

FINAL REPORT

Interaction of Microbial & Abiotic Processes in Soil Leading
to the (Bio)Conversion and Ultimate Attenuation of New
Insensitive Munitions Compounds

SERDP Project ER-2221

DECEMBER 2016

Jim A. Field
Jon Chorover
Reyes Sierra-Alvarez
Leif Abrell
University of Arizona, Tucson, AZ

John Coffey II
CH2M HILL

Distribution Statement A

This document has been cleared for public release



Page Intentionally Left Blank

This report was prepared under contract to the Department of Defense Strategic Environmental Research and Development Program (SERDP). The publication of this report does not indicate endorsement by the Department of Defense, nor should the contents be construed as reflecting the official policy or position of the Department of Defense. Reference herein to any specific commercial product, process, or service by trade name, trademark, manufacturer, or otherwise, does not necessarily constitute or imply its endorsement, recommendation, or favoring by the Department of Defense.

Page Intentionally Left Blank

REPORT DOCUMENTATION PAGE			Form Approved OMB No. 0704-0188		
1. REPORT DATE (DD-MM-YYYY) 30-12-2016		2. REPORT TYPE FinalReport		3. DATES COVERED (From - To) Feb9th 2012- Feb 8 th 2017	
4. TITLE AND SUBTITLE Interaction of Microbial & Abiotic Processes in Soil Leading to the (Bio)Conversion and Ultimate Attenuation of New Insensitive Munitions Compounds			5a. CONTRACT NUMBER W912HQ-12-C-0021		
			5b. GRANT NUMBER SERDP ER-2221		
			5c. PROGRAM ELEMENT NUMBER		
6. AUTHOR(S) Jim A Field Jon Chorover Reyes Sierra-Alvarez Leif Abrell John Coffey II			5d. PROJECT NUMBER ER-2221		
			5e. TASK NUMBER		
			5f. WORK UNIT NUMBER		
7. PERFORMING ORGANIZATION NAME(S) AND ADDRESS(ES) University of Arizona 888 N Euclid, Room 104 Tucson, AZ 85719			8. PERFORMING ORGANIZATION REPORT University of Arizona		
9. SPONSORING / MONITORING AGENCY NAME(S) AND ADDRESS(ES) Strategic Environmental Research and Development Program 4800 Mark Center Drive, Suite 17D03 Alexandria, VA 22350-3605			10. SPONSOR/MONITOR'S ACRONYM(S) SERDP		
			11. SPONSOR/MONITOR'S REPORT NUMBER(S) ER-2221		
12. DISTRIBUTION / AVAILABILITY STATEMENT Approved for public release; distribution is unlimited after embargo ending on June 1st, 2017					
13. SUPPLEMENTARY NOTES					
14. ABSTRACT Relatively little is known on insensitive munitions compounds, 2,4-dinitroanisole (DNAN) and 3-nitro-1,2,4-triazol-5-one (NTO), perform in the environment. The objectives of this study were to evaluate the interaction of abiotic and biotic factors contributing to the attenuation of IMCs in the soil leading to the formation of environmentally safe end-points. Anaerobic conditions favored the biological and/or chemical reduction of the nitro groups leading to the formation of amines intermediates. The amines retained toxicity thus further conversion was required. The amines formed from DNAN eventually became covalently incorporated into soil organic matter. The amine from NTO became mineralized by soil bacteria or manganese dioxide to carbon dioxide and inorganic nitrogen.					
15. SUBJECT TERMS Insensitive munitions compounds; 2,4-dinitroanisole (DNAN); 3-nitro-1,2,4-triazol-5-one (NTO); explosives; nitroaromatic compounds (NACs); nitroheterocyclic compounds; aromatic amines; 3-amino-1,2,4-triazol-5-one (ATO); 2-methoxy-5-nitroaniline (MENA); 2-amino-4-nitroanisole; 2,5-diaminosnidole (DAAN); biodegradation; biotransformation, bioconversion, bacteria; soil; transformation					
16. SECURITY CLASSIFICATION OF:			17. LIMITATION OF ABSTRACT	18. NUMBER OF PAGES	19a. NAME OF RESPONSIBLE PERSON
a. REPORT	b. ABSTRACT	c. THIS PAGE			Jim Field
UNCLASS	UNCLASS	UNCLASS	UNCLASS	204	19b. TELEPHONE NUMBER (include area code) 520-621- 0704

Page Intentionally Left Blank

Table of Contents

ABSTRACT	1
1. OBJECTIVES	3
2. BACKGROUND	4
2.1. Background on Insensitive Munitions Compounds	4
2.2. Background on Adsorption of Insensitive Munitions Compounds by Soil Components	5
2.3. Background on Biodegradation and Biotransformation of IMC	6
2.3.1. Biodegradation and biotransformation of DNAN.....	7
2.3.2. Biodegradation and biotransformation of NTO	8
2.3.3. Irreversible covalent incorporation of aromatic amines into humus	8
2.4. Ecotoxicity of DNAN and NTO	9
3. MATERIAL AND METHODS	11
3.1. Materials	11
3.1.1. Chemicals.....	11
3.1.2. Soils and inoculum.....	11
3.1.3. Humin purification.....	11
3.2. Analytical Methods.....	12
3.2.1. HPLC-DAD	12
3.2.2. UHPLC-Q-ToF-MS	12
3.2.3. Ion chromatography	13
3.2.4. Methane analysis by GC-FID	13
3.2.5. Nitrogen and carbon dioxide analysis by GC-TCD.....	13
3.2.6. Ultraviolet-visible (UV-Vis) analyses coupled to zebrafish toxicity..	13
3.2.7. Solid phase characterization of the soils.....	13
3.2.8. ¹⁴ C - fractionation	14
3.3 Bioassays.....	15
3.3.1. Inocula and basal medium	15

3.3.2. Biotransformation assays	16
3.3.3. Inhibition Bioassays.....	17
3.4. NTO/ATO Column Experiments	20
3.5. Adsorption Studies.....	22
3.5.1. Mineral synthesis and clay preparation.....	22
3.5.2. Batch sorption-desorption method.....	22
3.6. Oxidation of IMCs and IMC-Daughter Products by Minerals	23
3.7. Clone Library Methods to Characterize an ATO-Biodegrading Enrichment Culture	25
3.7.1. MR DNA primers and methods	25
3.7.2. Conventional clone library.....	25
4. RESULTS AND DISCUSSION	27
4.1. Adsorption of IMCs by Mineral Components of the Soil.....	27
4.1.1. Results: SR-XRD: Synthesis products and clay characterization.....	27
4.1.2. Results: adsorption isotherms	27
4.1.3. Results: Oxidation of MENA by acid birnessite.....	33
4.1.4. Discussion: Adsorption trends for Na ⁺ and K ⁺ smectite	33
4.1.5. Discussion: Adsorption to metal oxides	36
4.1.6. Discussion: Adsorption reversibility.....	36
4.1.7. Discussion: Preliminary Indications of Oxidation of MENA and ATO by Acid Birnessite.....	37
4.1.8. Conclusions adsorption work.....	37
4.2. Reaction of DNAN and Daughter Products with Birnessite and Ferrihydrite	39
4.2.1. Results: Reaction of DNA, MENA and DAAN with ferrihydrite	39
4.2.2. Results: Reaction of DNA, MENA and DAAN with birnessite.....	40
4.2.3. Results: Extent of mineralization.....	41
4.2.4. Transformation of birnessite based on X-ray diffraction (XRD) and X-ray photoelectron spectroscopy (XPS).....	42
4.2.5. Discussion DNAN and daughter product reaction with birnessite and ferrihydrite.	44
4.3. Reaction of NTO and Daughter Products with Birnessite and Ferrihydrite ...	47
4.3.1. Results: Oxidation assessment of NTO and ATO by birnessite	47

4.3.2. Results: Adsorption of IMCs to ferrihydrite:.....	51
4.3.4. Discussion: Oxidation assessment of NTO and ATO by birnessite ...	53
4.3.5. Discussion: Adsorptive loss from solution with ferrihydrite	55
4.3.6. Conclusion: Reaction of NTO and Daughter Products with Birnessite and Ferrihydrite	55
4.4. Reduction of IMCs with Green Rust	56
4.4.1. Results and discussion: reduction with green rust	56
4.4.2 Conclusion: reduction with green rust	59
4.5. Pathways of Reductive 2,4- DNAN Biotransformation in Sludge	60
4.5.2. Results: Aerobic conditions	60
4.5.3. Results: Microaerophilic aerobic conditions	62
4.5.4. Results: Anaerobic conditions	62
4.5.5. Results: Rates	65
4.5.6. Results: Identification of metabolites	65
4.5.7. Discussion: Reductive biotransformation	68
4.5.8. Discussion: Biotransformation pathways	68
4.5.9. Conclusions: Reductive DNAN biotransformation in sludge.....	69
4.6. (Bio)Transformation of 2,4-Dinitroanisole (DNAN) in Soils	70
4.6.2. Results: Aerobic soil survey for biotransformation	70
4.6.3. Results: Anaerobic soil survey for biotransformation	70
4.6.4. Results: Products identified in UHPLC and infusion Q-ToF-MS	73
4.6.5. Discussion: Aerobic transformation	74
4.6.6. Discussion: Anaerobic transformation.....	74
4.6.7. Discussion: Products of anaerobic conversion and biotransformation pathway	77
4.6.8. Conclusions: (Bio)Transformation of DNAN in soils	80
4.7. Environmental Fate of ¹⁴ C-2,4-DNAN in Soil Microcosms.....	81
4.7.1 Objectives: Fate ¹⁴ C-DNAN in soil microcosms	81
4.7.2. Results and discussion: DNAN reductive biotransformation.	81
4.7.3. Results and discussion: ¹⁴ C label distribution during DNAN biotransformation	82
4.7.4. Results and discussion: Aerobic vs. aerobic conditions	84
4.7.5. Anaerobic-aerobic sequential experiments.	86

4.7.6. Humic and organic carbon addition for higher incorporation	88
4.7.7. Conclusions: Fate ¹⁴ C-DNAN in soil.....	93
4.8. Biotransformation and Degradation of NTO by Soil Bacterial Communities	95
4.8.1. Results: Anaerobic reduction of NTO to ATO	95
4.8.1. Results: Lack of aerobic degradation of NTO	96
4.8.2. Results: Degradation of ATO	96
4.8.3. Discussion: Lack of NTO biodegradation under aerobic conditions..	99
4.8.4. Discussion: Anaerobic biotransformation.....	99
4.8.5. Discussion: Nitroreductases.....	99
4.8.6. Discussion Physiology	100
4.8.7. Discussion: Degradation products	100
4.9. Sequential Anaerobic-Aerobic Biodegradation of NTO.....	103
4.9.1. Results: Batch bioassays	103
4.9.2. Results: Continuous flow reactor experiments	104
4.9.3. Discussion: NTO reduction.....	107
4.9.4. Discussion: ATO degradation.....	107
4.9.5. Discussion: Sequential anaerobic-aerobic approach.....	108
4.9.6. Discussion: Concurrent aerobic and anaerobic reactions	108
4.9.7. Conclusions: Sequential biodegradation of NTO	109
4.10. Aerobic ATO-Biodegrading Enrichment Culture Study	110
4.10.1. Objectives:ATO enrichment culture study	110
4.10.2. Results and discussion: ATO-carbon-mineralization	111
4.10.3. Results and discussion: ATO-N mineralization.....	112
4.10.3. Results and discussion: Stoichiometry.....	114
4.10.4. Results and discussion: ATO EC clone libraries	115
4.10.4. Conclusions: ATO Enrichment culture.....	120
4.11. Microbial toxicity of DNAN and Aromatic Amine Daughter Products	121
4.11.1. Objectives	121
4.11.3. Results: Inhibition of aerobic heterotrophic bacteria	122
4.11.4. Results: Inhibition of nitrification.....	122
4.11.5. Results: Inhibition towards <i>Aliivibrio fischeri</i>	125

4.11.6. Discussion: Microbial toxicity of DNAN	125
4.11.7. Discussion: Microbial toxicity of DNAN metabolites.....	126
4.11.8. Conclusions: Microbial toxicity of DNAN and its daughter products .	126
4.12.2. Results and Discussion: Toxicity of model compounds and surrogates.	127
4.12.3. Results and Discussion: Exposures to DNAN (bio)transformation mixtures	130
4.12.3. Implications of microbial toxicity and (bio)transformation product profiles	138
4.13. Zebrafish Embryo Toxicity of DNAN Anaerobic Biotransformation Products .	139
4.13.1. Objectives: Zebrafish embryo toxicity.....	139
4.13.4. Toxicity implications of DNAN biotransformation.....	147
5. CONCLUSIONS	148
5.1. Reactivity of IMCs and IMC Daughter Products with Soil Minerals.....	148
5.1.1. Adsorption.....	148
5.1.2. Transformation.....	148
5.2. Bioconversion DNAN.....	149
5.2.1. DNAN transformation in anaerobic sludge	149
5.2.2. DNAN transformation in soil.....	150
5.2.3. ¹⁴ C-DNAN study.....	150
5.3. Bioconversion NTO	151
5.3.1. Biotransformation of NTO in soil.....	151
5.3.2. Sequential anaerobic-aerobic biodegradation of NTO	151
5.3.3. ATO-degrading enrichment culture.....	151
5.4. Toxicity	152
5.4.1. Microbial toxicity of DNAN.....	152
5.4.2. Microbial Toxicity of DNAN (bio)transformation products and product mixtures	152

5.5. Overview and Benefits.....	153
APPENDIX	176
A. Supporting Data	176
B. Scientific Publications.....	176
C. Other Supporting Materials	178

List of Tables

Table	Page
Table 2.1-1. Important properties of IMC relevant for environmental chemistry in comparison to conventional explosives they replace	4
Table 3.3-1. Zebrafish embryo toxicity endpoints assessed	19
Table 3.4-1. Operational conditions and performance of a laboratory-scale continuous flow reactor treating water containing ATO or NTO during different periods	21
Table 4.1-1. Distribution coefficients (K_d) and hysteresis indices (HI) calculated from the isotherms	32
Table 4.1-2. Maximum adsorption versus available surface area calculations	35
Table 4.2-1. First order rate constants (k) of IMC and daughter product oxidation by birnessite and ferrihydrite supplied at various concentrations	39
Table 4.3-1. First order rate constants (k) of ATO oxidation by birnessite and NTO/ATO adsorptive removal by ferrihydrite supplied at various concentrations.	49
Table 4.5-1. Molecular Formula, Retention Times Determined by UHPLC-MS, Calculated m/z Values, and m/z Values measured by TOFMS for the Various Identified Metabolites	67
Table 4.6-1. Rates of anaerobic biotransformation of DNAN with H_2 for the seven soils surveyed.	72
Table 4.6-2. Molecular Formulae, Retention Times, Calculated and Measured m/z Values, and Spectral Data Determined by UHPLC and Infusion Q-ToF-MS for the Identified Transformation Products. Retention time (RT)	76
Table 4.8-1. Selected properties of the soils used in this study	102
Table 4.9-1. Operational conditions and performance of a laboratory-scale continuous flow reactor treating water containing ATO or NTO during different periods	105
Table 4.10-1. Conventional clone library of ATO EC without YE after 17 transfer with primer set 27F and 1522R of the 16SrRNA gene. Shown are selected clones with $\geq 97\%$ sequence similarity.	117
Table 4.10-2. Conventional clone library of ATO EC with YE (1 mg L^{-1}) after 17 transfers with primer set 27F and 1522R of the 16SrRNA gene. Shown are selected clones with $\geq 97\%$ sequence similarity	118
Table 4.10-3. Clones with $\geq 97\%$ sequence homology in the MR DNA clone library of ATO EC without and with YE (1 mg L^{-1}) after 34 transfers with primer set 515F and 806F for the 16SrRNA gene. Dominant clones and clones related to conventional clone library. The number of recovered sequences are 127,239 for ATO EC without YE and 152,762 for ATO SC with YE.	119
Table 4.11-1. Summary of inhibitory concentrations determined for DNAN and its metabolites MENA and DAAN in various microbial toxicity bioassays	124
Table 4.12-1. Summary of inhibitory concentrations for DNAN, (bio)transformation products and best available surrogates to acetoclastic methanogens and <i>A. fischeri</i> (Microtox)	128
Table 4.12-2. Selected parent/daughter ion list for semi-quantitative LC-MS determination of soluble products formed during anaerobic MENA soil (bio)transformation. Daughter ions shown indicate they were used to determine the	136

abundance of the products. A total tolerance of 10 ppm for the mass bias was allowed for peak integration of the measured $[M+H]^+$ ions	
Table 4.13-1. Developmental Lowest Observable Effect Levels (LOELs) and endpoints with significant morbidity.	145
Table 4.13-2. Selected parent/daughter ion list for semi-quantitative LC-MS determination of soluble products formed during anaerobic MENA soil (bio)transformation. Daughter ions shown indicate they were used to determine the abundance of the products	145

List of Figures

Figure	Page
Figure 1.0-1. Overview of research project.	3
Figure 2.1-1. Chemical structures of DNAN and NTO	4
Figure 2.3-1. Pathway of reductive (bio)-transformation of nitro aromatic compounds to aromatic amines	6
Figure 2.3-2. Pathways of aerobic and anaerobic cometabolism reported in the literature.	7
Figure 2.3-3. Aerobic DNAN biodegradation pathway of <i>Nocardioides</i> sp strain JS1661	7
Figure 2.3-4. Pathways of NTO biotransformation and biodegradation	8
Figure 2.3-5. Postulated nucleophilic substitution of the aromatic amine, 2,4-diaminoanisole (DAAN), with a quinone moiety in humus. Mineral oxides of Fe and Mn are expected to regenerate quinone from hydroquinone. R = rest of molecule	8
Figure 2.3-6. Postulated one-electron oxidation of the aromatic amine, DAAN, to form a cation radical. The cation radicals either react with each other to form azo-dimers, diphenyl amines and oligomers or they couple with humus to become irreversibly covalently bound. Mineral oxides = manganese oxide. R = rest of molecule	9
Figure 3.2-1. Schematic of ¹⁴ C label recovery from different fractions after DNAN (bio)transformation: gaseous and volatile species (VOCs, CO ₂), aqueous (fulvic acids and water-soluble products), loosely bound (sequential liquid extractions with methanol (MeOH) and ethyl acetate (EtOAc), 0.5 M NaOH extraction (humic acids), and combustion in Harvey Oxidizier (unextractable and humin-bound residues).	15
Figure 3.4-1. Scheme of 350 mL aerated bioreactor used for NTO and ATO degradation. Legend: bottle containing influent (a), peristaltic pump (b), polyurethane foam blocks (c), air compressor (d), humid air inlet (e), effluent sampling port (f), and bottle containing effluent (g). The arrow indicates the direction of the flow. Influent samples were collected from bottle (a) and effluent samples were collected from tube (f).	20
Figure 4.1-1. Adsorption and desorption isotherms at pH 7.0 showing the uptake and release of 2,4-dinitroanisole (DNAN) at each mineral surface. Background electrolytes were 0.01 M NaCl for Na ⁺ -montmorillonite, goethite, and birnessite and 0.01 M KCl for K ⁺ -montmorillonite	28
Figure 4.1-2. Adsorption and desorption isotherms at pH 7.0 showing the uptake and release of 2-methoxy-5-nitroaniline (MENA) from each mineral surface (plot d is 'apparent' adsorption on basis of loss from solution, later recognized to include oxidative transformation as discussed in Section 5.2). Background electrolytes were 0.01 M NaCl for Na ⁺ -montmorillonite, goethite, and birnessite and 0.01 M KCl for K ⁺ -montmorillonite.	29
Figure 4.1-3. Adsorption and desorption isotherms at pH 7.0 showing the uptake and release of 3-nitro-1,2,4-triazole-5-one (NTO) on each mineral surface. Background electrolytes were 0.01 M NaCl for Na ⁺ -montmorillonite, goethite, and birnessite and 0.01 M KCl for K ⁺ -montmorillonite. Freundlich (non-linear) fits are shown for adsorption isotherms along with linear fits used for distribution coefficient calculations	30
Figure 4.1-4. Adsorption and desorption isotherms at pH 7.0 for 3-amino-1,2,4-triazole-5-one (ATO) on Na ⁺ -montmorillonite, K ⁺ -montmorillonite, and goethite. Background electrolytes were 0.01 M NaCl for Na ⁺ -montmorillonite, goethite, and birnessite and 0.01 M KCl for K ⁺ -montmorillonite. Note that the higher surface excess values following	31

desorption legs for montmorillonite are based on direct analytical application Equations shown in Section of and are therefore apparent. Surface exclusion of ATO gives a negative value for the difference within parentheses of eq. 2 in the Materials and Methods section (i.e., $C_{e,ads}$ overestimates adsorptive concentration in the entrained solution, M_{ENT})	
Figure 4.1-5. XRD patterns for K^+ -montmorillonite (a) and Na^+ -montmorillonite (b) clays after aqueous adsorption “ads” followed by desorption “des” of the nitro-aromatics DNAN and MENA for samples reacted at the highest adsorptive species concentrations shown in Figures 4.1.2-1 and 4.1.2-2. Note the increase in d-001 spacing (indicated by a downward shift in position $2^\circ \Theta$) with adsorption of MENA and DNAN. Greater relative expansion occurs in KCl solution and for DNAN relative to MENA, consistent with the surface excess results shown in Figures. 4.1-1 and 4.1-2.	35
Figure 4.2-1. Transformation of DNAN, MENA and DAAN by birnessite at (A) 15 g kg^{-1} , (B) 1.5 g kg^{-1} and (C) 0.15 g kg^{-1} solid to solution ratio at pH 7.0, and (D) log plots for MENA and DAAN reaction with birnessite at 0.15, 1.5 and 15 g kg^{-1} solid to solution ratio.	40
Figure 4.2-2. Comparative time course of DAAN loss from solution at birnessite and ferrihydrite SSR of 1.5 g kg^{-1} .	41
Figure 4.2-3. (A) The percent conversion of MENA/DAAN-C to CO_2 during incubations with birnessite 15 g kg^{-1} solid to solution ratio over a 3 h incubation period with 0, 5 and 20% O_2 in the headspace. DAAN CO_2 emission was tested with 20 % O_2 in the headspace only;(B) Nitrite recovery from MENA birnessite reaction at 15 g kg^{-1} solid to solution ratio at pH 7.0. *NT=not tested.	42
Figure 4.2-4. (A) XRD pattern of birnessite (MnO_2) and its transformation product after treatment with 1 mM MENA at pH 7. Peaks are labeled with the assigned diffracting planes (hkl) and d-spacing (\AA). Insets are the (002) and (220/110) peaks to show the offset of the MENA reacted birnessite. (B) High resolution Mn 3s scan for unreacted and post MENA reacted birnessite (15 g kg^{-1}) at pH 7.0. The increase in binding energy difference indicates reductive dissolution of birnessite and incorporation of reduced Mn forms back to the solids. Background electrolyte = 10 mM NaCl.	43
Figure 4.3-1. Transformation of IMCs by birnessite at (A) 15 g kg^{-1} , (B) 1.5 g kg^{-1} and (C) 0.15 g kg^{-1} solid to solution ratio at pH 7.0.	48
Figure 4.3-2. Log plots for ATO reaction with birnessite at 0.15, 1.5 and 15 g kg^{-1} solid to solution ratio. The error bars indicate 95 % confidence interval.	49
Figure 4.3-3. The fractional conversion of ATO carbon and nitrogen to detected products including total inorganic carbon ($CO_{2(g)} +$ dissolved carbonate species, indicated here by $CO_2\text{-C}$), $N_{2(g)}$, and urea following incubation with birnessite at 15 g kg^{-1} solid to solution ratio over a 3 h period with 20% headspace O_2 .	50
Figure 4.3.4. ATO remaining in solution upon reaction with birnessite at 15 g kg^{-1} solid to solution ratio over a 3 h incubation period with 0, 5 and 20% O_2 in the headspace with He.	51
Figure 4.3-5. Adsorption/desorption and fractional plots of NTO and ATO to ferrihydrite surface. Left axis q shows the mass of sorbed IMC per unit mass of solid at equilibrium. Right axis shows fraction of IMC sorbed to ferrihydrite surface at various steps.	52

Figure 4.3-6. High resolution Mn 3s scan for unreacted and post ATO reacted birnessite (15 g kg ⁻¹) at pH 7.0. The increase in binding energy difference indicates reductive dissolution of birnessite and incorporation of reduced Mn forms back to the solids.	53
Figure 4.4-1. Transformation of IMCs (A) NTO and (B) DNAN by sulfate green rust at 10 g kg ⁻¹ solid to solution ratio at pH 8.4.	57
Figure 4.4-2. Normalized absorbance (A) and normalized first derivative (B) Fe K α XANES spectra of pre- and post-reaction sulfate green rust (GR) with IMCs DNAN and NTO. Relative oxidation of GR and transformation to lepidocrocite (Lp) was examined by fractional convolution of reference spectra using linear combination fits (LCF) of reacted samples to reference compounds. Data are shown in black, fractional fits are shown in dots. Results show clear shift of oxidation state from mixed valent Fe ^{II} /Fe ^{III} (green rust) to Fe ^{III} (lepidocrocite) upon reaction with IMCs.	58
Figure 4.5-1. Aerobic biotransformation of DNAN (●) into MENA (□) and DAAN (▲). Panels: heat-killed sludge (A), live sludge (B), and live sludge supplemented with acetate as co-substrate (C). The dotted dashed line shows the molar sum of the three compounds.	61
Figure 4.5-2. Microaerophilic biotransformation of DNAN (●) into MENA (□) and DAAN (▲). Panels: heat-killed sludge (A), live sludge (B), and live sludge supplemented with acetate as co-substrate (C). The dotted dashed line shows the molar sum of the three compounds	63
Figure 4.5-3. Anaerobic biotransformation of DNAN (●) into MENA (□) and DAAN (▲). Panels: heat-killed sludge (A), live sludge (B), and live sludge supplemented with H ₂ as co-substrate (C). The dotted dashed line shows the molar sum of the three compounds	64
Figure 4.5-4. Comparison of the DNAN biotransformation rates in different redox conditions. Treatments: heat-killed sludge (■), endogenous (⊞), and cosubstrate (□). Expressed per unit of added biomass, the DNAN biotransformation rates in heat-killed sludge, endogenous and cosubstrate treatments were as follows (in $\mu\text{mol}\cdot\text{h}^{-1}\text{ g}^{-1}\text{ VSS}$): anaerobic (0.16, 5.86 and 11.0), microaerophilic (0.10, 9.08 and 7.79), and aerobic assays (0.08, 0.41 and 3.49).	65
Figure 4.5-5. DNAN biotransformation pathways by anaerobic sludge amended with H ₂ as a cosubstrate. Dashed lines represent hypothetical routes. Compounds in brackets were not detected but are potential metabolites. Main pathways are shown inside the black box. Secondary routes are presented outside of the box.	66
Figure 4.5-6. Nucleophilic attack of aromatic amine with nitrobenzene to form azo dimer. A similar reaction can occur between nitrosobenzene and hydroxylamines to form an azoxy dimer, which can account for previously observed formation of azoxy dimers as metabolites of DNAN reductive cometabolism in aerobic bacteria. Azoxy dimers can be reduced to azo dimers.	68
Figure 4.6-1. Aerobic removal of DNAN in soils (50 g wet wt L ⁻¹) in mineral medium. Live treatments (continuous line): Camp Butner (■), Camp Ripley (●), Catlin (▲), Camp Navajo (◆), Florence (X). Heat-killed treatments (dashed line): Camp Butner (□), Camp Ripley (○), and Catlin (Δ). No heat-killed treatment available for Florence and Camp Navajo. Averages with error bars are reported	71
Figure 4.6-2. Anaerobic transformation of DNAN in soils (50 wet g L ⁻¹) in mineral medium and amended with H ₂ : Camp Butner (■), Camp Ripley (●), Catlin (▲), Camp Navajo (◆), and Florence (X). Averages with error bars are reported.	71

Figure 4.6-3. Correlations of zero-order rate constant with soil organic carbon (OC) content (Panel A) and soil bioavailable Fe (Panel B) during DNAN anaerobic soil biotransformation assays. Rate was calculated from the end of the lag phase (Table 4.6-1) until DNAN was no longer detected. The vertical dashed line indicates threshold of linear correlation of rate constant with OC. Linear regression for OC in Panel A valid for 0-2.07% OC. Two-sided t-test, $n = 5$, $p \leq 0.005$	72
Figure 4.6-4. Concentrations of DNAN (●), MENA (■), and DAAN (▲) and their sum (---) during the anaerobic (bio)transformation of DNAN with 50 wet g L ⁻¹ soil for Catlin (A), Camp Butner (B), and Camp Navajo (C) soils. H ₂ added as electron donor (1), live soil (endogenous) (2), and heat-killed soil (3). Averages with error bars are reported	75
Figure 4.6-5. Possible mechanisms for coupling between reduced intermediates of nitroaromatic compounds: A) coupling of nitrosobenzenes with aromatic amines; B) coupling of nitrosobenzenes with phenylhydroxylamines	77
Figure 4.6-6. Metabolites detected with infusion and UHPLC Q-ToF-MS experiments and transformation pathway proposed. Compounds in parentheses were not detected in this work but are known intermediates in the literature. Double arrows indicate that reactions require multiple steps.	78
Figure 4.7-1. Incorporation of ¹⁴ C into soil components during DNAN (■) anaerobic (bio)transformation in soils and sludge amended with 10 mM pyruvate. Panel A: CN soil (10 g L ⁻¹). Panel B: CB soil (10 g L ⁻¹). Panel C: anaerobic sludge. No detectable ¹⁴ C label was obtained in the gas phase (volatile organic compounds (VOCs) and CO ₂). In this experiment, the aqueous samples were not corrected for scintillation quenching due to coloration. The upper line is the sum of all labeled fractions	83
Figure 4.7-2. Impact of redox conditions on extent and rate of ¹⁴ C-ring DNAN labeled carbon incorporation into different extractable liquid and residual solid fractions during (bio)transformation in CN soil (25 g L ⁻¹). Treatments included 10 mM pyruvate amended anaerobic (Pyr-Anaer), endogenous anaerobic without pyruvate added (Anaer) and endogenous aerobic without pyruvate added (Aer) conditions. Panel A: ¹⁴ C label distribution at 40 days of incubation. Panel B: ¹⁴ C-incorporation rate (0-40d, period of maximum slope) into the humin. Humin was measured with ¹⁴ CO ₂ from the combustion of the residual soil in a Harvey Oxidizer after all the extractions.	85
Figure 4.7-3. Effect of pyruvate and horseradish peroxidase addition on radiolabelled carbon soil incorporation during sequential anaerobic(0-40d)-aerobic(40-104d) biotransformation of ¹⁴ C-ring DNAN in CN soil (25 g L ⁻¹). Panel A: endogenous. Panel B: amended with 10 mM pyruvate at day 0. Panel C: endogenous with horseradish peroxidase (HRP) and H ₂ O ₂ added at day 40	87
Figure 4.7-4. Increased incorporation of ¹⁴ C into soil humus with increased organic carbon added as natural soil or by spiking soil with humin during the course of DNAN biotransformation amended with 10 mM pyruvate in anaerobic conditions. Panel A: Incubations with different CN amounts of soil extracted at day 40. Panel B: Incubations with CB soil (25 g L ⁻¹) and different amounts of purified humin added	90
Figure 4.7-5. Correlation of organic carbon to DNAN ratio with ¹⁴ C-ring labeled DNAN incorporation into humin extracted at 30-50d of anaerobic incubation amended with 10 mM pyruvate. CN soil (○), CB soil (□), CB soil amended with humin: experiment 1 (■) and experiment 2 (▲) incubations.	91

Figure 4.7-6. A suggested conceptual structure of DAAN covalently bound to two quinone moieties in humus, using 2-methoxy-1,4-hydroquinone as a model of the OC in humus. This conceptual structure would correspond to OC:DNAN (mg:mg ⁻¹) ratio of 0.85.	91
Figure 4.7-7. Predicted reaction between DAAN and 2-methoxy-1,4-benzoquinone.	92
Figure 4.7-8. Hypothesized formation of Fe(III) oxide minerals during Fe ²⁺ mediated reduction of nitroaromatic compounds to aromatic amines that enables the oxidation of hydroquinones to quinones which in turn can form irreversible covalent bonds with aromatic amines via nucleophilic substitution reactions. A total of 6 mol Fe(III) can be formed by reduction of each nitro group which is sufficient to oxidize 3 hydroquinones to quinone and only one quinone is required to form a covalent bond.	92
Figure 4.7-9. Reaction of aromatic amines with MnO ₂ involving a cation radical mechanism, formation of dimeric intermediates and the ultimate irreversible covalent bonding of the aromatic amines and dimers with the soil humus (natural organic matter, NOM). R = rest of molecule.	93
Figure 4.8.1. The anaerobic degradation of NTO to ATO in microcosms inoculated with (A) Camp Navajo (AZ) soil, and (B) Florence (AZ) soil in H ₂ amended microcosms (squares) endogenous controls (triangles), and killed controls (circles). NTO concentrations are shown with solid symbols and solid lines and ATO concentrations are shown with open symbols, dotted lines). Error bars indicate standard deviation of duplicate microcosms	96
Figure 4.8-2. Degradation of NTO to ATO in microcosms with H ₂ as an electron donor without YE (A) and with 10 mg L ⁻¹ YE (B), or with 20 mM of citrate without YE (C) and with 10 mg L ⁻¹ YE (D), or with 20 mM pyruvate without YE (E) and with 10 mg L ⁻¹ YE (F). The concentration of NTO (black squares) and ATO (triangles) are shown on the primary axis; the concentration of the hydroxyl-amino intermediate (circles) is shown on the secondary axis. Error bars indicate standard deviations of duplicate microcosms	97
Figure 4.8.3. Degradation of ATO under aerobic conditions and release of N species: (A) Camp Butner soil, pH 7.2; (B) Camp Navajo soil, pH 7.2; (C) Camp Butner soil, pH 8.5; (D) Camp Navajo soil, pH 8.5; (E) Camp Butner soil, pH 7.2, with glucose; (F) Camp Navajo soil, pH 7.2, with glucose; (G) Camp Butner soil, pH 8.5, with glucose; (H) Camp Navajo soil, pH 8.5, with glucose. Solid triangles show ATO concentrations (as per mol of N), squares correspond to ammonia, circles to nitrite, diamonds to nitrate, and dashed line represents the sum of N species concentrations (both inorganic and ATO). Mineral medium used initially contained 0.5 mM of inorganic N (as ammonia).	98
Figure 4.8-4. The biotransformation and degradation pathway of NTO found in this study.	100
Figure 4.9-1. NTO bioconversion under various redox regimens in a soil suspension (Gortner soil 10 g L ⁻¹) with pyruvate (2.7 mM). The aerobic incubation did not contain pyruvate and yeast extract. (A): Sequenced anaerobic-aerobic incubation. (B): Anaerobic incubation. (C): Aerobic incubation. Legend: NTO live culture (■), ATO live culture (□).	103
Figure. 4.9-2. Disappearance of ATO in aerated continuous flow reactor during periods I (no ATO addition, average flow rate = 154 mL day ⁻¹), IIa (600 μM ATO, average flow rate = 146 mL day ⁻¹), and IIb (1000 μM ATO, average flow rate = 213 mL day ⁻¹).	104

Legend: ATO concentration measured in the influent (■), ATO concentration measured in the effluent (□)	
Figure 4.9-3. Disappearance of NTO and ATO in an aerated continuous-flow reactor during period III (average flow rate = 204 mL day ⁻¹). NTO was added as the target substrate (1000 μM) and sodium pyruvate was added as a cosubstrate (1800 μM). Legend: NTO (▲) and ATO (■) concentration measured in the influent, NTO (Δ) and ATO (□) concentration measured in the effluent.	105
Figure 4.9-4. Mineralization of N and formation of a metabolite through ATO degradation in an aerated continuous flow reactor. (A): Concentration of inorganic N ions in the effluent. (B): Metabolite peak area measured in the effluent. Legend: Ammonium (○), nitrite (□), and nitrate (Δ) concentration, total N ions (—) concentration, and metabolite peak area (■) in the effluent.	106
Figure 4.10-1. ATO as main daughter product of NTO	110
Figure 4.10-2. Schematic of the aerobic ATO enrichment culture (EC) strategy	110
Figure 4.10-3. ATO concentration decrease in comparison with CO ₂ formation by the series A enrichment culture from the 27 th transfer in basal medium containing 1 mg L ⁻¹ YE. The data are normalized to the C concentration of ATO at time zero. ATO was supplied at 1.5 mM.	111
Figure 4.10-4. ATO concentration decrease in comparison with CO ₂ formation by the series B enrichment culture from the 28 th transfer in basal medium without YE. The data are normalized to the C concentration of ATO at time zero. ATO was supplied at 1.5 mM.	112
Figure 4.10-5. ATO concentration decrease in comparison with the formation of inorganic N species by the series A enrichment culture from the 37 th transfer in basal medium containing 1 mg L ⁻¹ YE. The data are normalized to the N mass of ATO at time zero. ATO was supplied at 3.9 mM. The ionic species were composed almost exclusively of NH ₄ ⁺	113
Figure 4.10-6. ATO concentration decrease in comparison with the formation of inorganic N species by the series B enrichment culture from the 35 th transfer in basal medium without YE. The data are normalized to the N mass of ATO at time zero. ATO was supplied at 3.5 mM. The ionic species were composed almost exclusively of NH ₄ ⁺	114
Figure 4.11-1. (A) CH ₄ production by anaerobic sludge amended with acetate (26 mM) and DNAN (in μM): 0 (□), 13 (◆), 26 (□), 52 (●), 78 (◇), 104 (■), and 130 (○). (B) DNAN bio-transformation, and formation of DNAN metabolites, and CH ₄ production by anaerobic sludge amended with acetate (26 mM) and DNAN (133 μM). Legends: DNAN (●), and MENA (□), DAAN (▲), and methane (◇).	121
Figure 4.11-2. DNAN, MENA and DAAN inhibition (expressed as percentage of the control activity) towards methanogenic (A), and aerobic microorganisms (B). <u>Panel A-</u> Methanogenic assays: DNAN (●), MENA (□), DAAN (▲). <u>Panel B-</u> Aerobic heterotrophic assays: DNAN (○), MENA (■); Nitrification assays: DNAN (●), MENA (□).	122
Figure 4.11-3. (A) Time course of O ₂ consumption by aerobic activated sludge amended with acetate (28 mM) when exposed to DNAN (in μM): 0 (◇), 130 (●), 260 (▲), and 390 (□). Endogenous control lacking acetate and DNAN (◆). (B) Time course of NH ₄ ⁺	123

consumption by nitrifiers in activated sludge in the presence of DNAN (in μM): 0 (\blacklozenge), 65 (\circ), 130 (\blacktriangle), 260 (\square), 520 (\bullet)	
Figure 4.11-4. Toxicity of DNAN (\bullet), MENA (\square), and DAAN (\blacktriangle) to <i>A. fischeri</i> after 30 min of exposure. Toxicity is expressed as percentage of toxicant-free activity	125
Figure 4.12-1. Panel A: (Bio)transformation pathways of DNAN in anaerobic incubations of soils and sludge. Microbial toxicity was evaluated for shown monomer compounds. Panel B: Azo-oligomer surrogate compounds used for microbial toxicity. Notation: OMe = methoxy; Ac = acetyl.	127
Figure 5.12-2. Methanogenic inhibition (A1, A2) and <i>A. fischeri</i> bioluminescence (B1, B2) based on toxicant concentration. Column 1: iMENA (\blacksquare), Ac-DAAN (\blacktriangle), dimer L (\bullet). Column 2: BBY (\blacktriangledown).	129
Figure 4.12-3. Fifty-percent inhibition concentrations (IC_{50}) for acetoclastic methanogens (\blacksquare) and <i>A. fischeri</i> (\bullet) for DNAN and its (bio)transformation products and azo-oligomer surrogates. Shaded area indicates DNAN IC_{50} range. Open symbols in dimer L show adjusted concentrations to monomer equivalents. Ac-DAAN did not cause inhibition to methanogens and the highest concentration tested (8000 μM) is shown instead with an asterisk above the symbol. The BBY IC_{50} for both models was 0.7 μM .	130
Figure 4.12-4. Workflow pictogram for DNAN staggered (bio)transformation assay, followed by product mixture semi-quantitative analysis and microbial toxicity assessment. Anaerobic incubations were set starting at different days so that when all the samples were taken the (bio)transformation product mixture would be a representative mixture for different stages of DNAN (bio)transformation (0, 1, 5, 10, 20, 30, 40, and 50 days of incubation). Samples were collected for (semi)-quantitation of the products formed, and subjected to methanogen and Microtox toxicity assays in order to reconstruct the changes in toxicity of the aqueous phase during the course of DNAN (bio)transformation.	131
Figure 4.12-5. DNAN anaerobic (bio)transformation in Camp Butner soil and their collective toxicity impact. Panel A: DNAN (\square) formed transformation products (stacked area, from light to dark in ascending molecular mass): 139.0866, 165.0659, 169.0608, 181.0972, 185.0652, 193.0607, 228.0768, 243.0877, 243.1241, 245.1300, 247.0425, 259.1190, 267.0975, 269.1397, 273.1347, 274.0715, 275.1503, 285.1347, 299.1179, 301.1289, 313.1289, 325.1659, 327.1452, 431.1569. Predominant $[\text{M}+\text{H}]^+$ values are shown. Panel B: Impact of mixtures of transformation products formed during (bio)transformation on <i>A. fischeri</i> bioluminescence (\blacksquare) and acetoclastic methanogens (\bullet).	133
Figure 4.12-6. DNAN anaerobic (bio)transformation in Camp Navajo soil and their collective toxicity impact. Panel A: DNAN (\square) formed transformation products (stacked area, from light to dark in ascending molecular mass): 139.0866, 165.0659, 169.0608, 181.0972, 185.0652, 193.0607, 228.0768, 243.0877, 243.1241, 245.1300, 247.0425, 259.1190, 267.0975, 269.1397, 273.1347, 274.0715, 275.1503, 285.1347, 299.1179, 301.1289, 313.1289, 325.1659, 327.1452, 431.1569. Predominant $[\text{M}+\text{H}]^+$ values are shown. Panel B: Impact of mixtures of transformation products formed during (bio)transformation on <i>A. fischeri</i> bioluminescence (\blacksquare) and acetoclastic methanogens (\bullet).	134
Figure 4.12-7. DNAN anaerobic (bio)transformation in anaerobic sludge and their collective toxicity impact. Panel A: DNAN (\square) formed transformation products (stacked	135

area, from light to dark in ascending molecular mass): 139.0866, 165.0659, 169.0608, 181.0972, 185.0652, 193.0607, 228.0768, 243.0877, 243.1241, 245.1300, 247.0425, 259.1190, 267.0975, 269.1397, 273.1347, 274.0715, 275.1503, 285.1347, 299.1179, 301.1289, 313.1289, 325.1659, 327.1452, 431.1569. Predominant $[M+H]^+$ values are shown. Panel B: Impact of mixtures of transformation products formed during (bio)transformation on <i>A. fischeri</i> bioluminescence (■) and acetoclastic methanogens (●).	
Figure 4.13-1. Main anaerobic DNAN (bio)transformation pathway (structures inside box): DNAN undergoes nitro reduction to MENA and DAAN. Reactive intermediates formed during nitro-group reduction enable coupling reactions that form dimers and other oligomers by reacting with aromatic amine. Chemical structures of individual compounds tested based on previously identified DNAN (bio)transformation products (§) or best available surrogates (§).	140
Figure 4.13-2. Developmental endpoints that caused significant malformations in the zebrafish embryo assay for dimer L. White bars indicate hits above the statistically significant threshold ($p \leq 0.05$). The rest of the endpoints did not show significant activity.	141
Figure 4.13-2. Developmental endpoints that caused significant malformations in the zebrafish embryo assay for dimer L. White bars indicate hits above the statistically significant threshold ($p \leq 0.05$). The rest of the endpoints did not show significant activity.	142
Figure 4.13-4. Average long distance swum recorded in locomotor response Viewpoint assay for 120 hpf zebrafish larvae exposed to DAAN (0-640 μ M) in dark (A) and light (B) stages.	143
Figure 4.13-5. Characterization of products formed during MENA (bio)transformation coupled to zebrafish toxicity. Panel A: Temporal semi-quantitation of transformation products ($[M+H]^+$ $m/z = 139, 181, 243, 313, 393$) shown with stacked areas and increasing m/z shown with darker shades and zebrafish mortality assessed at 120 hpf (■). Mortality statistical significance ($p < 0.05$) is above 4 hits ($n = 32$). Panel B: MENA concentration (●) and 400 nm/ 254 nm absorbance index (□) during MENA (bio)transformation.	146
Figure 5.5-1. Shared and divergent pathways of IMC biotransformation to environmentally safe end products (NOM refers to natural organic matter or humus)	153

List of Acronyms

Abbreviation	Definition
^{14}C -	^{14}C -labeled
^{15}N	^{15}N -labeled
16S rRNA	16S ribosomal ribonucleic acid
3,4-DCA	3,4-dichloroaniline
4-CA	4-chloroaniline
Ac-DAAN	N-acetyl-2,4-diaminoanisole
AGS	anaerobic methanogenic sludge
ATO	3-Amino-1,2,4-triazol-5-one
BBY	Bismarck brown Y (diazodye)
BET	Brunauer–Emmett–Teller specific surface area
C	carbon
CAP	4-chloro-2-aminophenol
CAP	4-chloro-2-aminophenol
CB	Camp Butner soil
CH_4	methane
CHO	chinese hamster ovary cells
CN	Camp Navajo soil
CNP	4-chloro-2-nitrophenol
CNP	4-chloro-2-nitrophenol
COD	chemical oxygen demand
DAAN	2,4-diaminoanisole
DAD	diode array detection
Dimer L	2,2'-dimethoxy-4,4'-azodianiline
DMSO	dimethylsulfoxide
DNAN	2,4-dinitroanisole
DNP	2,4-dinitrophenol
DoD	Department of defense
EC	enrichment culture
EDA	electron donor-acceptor (
E-donor	electron donor
eeq	electron equivalents
EM	embryo medium
EM	embryo medium
EtOAc	ethyl acetate
Fe	iron
FWHM	full width at half maximum
GR	green rust

H4IIE	H4IIE rat hepatoma cells
HI	hysteresis indices
hpf	hours post fertilization
HPLC-UV	High performance liquid chromatography with ultraviolet detection
HRP	horseradish peroxidase
HRT	Hydraulic retention time
HTO	hydroxylamino-1,2,4-triazol-5-one
HTO	3-hydroxylamine-1,2,4-triazol-5-one
IC ₅₀	50% inhibiting concentrations (IC ₅₀)
IMCs	insensitive munitions
iMENA	4-methoxy-3-nitroaniline
K _d	distribution coefficients
K _{oc}	organic carbon to water partitioning coefficients
LC	liquid chromatography
LC ₅₀	fifty-percent lethal concentrations
LCF	linear combination fits
LC-MSMS	liquid chromatography – tandem mass spectrometry
LOEC	lowest observed effect concentration
LOEL	lowest observable effect level
Log K _{ow}	octanol-water coefficient
L _p	lepidocrocite
LSC	liquid scintillation counting
MENA	2-methoxy-5-nitroaniline
MeOH	methanol
Mn	manganese
MnO ₂	manganese dioxide (birnessite)
MR DNA	Molecular Research LP
N	nitrogen
NA	not available
NACs	nitroaromatic compounds
NAD(P)H	reduced nicotinamide adenine dinucleotide (phosphate)
NC	Camp Butner soil (alternative abbreviation, soil is from North Carolina)
NCBI	National Center for Biotechnology Information
NHCs	nitroheterocyclic compounds
NMR	nuclear magnetic resonance spectroscopy
NOEL	no observable effect level
NOM	natural organic matter
NOM	natural organic matter
NTO	3-nitro-1,2,4-triazol-5-one
OC	Organic carbon

PZNC	point of zero net charge
qPCR	quantitative polymerase chain reaction
QSAR	quantitative structure-activity relationships
QToF	quadrupole time-of-flight
RAS	return activated sludge
RDX	1,3,5-trinitroperhydro-1,3,5-triazine
RT	retention time
SOC	soil organic carbon content
SOM	soil organic matter
SR-XRD	synchrotron radiation X-ray diffraction
SSR	solid to solution ratio
SSRL	Stanford Synchrotron Radiation Light-source
TAT	2,4,6-triaminotoluene
TC	total carbon
TN	total nitrogen
TNT	2,4,6-trinitrotoluene
TOC	total organic carbon
TOF-MS	time of flight mass spectrometry
UHPLC-DAD	an ultra-high performance liquid chromatograph - diode array detector
UV-Vis	ultraviolet-visible
VOCs	volatile organic compounds
VSS	volatile suspended solid
XANES	X-ray absorption near edge structure
XPS	X-ray photoelectron spectroscopy
XRD	X-ray diffractometer
YE	yeast extract
ZVI	zero valent iron

Keywords

Insensitive munitions compounds,; 2,4-dinitroanisole (DNAN); 3-nitro-1,2,4-triazol-5-one (NTO); explosives; nitroaromatic compounds (NACs); nitroheterocyclic compounds; aromatic amines; 3-amino-1,2,4-triazol-5-one (ATO); 2-methoxy-5-nitroaniline (MENA); 2-amino-4-nitroanisole; 2,5-diaminosidole (DAAN); biodegradation; biotransformation, bioconversion, bacteria; soil; transformation, manganese dioxide; MnO₂; Mn(IV); birnessite; ferrihydrite, green rust; goethite; iron oxide; Fe(III); Fe(II); manganese; iron; enrichment culture; mineralization; mineral; bioremediation; natural organic matter (NOM); humus; humin; organic matter (OM); organic carbon (OC); soil organic carbon; incorporation; covalent binding; irreversible binding; adsorption

ABSTRACT

Objectives. 2,4-Dinitroanisole (DNAN) and 3-nitro-1,2,4-triazol-5-one (NTO) are two insensitive munitions compounds (IMCs) being used to replace conventional munitions, TNT and RDX, respectively. Relatively little is known on how these compounds will perform in the environment with respect to their biotransformation and retention in soil systems. The objectives of this study were to evaluate the interaction of abiotic and biotic factors contributing to the attenuation of IMCs in the soil leading to the formation of environmentally safe end-points.

Technical Approach. A series of soil or soil mineral microcosm experiments were conducted in which IMC biotransformation products or IMC sorption were monitored with liquid chromatography (including quadrupole time of flight mass spectrometry detection), toxicity assays and ^{14}C fractionation studies. Staggered toxicity tests were used in which microbial and zebrafish embryo toxicity was monitored as a function of biotransformation time and product composition. To evaluate mineralization of IMC, common N ions were measured with an ion chromatograph and CO_2 and N_2 were measured with a gas chromatograph.

Results. DNAN was initially converted to 2-methoxy-4-nitroaniline (MENA) and 2,4-diaminoanisole (DAAN) in soil especially under reducing conditions provided with electron donating substrate in a reaction involving both abiotic and biotic mechanisms. The rate of reduction was correlated strongly to the soil organic carbon (OC). The aromatic amines reacted chemically with nitroso-intermediates of DNAN reduction to form azo-linked dimers and subsequently both the aromatic amines and dimers were subjected to secondary metabolism causing O-demethylation and N-methylation and N-acetylation. The aromatic amines also reacted with soil organic (NOM) to become covalently and irreversibly bound with the insoluble humus fraction (humins). The extent of ^{14}C -DNAN incorporation into humins could be accurately predicted by the mass ratio of organic carbon (OC) and initial DNAN ($\text{OC}:\text{DNAN}_{\text{initial}}$ mg:mg) regardless of the source of the soil organic matter. Comparing incubations conditions indicates that the most rapid incorporation of ^{14}C -DNAN into humins occurs under completely anaerobic conditions. The most likely mechanism of anaerobic incorporation is a nucleophilic substitution reaction between quinone moieties in humus and the aromatic amine daughter products.

The biotransformation intermediates of DNAN were observed to be toxic to some microbial systems such as acetoclastic methanogenesis, nitrification and the marine bioluminescent marine bacterium, *Aliivibrio fischeri* (Microtox assay). The toxicity was often either in the same range or moderately lower than the parent DNAN depending on the test system and the specific intermediate. However, only an N-acetylated DAAN metabolite was distinctly less toxic than DNAN by many orders of magnitude. Staggered bioassays revealed methanogen inhibition increased sharply early as reactive intermediates formed during nitro-group reduction but the inhibition reversed when dimers were formed. *Aliivibrio fischeri* tolerated the early intermediates but progressively became more inhibited as dimer levels accumulated over longer biotransformation time periods. To evaluate ecotoxicity, zebrafish embryo were utilized as the model system. Intermediates of DNAN biotransformation caused detectable developmental and behavioral toxicity in zebrafish embryos. Most concerning was the high level of developmental toxicity caused by a surrogate azo-dimer intermediate and 4-methoxy-5-nitroaniline (iMENA) (both at $6.4\ \mu\text{M}$) as well as evidence of locomotor toxicity caused by DAAN at higher concentrations. In staggered assays significant increase in acute mortality was observed at the onset of dimer formation. The toxicity tests clearly indicate that intermediates of DNAN biotransformation are often still quite toxic, thus the goal of remediation should be to achieve

environmentally safe end points such as irreversible covalent incorporation into humin (“bound residue”) or complete biodegradation to mineralized products (“mineralization”).

NTO was also readily reduced to its corresponding heterocyclic amine, 3-amino-1,2,4-triazol-5-one (ATO) under anaerobic conditions in soil via a microbially catalyzed reaction requiring an electron donor. Under aerobic conditions in aqueous soil suspensions, NTO was not biotransformed; whereas, under anaerobic conditions ATO was not degraded further. Full biodegradation could be achieved by properly sequencing redox reactions. NTO must first be reduced to ATO to subsequently be able to mineralize it under aerobic conditions. NTO degradation was achieved in a continuously fed aerobic biotrickle reactor. The reduction of NTO in an aerobic bulk environment of the reactor was plausible due to the presence of putative anaerobic microniches in the reactor’s biofilm. ATO was fully biodegraded as the sole C and N source by a sustainable enrichment culture (EC) developed from soil inoculum. The EC mineralizes C in ATO completely to CO₂ and the N in ATO by approximately 50% to NH₃ and the other 50% to N₂. The EC requires O₂, indicating at least one O₂- dependent step. Clone library studies indicated a possible role of *Hydrogenophaga* previously implicated in oxidative 4-aminobenzenesulfonate degradation and *Hyphomicrobium*, known for C1 metabolism. IMC adsorption studies were carried out with the clay, montmorillonite and the iron oxides, goethite and ferrihydrite. DNAN and its daughter product, MENA were adsorbed strongly by the layer silicate clay; whereas NTO and to a lesser extent ATO was adsorbed by the iron oxides. K⁺ enhanced DNAN adsorption to the clay due to its lower hydration shell compared to other major cations, enhancing the innersphere complexes.

Common occurring soil minerals can cause transformation reactions. Birnessite (MnO₂) and ferrihydrite. During reductive (bio)transformation of DNAN and NTO, the progressive replacement of electron withdrawing nitro-groups by amino groups, increases the oxidative susceptibility of the IMC molecules and they were rapidly oxidized by birnessite. In contrast, the parent compounds, DNAN and ATO were completely resistant to oxidation. ATO was extensively oxidized to safe end products consisting of CO₂, NH₃ and urea during the reaction with birnessite. Lastly, the mixed valent iron containing mineral, green rust, reduced DNAN in the time scale of a few days and NTO in the time scale of minutes to the corresponding amine daughter products.

Benefits. The most important benefit of the project is the recognition that IMCs can be converted by a sequence of reduction and oxidation (or substitution) reactions to environmentally safe end points. The sequence is required since our study shows that primary daughter products are still quite toxic and yet significantly more prone to oxidation. The sequence enables extensive degradation of NTO by forming ATO which in turn is extensively mineralized by aerobic bacteria or birnessite to CO₂, NH₃, N₂ and urea. The sequence also enables extensive incorporation of DNAN into NOM by first reducing it to aromatic amines that later undergo nucleophilic substitution reactions with quinone moieties in NOM creating irreversible covalent bonds. The mass ratio of OC to DNAN was identified as a parameter predicting humus-bound residue formation, with the implication of NOM addition enhancing the remediation of amines.

Other benefits include the discovery that iron oxides in soil can significantly adsorb NTO. Adsorption of DNAN in clay soils can be greatly increased by adding K⁺ to soil. The project also demonstrates the importance of both soil minerals and bacteria in the transformation of IMCs. And lastly, an enrichment culture was developed that reliably mineralizes ATO as sole C and N-source to benign products, CO₂, NH₃ and N₂, with potential for bioaugmentation applications.

1. OBJECTIVES

The Department of Defense (DoD) plans to increase the use of two new insensitive munitions compounds (IMC), 3-nitro-1,2,4-triazole-5-one (NTO) and 2,4-dinitroanisole (DNAN), yet little is known about their environmental behavior. In order to better understand the environmental fate of these IMCs, the goal of this project is to study the interaction of biological and abiotic processes in the soil that collectively contribute to their conversion and attenuation under different biogeochemical conditions. The project sought to provide a better understanding of the potential risk for the accumulation of toxic (bio)transformation intermediates and provide a scientific basis to predict the long-term fate of the IMCs to either mineralized products, bound residue in humus or tightly adsorbed species based on soil composition and biogeochemical conditions.

This study evaluated the interaction of microbial and abiotic factors in soil leading to the conversion of IMCs to potentially toxic (bio)-transformation intermediates and environmentally safe end points such as mineralized products or bound residue in humus (Figure 1.0-1.). The first goal was to evaluate the environmental fate of IMCs as a function of soil type from selected soils representing a range of soil characteristics. The fates that were monitored included IMC sorption to soil, and (bio)transformation yielding intermediate compounds, mineralized products and/or humus-bound residue. Based on the fates observed, soils were selected for further study to elucidate the main mechanisms of sorption, biodegradation and/or abiotic transformation. This information was combined to test the hypothesis that small structural modifications catalyzed by abiotic or biotic reactions will determine the ultimate fate of IMCs (mineralized *versus* bound residue in humus). Lastly, the consequences of the findings were assessed by evaluating the microbial and ecological toxicity of IMCs and their (bio)transformation products. The overall objective was to understand which mechanisms lead to the conversion of IMCs to safe end products so as to predict which soil conditions are suitable for attenuating IMCs and to apply measures for improving attenuation. The specific objectives of the project dictated the five main research tasks:

- 1) Attenuation and fate of IMCs over a range of upland soil types;
- 2) Mechanisms of biodegradation and biotransformation of IMCs in soils;
- 3) Mechanisms of sorption and abiotic transformation of IMCs in soils;
- 4) Interaction of biotic/abiotic mechanisms dictating the fate of IMCs
- 5) Microbial and ecological toxicity of IMCs and their (bio)transformation products

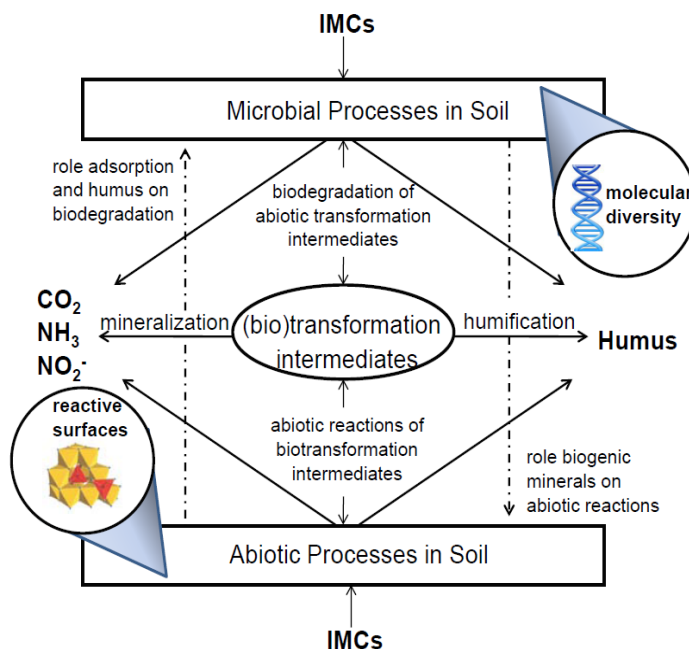


Figure 1.0-1. Overview of research project.

2. BACKGROUND

2.1. Background on Insensitive Munitions Compounds

Conventional explosive compounds such as 2,4,6-trinitrotoluene (TNT) and 1,3,5-trinitroperhydro-1,3,5-triazine (RDX) are falling out of favor with the military because they are prone to serious accidental explosions². The military is thus replacing conventional explosives with new insensitive munitions. Insensitive munitions are those munitions which reliably fulfill their performance, readiness and operational requirements on demand, but which will minimize the violence of a reaction and subsequent collateral damage when subjected to unplanned heat, shock, mechanical stress, electromagnetic energy, or radiation³⁻⁵. Two insensitive munitions compounds (IMCs) have become the most widely used replacements in munitions formulations. They are 2,4-dinitroanisole (DNAN)^{2,5} and 3-nitro-1,2,4-triazol-5-one (NTO)⁵⁻⁷ (Figure 2.1-1), which are used to replace TNT and RDX, respectively.

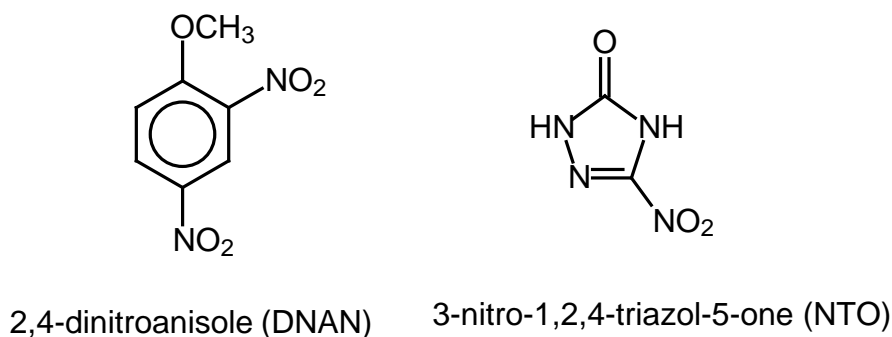


Figure 2.1-1. Chemical structures of DNAN and NTO

Table 2.1-1. Important properties of IMC relevant for environmental chemistry in comparison to conventional explosives they replace†

IMC	MW g mol ⁻¹	pKa	aqueous solubility mg L ⁻¹	Log Kow
TNT	227	N/A*	100	1.62
DNAN	198	N/A	276	1.61
RDX	222	N/A	60	0.87
NTO	130	3.76	12,800	0.21

*Not applicable.

†References for DNAN⁸; references for NTO^{7,9,10}; references for TNT and RDX^{11,12}.

Important environmental chemistry properties of DNAN and NTO are provided in Table 2.1-1. DNAN has a limited solubility of a few hundred mg L⁻¹ at room temperature. Nonetheless DNAN is somewhat more soluble in water than TNT. However NTO is very soluble with an aqueous solubility of tens of thousands of mg L⁻¹, greatly exceeding that of RDX by three orders of magnitude, indicating that NTO is much more polar and soluble than any of the commonly used

explosive compounds. Similar trends are also evident for the logarithm of the octanol-water coefficient (Log Kow, a measure of hydrophobicity). DNAN is moderately hydrophobic with a Log Kow value almost the same as TNT. On the other hand NTO has an estimated Log Kow value that indicates it is very polar ¹⁰, which is distinct from the clearly more hydrophobic Log Kow value for RDX.

2.2. Background on Adsorption of Insensitive Munitions Compounds by Soil Components

The IMCs DNAN and NTO^{13,14} have been shown to undergo microbially-mediated reductive transformation under anoxic conditions, as commonly occurs within bio-active soil aggregates subjected to precipitation events. As indicated elsewhere in this report, DNAN, the nitroaromatic IMC, undergoes biotransformation under anoxic conditions to form 2-methoxy-5-nitroaniline (MENA) ¹⁵. Likewise, previous work has shown that NTO undergoes reductive biotransformation to 3-amino-1,2,4, triazole-5-one (ATO)¹⁶. Therefore, an assessment of adsorptive partitioning of DNAN and NTO on surfaces should also include their (bio)transformation products MENA and ATO in order to predict more comprehensively the environmental fate of these IMCs.

Organic matter is commonly assumed to dominate the sorptive retention of hydrophobic organic contaminants in soils, but the affinity of organic compounds for mineral surfaces can also be very high, particularly for compounds comprising polar functional groups, such that significant underestimates of contaminant retention may result from consideration of organic matter alone ¹⁷. The siloxane surfaces of layer silicate clays, such as smectite, have been shown to be effective sorbents for nitroaromatic compounds (NACs) ¹⁷⁻¹⁹. The type of exchangeable interlayer cation (e.g., K⁺ versus Na⁺) has also been shown to affect the uptake of nitroaromatics by layer silicate clays: cations of lower hydration energy (e.g., K⁺ relative to Na⁺) may increase adsorptive affinity ^{17,18,20}, highlighting the potential for significant effects on organic sorptive retention of relatively small changes in mineral surface chemistry. In prior work, silicate clays have been shown to exhibit pH-dependent affinity for nitrogen heterocyclic compounds (NHCs) such as acridine ²¹ or quinoline ²², although with significant modulating effects of exchangeable cation or adsorbed natural organic matter.

Metal (oxyhydr)oxides are ubiquitous soil constituents that can also affect contaminant retention at their variably-charged hydroxylated surfaces. Iron (oxyhydr)oxides such as goethite and lepidocrocite present polar, pH-dependent charged surfaces that can affect electrostatic or covalent bonding of aromatic compounds comprising charged or polar functionalities ^{23,24}. Whereas manganese (III, IV) oxides also represent a significant fraction of reactive interface in soils, they are among the strongest oxidants outside of molecular oxygen present in soils ²⁵. For example, the Mn(IV) oxide birnessite was observed to oxidize aromatic amines such as toxic *p*-methoxyaniline and α -naphthylamine²⁶ and converted catechol (dihydroxybenzene) to polymerized products and CO₂ ²⁷. The oxidation and subsequent polymerization of aromatic amines into larger and/or smaller molecular weight compounds is a potential mechanism for reducing their mobility in soils.

Despite the fact that layer silicate clays and metal oxides dominate the reactive interfacial area of soil systems ²⁸, the adsorption-desorption behavior of new IMCs at such surfaces remained poorly known prior to this project. This left a significant gap in our ability to develop mechanistic models of the transport and fate of these contaminants in aqueous mineral soil systems, which are the principal recipients unexploded IMC residues. An improved understanding of IMC

environmental fate requires a knowledge of how these contaminants react at representative mineral surfaces, including the charged siloxane surfaces of layer silicate clays and the hydroxylated surfaces of metal (oxy)hydroxides. Therefore, the objectives of the adsorption experiments conducted as part of the study (discussed in Sections 3.4 and 4.1 of this report) were to (1) determine the adsorption affinity of the IMCs DNAN and NTO, as well as their microbial reduction products MENA and ATO, in abiotic aqueous suspensions of smectite, goethite and birnessite and (2) assess whether any abiotic transformation reactions may ensue as a result of sorbent-sorbate interaction.

2.3. Background on Biodegradation and Biotransformation of IMC

Nitroaromatic compounds (NAC) with two or more nitrogroups are not prone to becoming extensively biodegraded by a large diversity of microorganisms. The electron withdrawing character of the nitro-group impedes oxidative mechanisms of attacking polynitroaromatic compounds^{29,30}. This accounts for the persistence of explosive compounds in aerobic subsurface environments for decades^{31,32}. A few remarkable strains of aerobic bacteria have developed mechanisms of extensively biodegrading NAC with two nitro-groups such as via the formation of a Meisenheimer hydride complex resulting from the reduction of the aromatic ring³³. In contrast, TNT with three nitro groups is not extensively biodegraded to mineralized products, instead TNT is susceptible to reductive biotransformation whereby the nitro-groups are reduced to hydroxylamine and amine groups^{29,34}.

Nitro-group reduction proceeds via three two-electron transfers generating nitroso- and hydroxylamine intermediates before fully reducing the nitro-group to an amine (Figure 2.3-1)³⁵.

The nitro-groups of NAC are susceptible to abiotic reduction such as by iron (Fe^{2+}) adsorbed onto iron oxides³⁶⁻³⁸ or via redox mediators, transferring electrons from hydrogen sulfide (H_2S)³⁸⁻⁴⁰. In the subsurface, Fe^{2+} and H_2S are biogenic compounds produced by iron-reducing and sulfate reducing bacteria. Riboflavin produced by a bacterium⁴¹ abiotically reduced a RDX. Likewise

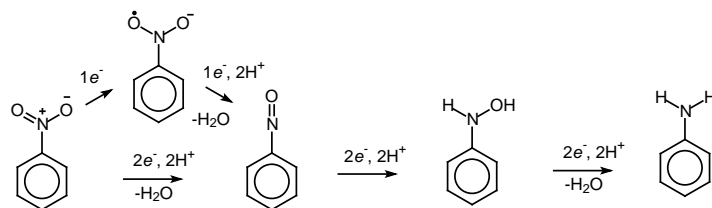


Figure 2.3-1. Pathway of reductive (bio)-transformation of nitro aromatic compounds to aromatic amines

NAC are reduced by a wide diversity of microorganisms such as methanogens, sulfate reducing bacteria, *Clostridium* spp and intestinal bacteria^{34,42-44}. The best described enzymes are broad-spectrum nitroreductases (containing flavin groups) in microorganisms³⁵. Aside from nitroreductases, there are potentially other enzymes in anaerobic microorganisms that reduce nitroaromatic compounds. For example, an Fe-only hydrogenase from *Clostridium acetobutylicum* reduced TNT to hydroxylamine intermediates⁴⁵.

Nitro-group reduction is thus carried out by a combination of abiotic and/or biotic factors, necessitating the term, “(bio)transformation” to describe the reductive transformation of explosives. Both chemical and enzymatic reactions are responsible for reducing nitro-groups and bulk chemical reducing agents (Fe^{2+} and H_2S) and some redox mediators (e.g. riboflavin) are themselves biogenic compounds produced by microbial activity.

2.3.1. Biodegradation and biotransformation of DNAN

There have previously only been a few studies examining the biodegradation and biotransformation of DNAN. Most studies have examined reductive cometabolism of DNAN resulting in the reduction of one or two of the nitro-groups. In anaerobic bioreactors, DNAN was reduced to 2,4-diaminoanisole (DAAN) ⁴⁶. Under anaerobic conditions, several pure strains of bacteria reduced DNAN to 2-methoxy-5-nitroaniline (MENA) and DAAN ⁴⁷. Under aerobic conditions DNAN was reduced to MENA in a soil slurry supplemented with carbon and nitrogen. A *Bacillus* strain isolated from the soil converted DNAN to MENA and 2-hydroxylamino-4-nitroanisole, 2-N-acetyl-4-nitroanisole and 2-N-acetyl-4-nitrophenol ⁴⁸. The O-demethylation of the methoxy group was confirmed by formation of formaldehyde. Cell free extracts of the *Bacillus* culture yielded formation of 2-nitroso-4-nitroanisole. Collectively the cometabolism of DNAN indicates the pathways illustrated in Figure 2.3-2.

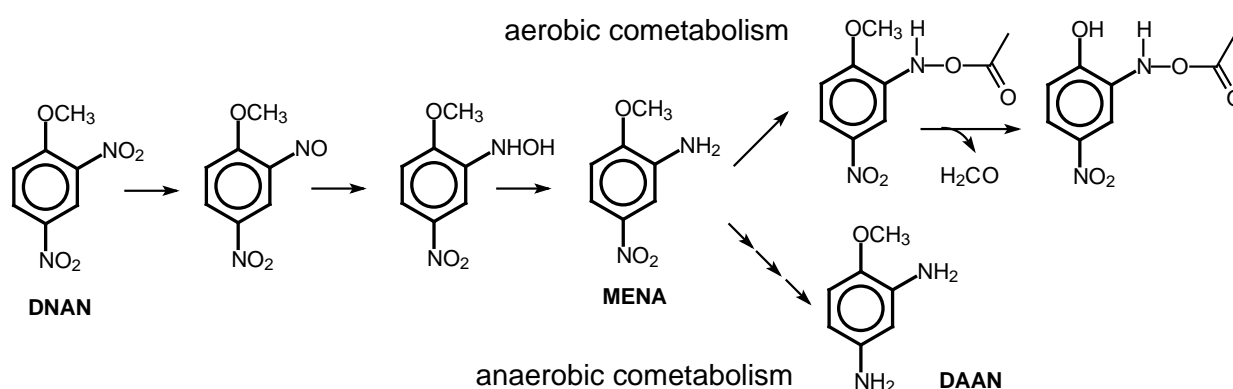


Figure 2.3-2. Pathways of aerobic and anaerobic cometabolism reported in the literature.

Under aerobic conditions, a highly specialized bacterial strain, *Nocardioides* sp strain JS1661, was recently shown to catalyze the O-demethylation of DNAN to 2,4-dinitrophenol (DNP) and subsequently extensively degrade DNP via a Meisenheimer hydride complex as evidenced by the stoichiometric release of nitrite ^{49,50}. A proposed pathway is provided in Figure 2.3-3.

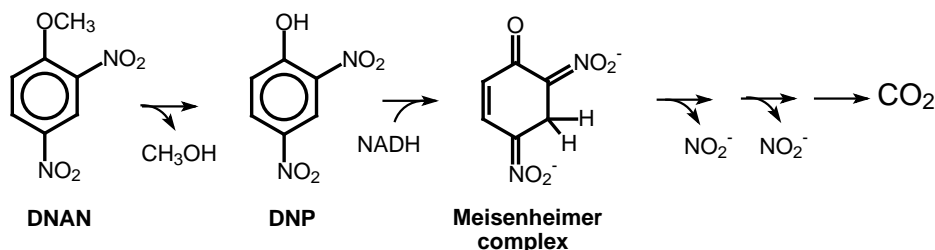


Figure 2.3-3. Aerobic DNAN biodegradation pathway of *Nocardioides* sp strain JS1661

2.3.2. Biodegradation and biotransformation of NTO

The first studies of NTO biodegradation were conducted by Le Campion et al.^{16,51}. The bacterium, *Bacillus licheniformis*, utilized in their studies was found to cometabolize NTO in the presence of 15 g L⁻¹ sucrose at pH 6 by reducing the nitro-group to an amino group yielding 3-amino-1,2,4-triazol-5-one (ATO) as an intermediate. Subsequently after raising the pH to 8, *B. licheniformis* biodegraded ATO to CO₂ and urea¹⁶ as shown in Figure 2.3-4. The microsomal fraction of rat liver also reduced NTO to ATO when incubated anaerobically with NADH. However when microsomal fraction of the rat liver is exposed to air, NTO is converted to urazole and nitrite is released in the process⁵¹ as illustrated in Figure 2.3-4. Circumstantial evidence of NTO biotransformation has also been witnessed by observing greater decrease of NTO concentration in soil as compared to heat sterilized soil^{52,53}.

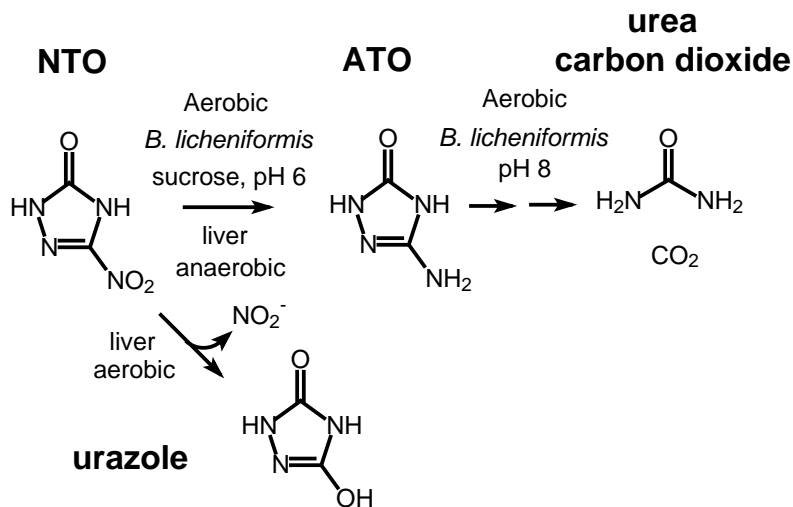


Figure 2.3-4. Pathways of NTO biotransformation and biodegradation

2.3.3. Irreversible covalent incorporation of aromatic amines into humus

The cometabolic and anaerobic (bio)transformation of DNAN results in the formation of aromatic amines. The aromatic amines are reactive in soils and sediments. There is strong evidence that they become covalently linked with the soil humus⁵⁴⁻⁵⁷. As such, the aromatic amines become irreversibly incorporated into soil humus with an expected low bioavailability that coincides with a demonstrated lowered ecotoxicity^{58,59}. Two major mechanisms can account for extensive incorporation into humus. The first mechanism involves substitution reactions that cause covalent bonding of amines with ketones and quinones⁶⁰⁻⁶³ as shown in Figure 2.3-5, illustrating the formation anilino-hydroquinone by reaction of an aromatic amine with a 1,4-benzoquinone. The second mechanism involves the one-electron oxidation of aromatic amines resulting in the formation of cation radicals. The formation of the cation radical causes coupling between aromatic amines or between aromatic amines and soil humus. Extracellular oxidative enzymes such as laccases and peroxidases⁶⁴⁻⁶⁷ can catalyze the oxidative coupling under aerobic conditions; however oxidized manganese-containing minerals (e.g MnO₂) also catalyze the one electron

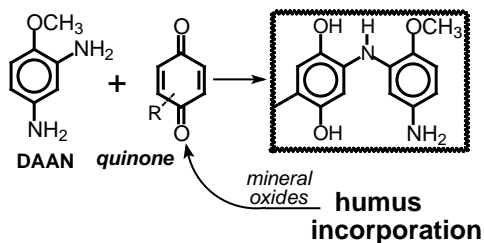


Figure 2.3-5. Postulated nucleophilic substitution of the aromatic amine, 2,4-diaminoanisole (DAAN), with a quinone moiety in humus. Mineral oxides of Fe and Mn are expected to regenerate quinone from hydroquinone. R = rest of molecule.

oxidation of aromatic amines and subsequent coupling in anaerobic environments^{25,26,68} as shown in Figure 2.3-6.

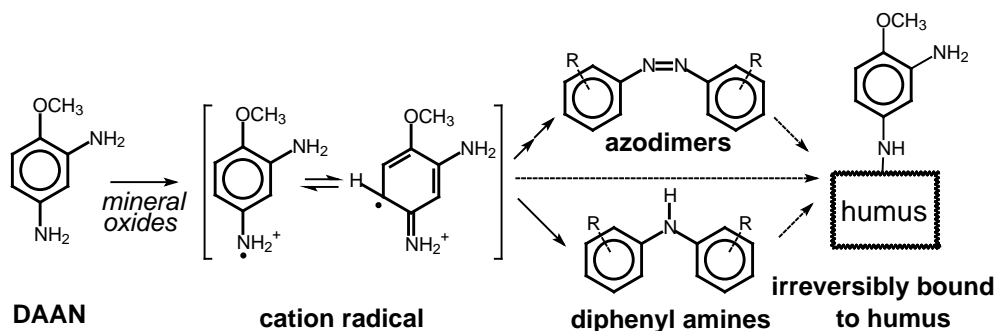


Figure 2.3-6. Postulated one-electron oxidation of the aromatic amine, DAAN, to form a cation radical. The cation radicals either react with each other to form azo-dimers, diphenyl amines and oligomers or they couple with humus to become irreversibly covalently bound. Mineral oxides = manganese oxide. R = rest of molecule.

2.4. Ecotoxicity of DNAN and NTO

In the last five years, considerable development has occurred in toxicity evaluation of DNAN to aquatic, terrestrial, and other relevant ecological toxicity organism models^{69,70}. The fifty-percent lethal concentrations (LC_{50}) of DNAN for different species have been determined: freshwater crustaceans (*Daphnia carinata* 48-h LC_{50} = 14.9 mg L^{-1} ⁷¹; *Ceriodaphnia dubia* 48-h LC_{50} = 42 mg L^{-1} ; *Daphnia pulex* 3-d LC_{50} = 18-20.3 mg L^{-1})⁷⁰, Northern leopard frog (*Rana pipiens* 96-h LC_{50} = 24.3 mg L^{-1})⁷², earthworm (*Einsinia andrei* 7 d- LC_{50} = 98 mg kg^{-1})⁶⁹, fathead minnow (*Pimephales promelas* 48-h LC_{50} 37 mg L^{-1})⁷⁰, and adult zebrafish (*Danio rerio*, 48 h- LC_{50} = 35 mg L^{-1})^{73,74}. In addition to mortality, there are also considerable toxic effects at sublethal concentrations. A median effective concentration (EC_{50}) that was less than half the lethal values (48h- EC_{50} = 31 mg kg^{-1} soil) was determined in toxicant avoidance tests with *E. andrei*⁶⁹. The phytotoxicity of DNAN has been evaluated in ryegrass growth assays monitoring shoot elongation (*Lolium perenne*, 19 d- EC_{50} = 7 mg kg^{-1})⁶⁹. While the primary endpoint in ecotoxicity studies has been lethality, DNAN sublethal effects should also be evaluated in *in vivo* models since many NACs are mutagenic to different types of organisms, including bacteria, algae, plants, invertebrates, and mammals⁷⁵⁻⁷⁷. Recently, exposure to sub-acute toxicity concentrations of DNAN was also found to induce significant DNA damage in a freshwater crustacean *D. carinata*⁷¹.

In some assays DNAN has been shown to be significantly less toxic than TNT, for example the lethal concentration calculated for DNAN in bioassays with larval fathead minnows (*P. promelas*) was one order of magnitude higher (96-h LC_{50} = 37 mg L^{-1})⁷⁰ compared to the corresponding value reported for TNT (3.1 mg L^{-1})⁷⁸. Likewise, DNAN was seven-fold less toxic to *D. carinata* (48-h LC_{50} = 14.9 mg L^{-1}) than TNT (2.3 mg L^{-1})⁷¹.

Information about the ecotoxicity of NTO is still limited. Concern about the potential environmental impact of NTO is compounded by the high mobility of this chemical.

Measurements of the dissolution of different IMC formulations showed that those containing NTO are likely to reach the groundwater in the absence of biotransformation ⁷⁹.

A few recent studies have reported on the aquatic toxicity of NTO. This compound was shown to exert very low toxicity in growth inhibition assays with the freshwater organism *C. dubia* (48-h LC₅₀ = 460 mg L⁻¹) and the unicellular green algae *Selenastrum capricornutum* (lowest observable effect concentration or LOEC = 2680 mg L⁻¹) ⁸⁰. NTO, however, was found to be more toxic to tadpoles. In toxicity assays performed with leopard frog tadpoles, the lowest observed effect concentration for survival (28-d LOEC) for NTO was 5 mg L⁻¹, while the LOEC value for TNT was 0.003 mg L⁻¹ ⁷². Although these results suggest that NTO is less toxic than traditional explosives, only a limited number of organisms have been tested to date. With regard to the mutagenic potential of NTO to aquatic species, Reddy and coworkers ⁸¹ reported that this IMC was not mutagenic in the Ames test or in *Escherichia coli* ⁸¹. No work has been done prior to this SERDP project on the toxicity of IMC biotransformation projects.

3. MATERIAL AND METHODS

3.1. Materials

3.1.1. Chemicals

3-nitro-1,2,4-triazol-5-one (CAS# 932-64-9, NTO, purity > 95%) was purchased from Interchem (San Pedro, CA, USA) and ATO (CAS# 1003-35-6, purity > 95%) from Princeton BioMolecular Research (Monmouth Junction, NJ, USA) or synthesized.^{82,83} 3-hydroxyamino-1,2,4-triazol-5-one (CAS# 134706-78-8, HTO) was also synthesized based on a method adapted from Le Campion and Ouazzani.⁸⁴ The structures of ATO and HTO were verified with high resolution quadrupole-time-of-flight mass spectrometry (QToF-MS, see below).⁸² Uniformly ring labelled ¹⁴C-DNAN (77 mCi mmol⁻¹) was obtained from American Radiolabeled Chemicals, Inc. (St. Louis, MO, USA). 2,4-dinitroanisole (DNAN; CAS # 119-27-7, 98% purity) was purchased from Alfa Aesar (Ward Hill, MA) and 2-methoxy-5-nitroaniline (MENA; CAS # 99-59-2, 98% purity) and DAAN (CAS# 615-05-4, analytical standard) were purchased from Sigma-Aldrich (St. Louis, MO).^{85,86} To study the toxicity of DNAN (bio)transformation products, monomer products and azo-dimer and trimer surrogates were acquired for bioassay with acetoclastic methanogens and the marine bioluminescent bacterium, *Allivibrio fischeri*.⁸⁷ 3-nitro-4-methoxyaniline (CAS# 577-72-0, denoted “iMENA”, purity 97%) was obtained from Accela ChemBio Inc. (San Diego, CA, USA). *N*-(5-amino-2-methoxyphenyl) acetamide (CAS# 64353-88-4, denoted “Ac-DAAN”, purity 95%) was purchased from ChemBridge Corporation (San Diego, CA, USA). 2,2'-dimethoxy-4,4'-azodianiline (CAS# 6364-31-4, denoted “dimer L”, purity >90%) was acquired from MolMall Sarl (Lonay, Switzerland). Bismarck Brown Y (*m*-Bis(2,4-diaminophenylazo)-benzene, CAS# 8005-77-4, denoted “BBY”, dye purity 46%) was obtained from Chem-Impex International (Wood Dale, IL, USA). *N*-methyl-*p*-nitroaniline (CAS # 100-15-2, MNA, 97% purity) was obtained from Alfa-Aesar (Ward Hill, MA, USA) and *N*-methyl-*p*-phenylenediamine (CAS# 5395-70-0, MPD, 98% purity) was acquired from AK Scientific (Union City, CA, USA).⁸⁸ All other chemicals used were analytical reagent or HPLC grade.

3.1.2. Soils and inoculum

All soils were collected within 20 cm from the surface. Roger Road soil was collected from the University of Arizona Campus Agricultural Center in Tucson, AZ. Catlin agricultural soil was from Illinois.⁸⁹ Maricopa soil was collected from the University of Arizona Maricopa County Agricultural Station in Maricopa County, AZ. Camp Navajo (AZ), Camp Butner (NC), Camp Ripley (MN), and Florence (AZ) soils were collected by CH2M HILL at U.S. National Guard bases. All soils, with the exception of Catlin and Roger Road soils, were immediately placed on ice and shipped overnight to the laboratory. Roger Road (AZ) soil was immediately transferred to the laboratory. All soils with the exception of Catlin were sealed to maintain original moisture, while Catlin soil was air-dried. All soils were sieved (2 mm) and stored at 4 °C until used in experiments. Soil used to understand sequential anaerobic-aerobic biodegradation of NTO⁹⁰ was collected from the garden of Gortner Laboratory on the University of Minnesota campus (St. Paul, MN, USA). Granular sludge⁸⁵ was obtained from a full-scale upflow anaerobic sludge blanket reactor located at an industrial brewery wastewater bioreactor (Mahou, Guadalajara, Spain).

3.1.3. Humin purification

Humin was purified from IHSS (International Humic Substances Society)⁹¹ Pahokee Peat soil in order to investigate if additional endogenous organic carbon from soil and artificially added humin would increase significantly the amount of ¹⁴C-labeled DNAN incorporation. Five grams of Pahokee Peat Soil were added to 50 mL of 0.5 M NaOH, and placed in a rotating tumbler for four hours. Then, samples were centrifuged (10 min, 4,000 rpm) and the liquid was decanted. This alkaline hydrolysis cycle was repeated ten times. Remaining solids were washed with a 18 mM phosphate buffer (pH=7.2) until circumneutral pH was achieved. Purified humin was dried overnight in an oven (60 °C) and ground in a mortar before use.

3.2. Analytical Methods

3.2.1. HPLC-DAD

DNAN, MENA, and DAAN were quantified on an ultra-high performance liquid chromatograph coupled to a diode array detector (UHPLC-DAD) with an Acclaim RSLC Explosives E2 column (2.1×100 mm, 2.2 μm) (Thermo Fisher Scientific, Waltham, WA, USA) and a methanol/H₂O eluent (isocratic 40/60, v/v, 0.25 mL min⁻¹) at room temperature.^{83,87} Detection wavelengths and retention times were (nm:min) 300:9, 254:5, and 210:2.3 for DNAN, MENA, and DAAN, respectively. NTO, HTO, and ATO were also analyzed by UHPLC-DAD (using an Agilent 1200 series instrument; Santa Clara, CA).^{82,83,90} Samples were diluted (1:3) into 0.1% trifluoroacetic acid (TFA) buffer prior to analysis. Injections (5 μL) were separated with a Hypercarb column (150 mm × 4.6 mm, 5 μm pore size) at a temperature of 30 °C based on Le Campion et al.⁹² The mobile phase (1 mL min⁻¹) was operated under the following v/v ratios of 0.1% TFA aqueous buffer and acetonitrile: 0–3 min 100/0; 11 min 85/15; 15 min 50/50; 17 min 50/50; 19 min 100/0; 20 min 100/0. NTO was detected at 15 min/340 nm, HTO at 13 min/360 nm, and ATO at 8.9 min/216.5 nm.

3.2.2. UHPLC-Q-ToF-MS

MENA, DAAN, and oligomer products in the liquid phase were semi-quantified without internal standards on an UltiMate 3000 UHPLC (Dionex, Sunnyvale, CA) using the same chromatography parameters and column described above for UHPLC-DAD, that was coupled to a TripleTOF 5600 quadrupole time-of-flight mass spectrometer (Q-ToF-MS) (AB Sciex, Framingham, MA, USA).^{85,87} Oligomeric products of MNA were also characterized by Q-ToF-MS as described herein.⁸⁸ The Q-ToF-MS was run with an electrospray ionization source in positive mode at 450 °C with a capillary setting of 5.5 kV, and a declustering potential of 80 V. N₂ was used as curtain gas, desolvation gas, and nebulizer gas at 30, 35, and 35 psi, respectively. Transformation products were detected and quantified by integrating accurate, selected parent ion (M+H⁺) mass chromatogram peaks from a survey scan (*m/z* 30–1000) based on newly detected, and previously characterized, transformation products. Semi-quantitative comparisons of transformation product abundances were determined based on integrated peak areas of parent mass ions extracted from mass chromatograms using a 10 mDa window centered on the calculated masses. AnalystTF 1.6 with PeakView 1.2.0.3 and MultiQuant version 2.1 were used to develop ion lists and to quantify individual ion masses from integrated mass chromatogram peaks.

QToF-MS analysis was used to confirm the exact mass of ATO and HTO⁸² as well as inspect any ATO-birnesite products.⁸³ ATO ([M + H]⁺ = 101.0447 detected, 1.1 ppm from expected) was verified via direct infusion of a 1 mg L⁻¹ solution in positive mode. HTO ([M + H]⁺ = 117.0390

observed, 1.7 ppm from expected) was verified as well. QToF-MS analyses were also used to screen for metabolites in selected microcosms. Microcosm contents were centrifuged and diluted (1:10–1:20 final dilution in water v/v) before infused directly into the QToF-MS. Spectra were obtained in both positive and negative mode, and a mass range of 35–600 m/z was acquired. Analyst TF 1.5.1 (and later Analyst TF 1.6) and Formula Finder 2.02.0 were used to process data.

3.2.3. Ion chromatography

Ammonium (NH_4^+), nitrite (NO_2^-), and nitrate (NO_3^-) were measured with ion chromatography (IC) for assays investigating the aerobic degradation of ATO.⁸² The IC analyses were performed on an ICS-3000 system (Dionex, Sunnyvale, CA) with a split flow for simultaneous anion and cation analysis on an AG18 RFIC column (4 × 50 mm, Dionex) and IonPac CG16 RFIC column (3 × 50 mm, Dionex), respectively. The eluent flow rate for anion analysis was 1 mL min⁻¹ and for cation analysis 0.5 mL min⁻¹.

3.2.4. Methane analysis by GC-FID

The concentration of methane in serum flasks headspace was determined by gas chromatography using an HP5890 Series II system (Agilent Technologies, Palo Alto, CA) equipped with a flame ionization detector (GC-FID)⁸⁸ and a DB-FFAP capillary column (J&W Scientific, Palo Alto, CA) with helium at a flow rate of 9.3 mL/min and a split flow of 32.4 mL/min. according to Ochoa et al.⁹³ Headspace samples (100 mL) were collected using a pressure-lock gas syringe.

3.2.5. Nitrogen and carbon dioxide analysis by GC-TCD

An Agilent Technologies 7890A Gas Chromatography (Santa Clara, CA) was used to measure the concentration of gas phase N₂. The GC was equipped with a Supelco Mol Sieve 5A PLOT column (30 m x 0.32 mm). The inlet was heated to 150 °C (splitless mode). Helium was used as carrier gas at a flow rate of 7 mL min⁻¹. The oven temperature was kept at 32 °C, and the TCD detector was heated to 230 °C. To measure the carbon dioxide from closed bottle systems the same GC system was utilized an Agilent Technologies J&W 113-4332 GS-GASPRO column was used (30 m x 0.32 mm). A helium gas flow was heated to 200 °C and kept at a pressure of 14.68 psi. The total flow rate was 25.9 mL min⁻¹. A total carbon detector was used to measure the signal at 50 Hz.

3.2.6. Ultraviolet-visible (UV-Vis) analyses coupled to zebrafish toxicity

In an effort to consider transformation products of MENA (2-methoxy-5-nitroaniline) that might be difficult to separate chromatographically or ionize by electrospray ionization, and couple them to zebrafish toxicity,⁹⁴ UV-vis spectra were recorded along the incubation course and summarized as an oligomer index, based on the ratio of absorbance at 400 nm to 254 nm, the former wavelength being chosen to quantify polymers⁹⁵ that have visible absorbance (e.g., azo dyes) and the latter being a common wavelength for aromaticity. Ultraviolet-visible (UV-vis) spectra of the supernatant from MENA samples incubated for 1 d, 6 d, 9 d, 20 d, and 30 d were recorded (200–600 nm) in quartz cuvettes with a UV-1800 Shimadzu spectrophotometer. Samples were diluted with a 50mM phosphate buffer (pH 7).

3.2.7. Solid phase characterization of the soils

Soils were characterized for various soil properties including pH, total organic carbon (TOC), particle size distribution, and Brunauer–Emmett–Teller (BET) specific surface area. The

mineralogy was also characterized. The pH was measured on a 1:5 (w/w) mixture of soil and water using a VWR Symphony pH Electrode (VWR International, Randor, PA). External specific surface area was determined using the BET dinitrogen gas adsorption method (Beckman Coulter SA-3100). TOC was calculated from the difference between total carbon, and total inorganic carbon. Total carbon was determined by combustion at 900 °C, and total inorganic carbon was determined by phosphoric acid addition followed by combustion at 200 °C using a Shimadzu 5000A-SSM TOC Analyzer (Columbia, MD). In some cases soil organic carbon was determined by loss on ignition.⁹⁶ For particle size analysis, samples were pretreated for organic matter removal and analyzed with a fully automated Beckman Coulter LS 13 320 Laser Diffraction Particle Size Analyzer (Fullerton, CA). Mineralogical analysis was conducted on both the bulk soil (powder) and oriented clays using a PANalytical X'Pert Pro MPD X-ray Diffractometer (XRD) with Cu-K α radiation source for qualitative and quantitative identification of the soil minerals. Samples were pretreated for the organic matter removal by oxidation with sodium hypochlorite. For oriented clay slides, the soil was dispersed using sodium hexametaphosphate and allowed to settle overnight. The clay suspension was used for preparing the oriented aggregate for clay mineral identification. Minerals were identified based on the expansion and contraction of d-spacing of clay minerals with various treatments. The treatments include saturation with MgCl₂, ethylene glycol, KCl at 25 °C, and subsequent heating at 300 and 550 °C. Quantitative phase analysis was performed using the Rietveld module in X'Pert High Score Plus software following the methodology described previously.⁹⁷

3.2.8. ¹⁴C - fractionation

A protocol for ¹⁴C recovery from the gas, liquid, and solid phases of the biotransformation soil assays (Figure 3.2-1) was adapted from Dryzga et al.⁹⁸ The headspace of the flask was trapped by purging with nitrogen gas through a series of two 20 mL traps: the first consisted of Opti-Fluor scintillation cocktail (Perkin Elmer, Waltham, MA, USA) to trap volatile organic compounds (VOCs), and the second was alkaline solution (0.1 M NaOH) to trap CO₂. For Liquid Scintillation Counting (LSC) the entire contents of the VOC trap were transferred, while only 2 mL of the CO₂ trap were added to 18 mL of Opti-Fluor for the (LSC). For liquid and solid phase analyses, the anaerobic tubes were opened and the contents transferred to 15 mL centrifuge tubes. The samples were centrifuged (10 min, 4000 rpm). Two mL of the supernatant were mixed with Opti-Fluor for LSC. The remaining of the liquid was decanted before addition of 10 mL MeOH to the pellet, followed by sonication (15 min) and centrifugation. One mL of supernatant was sampled for LSC and mixed with 18 mL of Opti-Fluor for LSC. The procedure was repeated with ethyl-acetate and 0.5 M NaOH (with 2 mL of extract mixed with 18 mL of Opti-Fluor). After these sequential liquid extractions, remaining solids were left to dry at 60 °C overnight. The dry solids (~50 mg) were weighed and combusted in a 400x Harvey Oxidizer (R.J. Harvey Instrument Corp., Tappan, NY, USA). The oven and the catalyst zones were set to 900 and 700 °C, respectively. N₂ and O₂ flows were 340 and 330 cc min⁻¹, respectively. 20 mL of 0.1M NaOH was used to trap CO₂. Two mL of the traps were added to 18 mL of Opti-Fluor for LSC. Soil hydrolyzable products with 0.5 M NaOH were operationally defined as fulvic and humic acid fraction in soils, whereas the remaining organic carbon combusted in the Harvey Oxidizer was operationally defined as humin. The Harvey Oxidizer efficiency was 60%, based on unlabeled mannitol combustion using a BaCl₂ phenolphthalein titration method to quantify CO₂ trapped in the 0.1 M NaOH solution.⁹⁹

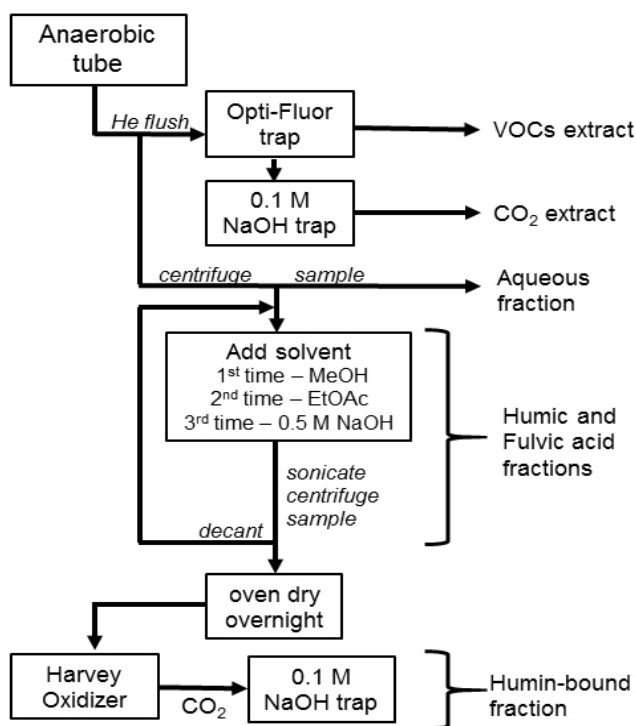


Figure 3.2-1. Schematic of ^{14}C label recovery from different fractions after DNAN (bio)transformation: gaseous and volatile species (VOCs, CO_2), aqueous (fulvic acids and water-soluble products), loosely bound (sequential liquid extractions with methanol (MeOH) and ethyl acetate (EtOAc), 0.5 M NaOH extraction (humic acids), and combustion in Harvey Oxidizer (unextractable and humin-bound residues).

^{14}C in samples containing Opti-Fluor scintillation cocktail were measured using a Tricarb 1500 Liquid Scintillation Counter (LSC) (Packard, Downers Grove, IL, USA). Measurements were performed in triplicate for 1 min counting intervals. LSC efficiency was above 85%. Unless otherwise noted, corrections for cpm signal quenching due to coloration was performed in all aqueous phases and 0.5 M NaOH samples by adding a known amount of ^{14}C -DNAN after sampling to each individual sample and measuring the amount of radiolabel recorded by the LSC.

3.3 Bioassays

3.3.1. Inocula and basal medium

3.3.1.1. Sludges and soil.

Anaerobic methanogenic sludge (AGS), aerobic return activated sludge (RAS), and nitrifying sludge were used as inoculum. AGS was obtained from a full-scale upward-flow anaerobic sludge blanket reactor treating wastewater at a brewery (Mahou, Guadalajara, Spain). The sludge was washed and sieved to remove fine particles before use in the bioassays. RAS and the nitrifying inoculum were collected from local municipal wastewater treatment plants; Ina Road and Randolph Park Wastewater Reclamation Facilities (Tucson, AZ, USA), respectively. All sludge samples were stored at 4°C . The volatile suspended solid (VSS) content in the methanogenic, RAS, and nitrifying sludge was 7.92, 0.25, and 0.53% (wet wt), respectively. The aerobic inocula were centrifuged (20 min at 4,000 rpm) and the supernatant was discarded before use in bioassays.

Seven different agricultural or military surface soils, characterized previously by Krzmarzick et al¹⁰⁰ were used as inocula. Prior to use, soils were sieved using a 2 mm mesh, and stored in sealed plastic bags at 4°C .

3.3.1.2. Basal medium.

All experiments were performed with the basal mineral medium labeled “medium 1”, unless otherwise indicated. “Medium 1” was prepared with ultrapure water (NANOpure Infinity™, Barnstead International, Dubuque, IA, USA) and was composed of (in mg L⁻¹): K₂HPO₄ (250), CaCl₂•2H₂O (10), MgSO₄•7H₂O (100), MgCl₂•6H₂O (100), NH₄Cl (280), and yeast extract (YE, varying concentrations depending on assay). Resazurin (200 mg L⁻¹) was used as a redox indicator 1 in some experiments. A bicarbonate (48 mM) based buffer was used (with 20% CO₂ in headspace) for anaerobic assays, while a phosphate buffer (20 mM) was used for aerobic assays. Nitrification toxicity bioassays utilized “medium 2” which contained (in mg L⁻¹): NaH₂PO₄ (1,500), Na₂HPO₄ (894), NH₄Cl (164), NaHCO₃ (899). All media were supplemented with trace element solution 2, 0.2-1.0 mL L⁻¹ depending on the assay. The final pH of the basal medium was adjusted to 7.0-7.2 with HCl, unless otherwise indicated.

3.3.2. Biotransformation assays

3.3.2.1. Conventional biotransformation assays with sludge/soil as inoculum.

The biotransformation of DNAN, NTO and selected DNAN/NTO biotransformation products was investigated in aerobic, microaerophilic and/or anaerobic biotransformation assays. The liquid volume in all bioassays was 50 or 100 mL, depending on the assay. Aerobic biotransformation assays were conducted in glass Erlenmeyer flasks (200 mL) capped with cotton gauze and placed on an orbital shaker at 180 rpm. Microaerophilic biotransformation assays were performed in glass serum flasks (160 mL) capped with cotton gauze and placed on an orbital shaker at 115 rpm. Due to the lower shaking intensity and the higher depth of the liquid medium, the shaking was notably less aggressive compared to the fully aerobic treatment. Water was added to compensate evaporation during the incubation as assessed weekly by weight measurements. Anaerobic biotransformation assays were conducted in glass serum flasks (160 mL) sealed with butyl rubber stoppers and aluminum crimp caps. The culture medium and the headspace were flushed with N₂/CO₂ (80:20, v/v) for 5 min to create anaerobic conditions.

All bioassays included inoculated treatments spiked with the target compound with or without cosubstrate; H₂ or acetate depending on the experiment. Abiotic and heat-killed sludge control experiments were included to account for the potential removal of the target compound by abiotic mechanisms. Inoculated aerobic and microaerophilic bioassays were supplied with RAS (0.5 g VSS L⁻¹) or soil (50 g wet weight L⁻¹ in assays with DNAN/MENA, 5-10 g wet weight L⁻¹ in assays with AT)/NTO). Prior to addition, RAS was centrifuged (20 min at 2,880 g) and the liquid medium was discarded. Anaerobic bioassays were inoculated with sieved AGS (1.5 g VSS L⁻¹) or soil (50 g wet weight L⁻¹ in assays with DNAN/MENA, 5-10 g wet weight L⁻¹ in assays with ATO/NTO). Heat-killed sludge/soil was prepared by autoclaving the sludge (121°C) for three consecutive days for 50 min the first day and 20 min the next two days. In selected assays, the soil was sterilized with 6 mL of a solution of 6% formaldehyde (v/v) for 18 h¹⁰¹. In one study, acetate (1.9 g L⁻¹) was used as a cosubstrate in both aerobic and microaerophilic biotransformation assays with DNAN⁸⁵. H₂ was used as an electron-donor in the anaerobic biotransformation assay with DNAN^{85,102}, in selected anaerobic biotransformation assays with NTO/ATO¹, and was supplied by pressurizing the flask headspace to 1.0-1.5 atm with a gas mixture (H₂/CO₂, 80:20 v/v) after flushing with N₂/CO₂. Additional anaerobic NTO biodegradation experiments were conducted with various electron donors (20 mM), with and without YE, with Camp Butner soil and included the following: acetate, lactate, ethanol, methanol, glucose, pyruvate, citrate, lactose, butyrate,

propionate, and formate^{1,101}. The impact of pH and glucose amendment on NTO and ATO degradation was also investigated as described elsewhere¹. The assays were incubated in the dark at 30°C. In the anaerobic biotransformation assays, the flasks were pre-incubated overnight to ensure that the sludge adapted to the medium conditions. The target compound was added to the flasks in the following morning. All assays were performed in duplicate.

Liquid samples were collected periodically for analysis of the target compound (e.g. DNAN) and its transformation products. Liquid samples (0.5 mL) were centrifuged immediately (10 min at 9,600-13,000 g) and diluted (1:3 to 1:4) in 250-375 mg L⁻¹ ascorbic acid (anaerobic assays) to prevent autoxidation of amine products upon air exposure^{47,103}, and stored at 4°C. Samples were analyzed by UHPLC-DAD to evaluate changes in the concentration of the parent compound and organic degradation products. UHPLC-QToF-MS analysis was used for structural elucidation and quantification of unknown organic degradation products. In selected assays, carbon dioxide (CO₂), dinitrogen gas (N₂) and inorganic nitrogen species (*i.e.*, ammonium, nitrate and nitrite) were monitored to evaluate the conversion of the target compound to mineralized products. Samples were analyzed within three days, with the exception of some of the samples evaluated with UHPLC-QToF-MS. Samples requiring storage for over 3 days were frozen. Dissolved oxygen (DO) and oxidation-reduction potential (ORP) were monitored in experiments replicating the endogenous and cosubstrate conditions for aerobic, microaerophilic, and anaerobic conditions.

3.3.2.2. Staggered soil/sludge (bio)transformation assays

Anaerobic bioassays were performed to obtain mixtures of the metabolites formed during different stages of the (bio)transformation of DNAN and MENA in soil or sludge microcosms, and evaluate their chemical nature and toxicity. Anaerobic tubes (Bellco Glass Inc., Vineland, NJ, USA) were filled with 10 mL of mineral medium (pH 7.2, 18 mM phosphate buffer⁸⁵) and 500 µM DNAN or MENA. The solution was inoculated with 100 mg of fresh Camp Navajo soil, 100 mg of wet Camp Butner soil or 75 mg of wet anaerobic sludge. Assays supplemented with MENA were amended with 10 mM pyruvate as an exogenous electron donor. The tubes were flushed with He/CO₂ (80/20 %), closed with t-butyl caps and aluminum seals, and subsequently incubated in the dark at 30°C in an orbital shaker at 115 rpm. The tubes were incubated according to a staggered timeline to ensure that all liquid samples were collected on the same day to facilitate simultaneous toxicity testing of all samples and minimize test variability.

Sampling was performed inside an anaerobic hood to minimize autoxidation from reactive products with oxygen. Samples were centrifuged (10 min, 9,600×g), sealed inside the anaerobic chamber, and kept at 4 °C before methanogenic and *A. fischeri* toxicity assays. Aliquots of the supernatant were collected for immediate analysis by UHPLC-Q-ToF-MS and for toxicity testing. The latter samples were sealed under N₂ gas and then frozen (-20°C) for 2 weeks until the zebrafish embryo toxicity assays were performed. All experiments were performed in duplicate.

3.3.3. Inhibition Bioassays

3.3.3.1. Methanogenic toxicity assay.

Assays were conducted in glass flasks (160 mL) with basal medium 1 (25 mL) supplemented with acetate (26 mM) and methanogenic sludge (1.5 g VSS L⁻¹). All flasks were sealed with butyl rubber stoppers and then flushed with N₂/CO₂ (80:20, v/v) for 5 min to create anaerobic conditions. The flasks were pre-incubated overnight to ensure that the sludge was adapted to the assay conditions. The following day the toxicants were added from concentrated stock solutions. In addition to the individual inhibitory compounds, mixtures of biotransformation products in aqueous solutions at

a single dilution of 54-fold (with a starting DNAN concentration of 500 μM) were assayed with the methanogenic sludge. Separate samples of these aqueous solutions containing mixtures of biotransformation products were harvested at different stages of DNAN (bio)transformation in order to detect temporal changes in toxicity due to shifting mixture of intermediates and products during (bio)transformation. The methane content in the headspace of each flask was measured periodically until the production of methane became constant in the toxicant-free controls. The maximum specific methanogenic activity of the control was 0.16 g $\text{CH}_4\text{-COD g VSS}^{-1} \text{ d}^{-1}$.

3.3.3.2. Aerobic heterotrophic inhibition assay

Assays were conducted in serum flasks (160 mL) with medium 1 (25 mL) supplemented with acetate (28 mM) and RAS (0.5 g VSS L^{-1}). Flasks were spiked with different concentrations of the toxicant, sealed with butyl rubber stoppers, and flushed with $\text{He/CO}_2/\text{O}_2$ (60:20:20, v/v) for 5 min. The O_2 content in the headspace of each flask was measured periodically until the O_2 consumption rate resembled that of the endogenous control lacking acetate and toxicant addition. The maximum specific O_2 consumption activity of the uninhibited control was 28 mg $\text{COD g VSS}^{-1} \text{ d}^{-1}$.

3.3.3.3. Nitrification inhibition assays

Assays were conducted in Erlenmeyer flasks (125 mL) containing basal medium 2 (50 mL) and nitrifying sludge (0.5 g VSS L^{-1}). The flasks were spiked with different concentrations of the toxicant, and then capped with cotton gauzes to facilitate gas exchange. Liquid samples were collected periodically for ammonium analysis. The nitrifying activity of the uninhibited control was 19.3 mg $\text{NH}_4^+\text{-N g VSS}^{-1} \text{ d}^{-1}$.

3.3.3.4. Microtox

The Microtox assay was used to characterize the toxicity of the (bio)transformation products and surrogates. Exposure at 30 min was monitored for individual toxicants. Microtox was also used to evaluate aqueous mixtures biotransformation compounds recovered from different stages of DNAN (bio)transformation at a single dilution of 36-fold (with a starting DNAN concentration of 500 μM). A Microtox® Model 500 analyzer (Strategic Diagnostics, Inc. SDIX, Newark, DE, USA) was used to measure changes in the bioluminescence produced by the marine bacterium *Aliivibrio fischeri* (lyophilized culture of *A. fischeri* NRRL-B-11177, AZUR Environmental, Carlsbad, CA, USA) when exposed to increasing concentrations of the toxicant. Microbial inhibition in Microtox was measured at 25°C in triplicate experiments as previously described¹⁰⁴.

All microbial toxicity experiments were conducted in duplicate, unless otherwise indicated. The bioassays using sludge were incubated at 30°C in an orbital shaker (115 rpm) in the dark. Flasks without toxicant were included in all the assays and served as uninhibited controls. The maximum specific O_2 consumption, as well as the nitrifying and methanogenic activities were calculated from the slope of O_2 consumption, ammonium concentration, and cumulative methane production; respectively. The activities were normalized with respect to the biomass concentration. The initial concentrations of toxicant causing 20, 50 and 80% reduction in activity compared to an uninhibited control were referred to as IC_{20} , IC_{50} and IC_{80} , respectively.

3.3.3.5. Zebrafish embryo assays

A previously reported protocol¹⁰⁵ was used with slight modifications. Embryos with intact chorions were manually placed in 96-well plates containing embryo medium (EM) at 6 hours post fertilization (hpf) and exposed to individual toxicants (10 μL + 90 μL EM) or supernatant solutions

of different stages of MENA (bio)transformation (50 μ L + 50 μ L EM). 32 embryos were exposed per concentration and toxicant, and all controls and treatments included 0.64% dimethylsulfoxide (DMSO) to aid toxicant dissolution). This concentration of DMSO is known to not cause effects in zebrafish embryo assays. Zebrafish embryos were exposed to 0-64 μ M concentrations of the test compounds, with the exception of MENA and DAAN which had a range 0-640 μ M. In all cases the concentrations tested were chosen to span five orders of magnitude. The plates were incubated at 28°C in the dark. At 24 and 120 hpf, development abnormality and mortality assessments were performed (endpoints shown in Table 3.3-1.)¹⁰⁵. Endpoint scoring and statistical analyses were performed in R software as described previously¹⁰⁵.

In addition, at 120 hpf a larval locomotor behavior assay was performed with alternating light/dark cycles in a Viewpoint Zebrabox (software version 3.0, Life Sciences, Lyon, France)¹⁰⁶. Briefly, at 120 hpf, plates were inserted into the Viewpoint Zebrabox where movement was recorded during the following light/dark cycle: initial light acclimation (10 min), light (10 min), dark (5 min). Long swimming distance (> 2.5 mm min⁻¹) was averaged across all surviving replicates at 120 hpf for a single concentration. Malformed and dead zebrafish were not considered in the locomotor assay. Endpoint scoring and statistical analyses were performed according to the protocols described^{105,106}.

Table 3.3-1. Zebrafish embryo toxicity endpoints assessed.

Time	Endpoints
24 hpf	mortality, developmental delay, spontaneous movement, notochord
120 hpf	mortality, notochord, yolk sac edema, body axis, eye defect, snout, jaw, otic vesicle, pericardial edema, brain somite, pectoral fin, caudal fin, pigment, circulation, truncated body, touch response

3.4. NTO/ATO Column Experiments

The degradation of ATO and NTO was studied in a continuous flow reactor using 54 g of soil as inoculum. The reactor was made of acrylic material, and its volume was 350 mL (diameter of 5 cm and column height of 17.8 cm). Approximately 50% of this volume was filled with 1 cm³ polyurethane sponge blocks (Figure 3.4-1.). The reactor was covered with aluminum foil to avoid exposure to light. Humid air was supplied by an air compressor at the bottom of the reactor at a flow rate of approximately 400 cm³ min⁻¹ during all the operation periods. The influent was supplied at the top of the reactor using a peristaltic pump. The influent (pH 7.4) contained the following chemicals (in mg L⁻¹): MgSO₄·7H₂O (20), CaCl₂·2H₂O (10), MgCl₂·6H₂O (20), yeast extract (4), KH₂PO₄ (154), K₂HPO₄ (673), and 0.2 mL L⁻¹ of a trace elements solution (previously described). Initially, the medium did not contain ATO. On day 13, the medium was supplemented with ATO (0.6 mM). On day 76, the concentration of ATO was increased to 1.0 mM, and this concentration was maintained during the next 152 days. After day 228, ATO was replaced by NTO (1.0 mM) and sodium pyruvate (1.8 mM, as an electron donor to drive NTO reduction). The reactor was maintained at 22±2°C and it was operated at an empty bed hydraulic retention time (HRT) of 42 h during most part of the experiment. The reactor contained a recirculation system, and its flow rate was adjusted to 720 mL day⁻¹. The operation of the reactor was divided in four periods (I, IIa, IIb and III), as described in Table 3.4-1.

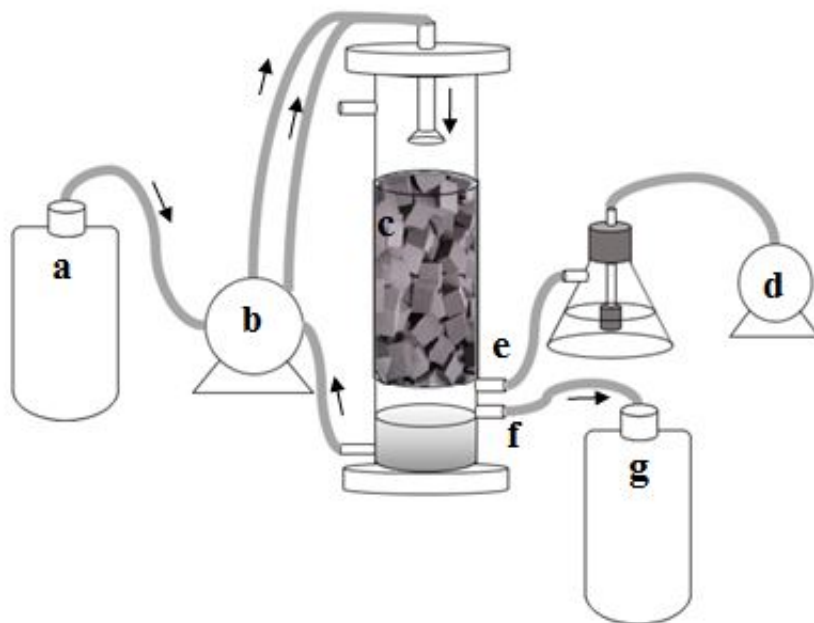


Figure 3.4-1. Scheme of 350 mL aerated bioreactor used for NTO and ATO degradation. Legend: bottle containing influent (a), peristaltic pump (b), polyurethane foam blocks (c), air compressor (d), humid air inlet (e), effluent sampling port (f), and bottle containing effluent (g). The arrow indicates the direction of the flow. Influent samples were collected from bottle (a) and effluent samples were collected from tube (f).

Table 3.4-1. Operational conditions and performance of a laboratory-scale continuous flow reactor treating water containing ATO or NTO during different periods.

Period	Compound Added	Days	Flow Rate	ATO influent	NTO influent	ATO removal	NTO removal	N-mineralization to ions (NH ₄ ⁺ , NO ₂ ⁻ , NO ₃ ⁻)
			(mL day ⁻¹)	(μM)	(μM)	(%)	(%)	(%)
I	-	13	154.4±17.2	0±0	0±0	-	-	-
IIa	ATO	63	146.3±11.7	649.1±107.1	0±0	100±0	-	36.1±21.5
IIb	ATO	152	213.4±48.2	1024.4±54.5	0±0	99.7±1.1	-	37.8±4.5
III^a	NTO	79	204.2±18.7	48.1±91.3	931±101	-	93.5±5.6 ^b	41.5±5.1

^a Addition of 1.8 mM sodium pyruvate as electron donor

^b Removal efficiency after the reactor reached steady state (day 298 to 310)

3.5. Adsorption Studies

The adsorption and desorption of DNAN, MENA, NTO and ATO on representative soil mineral sorbents including a 2:1 layer silicate (montmorillonite), an iron oxyhydroxide (goethite), and a manganese oxide (acid-birnessite) was quantified as described below.⁸³ These specimen mineral constituents were chosen due to their ubiquitous occurrence in soils worldwide, and for their representative range of surface chemical properties. The effects of saturated interlayer cation type (K^+ , Na^+) on IMC sorption was also investigated.

3.5.1. Mineral synthesis and clay preparation.

Wyoming montmorillonite (SWy-2) was acquired from the Source Clay Minerals Repository, University of Missouri, and added to ultrapure ($18\text{ m}\Omega\text{ cm}^{-1}$) water (1:25 ratio) and dispersed for size fractionation by adjustment of the suspension pH value to 8.0 through the addition of 0.01 M NaOH. The $< 2\mu\text{m}$ size fraction was collected by extraction of the supernatant suspension following centrifugation for five minutes at 1000 rpm. The suspension was then flocculated by addition of 0.001 M HCl in 1.0 M NaCl for 20 min, followed by centrifugation for 10 min at 7500 rpm, and repeated until the pH values of the supernatant and wash solution were equivalent (pH 3). Clays were then dispersed in 0.01 M NaCl for 20 min, followed by centrifugation for 10 min at 7500 rpm, and the process repeated until the pH value of the supernatant reached pH 5.5. The clays, suspended in 0.01 M NaCl, were then stored at 2.8°C . The same protocol was followed for K^+ saturation of the montmorillonite.⁸³ Goethite was synthesized from 2.5 M KOH and 0.15 M $\text{Fe}(\text{NO}_3)_3 \cdot 9\text{H}_2\text{O}$ $18\text{ m}\Omega\text{ cm}^{-1}$ water (4:33 ratio) at 60°C for 24 h. Solids were decanted and washed with 0.1 mM HCl solution until the supernatant reached pH 5 and residual nitrate was removed.¹⁰⁷ Birnessite was synthesized by addition of 12 M HCl to boiling 0.4 M potassium permanganate solution (33:500 ratio). The precipitate was mixed with 1 mM HCl for 30 min, centrifuged at 18,000 rpm for 10 min, and repeated until the supernatant reached pH 4, before freeze-drying.¹⁰⁸ Successful birnessite and goethite mineral synthesis was confirmed by synchrotron radiation X-ray diffraction (SR-XRD) analysis at the Stanford Synchrotron Radiation Lightsource (SSRL) and by comparison to previously measured specimen minerals prepared the same methods.¹⁰⁹

3.5.2. Batch sorption-desorption method

IMCs were dissolved in 0.01 M NaCl or 0.01 M KCl solutions at maximum solution phase concentrations of 1.0 mmol kg^{-1} (below aqueous solubility). IMC solution pH was adjusted to 7 by addition of 0.01 M NaOH or 0.01 M HCl. Approximately 0.4 mL of clay suspension were added to perfluoroalkoxy microcentrifuge tubes (reaction vessels; Savillex Corporation, Eden Prairie, MN), resulting in a solid concentrations of 9.1 g L^{-1} and 7.5 g L^{-1} for Na^+ -saturated montmorillonite and K^+ -saturated montmorillonite, respectively. IMC solutions were diluted with 0.01 M NaCl or 0.01 M KCl to achieve known initial concentrations.

Solid birnessite, goethite and ferrihydrite were added to reaction vessels in solid form to prepare suspensions of approximately 15 g L^{-1} . For ferrihydrite, desorption was carried out, also at pH 7, in two sequential steps, initially with 0.03 M CaCl_2 and then with 0.03 M NaH_2PO_4 . For birnessite and goethite experiments, IMC solutions were diluted with 0.01 M NaCl to achieve known initial concentrations. All reaction vessels were mixed at 10 rpm on a rotational (end-over-end) mixer for three hours in the dark at room temperature. Following mixing, solids were separated via centrifugation at 12,000 rpm for 10 min using an Eppendorf 5417C bench top microcentrifuge. Sorbed concentrations of IMCs were determined by the difference between

aqueous initial and final equilibrium concentrations as measured by ultra-high performance liquid chromatography (describe above) with diode array detection (DAD) using:

$$q_{ads} = \frac{C_i - C_e}{M_{SLD}} M_{SLN} \quad [1]$$

where q_{ads} is the mass of sorbed IMC per unit mass of solid sorbent ($\text{mmol kg}^{-1}_{SLD}$) at equilibrium after the adsorption step, C_i and C_e are the initial and equilibrium IMC concentrations ($\text{mmol kg}^{-1}_{SLN}$), M_{SLD} is the total mass of solid (kg), and M_{SLN} is the total mass of solution (kg).⁸³

Following the adsorption step, excess solution was decanted and sedimented pellets were suspended in the appropriate background electrolyte solution (0.01 M NaCl or 0.01 M KCl) to determine the extent of desorption. Adsorbed IMC concentrations after the desorption step were determined by:

$$q_{des} = q_{ads} - \left(\left(\frac{C_{e,des} M_{SLN}}{M_{SLD}} \right) - \left(\frac{C_{e,ads} M_{ENT}}{M_{SLD}} \right) \right) \quad [2]$$

where q_{des} is the mass of sorbed IMC per unit mass of solid sorbent ($\text{mmol kg}^{-1}_{SLD}$) at equilibrium after the desorption step, $C_{e,des}$ and $C_{e,ads}$ are the measured equilibrium IMC concentrations in solution ($\text{mmol kg}^{-1}_{SLN}$) after the desorption and adsorption steps, respectively, and M_{ENT} is the mass of entrained solution remaining in the reaction vessel after decanting the supernatant solution (kg). Solid-solution partition coefficients (K_d) were calculated for linear isotherms. The K_d values were calculated by:

$$K_d = \frac{q_{ads}}{C_{e,ads}} \quad [3]$$

where q_{ads} is the mass of sorbed IMC per unit mass of solid sorbent ($\text{mmol kg}^{-1}_{SLD}$) and $C_{e,ads}$ is the solution phase IMC concentration ($\text{mmol kg}^{-1}_{SLN}$), both measured at equilibrium. Hysteresis index (HI) values were also calculated for several isotherms. HI is determined by comparing the surface excess values, q_{ads} and q_{des} , for the sorption and desorption steps at a fixed value of aqueous analyte concentration²⁴. The HI values were calculated by:

$$HI = \frac{q_{des} - q_{ads}}{q_{ads}} \quad [4]$$

For non-linear adsorption the Freundlich isotherm equation provided a better fit to the data than a linear equation. The Freundlich fit was calculated using:

$$q_{ads} = K C_{e,ads}^n \quad [5]$$

where q_{ads} is the mass of sorbed of IMC per unit mass of solid sorbent ($\text{mmol kg}^{-1}_{SLD}$) at equilibrium, K is the Freundlich constant, $C_{e,ads}$ is solution phase IMC concentration at equilibrium ($\text{mmol kg}^{-1}_{SLN}$), and n is the Freundlich exponent. K and n are both adjustable parameters calculated from a linearized log-log plot of surface excess versus aqueous analyte concentration.

3.6. Oxidation of IMCs and IMC-Daughter Products by Minerals

Time series experiments were conducted to quantify the abiotic transformation potential of IMCs by birnessite and ferrihydrite at solid to solution ratios (SSR) of 0.15, 1.5 and 15 g kg^{-1} . Birnessite synthesis is described above. Six line ferrihydrite was synthesized in the laboratory following the method described by Schwertmann and Cornell¹¹⁰. Twenty grams of $\text{Fe}(\text{NO}_3)_3 \cdot 9\text{H}_2\text{O}$ were added to 2 L of preheated distilled water at 75° C. The mixture was stirred rapidly for 12 mins and then rapidly cooled by plunging into ice water, transferred to dialysis bags and dialysed for at least 3 d,

with water changed several times each day, prior freeze drying. Both birnessite and ferrihydrite samples were tested for purity by x-ray diffraction (XRD).

One hundred mL of 1 mM DNAN, MENA, DAAN, NTO or ATO solution (in 10 mM NaCl as background electrolyte) were placed in a reactor with a magnetic stirrer and the appropriate dry mass of birnessite or ferrihydrite was added with rapid mixing to initiate the reaction at the desired SSR ratios. The pH was controlled at 7.0 by titration addition of 10 mM HCl or NaOH throughout the reaction. Samples were taken at time intervals between 0 and 180 min. Solids were separated via centrifugation at 41,500 g for 5 min and the supernatant solution was analyzed for equilibrium concentration of IMCs using high performance liquid chromatography with photodiode array detection (UHPLC-DAD described above). All time series experiments were conducted under oxic conditions (in equilibrium with atmospheric air) at 25°C. First order rate coefficients for oxidation kinetics were determined from the magnitude of the slope of the regression line resulting from plotting the log of normalized reactant concentration (C_t/C_0) vs time (h), where C_t is the concentration of compound at time t , and C_0 is the initial concentration of compound at time zero. To examine the role of O₂, selected reactions were run with suspensions equilibrated with partial pressures of O₂ in the headspace of 0, 0.05 and 0.2 atm.

Additional experiments were conducted to identify and quantify products from birnessite-ATO reaction. These experiments were carried out in closed serum bottles (Volume = 155.5 cm³) at initial pH of 7.0 in 10 mM NaCl background solution at room temperature. An aliquot of 40.0 g of 1 mM ATO solution was added to 0.60 g birnessite in triplicate to give SSR values of 15 g kg⁻¹ (1260 m² kg⁻¹). The samples were allowed to react for 3 h, and N₂ and CO₂ release to the headspace was measured following acidification of solution to pH 2.0 with 0.1 M HCl. Total CO₂ production was calculated from gas phase concentrations using Henry's law. Samples were also analyzed for dissolved organic transformation products using liquid chromatography tandem mass spectrometry (LC-MS/MS) as follows. An Acquity UHPLC and a triple quadrupole Quattro Premier XE mass spectrometer, with a sample organizer from Waters Corporation (Milford, MA) were run with an XBridge BEH C18 column (2.1 x 50 mm, 2.5 µm) at 30 °C (10 µL injection) and a mobile phase consisting of acetonitrile (ACN) and water (H₂O) with 0.1% formic acid in both (0.35 mL min⁻¹ for 5 min in a ACN/H₂O gradient as follows: 0-3 min 75/25, 3.3 min 90/10, 4.5 min 75/25). Mass spectra were obtained in positive ion mode with a capillary voltage of 2.95 kV. Urea (61.1 > 44) was quantified under multiple reaction monitoring (MRM) with 0.1 s per transition dwell time, 26 V cone voltage and 9 V cone energy. N₂ was used as both cone gas and desolvation gas, and high purity argon was used as the collision gas (8.08 E-03 psi). Mass lynx 4.1 software from Waters Corp. (Milford, MA) was used to for analyte identification and quantification.

Closed serum bottles (10 mM NaCl background and initial pH 7.0, at 25 °C) were used to measure the extent to which IMC and daughter product oxidation resulted in compound mineralization to CO_{2(g)}. Forty mL of 1 mM IMC solution were added to 0.6 g mineral in a serum bottle (Volume = 155.5 cm³) at SSR of 15 g kg⁻¹. The samples were allowed to react for 3 h, and CO₂ released to the headspace was measured as described above using gas chromatography after acidification (pH 2) of the solution with 0.1 M HCl. To measure production of inorganic nitrogen species from IMC oxidation, a separate set of experiments were conducted at 15 g kg⁻¹ SSR in deionized water, in the absence of added background electrolyte to avoid analytical interference from Na⁺ and Cl⁻ in quantification of inorganic N species. Samples were collected as a function of reaction time and analyzed for dissolved NH₄⁺, NO₂⁻ and NO₃⁻ as described above. Total solution

phase manganese was measured using an Elan DRC-II inductively coupled plasma mass spectrometer (ICP-MS) (Perkin Elmer, Waltham, MA, USA).

Bragg reflections from XRD were collected for freeze dried powders of the control- and reacted-oxides in transmission mode on beamline 11-3 at the Stanford Synchrotron Radiation Lightsource (SSRL) at fixed X-ray energy of 12.7 keV (0.9765 Å) and calibrated to a LaB₆ standard. Analysis of the diffractograms for peak position ($^{\circ}2\theta$ and d-spacing [Å]), height, full width at half maximum (FWHM), and peak area was performed using X'Pert HighScore Plus software (PANalytical).

Selected reacted and unreacted birnessite samples were analyzed by X-ray photoelectron spectroscopy (XPS) to detect changes in Mn oxidation state using a Kratos Axis 165 Ultra X-ray photoelectron spectrometer (Kratos Analytical Ltd, UK). The XPS employed an Al monochromatic source and an array of eight channeltrons as detector. The sample chamber was continuously purged with He, and Mn 3s spectra were collected at high resolution to identify changes in Mn redox speciation induced by reaction.

3.7. Clone Library Methods to Characterize an ATO-Biodegrading Enrichment Culture

3.7.1. MR DNA primers and methods

Amplicon diversity sequencing was performed by MR DNA (www.mrdnalab.com). The 16S rRNA gene V4 variable region was amplified with PCR using primers 515F (5'-GTG CCA GCM GCC GCG GTA A-3') and 806R (5'-GGA CTA CHV GGG TWT CTA AT-3')¹¹¹ with the HotStarTaq Plus Master Mix Kit (Qiagen, USA) under the following thermocycling conditions: 94°C for 3 minutes, followed by 28 cycles of 94°C for 30 seconds, 53°C for 40 second, and 72 °C for 1 minute, with a final elongation step of 72°C for 5 minutes. Sequencing was performed on an Ion Torrent Personal Genome Machine (PGM) following manufacturer's guidelines and sequence data were processed using a propriety analysis pipeline (MR DNA, Shallowater, TX, USA) where sequences were depleted of barcodes and primers, poor quality sequences were removed, sequences were denoised, OTUs were generated, and chimeras were removed. OTUs were defined by clustering at 97% similarity and classified using BLASTn against a database derived from RDPII (<http://rdp.cme.msu.edu>) and NCBI (www.ncbi.nlm.nih.gov). The number of sequences in the data set was 112,788 (Contamination control culture without yeast), 96,318 (Contamination control culture with yeast), 127,239 (Enrichment culture without yeast), and 152,762 (Enrichment culture with yeast).

3.7.2. Conventional clone library

Nearly complete 16S rRNA genes were amplified from the ATO enrichment cultures (both with and without yeast extract) using primers Bac27F (5'-AGA GTT TGA TCM TGG CTC AG-3') and 1522R (5'-AAG GAG GTG ATC CAN CCR CA-3')¹¹². PCR was performed in 50 µL reactions with 1 × GoTaq Reaction Buffer (Promega), 2.5 U GoTaq G2 Flexi DNA polymerase (Promega), 1 mM MgCl₂, 0.16 mM dNTPs (Promega), 0.5 mM each primer, and 1 µL of DNA extracted from 1 mL of enrichment cultures with the PowerSoil DNA extraction kit (MoBio). The thermocycling procedure contained an initial denaturing step at 95°C for 5 min, 30 cycles of 95°C for 45 s, 55°C for 30 s, 72°C for 1 min, and final extension step of 72°C for 5 min. PCR amplification products were cleaned with a PowerClean DNA Clean-Up kit (MoBio). Electrophoresis on a 1% agarose gel was performed on purified amplification products and visualized with a GelRed DNA stain

(Biotium) and a GelDoc XR+ with ImageLab software (BioRad) to ensure correct amplicon size (~1500 bp), using a DNA 100bp DNA ladder (Promega), and to ensure amplicon purity. Amplicons were ligated into pGEM-T Easy vectors and cloned into *E. coli* JM109 cells with the pGEM-T Easy Vector System II kit according to manufacturer's recommendations (Promega). Cells were plated on LB plates with 100 mg L⁻¹ ampicillin and with ChromoMax IPTG/X-Gal solution for colony screening (Fisher Scientific). Colonies were picked with sterile pipette tips, placed into 10 µL of DNase/RNase-free water, and frozen and thawed three times to lyse cells. PCR using primers M13F (5'-GTT TTC CCA GTC ACG AC-3') and M13R (5'-CAG GAA ACA GCT ATG AC-3') were used to amplify the section of the vectors containing the 16S rRNA gene inserts. PCR was performed in 50 µL reactions as above but with M13 primers and 1 µL of a 1:10 dilution of lysed cell contents for template. The thermocycling procedure contained an initial denaturing step at 95°C for 5 min, 30 cycles of 95°C for 45 s, 51°C for 1 min, 72°C for 1 min, and final extension step of 72°C for 5 min. PCR amplification products were cleaned with a PowerClean DNA Clean-Up kit (MoBio) and screened with electrophoresis on a 1% agarose gel for purity. The cleaned PCR amplification product was then sequenced at the Oklahoma State University DNA/Protein Core Facility using Sanger Sequencing on an Applied Biosystems 3730 DNA analyzer. Sequencing was performed in each direction for each 16S rRNA gene target with the M13F (5'-GTT TTC CCA GTC ACG AC-3') and M13R (5'-CAG GAA ACA GCT ATG AC-3') primers. Sequence reads were inputted into a DNA alignment with Mega 6.0 software¹¹³ and the raw sequencing reads were reviewed to confirm quality. For each sequence, 1000-1200 bp of high quality sequence data was found. For each bidirectional sequencing pair, the bp between the beginning of the runs and the Bac27F or Bac1522R primers were deleted, the Bac1522R containing sequence was converted to its reverse-complement, and the two sequences were merged into a nearly complete 16S rRNA gene consensus sequence. Consensus sequences were analyzed with BLASTn (NCBI, www.ncbi.nlm.nih.gov) to identify phylogeny. The number of consensus sequences analyzed was 26 for the culture with YE, and 25 for the culture without YE.

4. RESULTS AND DISCUSSION

4.1. Adsorption of IMCs by Mineral Components of the Soil

The objectives of the adsorption experiments were to (1) determine the adsorption affinity of the IMCs DNAN and NTO, as well as their microbial reduction products MENA and ATO, in abiotic aqueous suspensions of smectite, goethite and birnessite and (2) collect preliminary data to assess whether any abiotic transformation reactions may ensue as a result of sorbent-sorbate interaction.

4.1.1. Results: SR-XRD: Synthesis products and clay characterization

Goethite and birnessite mineral syntheses were verified by X-ray diffraction (XRD) analysis at the Stanford Synchrotron Radiation Laboratory (SSRL). Data for synthesis products were fitted to goethite and birnessite using a Rietveld simulation to the SR-XRD data. The synthesized manganese oxide appeared to have the closest fit to acid-birnessite¹¹⁴.

4.1.2. Results: adsorption isotherms

Adsorption-desorption isotherm experiments were conducted at pH 7.0 at 10 mM ionic strength for the IMCs DNAN and NTO, as well as their respective reduced daughter products, MENA and ATO. Four distinct mineral adsorbents were employed including (i) Na⁺- and (ii) K⁺- saturated montmorillonite, (iii) goethite, and (iv) birnessite (Figure 4.1-1., Table 4.1-1). The isotherms show IMC surface excess (q) values, calculated in accordance with equations shown in the Material and Methods section, as a function of equilibrium adsorptive species concentration in solution. Distribution coefficient (K_d) values (Table 4.1-1) are determined from a linear fit to the slope of each isotherm.

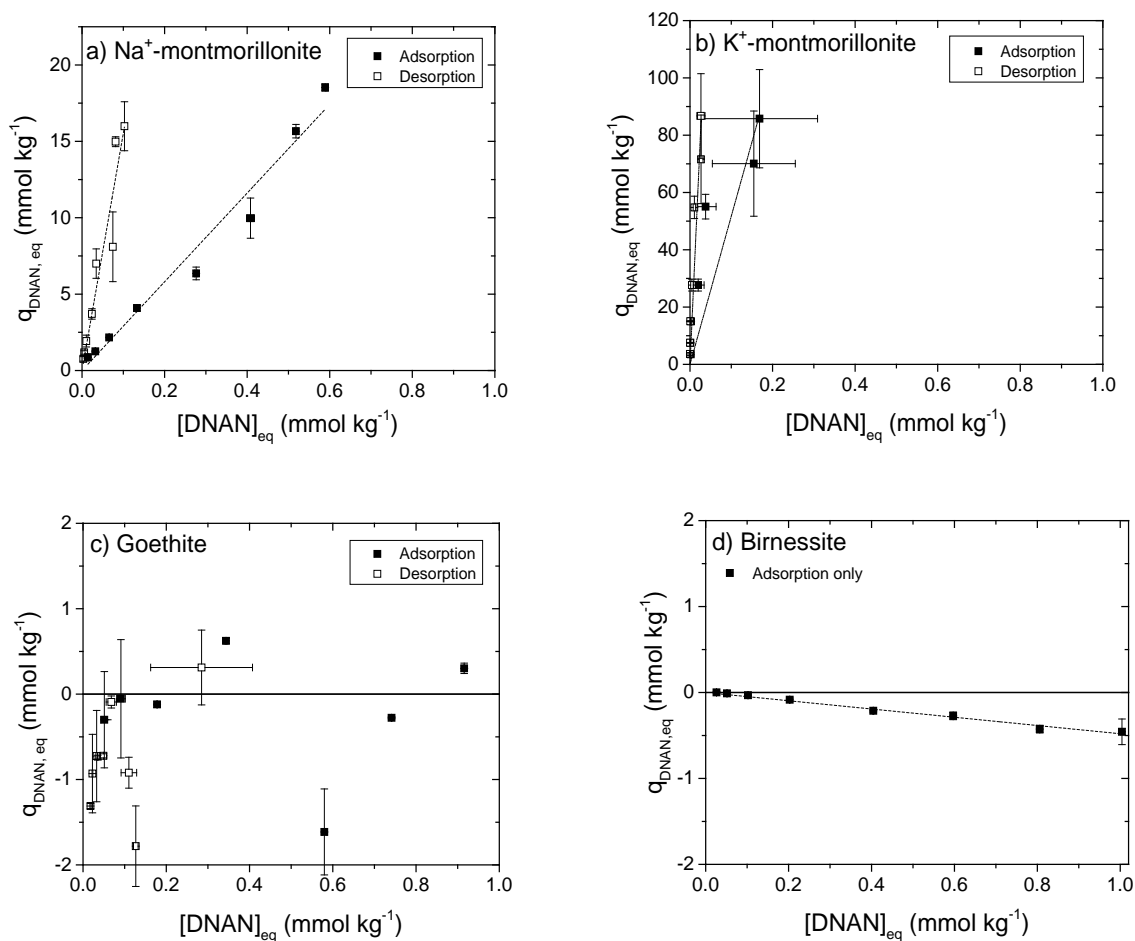


Figure 4.1-1. Adsorption and desorption isotherms at pH 7.0 showing the uptake and release of 2,4-dinitroanisole (DNAN) at each mineral surface. Background electrolytes were 0.01 M NaCl for Na⁺-montmorillonite, goethite, and birnessite and 0.01 M KCl for K⁺-montmorillonite.

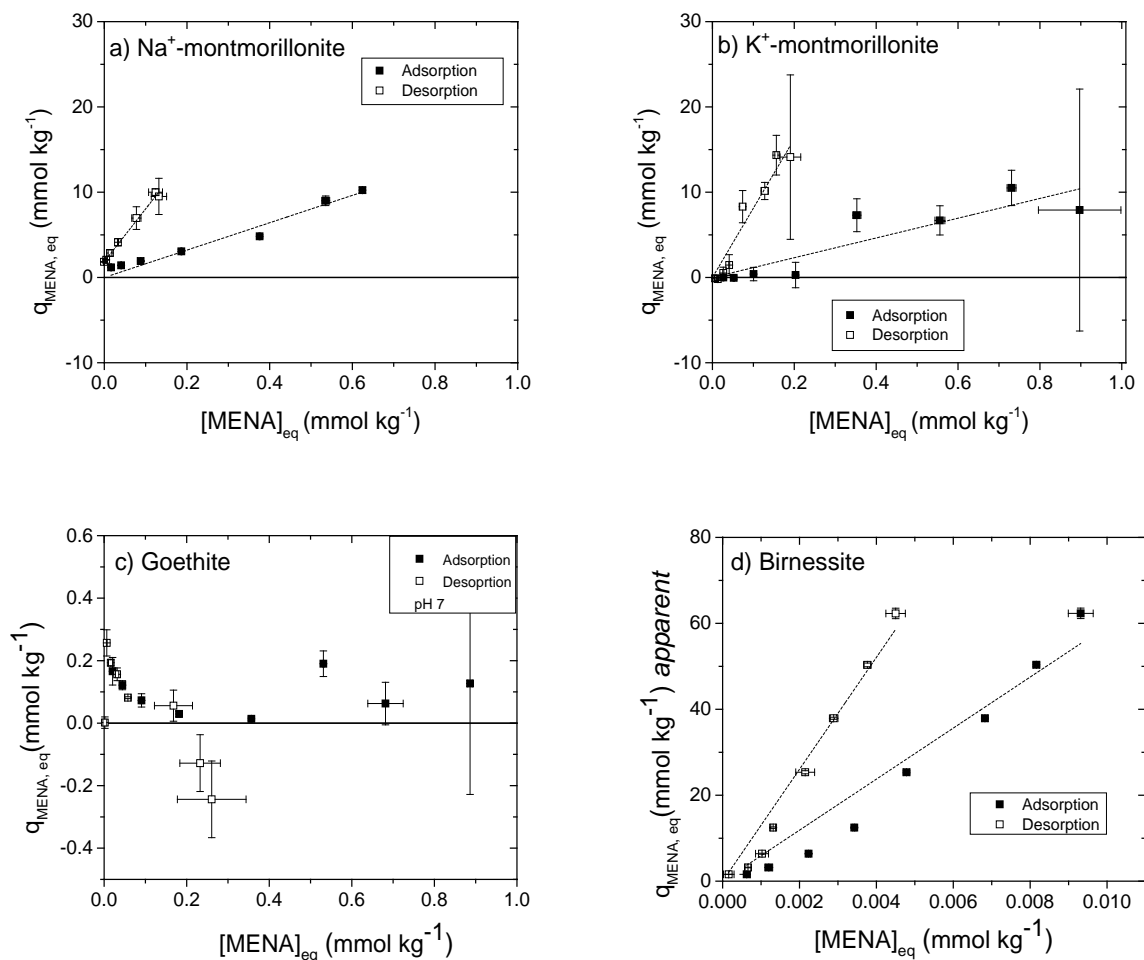


Figure 4.1-2. Adsorption and desorption isotherms at pH 7.0 showing the uptake and release of 2-methoxy-5-nitroaniline (MENA) from each mineral surface (plot d is ‘apparent’ adsorption on basis of loss from solution, later recognized to include oxidative transformation as discussed in Section 5.2). Background electrolytes were 0.01 M NaCl for Na⁺-montmorillonite, goethite, and birnessite and 0.01 M KCl for K⁺-montmorillonite.

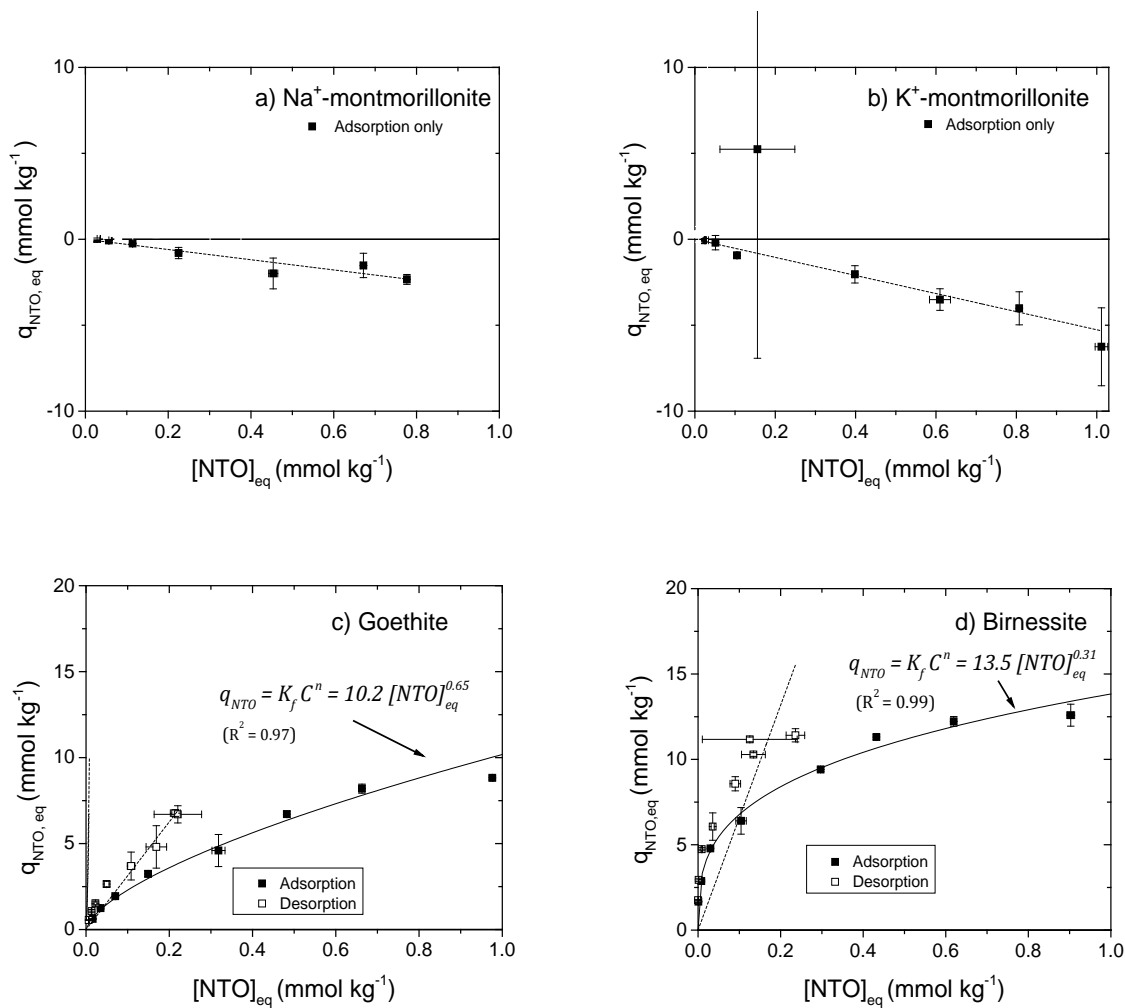


Figure 4.1-3. Adsorption and desorption isotherms at pH 7.0 showing the uptake and release of 3-nitro-1,2,4-triazole-5-one (NTO) on each mineral surface. Background electrolytes were 0.01 M NaCl for Na^+ -montmorillonite, goethite, and birnessite and 0.01 M KCl for K^+ -montmorillonite. Freundlich (non-linear) fits are shown for adsorption isotherms along with linear fits used for distribution coefficient calculations.

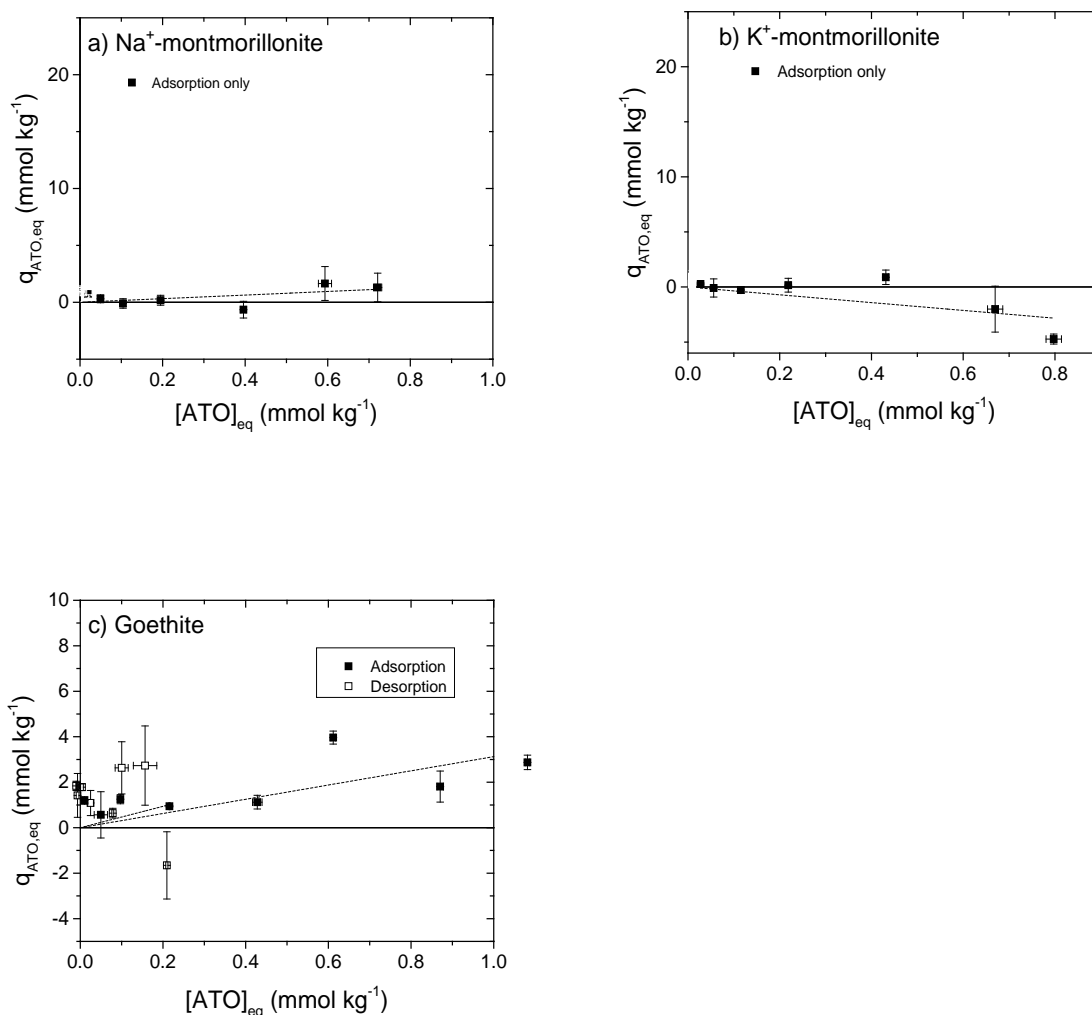


Figure 4.1-4. Adsorption and desorption isotherms at pH 7.0 for 3-amino-1,2,4-triazol-5-one (ATO) on Na⁺-montmorillonite, K⁺-montmorillonite, and goethite. Background electrolytes were 0.01 M NaCl for Na⁺-montmorillonite, goethite, and birnessite and 0.01 M KCl for K⁺-montmorillonite. Note that the higher surface excess values following desorption legs for montmorillonite are based on direct analytical application Equations shown in Section of and are therefore apparent. Surface exclusion of ATO gives a negative value for the difference within parentheses of eq. 2 in the Materials and Methods section (i.e., $C_{\text{e,ads}}$ overestimates adsorptive concentration in the entrained solution, M_{ENT}).

Table 4.1-1. Distribution coefficients (K_d) and hysteresis indices (HI) calculated from the isotherms.

Mineral Sorbent	Adsorption K_d / HI							
	DNAN		MENA		NTO		ATO	
Na ⁺ -montmorillonite	29.0	4.3	16.1	3.85	-3.0 ^b	0 ^c	1.6	NA ^a
K ⁺ -montmorillonite	517	5.1	11.6	6.0	-5.3 ^b	0 ^c	-3.5 ^b	0 ^c
Goethite	-0.04 ^b	0 ^c	0.2	0 ^c	11.1 ^d	1.8	3.1	0.50
Birnessite	-0.50 ^b	0 ^c	5940 ^e	1.2 ^a	18.5 ^d	2.6	ORS ^e	NA ^a

^aNA - not applicable

^bNegative slopes reported as K_d

^cHI not calculated for negative K_d values

^dBetter fit to Freundlich curve

^eORS - oxidative removal from solution

The data indicate that the nitro-aromatic compounds (NACs), DNAN (Figure 4.1-1) and MENA (Figure 4.1-2), have a positive affinity for montmorillonite but not for goethite. Comparing the Na⁺-montmorillonite and K⁺-montmorillonite isotherms in Figure 4.1-2a demonstrates the large effect of exchangeable cation type on surface excess. For example, the K_d of DNAN is *ca.* 18 times higher for K⁺- versus Na⁺-saturated montmorillonite.

MENA showed sorptive affinity for montmorillonite, though to a lesser extent than did DNAN; MENA showed a K_d for adsorption that was *ca.* 50% of that for DNAN in the case of Na⁺-montmorillonite and 2.2% in the case of K⁺-montmorillonite. In contrast to their affinity for the silicate clays, DNAN and MENA showed little adsorption affinity for the hydroxylated surface of goethite (Figures 4.1-1 and 4.1-2). Results from DNAN adsorption to birnessite also indicated near zero and negative adsorption, consistent with interfacial exclusion (Figure 4.1-1d). This result is in stark contrast to that of MENA-birnessite reaction, which appears high (Figure 4.1-2d) when calculated on the basis of loss from solution (eqs. 1 and 2 in section 3.5.2), which prompted the follow on studies (Section 4.2).

Isotherms and mineral-surface affinities for the NHCs (NTO and ATO, Figures 4.1.2-3 and 4.1.2-4) are distinctly different from those of the NACs (DNAN and MENA) presented above. When reacted with montmorillonite, the NHCs give negative or near zero surface excess values irrespective of exchangeable cation type, consistent with charge repulsion and exclusion at the clay interface (Figures 4.1-3 and 4.1-4, a & b). Conversely, NTO shows positive uptake to both metal oxides. NTO affinity for the goethite surface ($K_d = 11.06$, but better fit to a Freundlich isotherm equation, Figure 4.1.2-3c) greatly exceeds that of its metabolite ATO ($K_d = 3.13$, Figure 4.1-4c). NTO exhibited its highest affinity for the birnessite surface ($K_d = 18.48$, but also better fit to a Freundlich isotherm equation, Figure 4.1-3d).

Repulsion of anionic NTO and ATO from the negatively charged surfaces of montmorillonite (Figures 4.1-3a,b and 4.1-4a,b) results in a negative surface excess, where analyte concentration in the bulk supernatant solution is higher than that in the entrained solution because of organic anion exclusion from the mineral-water interface¹¹⁵. The same effect has also been observed for other organic anions such as the glucosinolates¹¹⁶, which are naturally sulfonated organic

compounds. Because of anion exclusion, the measured surface excess (q) values are shown for montmorillonite in Figures 4.1-3 and 4.1-4 only for the adsorption step. Calculation of surface excess following the desorption step leads to erroneous results as a result of a negative value for the difference within parentheses of eq. 2 (in section 3.5.2). Specifically, the use of $C_{e,ads}$ overestimates, in the case of anion exclusion, adsorptive concentration in the entrained solution (M_{ENT}).

Hysteresis index (HI) values calculated from the differences in slope following the adsorption and desorption steps (Figures 4.1-1 through 4.1-4) provide a measure of kinetic reversibility of a positive adsorption reaction. The largest HI value (least kinetically reversible reaction) was obtained for MENA reacted with K^+ -montmorillonite (HI = 6.0). Several of the HI values for DNAN and MENA were in a similar range (4.3, 5.1, 6.0), in contrast to the lower HI values of NTO and ATO (1.8, 2.6, 0.5).

4.1.3. Results: Oxidation of MENA by acid birnessite

Reaction of the DNAN bio-reduction product, MENA, with acid-birnessite resulted in near complete removal of MENA from solution, an assessment that is apparent from the equilibrium solution phase concentrations following the adsorption step (see the X axis scale values shown in Figure 4.1-2d). Average removal of MENA from solution was 98.4%. Organic degradation products were formed during MENA reaction with birnessite as evidenced by unknown (product) peak emergence during HPLC/DAD analysis. Pre- and post-reaction supernatant solutions were therefore analyzed by LC-QTOF-MS in an attempt to identify the degradation products. By differential analysis, mass spectral peaks with m/z values lower (160.9860) as well as higher (174.0166, 252.9588, 335.1346) than MENA were observed. Similarly, experiments with the NTO reduction product ATO also resulted in near complete ATO removal from solution. Upon analysis with both HPLC-DAD and QTOF-MS, no ATO was detectable in post-reaction supernatant.

4.1.4. Discussion: Adsorption trends for Na^+ and K^+ smectite

The DNAN and MENA adsorption trends for montmorillonite (Figures 4.1-1 and 4.1-2) show differential impact of exchangeable cations on NAC adsorption. Differences in affinity between Na^+ and K^+ exchanged forms of the clay suggest that the mechanisms of DNAN and MENA adsorption to montmorillonite are dominated by interaction of electronegative nitro groups on the NACs with the positive-charged exchangeable cations (Na^+ or K^+). DNAN adsorption to K^+ -montmorillonite was much greater than that for Na^+ -montmorillonite, presumably due to the lower hydration enthalpy of K^+ (-314 kJ mol^{-1}) relative to Na^+ (-397 kJ mol^{-1}), which is known to enhance the formation of inner-sphere cation complexes with NAC nitro groups¹⁷.

The observed high affinity adsorption of the DNAN and MENA to the cation-saturated silicate clays is likely driven, in part, by electron donor-acceptor (EDA) complexes. An EDA complex occurs when the electron deficient π -system of the NAC, caused by the electronegative nitro-groups extracting electron density from the ring, interacts with clay surface siloxane oxygen atoms. The siloxane oxygens serve as electron donors and the π -system of the NAC as the electron acceptor, giving rise to adsorption geometry of the ring structure that is parallel planar to the siloxane surface. This mechanism was proposed by Haderlein et al.¹⁸ in a study where interlayer cation effects on adsorption were also examined. Consistent with the results for DNAN and MENA reported here, Haderlein et al.¹⁸ found that K^+ -montmorillonite had the largest adsorption capacity (per unit mass) for different NACs across a range of homoionic clay minerals (montmorillonite, illite, kaolinite), and that K^+ had K_d values up to four orders of magnitude larger than other more

strongly hydrated exchangeable cations (Na^+ , Ca^{2+} , Mg^{2+}). Zhang et al.¹¹⁷ explored 1,3-dinitrobenzene adsorption to cation modified clays, and found again that adsorption was greatest with K^+ relative to Na^+ or Ca^{2+} saturated smectite. Boyd et al.¹⁷, using Fourier transform infrared (FTIR) spectroscopy to examine the adsorption mechanisms of NACs to smectite clays, showed, principally through shifts in the vibrational frequencies of the N-O bands, that adsorption was dominated by direct interaction of electronegative substituents with interlayer cations such as K^+ . These authors suggested that adsorption of NACs to smectite (including montmorillonite) is likely a cumulative effect of several factors, the dominant one being the relative stability of cation-oxygen bonds formed between siloxane-adsorbed cations and nitro functional groups of the NACs.

Differences in the magnitude of DNAN and MENA adsorption to montmorillonite (Figures 4.1-1 and 4.1-2) reflect the importance of nitro-cation bonding, since reduction of the ortho-nitro group to amine functionality results in significantly diminished montmorillonite affinity, particularly for adsorption to the K^+ -saturated clay (compare Figures 4.1-1b and 4.1-2b). For example, in the case of K^+ -montmorillonite, the DNAN K_d is 517, whereas the MENA K_d is 11.6. The effect of ortho-nitro group reduction is much smaller, but still present, in the case of Na^+ -saturation (Figures 4.1-1a and 4.1-2a), for which the DNAN $K_d = 29.04$, and MENA $K_d = 16.05$ (Table 4.1-1). From the perspective of fate and transport of IMCs and their metabolites in soil systems, this effect is very important, because it suggests that bio-reduction of a nitro-functionality can significantly diminish contaminant sorptive affinity for layer silicate surfaces. Thus, the bio-reduced form of DNAN (MENA), expected to be formed in sub-oxic pore waters, may for this reason be more mobile in the subsurface environment. Haderlein et al.¹⁸ argued that nitro-to-amine reduction donates electron density back to the benzene ring π -system, reducing the tendency to form an EDA complex and, hence, results in less adsorption. This EDA effect is likely superimposed on the low affinity of the $-\text{NH}_2$ group to complex even weakly hydrated cations such as K^+ . The reduction of DNAN (i.e., MENA formation) leads to less adsorption due to the loss of a substituent group capable of cation complexation.

Despite these differences in magnitude, both the mono- and di-nitro aromatics showed significant adsorption to the montmorillonite surface under conditions of both K^+ and Na^+ exchangeable cation saturation, raising the question of the extent to which the IMC and its biotransformation product were adsorbed into the expansible interlayer versus solely on the external or basal surfaces. X-ray diffraction (XRD) measurements showed an increase in the d_{001} interlayer spacing (indicated by a downward shift in position $2^\circ \Theta$) upon DNAN and MENA adsorption, with the largest increase observed for K^+ -saturated clays (Figure 4.1-5). This result signals interlayer (siloxane surface) adsorption of both DNAN and MENA. A model calculation also confirms that monolayer adsorption to external surfaces is insufficient to explain the moles of adsorbate of modeled molecular dimensions (Table 4.1-5), whereas co-planar orientation of the NAC adsorbate at interlayer surfaces, which is consistent with molecular modeling and prior spectroscopic studies¹⁷, can explain the mass balances measured in the isotherm experiments.

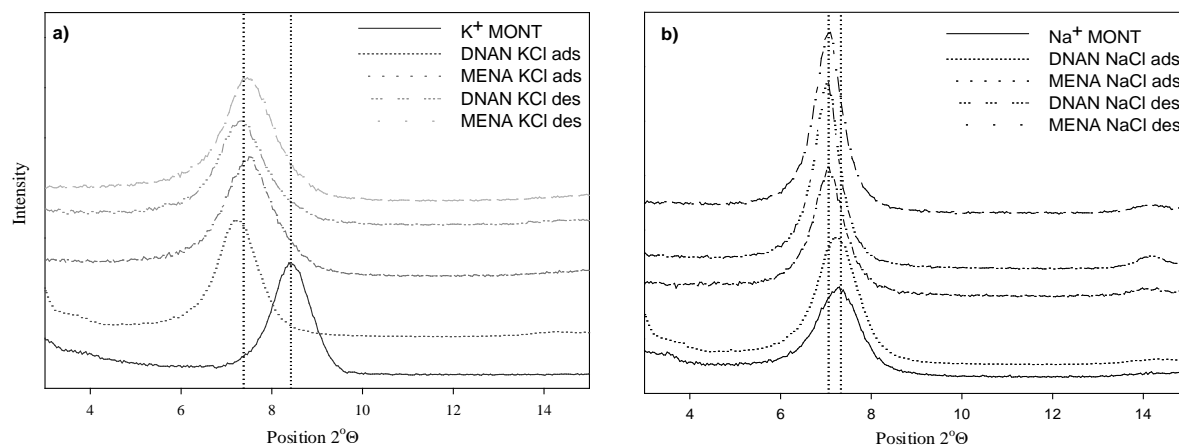


Figure 4.1-5. XRD patterns for K⁺-montmorillonite (a) and Na⁺-montmorillonite (b) clays after aqueous adsorption “ads” followed by desorption “des” of the nitro-aromatics DNAN and MENA for samples reacted at the highest adsorptive species concentrations shown in Figures 4.1.2-1 and 4.1.2-2. Note the increase in d-001 spacing (indicated by a downward shift in position 2° Θ) with adsorption of MENA and DNAN. Greater relative expansion occurs in KCl solution and for DNAN relative to MENA, consistent with the surface excess results shown in Figures. 4.1-1 and 4.1-2.

Table 4.1-2. Maximum adsorption versus available surface area calculations.

DNAN Surface area* (nm ²)	DNAN adsorption (mmol kg ⁻¹)	Montmorillonite surface area (m ² g ⁻¹)	DNAN surface density (molecules/nm ²)	Total surface area occupied (%)
1.64	85.8	596	0.087	14
1.64	85.8	36.4	1.42	232

*Connolly molecular surface area (ChemBio 3D Ultra 13.0)

Specifically, the surface area of the DNAN molecule was estimated using the Connolly molecular surface area calculation in ChemBio 3D Ultra 13.0. Given the calculated surface area of a planar DNAN molecule as 1.64 nm², adsorption of the aromatic ring co-planar with the siloxane surface enables adsorption of a *maximum* of 0.61 DNAN molecules per nm² of planar surface (i.e., in closest-packing mode). This DNAN surface density was compared with the maximum DNAN surface excess (maximum *q*) measured under the following assumed scenarios: (1) DNAN adsorption to both external and interlayer surfaces, and (2) DNAN adsorption only to external basal surfaces. Scenario (1) implies a DNAN surface density of approximately 0.09 DNAN molecules per nm², or 14% of available surfaces being occupied at maximum *q*. This DNAN surface density is less than the estimated maximum (0.09 DNAN molecules per nm² < 0.61

DNAN molecules per nm²) and the low surface area occupation percentage is viable, given that the isotherm is still linear at the maximum q measured. In contrast, scenario (2) implies a DNAN surface density of 1.42 DNAN molecules per nm², or occupation of approximately 232% of the available surface sites. This cannot be reconciled with the assumption of planar adsorption to the clay mineral particles. Hence, isotherm, XRD data and model calculations are all consistent with DNAN and MENA being adsorbed to interlayer siloxane sites in proportion to both their nitro functional group density and exchangeable cation composition of the clay.

Interaction of NTO with montmorillonite resulted in negative surface excess. With a pKa of 3.76, the NTO molecule is negatively charged at experimental pH (7). The negative charge of the sorbent evidently repels the sorptive solute, resulting in detectable levels of anion exclusion. Several authors, including, e.g., Polubesova and Borisover¹¹⁸ have shown that electrostatic repulsion creates a region of anion free solution in the nanoporous domains that present close proximity to the solid surface. This causes an increase in adsorptive concentration in the supernatant solution relative to that measured in the bulk solution control without clay colloids (eq. 1 in Materials and Methods). An increase in exclusion (i.e., negative surface excess) with increasing equilibrium concentration in bulk solution (Figure 4.1-2c), gives rise to the negative K_d values calculated with eq. 3 (in section 3.5.2) and reported in Table 4.1-1.

4.1.5. Discussion: Adsorption to metal oxides

NTO adsorption to the iron oxyhydroxide surface (Figure 4.1-3c) is consistent with electrostatic considerations. In an “indifferent” background electrolyte solution, such as the 0.01 M NaCl used here, goethite has a point of zero net charge (PZNC) of 7.5¹¹⁹, and thus is slightly positively charged at our experimental pH. This positive charge creates an electrostatic attraction between the anionic NTO and the goethite surface, giving rise to positive adsorption values. Interestingly, NTO data also suggested a relatively high affinity for the Mn oxide, birnessite. This interaction cannot be rationalized through electrostatics alone since acid-birnessite (MnO₂), has a PZNC of 1.9¹¹⁹, giving it a negative surface charge at the experimental pH. Nonetheless, we observed no new peak emergence in the HPLC-DAD chromatograms (despite extended run times) for the NTO-birnessite system, which argues against chemical transformation as a potential fate. It is plausible that NTO adsorption was localized at positively-charged surface sites and/or mediated by cation bridging interactions. In addition, the Freundlich isotherm equation appeared to closely approximate the adsorption of NTO to both metal oxides (Figures 4.1-3c and 4.1-3d), with R^2 values of 0.97 and 0.99, for goethite and birnessite, respectively.

4.1.6. Discussion: Adsorption reversibility

Hysteresis indices were measured for all isotherms to assess the kinetic reversibility of adsorption-desorption reactions¹²⁰. During the desorption step of the isotherm experiments, release from the surface of adsorbate occurs following perturbation by replacement of the equilibrium solution condition. When the colloidal suspensions were modified by removal of equilibrium IMC solution and replaced with an IMC-free (otherwise equivalent) electrolyte solution, the reduction in IMC concentration in solution is expected to promote IMC desorption (for positive q values) with approach to a new equilibrium value following the 3 h equilibration step (equal to that for adsorption) at a lower solution phase IMC concentration. A high HI value indicates high relative surface retention of adsorbate and, therefore, kinetic irreversibility, whereas a small or zero q value indicates adsorption-desorption that is kinetically reversible. DNAN adsorption-desorption on both the K⁺ and Na⁺ montmorillonite show significant hysteresis (Figures 4.1-1a and 4.1-1b). The

HI values are similar in scale, but HI is nonetheless 16% larger for K^+ - relative to Na^+ -exchanged clay. This difference in HI values is again consistent with weaker NAC ternary interaction with a strongly hydrated cation adsorbate. That is, the ternary ligand-metal-siloxane surface complexes appear to dissociate more readily for Na^+ than for K^+ exchanged forms, consistent with the lower metal-ligand stability that occurs in outer-sphere versus inner-sphere complexes.

For consistency across data sets, the NTO HI values were calculated using linear isotherm fits to the data shown in Figures 4.1-3c and 4.1-3d for goethite and birnessite, despite the fact that isotherms were non-linear, as indicated by the non-linearity factor, n , of both Freundlich fits being < 1.0 . The NTO/metal oxide HI values were *ca.* half as large as the DNAN/clays HI values, suggesting that even though similar surface excess values are achieved in the NAC-clay and NHC-oxide systems, the electrostatic interactions leading to nitrogen heterocyclic compound adsorption (e.g., NTO to goethite) are more reversible kinetically than those for NAC/clay adsorption.

4.1.7. Discussion: Preliminary Indications of Oxidation of MENA and ATO by Acid Birnessite

The synthetic acid-birnessite $[(Na_{0.3}Ca_{0.1}K_{0.1})(Mn^{4+}, Mn^{3+})_2O_4 \cdot 1.5H_2O]$ used in this study is a common secondary manganese oxide that is formed by bacteria and fungi in soils ¹²¹, and it is the most commonly observed secondary Mn(IV) solid phase. Importantly, results of our adsorption studies showed near complete removal of MENA and ATO, the bio-reduced (aminated) forms of the IMCs DNAN and NTO, respectively, during reaction with birnessite. Birnessite has previously been shown to remove parent aromatic amines from solution via oxidative transformation, as well as by adsorption ^{26,122}. Indeed, as discussed above, QToF-MS analysis indicated that birnessite induces oxidative transformation of MENA followed by potential fragment polymerization of oxidative transformation products, an observation supported also by prior work on other aromatic amines ²⁶ and polyphenols ²⁷.

ATO was also removed from solution during reaction with birnessite, and a similar oxidative transformation mechanism is hypothesized. Aromatic amine transformation by Mn(IV) oxide was investigated by Laha and Luthy ²⁵, who reported that azobenzene formed from the reaction of aniline with manganese dioxide. The formation of azobenzene, a larger polymer, resulted in the removal of the nitroaromatic from solution ²⁵.

4.1.8. Conclusions adsorption work

The adsorption and reactivity of IMCs with clay mineral and Fe and Mn oxide mineral constituents was determined as a means to better assess contaminant mobility and bioavailability in soils and sediments. The experimental results highlight the importance of interactions between (i) IMC chemical structure and (ii) soil mineral surface composition in controlling contaminant adsorptive affinity. Adsorption of IMCs at mineral surfaces is governed not only by functional group composition and charge of the IMCs themselves, but also by the surface functional group chemistry and (in the case of montmorillonite) exchangeable cation composition of the mineral adsorbents. For this reason, it was important to test adsorption reactions across a representative range of mineral surface chemistries characteristic of common soil mineral assemblages. While none of the minerals served as a high affinity adsorbent for all of the IMCs and metabolites studied, each of the compounds did exhibit a high adsorption affinity for at least one of the adsorbent types. This suggests that each of the compounds would be subjected to adsorptive retardation during subsurface transport, but likely as a result of accumulation at distinct mineral surfaces. Specifically, the NACs, DNAN and MENA, exhibited significant affinity for layer silicate clays,

whereas the NHCs showed greater affinity for metal oxide surfaces. NAC adsorption to layer silicate clays was apparently favored by inner-sphere complexation between nitro functional groups and exchangeable cations, whereas NHC adsorption was insignificant on the silicate clays because of charge repulsion. Conversely, the NHC NTO exhibited strong affinity for adsorption to both goethite and birnessite surfaces.

The microbially-catalyzed reduction of DNAN and NTO is expected to occur in sub-oxic soil pore waters and our results indicate that such bio-reduction to MENA and ATO, respectively, can alter subsequent contaminant reactivity with mineral surfaces. Specifically, reduction of nitro substituents to amine functionality diminishes NAC affinity for layer silicate surfaces, where they form ternary complexes with adsorbed metal cations. Nitro group reduction also decreases NHC sorptive affinity for goethite, but the amine functionality associated with both ATO and MENA appeared to increase their oxidative reactivity toward the mineral oxidant birnessite, supporting the assertion that a coupled biotic-abiotic degradation pathway that can lead to elimination of both parent and daughter compounds. This latter set of reactions was investigated in greater detail as described in the following section.

4.2. Reaction of DNAN and Daughter Products with Birnessite and Ferrihydrite

The results of adsorption-desorption experiments described in Section 4.1 suggested significant reactivity of IMC reduced daughter product MENA with Mn(IV) oxide and also potentially with Fe(III) oxide. Among the most common and reactive representatives of these oxide groups are birnessite and ferrihydrite, respectively. Therefore, the objectives of this portion of the project were (i) to quantify the kinetics and extent of oxidative transformation of DNAN and reduced daughter products MENA and DAAN at birnessite and ferrihydrite surfaces and (ii) to assess any resulting transformations in the mineral solids that accompany redox reactions.

4.2.1. Results: Reaction of DNA, MENA and DAAN with ferrihydrite

The reactivity of DNAN, MENA and DAAN was tested with ferrihydrite at a SSR of 15, 1.5 and 0.15 g kg⁻¹. There was no reaction of DNAN and MENA with ferrihydrite within the 3 h reaction time for all of the solid phase concentrations tested (Table 4.2-1). However, DAAN was reactive with ferrihydrite at 1.5 and 15 g kg⁻¹ SSR (Table 4.2-1). There was initial decline in DAAN concentration; but the reaction seems to stall and the amount of DAAN in solution reaches a near-steady value after 60 min for 1.5 g kg⁻¹ SSR. Conversely, for 15 g kg⁻¹ SSR, there was gradual decline in DAAN concentration up to a 3 hour reaction time.

Table 4.2-1. First order rate constants (*k*) of IMC and daughter product oxidation by birnessite and ferrihydrite supplied at various concentrations.

Mineral Surface	SSR [‡] g kg ⁻¹	1st Order Rate Constants (<i>k</i> , h ⁻¹)		
		DNAN	MENA	DAAN
Birnessite				
	0.15	0.00*	0.01 (0.21) [†]	0.11 (0.55)
	1.50	0.00	0.22 (0.96)	1.18 (0.99)
	15.0	0.00	1.36 (0.93)	≥ 90.5 ^{**} (N/A)
Ferrihydrite				
	0.15	0.00	0.00	-
	1.50	0.00	0.00	0.20(0.53)
	15.0	0.00	0.00	0.27(0.81)

*0.00 means no measurable reaction in 3h, in the case of DNAN + birnessite and DNAN/MENA

[†] ferrihydrite, no reactions was observed.

** value estimated by slope of first two data points only, as concentration reached zero at second sampling point (5min). The rate is even higher than estimated as actual reaction end point might be less than five minutes and is denoted by ≥ in the table. N/A Not applicable

[†]Values in parentheses are R2 values for the regression fit.

[‡] SSR = solids solution ratio.

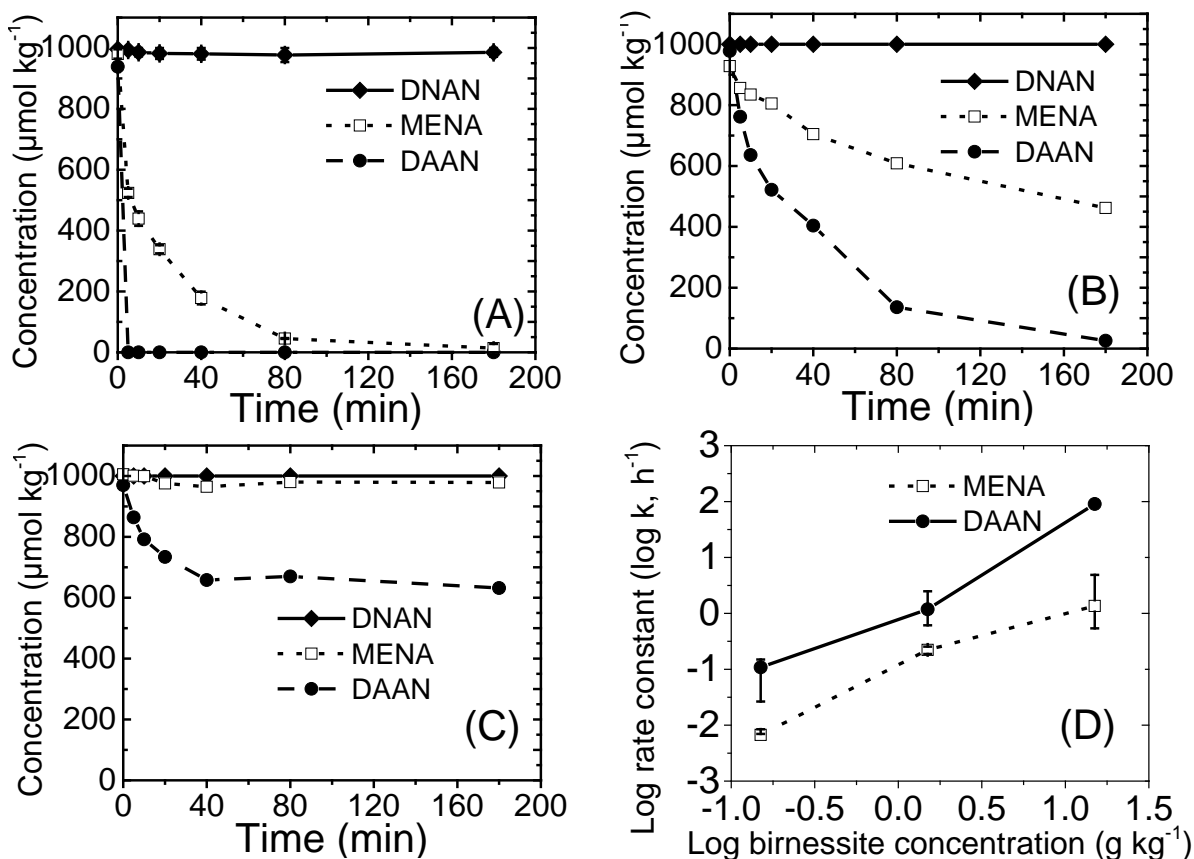


Figure 4.2-1. Transformation of DNAN, MENA and DAAN by birnessite at (A) 15 g kg⁻¹, (B) 1.5 g kg⁻¹ and (C) 0.15 g kg⁻¹ solid to solution ratio at pH 7.0, and (D) log plots for MENA and DAAN reaction with birnessite at 0.15, 1.5 and 15 g kg⁻¹ solid to solution ratio.

4.2.2. Results: Reaction of DNA, MENA and DAAN with birnessite

There was no detectable reaction of DNAN with birnessite under the experimental conditions tested over a 3 h period (Table 4.2-1, Figure 4.2-1). However, DNAN daughter products were transformed by birnessite oxidation within 3 h for MENA and within 5 min for DAAN at a SSR of 15 g kg⁻¹ (Figure 4.2-1A), corresponding to first order rate constants of 1.4 and ≥ 90 h⁻¹, respectively (Table 4.2-1). At a lower SSR of 1.5 g kg⁻¹ with birnessite (Figure 4.2-1B), the first order reaction produced rate constants of 0.22 and 1.18 h⁻¹ for MENA and DAAN, respectively, (Table 4.2-1).

A direct comparison for the oxidation of DAAN by birnessite and ferrihydrite at an SSR of 1.5 g kg⁻¹ (Figure 4.2-2) indicates a stark contrast in the ability of these minerals oxidize the daughter products of DNAN. Birnessite oxidized both MENA and DAAN; whereas only ferrihydrite only oxidized DAAN. Furthermore, the rate of DAAN oxidation was 6-fold faster

with birnessite compared to ferrihydrite when each was supplied at 1.5 g kg^{-1} mineral oxidant (Table 4.2-1).

The number of nitro- and amino- groups on the molecule controlled oxidation rate by birnessite. The parent compound DNAN, with two nitro-groups was not oxidized. However, the reduced daughter products were oxidized and the rates increased as the number of amino-groups increased and nitro-groups decreased. DAAN with two amino-groups was oxidized 5.4-fold faster than MENA which has one-amino and one-nitro group (Table 4.2-1). Even at the lowest tested SSR of 0.15 g kg^{-1} , the first order rate constant for DAAN oxidation by birnessite was 0.11 h^{-1} but the reaction then plateaued after 40 min (Figure 4.2-1C) indicating depletion of reactive oxidant. Conversely, there was no measurable MENA oxidation over a 3 h period at the lowest SSR value (Table 4.2-1). First order rate constants showed a strong log-log dependence on SSR (Figure 4.2-1D) for MENA and DAAN. The error bars represent 95 % confidence interval. Figure 4.2-1D also illustrates the higher reactivity of DAAN at all oxidant concentrations compared to MENA.

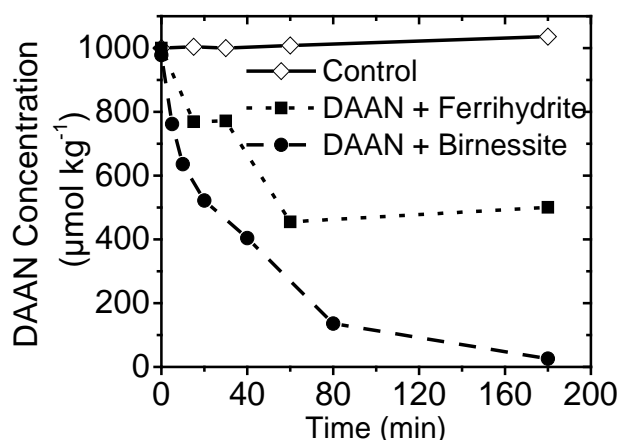


Figure 4.2-2. Comparative time course of DAAN loss from solution at birnessite and ferrihydrite SSR of 1.5 g kg^{-1} .

4.2.3. Results: Extent of mineralization

For those conditions showing maximum MENA and DAAN removal (15 g kg^{-1} birnessite), companion experiments were conducted to assess CO_2 evolution from the reaction. Data show that under oxic conditions ($20\% \text{ O}_2$), 15% and 12% of the C was mineralized to CO_2 for MENA and DAAN, respectively (Figure 4.2-3A). Furthermore, the data show that mineralization to CO_2 was not limited by presence of O_2 , since the fraction of MENA mineralized following reaction with birnessite in a 0.01 M NaCl background was independent of $\text{O}_{2(\text{g})}$ partial pressure (Figure 4.2-3A).

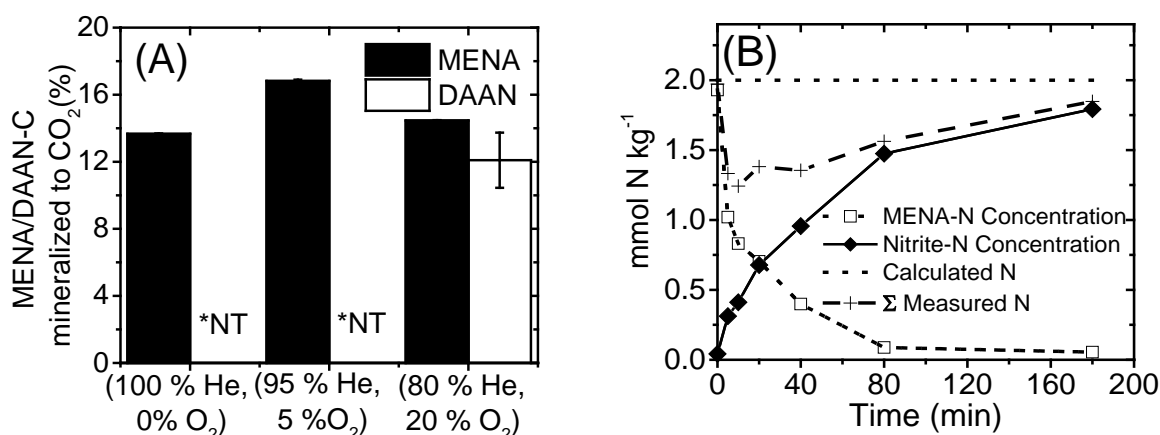


Figure 4.2-3. (A) The percent conversion of MENA/DAAN-C to CO₂ during incubations with birnessite 15 g kg⁻¹ solid to solution ratio over a 3 h incubation period with 0, 5 and 20% O₂ in the headspace. DAAN CO₂ emission was tested with 20 % O₂ in the headspace only; (B) Nitrite recovery from MENA birnessite reaction at 15 g kg⁻¹ solid to solution ratio at pH 7.0. *NT=not tested.

In addition to partial mineralization of IMC daughter organic C to CO₂, the release of organic N to inorganic forms was also observed for both MENA and DAAN reaction with birnessite, albeit to different extents. For MENA, results indicate nitrite (NO₂⁻) as the dominant N degradation product, with *ca.* 95 % of MENA nitrogen recovered in this inorganic form following 3 h of oxidation by birnessite (Figure 4.3-3B). A smaller yield of NO₂⁻ was observed for DAAN, equating to *ca.* 15 % of total DAAN-N (e.g., compare Figures A.2 and A.3). Much less NH₄⁺-N (<2%) and NO₃-N (<5%) and no N₂-N were detected as a product of either MENA or DAAN oxidation).

The yield of soluble Mn(II) was much less than that calculated based on stoichiometric conversion of birnessite Mn(IV) to soluble Mn(II) during reaction with IMC daughter products. For MENA and DAAN, only 34.5 μg kg⁻¹ and 782.4 μg kg⁻¹ of Mn(II) were recovered from solution respectively at the end of 3-hour reaction. These measured values are more than three orders of magnitude lower than the values of 935 and 988 mg kg⁻¹ Mn(II) calculated for complete stoichiometric conversion of MENA and DAAN to CO₂ and nitrite or N₂, respectively. Calculations of Mn²⁺_(aq) generated from 12% (MENA) and 15% (DAAN) conversion to mineralized products, as measured in the experiments, also give concentrations *ca.* 4000 and 152 times higher for Mn(II) concentrations in solution than those measured, indicating a solid-phase fate for the reduced Mn.

4.2.4. Transformation of birnessite based on X-ray diffraction (XRD) and X-ray photoelectron spectroscopy (XPS).

The unreacted birnessite showed the expected Bragg reflections including (001) at 7.294 Å, (002) at 3.633 Å, and the strongly asymmetrical (220/110) and (310/020) peaks at 2.468 Å and 1.424 Å respectively (Figure 4.2-4A). The MENA- reacted birnessite showed no change in the (001) peak position, height or FWHM. The (002) and (220/110) peak showed distortions with the (002)

reflection 0.017 Å closer, 11% lower in height, but at the same full width at half maximum (FWHM); the (220/110) reflection was 0.009 Å longer, no change in height, and a FWHM at 50% the value of the unreacted birnessite. The (020) showed no change in d-spacing, but a 20% decrease in the FWHM.

High resolution Mn3s spectra for birnessite reveal detectable changes in Mn oxidation state following reaction of MENA (Figure 4.2-4B) with 15 g kg⁻¹ SSR birnessite. The magnitude of peak splitting for Mn3s high resolution spectra is diagnostic for the oxidation state of Mn¹²³. Unreacted birnessite shows a binding energy difference between Mn3s splitting multiplex of 4.5 eV, consistent with predominance of Mn(IV) oxidation state, whereas following 3 h reaction with MENA, the binding energy difference between Mn3s splitting multiplex shifts to 5.05, indicating reduction of a portion of birnessite Mn (IV) to a mixture of Mn (II and III). The Mn shift towards higher binding energy is consistent with the low aqueous recovery of Mn discussed above, and suggests that reductive transformation of birnessite upon reaction with IMC daughter products results in subsequent re-incorporation of reduced Mn into the solids.

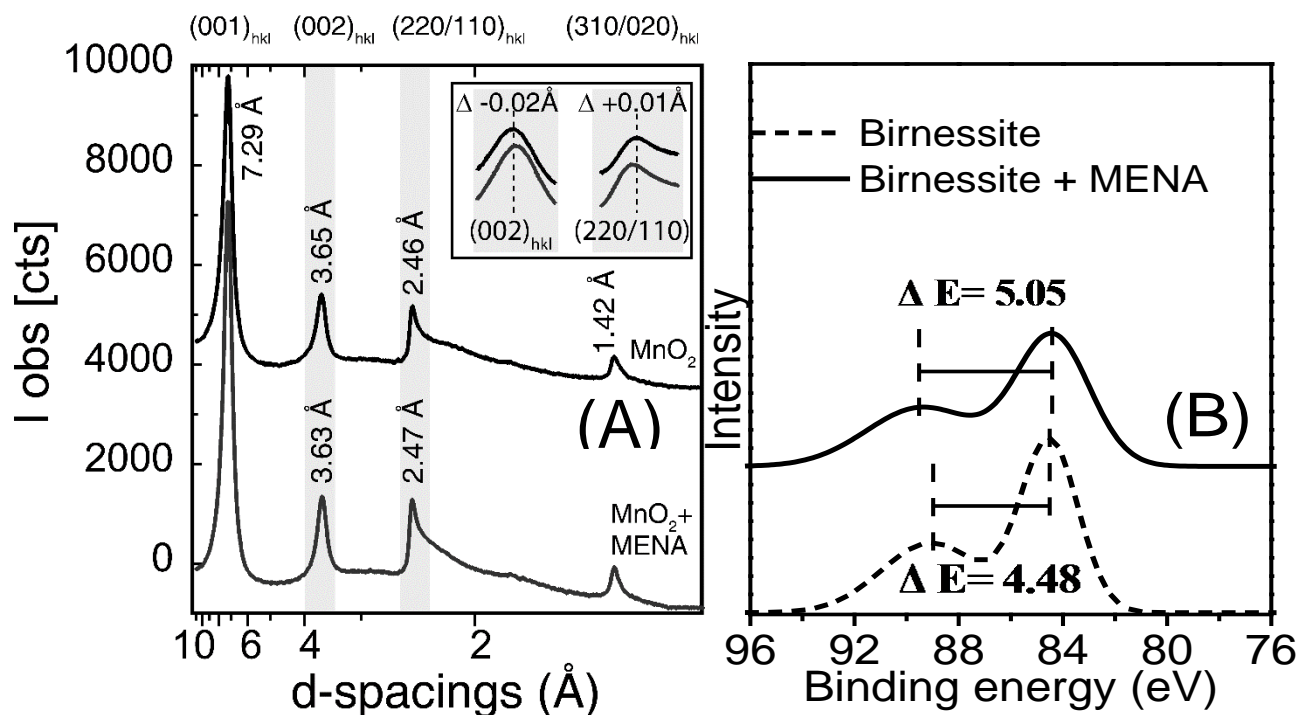


Figure 4.2-4. (A) XRD pattern of birnessite (MnO₂) and its transformation product after treatment with 1 mM MENA at pH 7. Peaks are labeled with the assigned diffracting planes (*hkl*) and d-spacing (Å). Insets are the (002) and (220/110) peaks to show the offset of the MENA reacted birnessite. (B) High resolution Mn 3s scan for unreacted and post MENA reacted birnessite (15 g kg⁻¹) at pH 7.0. The increase in binding energy difference indicates reductive dissolution of birnessite and incorporation of reduced Mn forms back to the solids. Background electrolyte = 10 mM NaCl.

4.2.5. Discussion DNAN and daughter product reaction with birnessite and ferrihydrite.

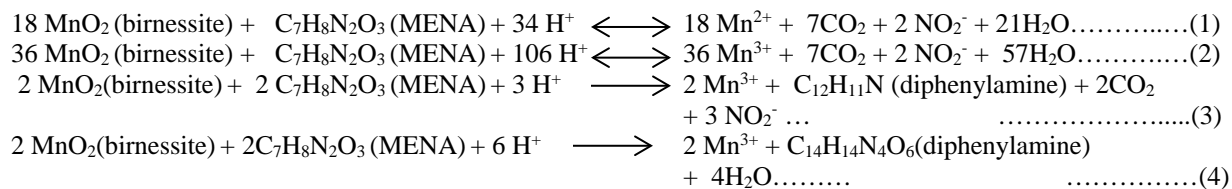
The metal oxides birnessite and ferrihydrite were tested for their reactivity with DNAN and its daughter products MENA and DAAN. The results indicate a strong dependence on mineral type and solid concentration. The parent compound DNAN was found to be stable and non-reactive with both birnessite and ferrihydrite. DNAN structure has two nitro groups in the ortho and para positions. The nitro groups in DNAN structure have a strong electronegativity resulting from the combined action of two electron withdrawing oxygen atoms bonded to the partially negative nitrogen atom¹²⁴. The nitro group strongly inhibits electrophilic substitution in the aromatic ring¹²⁵. Under reducing conditions, DNAN is found to undergo regioselective reduction to MENA, which then gets further reduced further to DAAN^{47,48,126,127}. In MENA, the ortho nitro group is replaced by an amine (-NH₂) (Table 4.2-1). The amine substituent acts as a nucleophile, where an active lone pair of electrons on the N atom are attracted to reaction with electrophilic Mn(IV) in birnessite^{26,128}. The presence of two amine groups in DAAN (Table 4.2-1) is, therefore, consistent with its faster oxidation rate by birnessite and even ferrihydrite. There have been some prior studies regarding oxidation of compounds like anilines and hydroquinone by ferrihydrite^{39,129,130}. So, DAAN may undergo abiotic oxidation by ferrihydrite. Both of the oxides (ferrihydrite and birnessite) are kinetically stable under oxic conditions. The reduction potential of ferrihydrite is approximately 0.0 eV, whereas birnessite has reduction potential of 0.6 eV^{131,132}, thus making birnessite a stronger oxidizing agent than ferrihydrite.

In our previous study⁸³, wherein MENA was reacted with goethite and birnessite, near complete removal of MENA from solution was observed upon reaction with birnessite, whereas a much lower removal, and trends consistent with surface adsorption, was observed for goethite. Others have previously compared the efficacy Mn(IV) and Fe(III) oxides for oxidation of the anilines 4-chloroaniline (4-CA), 3,4-dichloroaniline (3,4-DCA) and 3,5-DCA¹²⁹. At pH 6-7, oxidation of only 4-CA was observed, and only with Mn oxide, with no oxidation by Fe oxide. At pH 5, both 3,4-DCA and 4-CA were 65% oxidized by Mn oxide, whereas less than 5% oxidation occurred with Fe oxide; and at pH 4, 3,4-DCA, 3,5-DCA and 4-CA were completely (or nearly completely) oxidized by Mn oxide, whereas 5-15% oxidation was observed with Fe oxide. Products of oxidation were only identified when birnessite was used. Electron withdrawing groups (EWG) such as the nitro groups in MENA and DNAN increase the standard reduction potential and make the anilines less susceptible to oxidation whereas electron donating groups such as a *p*-methoxy group decrease the standard reduction potential and render the compounds more susceptible to oxidation^{68,133}. A kinetic rate study showed a *ca.* 1000-fold slower oxidation rate for *p*-nitroaniline as compared to aniline upon reaction with MnO₂ at pH 4¹³³. In contrast, oxidation of *p*-methoxyaniline was 3000-fold faster than aniline. Therefore, the progressive (bio) reduction of DNAN is expected to increase the oxidizability of the molecule, and this was reflected in the present study in terms of logarithmic impacts on the rate of oxidation.

Previous studies with non-phenolic aromatic amines such as aniline, *p*-methoxyaniline, nitroaniline and dichloroaniline indicate that the principal reaction with MnO₂ is a one-electron oxidation to a cation radical, and subsequent coupling to form azo-dimers and diphenylamines and oligomers connected by N=N and C-N bonds^{129,133}. Eventually these intermediates become polymerized as evidenced from the formation of oligomers and irreversible bound residue due to reaction of anilines with Mn in soil²⁶. No evidence of polymerized products was sought in this study, but in a previous study⁸³, some higher molar mass products were obtained from mass spectrometry data by reacting MENA with birnessite.

A unique finding in this study was that nonphenolic aromatic amines can become partially mineralized to CO₂, with yields of CO₂ ranging from 12-15%. The extent of the yield would suggest that the CO₂ was formed from one of seven C atoms in the MENA or DAAN molecule, possibly that of the methoxy group. The oxidation of methoxybenzenes by peroxidases via cation radical causes a quinone to form with the simultaneous releases of a methanol¹³⁴. A second unique finding is the high yield of nitrite formed from the oxidation of MENA by birnessite accounting for nearly all of the N in MENA. Release of N from aromatic amines has never been described previously in reactions involving metal oxides. Mineralization of the daughter products to CO_{2(g)} and NO_{2⁻(aq)} (the latter in the case of MENA) indicates partial mineralization. Mineralization of nonphenolic-aromatic amines during reaction with birnessite has never been described before. While it is well established that the carbon in phenolic compounds becomes partially mineralized during oxidation with birnessite, the major reaction is polymerization^{27,135}. We were able to recover only *ca.* 15 % CO₂ from birnessite MENA/DAAN reactions. The oxidant demand in each case of coupling for MENA and DAAN is much lower than that required for the full mineralization reaction. The rapid loss of daughter products with birnessite thus could also be attributed to formation of coupling products. The mass spec data showed complete loss of MENA (m/z 169.15) after the reaction with birnessite at 15 g kg⁻¹ SSR birnessite. The oxidative transformation of MENA could result in mineralization or oxidative coupling as observed by others for other nitroaromatic amines¹³⁶. High resolution MS spectra collected from m/z 35-1000, Da show more transformation products below 200 Da. The most dominant masses were m/z 158.0059, 116.9783, 130.0099. Relative abundance of higher mass peaks were very low. The peaks with various masses might be due to possible ring cleavage or release of substituents as observed by other researchers for contaminants reaction with birnessite^{27,136-138}.

Incomplete mineralization leading to polymerization forming diphenylamine and related coupling products can be considered as the major route of transformation for MENA with birnessite. Alternatively, complete mineralization of MENA by birnessite to CO₂ and NO_{2⁻} could be minor pathway for the reaction, yielding Mn(II) or Mn(III). The equilibrium reaction for each scenario with MENA as model example can be written as:



Although much lower aqueous Mn values are expected for the polymerization routes, measured values of Mn in solution were substantially lower than those predicted by these reactions. Aqueous Mn was 0.31 % of that calculated for Eq. 3, 0.31 % of that calculated for Eq. 4, and 0.04 % of that calculated for Eq. 1.

The XRD reflections in the control and reacted birnessite are broad, indicating poor crystallinity and/or nano-particulate crystallites. The asymmetry of the peaks is due to turbostratic stacking disorder. The ratio of the (220/110) to the (310/020) reflections is $\sqrt{3}$, indicating hexagonal layer symmetry, which is maintained after reaction with MENA. Additionally, the reflection at 1.42 Å is generally diagnostic of hexagonal layered birnessite¹³⁹. The MENA reacted birnessite shows no change in the (001) peak size, position, or shape relative to the control, indicating no distortion of the 10 Å spacing of the layered octahedral sheets. The change in the (002) and (220/110) peaks, -0.017 Å and +0.009 Å respectively, could be due to Jahn-Teller

distortion of the octahedrally coordinated $\text{Mn}^{(\text{IV})}\text{O}_6$ groups^{140,141}. The slight lengthening and sharpening of the (220/110) peak upon reaction with MENA indicates an increased ordering along the *b*-axis and lengthening along the *a*-axis of the unit cell¹³⁹. Hexagonal layered birnessite has about 0.25 cation vacancies per layer in the octahedral sheets that Mn(III) can fill either via comproportionation of Mn(II) and Mn(IV) following a two electron transfer from MENA or DAAN, or via a one electron transfer reaction. Either case results in Mn(III) occupying available vacant sites¹⁴². The affinity of hexagonal layered birnessite surface vacancies for Mn(II) adsorption and subsequent incorporation of Mn(III) into the sheets would result in the changes observed in the diffraction peaks and offers an explanation for the low recovery of aqueous phase Mn(II) after reaction with MENA.

This scenario is also consistent with the XPS data (Figure 4.2-4B), which shows a net reduction in Mn oxidation state at the birnessite surface¹³¹. The comproportionation reaction between Mn(II) adsorbed on vacant sites and the surrounding octahedrally-coordinated Mn(IV) in the layer structure to form Mn(III) formation, and the subsequent migration of the Mn(III) into vacancies with an ordered distribution in the birnessite layers has been reported recently¹⁴³, and we postulate that a similar process is occurring in our experiments, progressively altering the reactivity of the Mn oxide over time.

4.2.6. Conclusion DNAN and daughter product reaction with birnessite and ferrihydrite.

The results of this study suggest that the replacement of electron withdrawing nitro groups by amino increases the susceptibility of IMC molecules to oxidation by naturally occurring metal oxides in soil. The parent compound, DNAN, was found resistant to oxidation by both birnessite and ferrihydrite. The first daughter product MENA, resulting from substitution of an amine group for one nitro group was found reactive with birnessite but not with ferrihydrite. The second daughter product DAAN formed as a result of substitution of both the nitro groups by amines was found reactive both with birnessite and ferrihydrite, but birnessite was 6-fold more reactive. These results indicate that metal oxides in soil play a very important role in remediation of IMC daughter products in the natural environment.

4.3. Reaction of NTO and Daughter Products with Birnessite and Ferrihydrite

The results of adsorption-desorption experiments described in Section 4.1 suggested significant reactivity of IMC reduced daughter product ATO with Mn(IV) oxide. Furthermore, large irreversible loss from solution was observed for NTO reacted with goethite suggesting that such transformations may be potentially occurring as well with Fe(III) oxide. Among the most common and reactive representatives of these oxide groups are birnessite and ferrihydrite, respectively. Therefore, the objectives of this portion of the project were (i) to quantify the kinetics and extent of oxidative transformation of NTO and reduced daughter product ATO at birnessite and ferrihydrite surfaces, (ii) to distinguish such losses from strong surficial binding of the non-transformed compound, and (iii) to assess any resulting transformations in the mineral solids that accompany redox reactions.

4.3.1. Results: Oxidation assessment of NTO and ATO by birnessite

The time course results of NTO and ATO reaction with birnessite at solid-to-solution ratios (SSRs) of 15, 1.5 and 0.15 g kg⁻¹ are shown in Figure 4.3-1A, 4.3-1B and 4.3-1C, respectively. These data indicate that parent compound NTO was resistant to oxidation at all tested concentrations of birnessite for the full 3 h reaction time. However, its reduced daughter product, ATO, was subject to oxidative transformation. It was fully removed from solution after reaction with birnessite at 15 g kg⁻¹ SSR (pseudo-first order rate constant, $k \geq 90.2 \text{ h}^{-1}$) (Figure 4.3-1) with a half-life ($t_{1/2}$) of 27.5 s (Table 4.3-1). At lower birnessite concentrations of 1.5 g kg⁻¹ ($k=3.03 \text{ h}^{-1}$) and 0.15 g kg⁻¹ ($k=0.04 \text{ h}^{-1}$), reaction kinetics were slower for ATO (Panels B and C in Figure 4.3-1), and the reaction rate was pseudo-first order in ATO concentration at any given SSR (Table 4.3-1). The reaction rate was linearly dependent on birnessite concentration in log-log space (Figure 4.3-2).

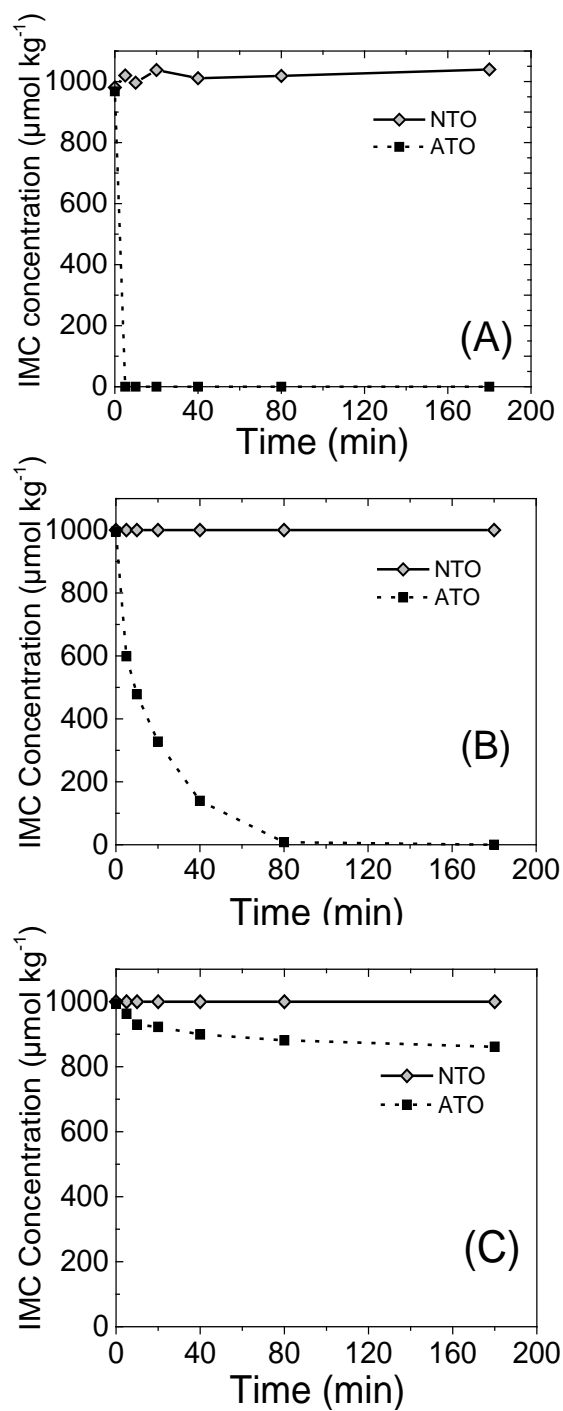


Figure 4.3-1. Transformation of IMCs by birnessite at (A) 15 g kg^{-1} , (B) 1.5 g kg^{-1} and (C) 0.15 g kg^{-1} solid to solution ratio at pH 7.0.

Table 4.3-1. First order rate constants (k) of ATO oxidation by birnessite and NTO/ATO adsorptive removal by ferrihydrite supplied at various concentrations.

Mineral Surface	Solid to Solution Ratio (SSR), g kg ⁻¹	1 st Order Rate Constants (<i>k</i> , h ⁻¹)			
		NTO	ATO	t _{1/2} (NTO), h	t _{1/2} (ATO), h
Birnessite					
	0.15	0.00	0.04 (0.70) [†]	N/A	17.9
	1.50	0.00	3.03 (0.99)	N/A	0.23
	15.0	0.00	≥ 90.2 (N/A) ^{***}	N/A	0.01
Ferrihydrite					
	0.15	0.03 (0.23)	0.12 (0.83)	20.49	5.9
	1.50	0.05 (0.22)	0.19 (0.86)	14.71	3.6
	15.0	10.40 (N/A) ^{***}	0.07 (0.49)	0.07	10.6

0.00 means no measurable reaction in 3h.

^{***} value estimated by slope of first two data points only, as concentration reached zero at second sampling point (5min/15min). The rate is even higher than estimated as actual reaction end point might be less than five minutes and is denoted by \geq in the table. N/A Not applicable

[†]Values in parentheses are R^2 values for the regression fit.

$t_{1/2}$ = half-life of reaction

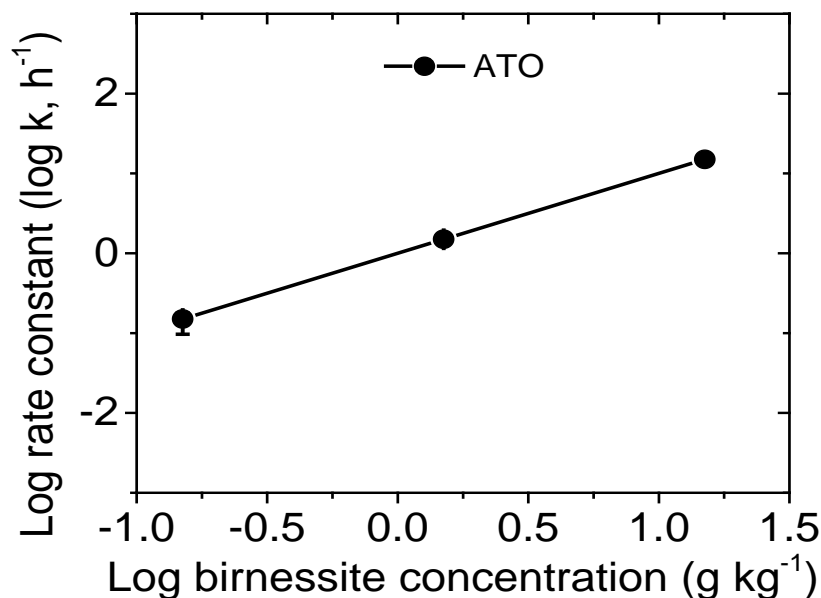


Figure 4.3-2. Log plots for ATO reaction with birnessite at 0.15, 1.5 and 15 g kg^{-1} solid to solution ratio. The error bars indicate 95 % confidence interval.

The birnessite experiment conducted to measure N_2 and CO_2 evolution under oxic conditions revealed mineralization of nearly half (47.8%) of ATO nitrogen to N_2 and slightly more than half (51.5%) of ATO carbon to CO_2 (Figure 4.3-3) at 15 g kg^{-1} SSR. Neither birnessite-free NTO controls nor compound-free birnessite controls produced N_2 and/or CO_2 . After the reaction we were able to recover less than 8 % of total N in the form of total inorganic ionic N species (NH_4^+ , NO_3^- and NO_2^-) at 15 g kg^{-1} SSR with IC. Further investigation on reaction products formed by LC- MS/MS revealed urea as a major transformation product that accounted for nearly 44 % of ATO lost from the solution (Figure 4.3-3). The transformation of ATO was also measured in the absence of dissolved oxygen (Figure 4.3-4) and the extent of ATO transformation was unaffected. Evidently, oxygenated conditions are not required for the oxidative transformation of ATO by birnessite.

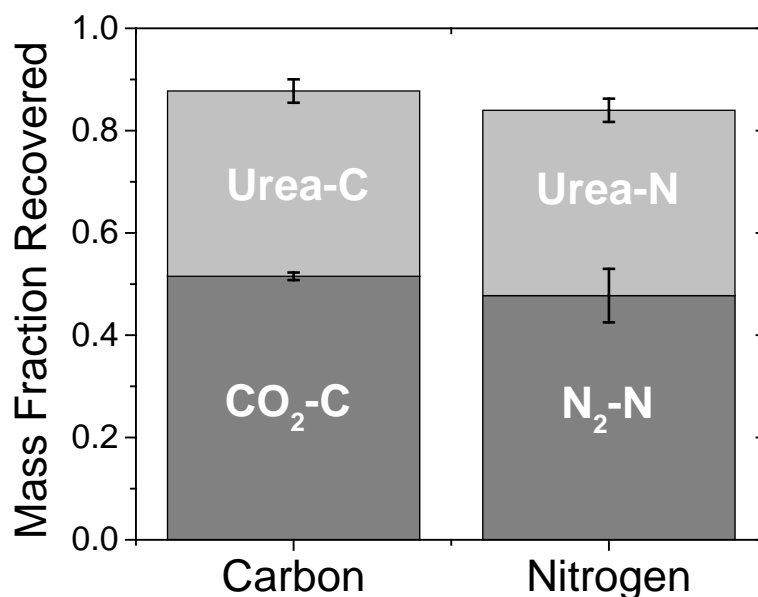


Figure 4.3-3. The fractional conversion of ATO carbon and nitrogen to detected products including total inorganic carbon ($CO_{2(g)}$ + dissolved carbonate species, indicated here by CO_2 -C), $N_{2(g)}$, and urea following incubation with birnessite at 15 g kg^{-1} solid to solution ratio over a 3 h period with 20% headspace O_2 .

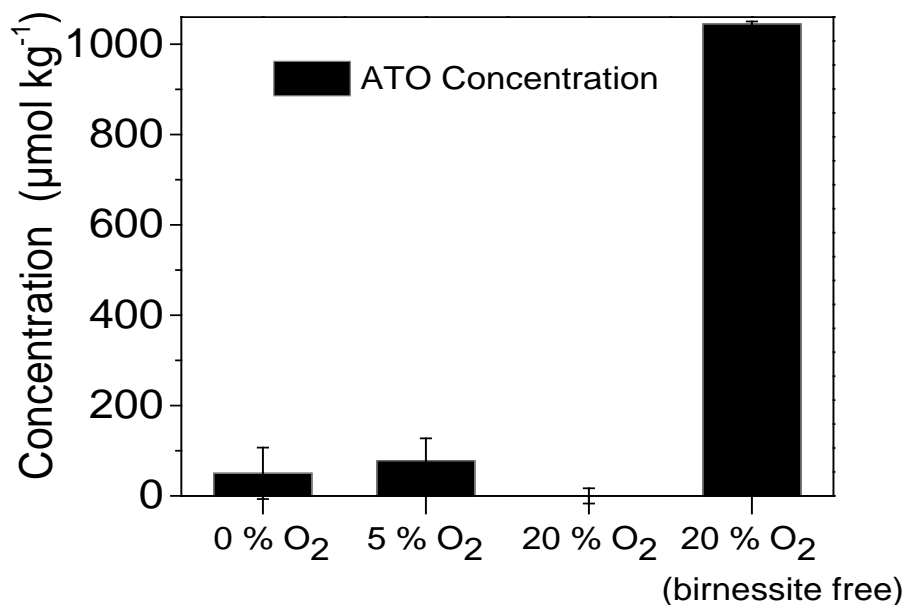


Figure 4.3.4. ATO remaining in solution upon reaction with birnessite at 15 g kg⁻¹ solid to solution ratio over a 3 h incubation period with 0, 5 and 20% O₂ in the headspace with He.

4.3.2. Results: Adsorption of IMCs to ferrihydrite:

There was an initial decrease in solution phase NTO concentration upon reaction with ferrihydrite that occurred within the first 15 min, which raised the question of whether ferrihydrite was also an effective oxidant of NTO. At the two lower SSR values (0.15 and 1.5 g kg⁻¹) the initial decrease was followed by a plateau in concentration after the first sampling time-point. At 15 g kg⁻¹ SSR, there was complete loss of NTO from solution. For ATO, the loss from the solution with ferrihydrite at 0.15, 1.5 and 15 g kg⁻¹ SSR increased with reaction time. However, further investigation through desorption experiments indicated that both NTO and ATO were adsorbed to the surface of ferrihydrite (Figure 4.3-5).

For NTO, at 15 g kg⁻¹ SSR, there was complete loss from the solution during an initial 3 hour reaction step. An initial desorption step with CaCl₂ brought no NTO into solution (Figure 4.3-5). However, a second desorption step with Na₂HPO₄ released 80 % of NTO back into solution, indicating strong adsorption to the surface. Similarly, for ATO there was about 40 % of ATO removed from solution upon 3 hour reaction, but subsequent desorption with CaCl₂ and Na₂HPO₄ was able to return nearly all of the ATO back to solution (Figure 4.3-5).

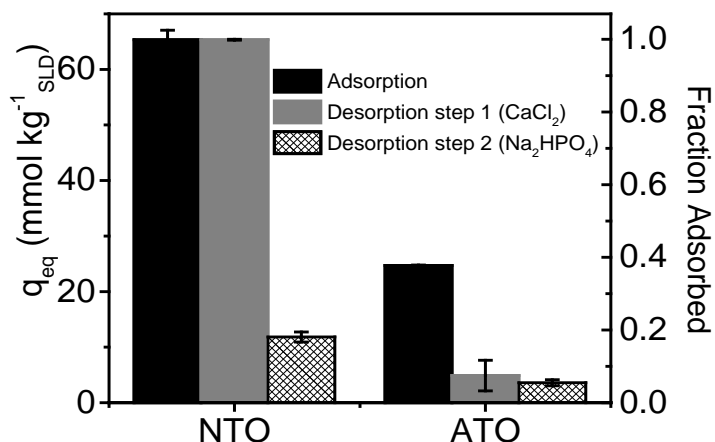


Figure 4.3-5. Adsorption/desorption and fractional plots of NTO and ATO to ferrihydrite surface. Left axis q shows the mass of sorbed IMC per unit mass of solid at equilibrium. Right axis shows fraction of IMC sorbed to ferrihydrite surface at various steps.

4.3.3. Results: Reductive transformation of birnessite:

High resolution Mn3s X-ray photoelectron (XPS) spectra for unreacted- and ATO-reacted birnessite are shown in Figure 4.3-6. As discussed in the previous section, the magnitude of peak splitting for Mn3s high resolution spectra is distinctive for Mn oxidation state. The unreacted birnessite has a binding energy difference between the Mn3s splitting multiplex of 4.5 eV, whereas for birnessite reacted with ATO, the binding energy difference between Mn3s splitting multiplex is 4.63 eV. This indicates reduction of birnessite Mn (IV) to a mixture of Mn (II, III and IV). The Mn shift towards higher binding energy indicates reductive transformation of birnessite with incorporation or retention of reduced Mn forms in the solid phase. The yield of soluble Mn(II) was much less than that calculated based on stoichiometric conversion of birnessite Mn(IV) to soluble Mn(II) during reaction with IMC daughter products. For ATO, only $19.27 \mu\text{g kg}^{-1}$ of Mn(II) was recovered from solution respectively at the end of 3 hour reaction.

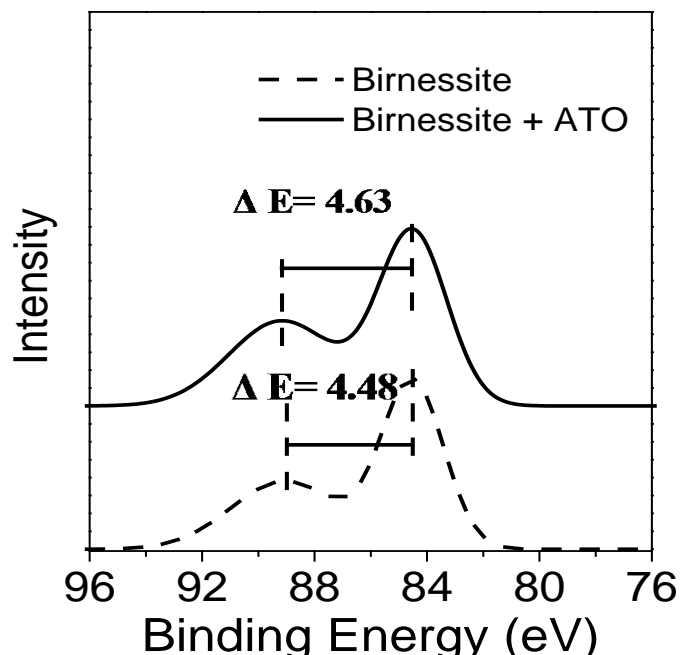


Figure 4.3-6. High resolution Mn 3s scan for unreacted and post ATO reacted birnessite (15 g kg^{-1}) at pH 7.0. The increase in binding energy difference indicates reductive dissolution of birnessite and incorporation of reduced Mn forms back to the solids.

4.3.4. Discussion: Oxidation assessment of NTO and ATO by birnessite

The mineral-surface mediated oxidation of heterocyclic IMC compounds was dependent on the compound structure itself, mineral type, and the metal oxide solid concentration. Reduction of the NTO nitro group is expected to enhance the tendency for organic compound oxidation by metal oxides because the presence of electron withdrawing nitro groups inhibits oxidation¹⁴⁴. This was observed in the current study as NTO was not oxidized by the metal oxides under any condition tested; however, ATO was rapidly oxidized by birnessite at all SSR tested.

This was the first study showing oxidative transformation of ATO by birnessite. Electron withdrawing nitro groups increase the standard reduction potential and make the compounds less susceptible to oxidation whereas electron donating amine groups decrease the standard reduction potential and make the compounds more susceptible to oxidation^{68,132,133,144}. A kinetic rate study showed a *ca.* 1000-fold slower oxidation rate for *p*-nitroaniline as compared to aniline upon reaction with MnO_2 at pH 4¹³³, whereas oxidation of *p*-methoxyaniline was 3000-fold faster than aniline. The nitroaromatic and aromatic amines can be easily oxidized either via mineralization or polymerization under aerobic conditions¹⁴⁵.

Ferrihydrite was not able to oxidize either NTO or ATO under the tested conditions; however, birnessite was capable of oxidation of ATO. The data from this study are consistent with the fact that birnessite is a stronger oxidizing agent than ferrihydrite; the standard reduction potential of ferrihydrite with $\text{Fe}^{2+}_{(aq)}$ as a product is approximately 0.0 eV, whereas the standard reduction potential of birnessite with $\text{Mn}^{2+}_{(aq)}$ as a product is 0.6 eV^{132,146}. The faster reaction rate with

birnessite can be attributed to its oxidation capacity that induced heterocyclic ring cleavage and mineralization of ATO to urea, N₂ and CO₂. First order rate constants showed strong log-log dependence with SSR (Figure 4.3-2) for ATO. Hence, even though the solid phase concentration of Mn oxides is lower than Fe oxides in soil environments, the former are such potent oxidants that their impact on oxidizing organic amines is likely greater than is the case for the more prevalent Fe oxides.

While we are not aware of prior studies that compared directly the reactivity of Fe(III) and Mn(IV) oxides toward oxidation of N-heterocyclic compounds, there have been direct comparisons pertaining to aromatic amines. For example, prior work showed higher reactivity of birnessite relative to Fe(III) oxyhydroxide for oxidation of 4-chloroaniline (4-CA), 3,4-dichloroaniline (3,4-DCA) and 3,5-DCA¹²⁹. At pH 6-7, Mn oxide was capable of oxidation of 4-CA only but there was no oxidation by Fe oxide. At pH 5, both 3,4-DCA and 4-CA were 65% oxidized by Mn oxide, but less than 5% oxidation occurred with Fe oxide; and at pH 4, 3,4-DCA, 3,5-DCA and 4-CA were near completely oxidized by Mn oxide, whereas 5-15% oxidation was observed with Fe oxide. Our results for NTO and ATO are comparable to those reported above for DNAN and MENA that indicated oxidative removal only of MENA (not of DNAN), and only in the presence of birnessite (not ferrihydrite)⁸³.

The fact that measured values of Mn in solution were substantially lower than those predicted by the stoichiometry leading to Mn²⁺ as a product are consistent with the reincorporation of Mn into the solid phase. Specifically, total aqueous Mn amounted to only 0.18 % of that predicted from reduction of birnessite to Mn²⁺. The low recovery of aqueous Mn(II) indicates resorption of reduced Mn at the surface and incorporation into birnessite. Indeed, as evident from the XPS data, the increase in binding energy for ATO-reacted birnessite indicates reduction of birnessite, dominated by Mn (IV), to a mixture of Mn redox states (II, III and IV). Initial adsorption of Mn(II) or Mn(III) to the birnessite surface is promoted by its structural charge (resulting from Mn(IV) vacancy sites) and low pH of zero net proton charge.

Further indications of birnessite transformation during ATO reaction derive from XRD data, but in this case, changes are more subtle. Reflections in the control and ATO-reacted birnessite are broad and asymmetric, indicating poor crystallinity and/or nano-particulate crystallites and turbostratic stacking disorder. The hexagonal layer symmetry of birnessite is maintained post reaction. The (001) reflection (along the c-axis) of the ATO-reacted birnessite shows a slight change in peak width and position indicating a small distortion of the 10 Å spacing of the layered octahedral sheets. If the change were due only to Jahn-Teller distortion of the octahedrally-coordinated Mn^(IV)O₆ groups, a lengthening of the *a*-axis would have been noted by an increase in the *d*-spacing (220) reflection^{140,141}. However, no change in the short range *d*-spacing reflections at 2.46 Å were observed. The slight shift of the (001) peak can thus be attributed to a slight compression of the interlayer separation accompanied by a narrowing of the (001) peak, observed as a slight decrease in FWHM from 0.508 Å to 0.466 Å after reaction, and a small decrease in the ratio of the peak-height to peak-area from 1.17 to 1.29 after reaction with ATO. The narrowing of the (001) peak indicates slightly larger crystallite sizes after reaction, estimated *ca.* 11 nm to 12 nm using the Scherer equation¹⁴⁷. We postulate that this is due to re-adsorption of released Mn(II) and subsequent comproportionation with structural Mn(IV). During oxidative transformation of ATO, birnessite undergoes reduction to a Mn(III/II)-bearing phase as observed by XPS. Indeed, our results are consistent with a comproportionation reaction between Mn(II) adsorbed to vacancy sites and the surrounding layer Mn(IV) to form Mn(III), followed by migration of Mn(III) into

vacancies, accompanied by an ordered distribution in the birnessite layers, as has been reported recently ¹⁴³.

4.3.5. Discussion: Adsorptive loss from solution with ferrihydrite

There was no adsorption of NTO to birnessite. Birnessite has a point of zero net charge of 1.9 and thus was negatively charged at all experimental pH values for this study ¹⁴⁸. As a result of labile N-H bonds that undergo dissociation above the pKa (3.14) ¹⁴⁹, the NTO molecule is anionic in bulk solution at the experimental pH (7.0). NTO has a nitro group in the structure, and the oxygen atoms in the nitro group are electron withdrawing and hence exhibit a negative polarity. Charge repulsion between NTO and birnessite resulted in negligible adsorptive uptake to the surface.

Conversely, there was adsorptive loss of NTO and ATO upon reaction with ferrihydrite. For NTO, at the two lower SSR values (0.15 and 1.5 g kg⁻¹) the initial decrease was followed by a plateau in concentration after the first sampling time-point, and there was complete loss from the solution at 15 g kg⁻¹ ferrihydrite, which is consistent with prior studies conducted with goethite ⁸³. NTO was difficult to remove from the ferrihydrite surface with CaCl₂ but it underwent nearly complete desorption upon reaction with Na₂HPO₄ indicating very strong affinity, likely retention via inner sphere complexation.

4.3.6. Conclusion: Reaction of NTO and Daughter Products with Birnessite and Ferrihydrite

This study aids in understanding the fate of parent compound NTO and its daughter product ATO on mineral surfaces. NTO was resistant to oxidation by both the birnessite and ferrihydrite at the tested concentrations. However, NTO was strongly adsorbed to the ferrihydrite surface, indicating an important potential mechanism for its attenuation in soils. ATO was also found to adsorb to the ferrihydrite surface but more weakly than NTO. However, ATO, which is readily produced from NTO in suboxic soil microsites by reduction of the nitro group to amine, was found to be highly reactive with birnessite. The reaction of ATO with birnessite results in its transformation to urea, N₂ and CO₂, indicating complete breakdown to safe end products.

4.4. Reduction of IMCs with Green Rust

4.4.1. Results and discussion: reduction with green rust

Both the parent compounds NTO and DNAN were susceptible to reduction by green rust at 10 g kg⁻¹ solid to solution ratio (SSR) (Figure 4.4-1). NTO was reductively transformed stoichiometrically to its corresponding amine daughter product, ATO, by green rust (Figure 4.4-1A). The reaction of NTO with green rust was faster than DNAN, nearly complete in 10 min, and NTO was not detectable at 20 min after reaction initiation. To the best of our knowledge, this is the first report of NTO reduction by a naturally-occurring mineral. The presence of the nitro group on the heterocyclic structure causes strong electron deficiency in the ring and surplus electron density on the nitro group, making the latter a favorable site for reduction by structural Fe(II) of green rust, leading to transformation to ATO. Research conducted on NTO with bimetallic Fe/Cu and Fe/Ni (solid to solution ratio of 1%) at pH 3 suggested NTO loss from the solution in one hour but no reduction products were reported¹⁵⁰. The product ATO has been also observed to form from microbially-mediated reduction of NTO^{16,82}. In an anaerobic soil microcosm study with H₂ added as electron donor, a stoichiometrically proportionate amount of ATO (95.3 %) was recovered from NTO biodegradation⁸².

DNAN was also reductively transformed, initially forming both iMENA and MENA. The reduction occurred with a staggered regioselectivity. Over the first 10 min, the *para*-nitro group of DNAN was selectively reduced, generating iMENA. Thereafter the *ortho* nitro group was preferentially reduced, generating MENA. Both iMENA and MENA subsequently transformed to the final reduction product DAAN within 1 d (Figure 4.4-1B). Previous research reported initial *biological* reduction of DNAN was regioselective favoring the nitro group in the *ortho* position to yield MENA^{48,126,127,151} before reduction of the second nitro-group to yield DAAN^{126,127,151}. Previous studies evaluated DNAN reduction with ZVI wherein it was converted to MENA^{47,152-154}, iMENA^{153,154} and DAAN^{47,152-154}. Most of these studies report only a small fraction of iMENA products. The formation of MENA is favored^{47,153}. However in the PAX-101 study, both MENA and iMENA are formed as important intermediates¹⁵⁴, which suggests a non-regioselective reduction of both *ortho*- and *para*-nitro groups of DNAN. The staggered regioselectivity of *para*- and *ortho* nitro-groups observed with green rust is unique. The relative differences in reduction of nitro group might also be due to the methoxy group substituent effect. Methoxy groups are electron supplying groups and the initial substitution favoring to *para* position as compared to *ortho* position may be due to steric hindrance by methyl group. Like DNAN, other aromatic compounds with multiple nitro-groups cause a strong electron deficiency in the carbon skeleton and increased electron density in nitro groups favoring their reductive biotransformation^{127,155-157}.

The initial abiotic reduction of nitro groups to amine is a major step in (bio) transformation of IMCs because of their inherent resistance to oxidation under oxic environment. The formation of aminated daughter compounds are found to show reactivity with soil minerals like birnessite and further transformed via polymerization or mineralization pathways^{83,132}. The daughter compounds MENA and ATO were found oxidatively removed from the solution by birnessite in our previous study⁸³ and also as discussed in the above sections. The oxidative removal of MENA from solution upon reaction with birnessite have been observed by other researchers as well¹³². Mineralized safe end products like N₂, CO₂, NO₂⁻ have been observed for these reduced IMCs upon reaction with birnessite. Also, biotransformation of reduced IMCs have been observed in incubation studies in sludge¹²⁷ and soils^{82,126}. So, initial reduction of the parent

IMCs by green rust is potentially very important from remediation point of view and this is the first study reporting reduction of new IMCs by green rust.

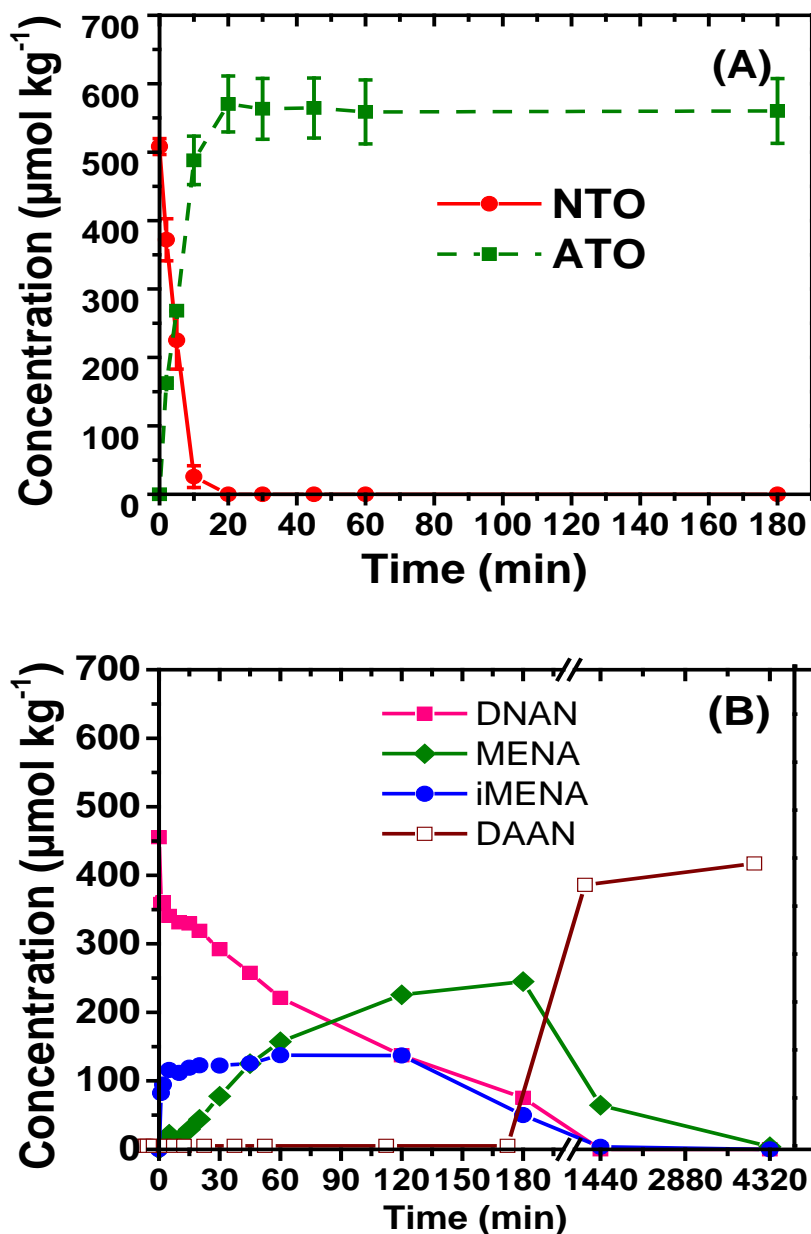


Figure 4.4-1. Transformation of IMCs (A) NTO and (B) DNAN by sulfate green rust at 10 g kg⁻¹ solid to solution ratio at pH 8.4.

The normalized absorbance and first derivative Fe-XANES spectra collected from reacted samples indicate oxidation of green rust to a lepidocrocite (γ -Fe^(III)O(OH))-like species during reductive transformation of DNAN and NTO, which was more evident in the case of NTO as compared to DNAN (Figure 4.4-2). Fe-XANES results show a clear shift of oxidation state from

$\text{Fe}^{\text{II}}/\text{Fe}^{\text{III}}$ (green rust) to Fe^{III} (lepidocrocite) upon reaction with IMCs. The LCF data suggested lepidocrocite-like mineralogy accounts for 94% of iron product with NTO and 62% with DNAN after reaction (Figure 4.4-2), consistent with the faster reductive transformation of NTO relative to DNAN (Figure 1). Green rust has been observed as a reactive intermediate in ZVI¹⁵⁸⁻¹⁶³ contaminant removal systems with the eventual formation of lepidocrocite as the final end product of green rust oxidation^{158,164}. Sulfate green rust is found to transform into lepidocrocite like form depending on pH and oxidation rate unlike the carbonate green rust which tends to form goethite like forms^{164,165}. Green rust is capable of reductive transformation of IMCs to their respective amines under anaerobic condition at the expense of being oxidized to lepidocrocite during the process.

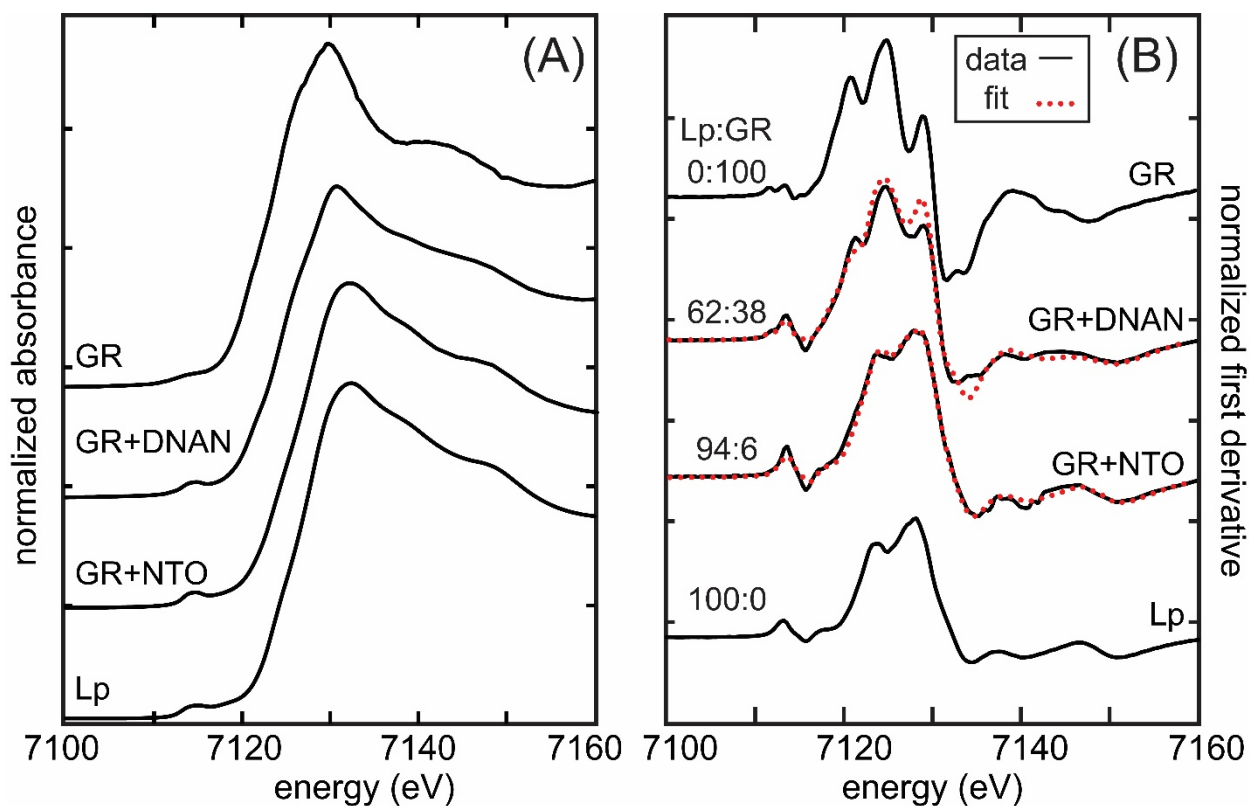


Figure 4.4-2. Normalized absorbance (A) and normalized first derivative (B) Fe K α XANES spectra of pre- and post-reaction sulfate green rust (GR) with IMCs DNAN and NTO. Relative oxidation of GR and transformation to lepidocrocite (Lp) was examined by fractional convolution of reference spectra using linear combination fits (LCF) of reacted samples to reference compounds. Data are shown in black, fractional fits are shown in dots. Results show clear shift of oxidation state from mixed valent $\text{Fe}^{\text{II}}/\text{Fe}^{\text{III}}$ (green rust) to Fe^{III} (lepidocrocite) upon reaction with IMCs.

4.4.2 Conclusion: reduction with green rust

Green rust is capable of reductive transformation of IMCs to their respective amines and is oxidized in the process to lepidocrocite. The transformation of DNAN and NTO to reduced, aminated daughter products as mediated by the green rust mineral surface is of importance for the geochemical transformation of these compounds in soil. This study also adds insight into the mechanism of contaminant transformation by reaction with ZVI where green rust is a major intermediate product formed driving the reductive transformation. Treatment of IMCs with green rust could be a useful technique for abiotic transformation of munition compounds.

4.5. Pathways of Reductive 2,4- DNAN Biotransformation in Sludge

Recent studies have begun to evaluate DNAN biotransformation under anaerobic⁴⁶ and aerobic⁴⁸ conditions, and some biotransformation metabolites have been elucidated. In the present study, we assessed DNAN biotransformation using mixed microbial cultures (*i.e.*, aerobic and anaerobic sludge) under aerobic, microaerophilic, and anaerobic conditions. Our aims were to compare DNAN biotransformation rates as a function of redox conditions, as well as to determine important biotransformation products. Our results confirmed that DNAN underwent biotransformation under all redox conditions investigated, and that conversion of the nitroaromatic compound was greatly enhanced under reducing conditions. A combination of ultra-high performance liquid chromatography coupled to triple quadrupole mass spectrometry (UHPLC-MS) and high-resolution time of flight mass spectrometry (TOFMS) allowed identification of seven new metabolites which are described here for the first time, and enabled elucidation of new biotransformation pathways.

4.5.2. Results: Aerobic conditions

The DNAN biotransformation rate under fully aerobic conditions was very low (Figure 4.5-1). Under the best condition (with cosubstrate addition), almost 700 h was required to remove most (87%) of the added DNAN. In the endogenous treatment, only 40% of the nitroaromatic compound was converted in the same time period. In the control with heat-killed sludge, only very minor conversion of DNAN occurred.

Based on HPLC-DAD analysis, MENA and DAAN were identified as products of DNAN biotransformation. In the killed sludge control and the endogenous treatments (no cosubstrate), an initial small decrease in DNAN occurred that may have been due to sludge adsorption. Thereafter, the mass balance indicates that further decreases in DNAN were accounted for by increases in the products; MENA and DAAN. After approximately 700 h, about 8% and 22% of DNAN was transformed to MENA and DAAN in the heat-killed sludge and endogenous treatments, respectively. In the treatment amended with acetate, conversion of DNAN to MENA and DAAN occurred from the start of the experiment. After 700 h, about 35% and 17% of DNAN was transformed to MENA and DAAN, respectively. The mass balance was not complete in the cosubstrate-amended treatment, since 40% of the DNAN originally added could not be accounted for by the chemical species detected with the HPLC-DAD.

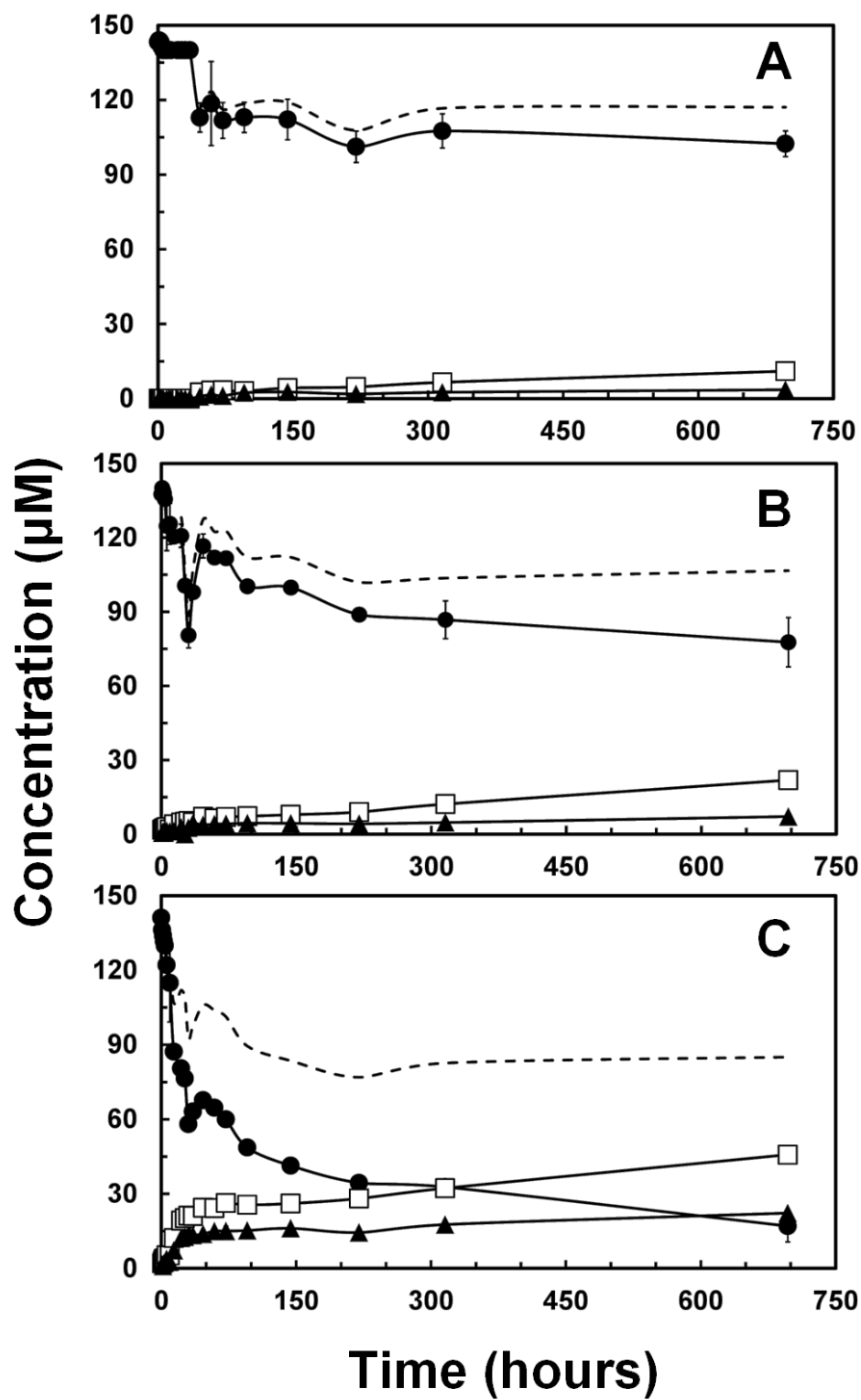


Figure 4.5-1. Aerobic biotransformation of DNAN (●) into MENA (□) and DAAN (▲). Panels: heat-killed sludge (A), live sludge (B), and live sludge supplemented with acetate as co-substrate (C). The dotted dashed line shows the molar sum of the three compounds.

4.5.3. Results: Microaerophilic aerobic conditions

Under microaerophilic conditions, the biotransformation of DNAN was much faster in all treatments (Figure 4.5-2) compared to the fully aerobic condition. In this case, the endogenous and cosubstrate treatments behaved similarly with 80% removal of DNAN in 35 and 52 h, respectively. In the treatments with live sludge, DNAN conversion was notably faster than with heat-killed sludge where only 8% of DNAN was transformed to other compounds during the whole experimental period of 150 h.

MENA and DAAN were also found with HPLC-DAD as the two main metabolites of DNAN biotransformation. MENA was the dominant product occurring in a 3:1 molar ratio compared to DAAN. After incubating for 20 h, the sum of the molar concentrations of DNAN (57 μM), MENA (47 μM), and DAAN (21 μM) was stable and nearly equal to the initial added concentration of DNAN (130 μM). The gap between initial added DNAN and the sum of the final compounds could be due to sludge sorption or to biomineralization. Thus it can be said that DNAN is transformed almost stoichiometrically under microaerophilic conditions to MENA and DAAN. In the treatment with heat-killed sludge, MENA was almost the only product formed.

4.5.4. Results: Anaerobic conditions

Under anaerobic conditions, the DNAN biotransformation occurred considerably faster and a higher conversion was observed compared to the aerobic and microaerophilic conditions (Figure 4.5-3). In the treatment with H_2 as cosubstrate, DNAN was nearly fully converted within 12 h. In the endogenous treatment, an almost complete conversion required only 33 h. The heat-killed sludge treatment also retained reducing capacity, converting 88% of the added DNAN by the end of the experimental period of 48 h.

According to the time course of biotransformation products (Figure 4.5-3), about 75% of DNAN was transformed to MENA in the heat-killed sludge. In the endogenous treatment, about 70% of DNAN was transformed to MENA in 33 h. Afterwards, MENA started to decrease and was transformed into DAAN. In the H_2 supplemented treatment, about 28% of DNAN was transformed to MENA during the first 12 h. Thereafter, MENA started to be transformed to DAAN as well. The mass balances in the endogenous and H_2 -supplemented treatments with live sludge were very poor. At the end of the experiment, the identified products only accounted for approximately 50% and 20% of the DNAN added at the start of the experiment, respectively, suggesting the formation of other biotransformation products that were not detected by HPLC-DAD or reaction of the aromatic amines with the natural organic matter in the anaerobic sludge.

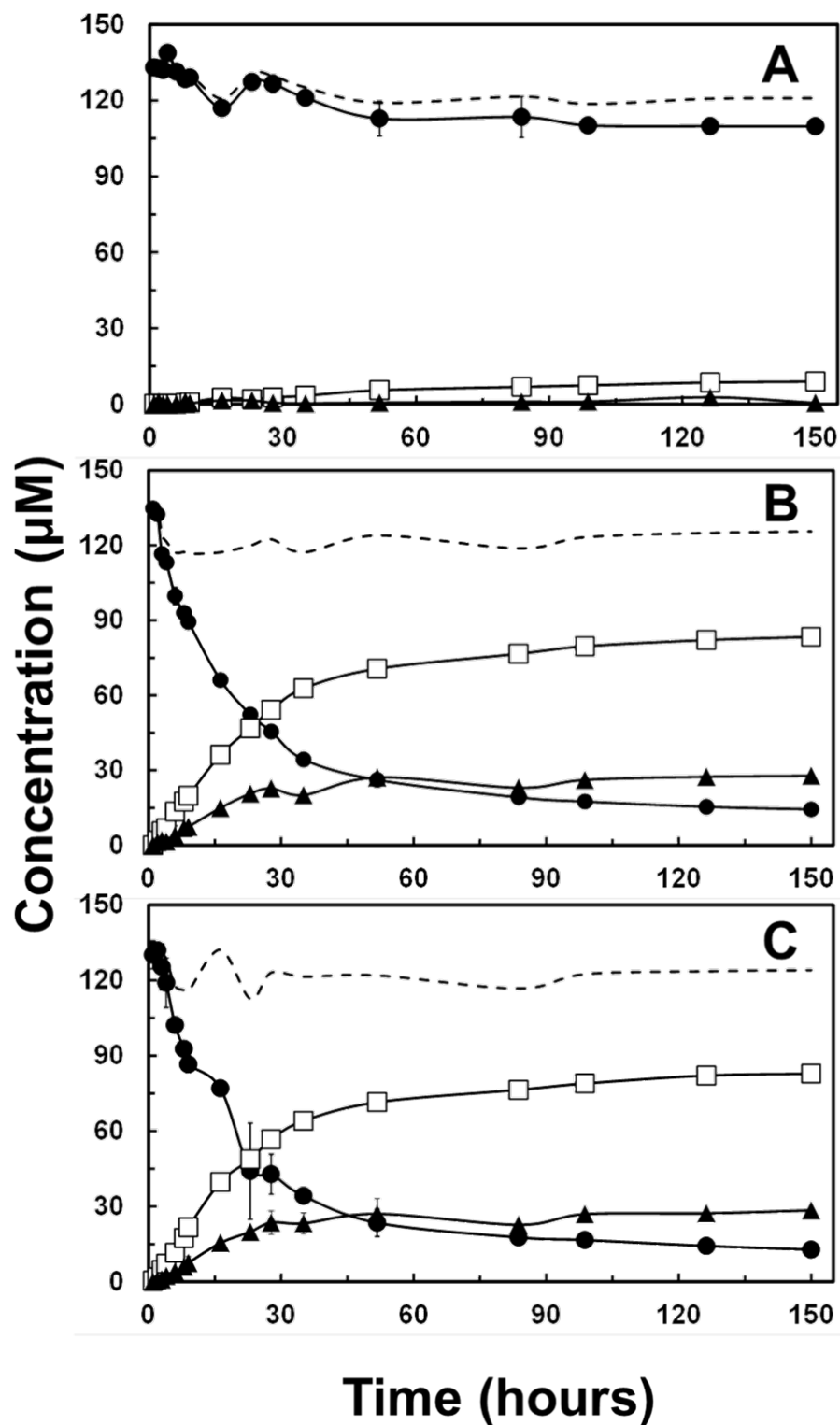


Figure 4.5-2. Microaerophilic biotransformation of DNAN (●) into MENA (□) and DAAN (▲). Panels: heat-killed sludge (A), live sludge (B), and live sludge supplemented with acetate as co-substrate (C). The dotted dashed line shows the molar sum of the three compounds

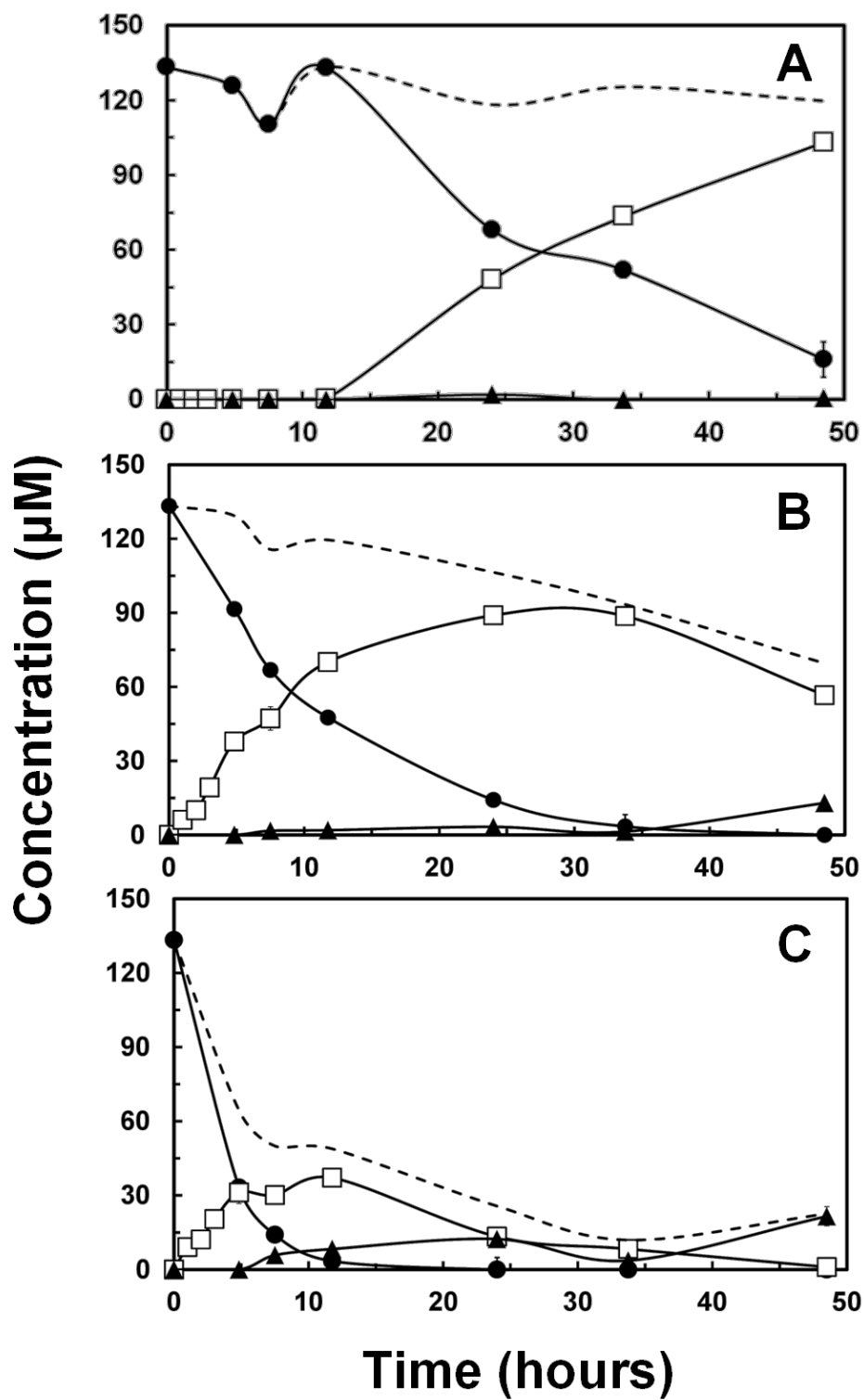


Figure 4.5-3. Anaerobic biotransformation of DNAN (●) into MENA (□) and DAAN (▲). Panels: heat-killed sludge (A), live sludge (B), and live sludge supplemented with H₂ as co-substrate (C). The dotted dashed line shows the molar sum of the three compounds

4.5.5. Results: Rates

Zero-order DNAN conversion rates under the different redox conditions are shown in Figure 4.5-4 and are representative of initial linear DNAN biotransformation during the first hours. Aerobic and microaerophilic conditions are directly comparable since both used the same inoculum, RAS. However, the anaerobic treatment had an anaerobic inoculum (AGS). The DNAN biotransformation rate increased as the redox conditions shifted from aerobic to anaerobic. The highest initial DNAN biotransformation rate of $16.4 \mu\text{mol}\cdot\text{L}^{-1} \text{ h}^{-1}$ was observed in the anaerobic bioassay with H_2 as cosubstrate. It was approximately 4.2 and 9.4 times higher than those observed in the microaerophilic and aerobic conditions with acetate as cosubstrate. The endogenous, anaerobic biotransformation rate was $8.8 \mu\text{mol}\cdot\text{L}^{-1} \text{ h}^{-1}$, which is 1.9 and 43.2 times higher than those observed in the endogenous microaerophilic and aerobic conditions, respectively. Considering specific biotransformation rates per unit of added volatile suspended solids (VSS), the rates in the live sludge had the same order of magnitude for the anaerobic and microaerophilic sludge (see data listed in caption of Figure 4.5-4).

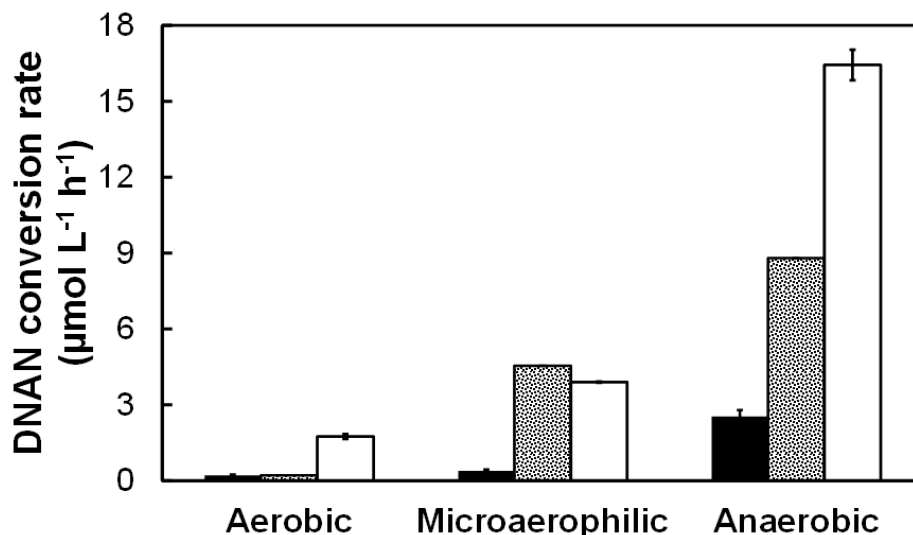


Figure 4.5-4. Comparison of the DNAN biotransformation rates in different redox conditions. Treatments: heat-killed sludge (■), endogenous (▨), and cosubstrate (□). Expressed per unit of added biomass, the DNAN biotransformation rates in heat-killed sludge, endogenous and cosubstrate treatments were as follows (in $\mu\text{mol}\cdot\text{h}^{-1} \text{ g}^{-1} \text{ VSS}$): anaerobic (0.16, 5.86 and 11.0), microaerophilic (0.10, 9.08 and 7.79), and aerobic assays (0.08, 0.41 and 3.49).

4.5.6. Results: Identification of metabolites

An additional experimental incubation was carried out to identify intermediates in the anaerobic culture using mass spectrometry. The anaerobic sludge supplemented with H_2 was spiked several times with DNAN to generate enough products to facilitate their analysis.

UHPLC-MS analysis of the products showed a protonated molecular mass $[\text{M}+\text{H}]^+$ at m/z 169 and 139 Da matching formulas of $\text{C}_7\text{H}_8\text{N}_2\text{O}_3$ and $\text{C}_7\text{H}_{10}\text{N}_2\text{O}$. They were also identified with the precursor-transitions: $169>154$ and $169>123$ for MENA (**2**; Figure 4.5-5) and $139>107$ for DAAN (**5**; Figure 4.5-5). In addition, MENA and DAAN were also confirmed with analytical standards using HPLC-DAD based on retention times. Other compounds detected with UHPLC-

MS and TOFMS included azo dimers (**7**, **10**, **11**, **12**, and **13**; Figure 4.5-5), hydrazine dimers (**8** and **14**; Figure 4.5-5), as well as intermediates wherein a primary amine was alkylated with methyl (**11**; Figure 4.5-5), methylene (**10** and **11**; Figure 4.5-5) and acetyl (**9**; Figure 4.5-5) moieties. Dimers were also observed showing evidence of O-demethylation (**12**; Figure Sludge5) and subsequent dehydroxylation (**13**; Figure 4.5-5) of the methoxy group. Chemical structures were deduced from molecular formulae determined using Formula Finder 2.0.2.0 wherein monoisotopic masses were measured. The structures were determined based on high resolution molecular formulae in concert with interpretation of possible chemical reactions that nitroaromatics are known to undergo. MENA, DAAN, as well as other compounds found are reported in Table 4.5-1. The chemical structures and mass spectra recorded for these metabolites can be found in the Supporting Data of the corresponding publication¹⁶⁶.

The retention times and measured and predicted exact masses determined for the various compounds in the UHPLC-MS analysis are reported on Table 4.5-1.

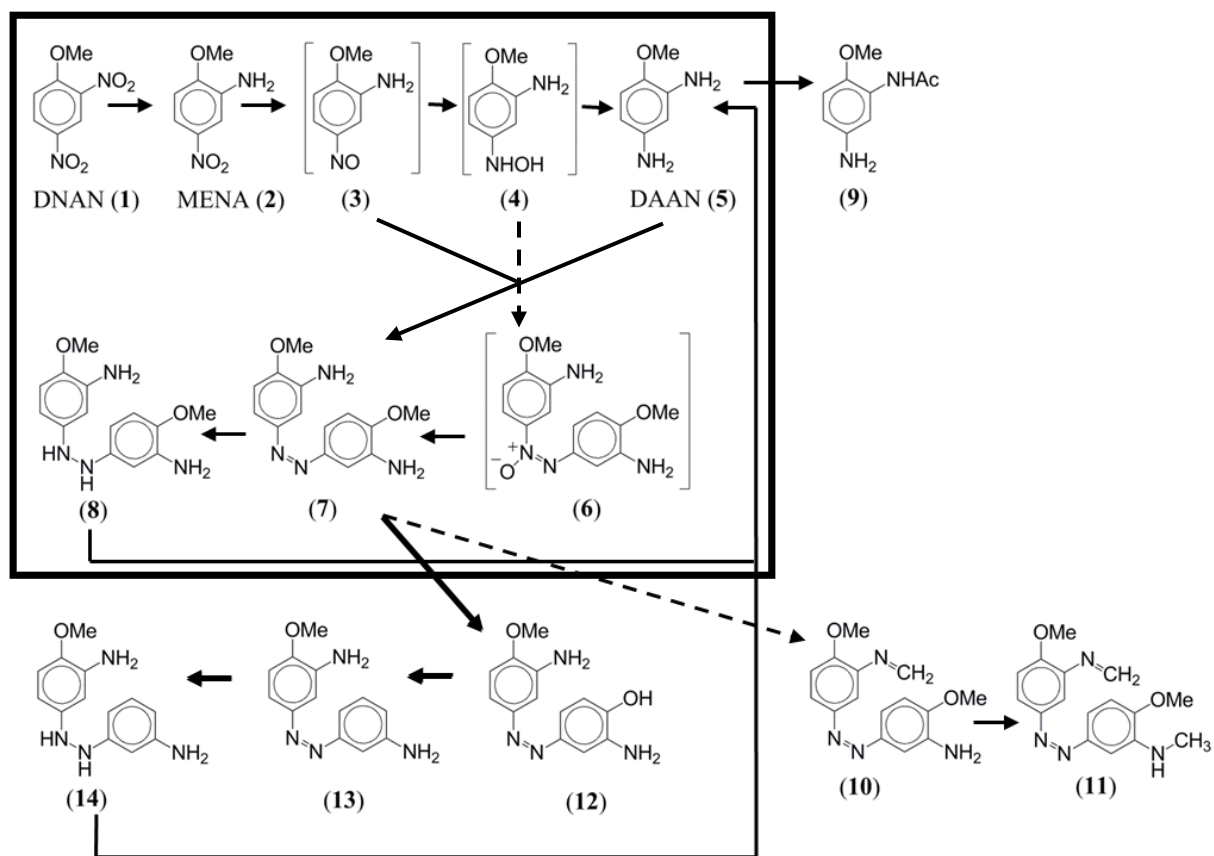


Figure 4.5-5. DNAN biotransformation pathways by anaerobic sludge amended with H₂ as a cosubstrate. Dashed lines represent hypothetical routes. Compounds in brackets were not detected but are potential metabolites. Main pathways are shown inside the black box. Secondary routes are presented outside of the box.

Table 4.5-1. Molecular Formula, Retention Times Determined by UHPLC-MS, Calculated m/z Values, and m/z Values measured by TOFMS for the Various Identified Metabolites.

Compound	Molecular formula [M]	Structure in Figure 3.6	Retention time (min)	Calculated [‡] [M+H] ⁺	Measured [M+H] ⁺
2-methoxy-5-nitroaniline (MENA)	C ₇ H ₈ N ₂ O ₃	2	1.5	169.0866	169.0864
2,4-diaminoanisole (DAAN)	C ₇ H ₁₀ N ₂ O	5	0.86	139.0608	139.0579
3,3'-diamino-4,4'-dimethoxy-azobenzene	C ₁₄ H ₁₆ N ₄ O ₂	7	3.7	273.1347	273.1315
3,3'-diamino-4,4'-dimethoxy-hydrazobenzene	C ₁₄ H ₁₈ N ₄ O ₂	8	3.6	275.1503	275.1499
N-(5-amino-2-methoxyphenyl) acetamide	C ₉ H ₁₂ N ₂ O ₂	9	3.2	181.0972	181.0968
5-((3-amino-4-methoxyphenyl)diazenyl)-2-methoxy-N-methylethaniline	C ₁₅ H ₁₆ N ₄ O ₂	10	4.3	285.1347	285.1346
2-methoxy-5-((4-methoxy-3-(methylamino)phenyl)diazenyl)-methylethaniline	C ₁₆ H ₁₈ N ₄ O ₂	11	5.3	299.1503	299.1503
3,3'-diamino-4-hydroxy-4'-methoxy-azobenzene	C ₁₃ H ₁₄ N ₄ O ₂	12	4.4	259.1190	259.1159
3,3'-diamino-4-methoxy-azobenzene	C ₁₃ H ₁₄ N ₄ O	13	2.5	243.1241	243.1207
3,3'-diamino-4-methoxy-hydrazobenzene	C ₁₃ H ₁₆ N ₄ O	14	3.3	245.13	245.0*

* m/z value measured by UHPLC-MS. The compound was not detected by TOFMS. ‡ ChemBioDraw Ultra 12.0.2.1076

4.5.7. Discussion: Reductive biotransformation

The multiple nitro functional groups of DNAN cause a strong electron deficiency in the carbon skeleton favoring reductive biotransformation as has been observed in many polynitroaromatic compounds in both aerobic and anaerobic conditions³⁵. We observed that the initial biological reduction of DNAN was regioselective favoring the nitro group in the *ortho* position to yield MENA, as other studies have shown for DNAN⁴⁶⁻⁴⁸. MENA was then further reduced to DAAN which has also been observed previously only in cases where there are strict anaerobic conditions^{46,47}.

Nitroreductases responsible for nitro group reduction are readily found in bacteria, and they may account for the facile reduction of DNAN in sludge. There are two main types of nitroreductases, -oxygen-sensitive and oxygen-insensitive nitroreductases. The latter may account for the reduction of DNAN under aerobic conditions. Oxygen-insensitive nitroreductases use a series of two electron transfer mechanisms and yield nitroso, hydroxylamine, and amino metabolites^{35,167}. The oxygen-insensitive reduction may be catalyzed by nitroreductases dependent on NAD(P)H as an electron donor, which often require flavin containing prosthetic groups^{35,167}.

In this study, we observed reduction of DNAN in the anaerobic and microaerophilic bioassays that contained heat-killed sludge, albeit at a rate that was slower than in the bioassays with live sludge. Several authors have reported that reduced components present in sludge can still be active after biological inactivation and cause some reduction of NACs. Donlon et al¹⁶⁸ detected reduction of 2-nitrophenol by autoclaved methanogenic granular sludge. In addition, the reduction of NACs such as 4-chloronitrobenzene was also attributed to Fe²⁺ adsorbed to Fe-containing minerals containing minerals³⁶, as well as to sulfide when electron transfer is mediated by natural organic matter¹⁶⁹.

4.5.8. Discussion: Biotransformation pathways

A large array of DNAN metabolites were detected, including seven new products not previously reported. A plausible pathway for DNAN anaerobic biotransformation is proposed in Figure 4.5-5 which accounts for the detected metabolites. Firstly, the nitro groups in DNAN were reduced leading to MENA and DAAN. Secondly, dimers were formed from reduced intermediates of DNAN. Azo compounds are known to be formed via nucleophilic reaction between aromatic amines and nitrosobenzenes according to scheme in Figure 4.5-6. The mechanism involves a coupling between nitroso-intermediates and aromatic amines. The coupling reaction is initiated by a nucleophilic attack of the amine to the nitroso-group which produces an intermediate compound, N-hydroxy-hydrazine^{170,171}. Upon loss of a water, this intermediate is directly converted to an azobenzene. The metabolites **7**, **10**, **11**, **12** and **13** were azo dimers.

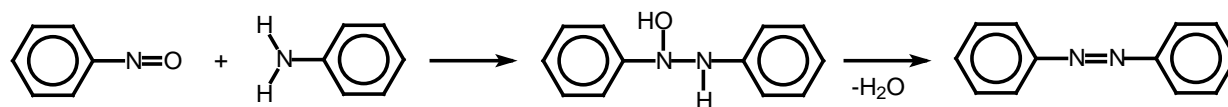


Figure 4.5-6. Nucleophilic attack of aromatic amine with nitrobenzene to form azo dimer. A similar reaction can occur between nitrosobenzene and hydroxylamines to form an azoxy dimer¹⁷², which can account for previously observed formation of azoxy dimers as metabolites of DNAN reductive cometabolism in aerobic bacteria⁴⁸. Azoxy dimers can be reduced to azo dimers¹⁷³.

Afterwards, azo compounds were reduced further to hydrazine metabolites (**8**, **11** and **14**), which in turn were cleaved to form aryl amines (e.g **5** (DAAN)). Hydrazine compounds have been

reported as intermediates during the biological reduction of azo dyes ¹⁷⁴⁻¹⁷⁶. Anaerobic sludge is well known to completely reduce azo dyes to their corresponding aromatic amines ^{177,178}.

Both aromatic amines and azo dimer products become subject to secondary reactions, such as O-demethylation (**12**), dihydroxylation (**13** and **14**), N-methylation (**10** and **11**) and N-acetylation (**9**). Of these processes, 2-N-acetyl-4-aminoanisole (**9**) detected as a metabolite in this study under strict anaerobic conditions was similar to a metabolite, 2-N-acetyl-4-nitroanisole, detected during aerobic DNAN cometabolism by a *Bacillus* strain ⁴⁸. Acetylation has been reported for 2,4-diamino-6-nitrotoluene by *Pseudomonas fluorescens* ¹⁷⁹. N-arylamine acetyl transferases in bacteria and eukaryotes are responsible for transferring acetyl groups from acetyl coenzyme A to xenobiotic compounds containing amino and hydroxylamine groups ¹⁸⁰. In this study evidence for the formation of N-methylene and N-methyl containing metabolites (**10** and **11**) is unique.

The metabolite with a free hydroxyl group (**12**) indicates the occurrence of O-demethylation. Aerobic cometabolism of DNAN also resulted in the identification of an O-demethylated metabolite, 2-N-acetyl-4-nitrophenol ⁴⁸. The aerobic bacteria, DNAN-biodegrading bacterium, *Nocardioides* sp JS1661, initiated the degradation of DNAN via an O-demethylation reaction ⁵⁰. *Rhodococcus* strains have also been reported to O-demethylate 4-nitroanisole ¹⁸¹. Several metabolites detected in our study lacked the hydroxyl group (**13** and **14**) putatively formed after O-demethylation. This suggests the removal of the hydroxyl group. Reductive dehydroxylation is a well-known reaction of the intermediate 4-hydroxybenzoyl-coenzyme-A, yielding benzoyl-coenzyme-A, during the anaerobic degradation of phenol ¹⁸².

4.5.9. Conclusions: Reductive DNAN biotransformation in sludge

DNAN was reduced by sludge to MENA and DAAN as the main metabolites, under all of the different conditions tested. The highest DNAN biotransformation rate was observed in anaerobic conditions enhanced by the addition of H₂, as a cosubstrate. The nitro group in the ortho position was first reduced to an amine to yield MENA, then the para nitro group was reduced to an amine to produce DAAN. During the reductive biotransformation, coupling of DNAN intermediates occurred, yielding azo compounds. These products were further reduced to hydrazine dimers. In addition, a diversity of products was created by parallel pathways of N-methylation, and N-acetylation of primary amines, as well as O-demethylation and dehydroxylation of methoxy groups. These insights on the fate and biotransformation of DNAN will help in understanding environmental health risks from DNAN and provide clues for the bioremediation of DNAN contamination.

4.6. (Bio)Transformation of 2,4-Dinitroanisole (DNAN) in Soils

Previous studies have focused on enriched cultures or pure cultures of bacteria, whose biodegradation and biotransformation mechanisms might differ from those occurring in natural systems where processes are driven by natural mixed soil microbial populations, as well as abiotic soil components. In order to elucidate key soil parameters and conditions that influence the fate of DNAN in natural systems, we performed (bio)transformation assays with a diversity of soils provided as suspensions under anaerobic and aerobic conditions. Our objectives were (1) to characterize the (bio)transformation potential for a diversity of soil types in aerobic and anaerobic conditions, (2) to assess inherent soil characteristics and culture conditions that enhance biotransformation, and (3) to resolve (bio)transformation pathways by identifying intermediates.

4.6.2. Results: Aerobic soil survey for biotransformation

The bioconversion of DNAN under aerobic conditions was investigated in seven different soils. (The soil properties are described in a previous publication¹⁰⁰. In some cases, heat-killed soil controls were included. Overall, there was slow conversion of DNAN in all of the soils surveyed (Figure 4.6-1). After rapid initial DNAN decrease (4-24 h), the removal rate was slow in the live treatments (0.42-2.28 $\mu\text{M d}^{-1}$). The rates and extent of DNAN removal achieved were similar to those observed in the heat-killed soil.

Initial DNAN removal was not associated with any significant HPLC resolvable transformation products except for minimal amounts of MENA (0-1.4% of DNAN). However, the removal was linearly correlated with the soil organic carbon (OC) ($R^2 = 0.9005$, $n = 5$, two-sided t-test $p=0.015$). This initial loss of DNAN could potentially be attributed to adsorption. The initial adsorption was followed by slow DNAN transformation. The transformation rate decreased after 4-8 d, suggesting that abiotic factors responsible for reducing DNAN became exhausted. By 15 days of incubation, Catlin, Camp Navajo and Camp Butner soils had the most DNAN removed due to adsorption and transformation (Figure 4.6-1); accounting for 64, 42, and 37% of DNAN, respectively. The soils that were incubated for a longer period (43 d) Catlin, Camp Butner, and Camp Ripley; showed an overall removal of 45-80 %.

4.6.3. Results: Anaerobic soil survey for biotransformation

DNAN bioconversion was investigated under anaerobic conditions using H_2 as an electron donor. Two main groups of soils can be distinguished by their respective fast and slow rates of DNAN (bio)transformation (Figure 4.6-2). Zero-order DNAN transformation rates for fast soils ranged between 38.9-73.1 $\mu\text{M DNAN d}^{-1}$ (Figure 4.6-3, Table 4.6-1). Complete DNAN removal was achieved within 6 d in the fast soils (Catlin, Camp Butner, Camp Navajo, and Camp Ripley). These soils had lag phases ranging from 0.2-2.6 d. Soils with slow (bio)transformation rates (Florence, Maricopa, Roger Rd.) transformed DNAN at 4.51-11.6 $\mu\text{M d}^{-1}$, providing $\leq 33\%$ of total DNAN removal after 9 d. In Figure 4.6-2, only Florence soil is shown as the example for the slow soils; data for Maricopa and Roger Rd are not shown but Table 4.6-1 summarizes DNAN anaerobic (bio)transformation data for all soils.

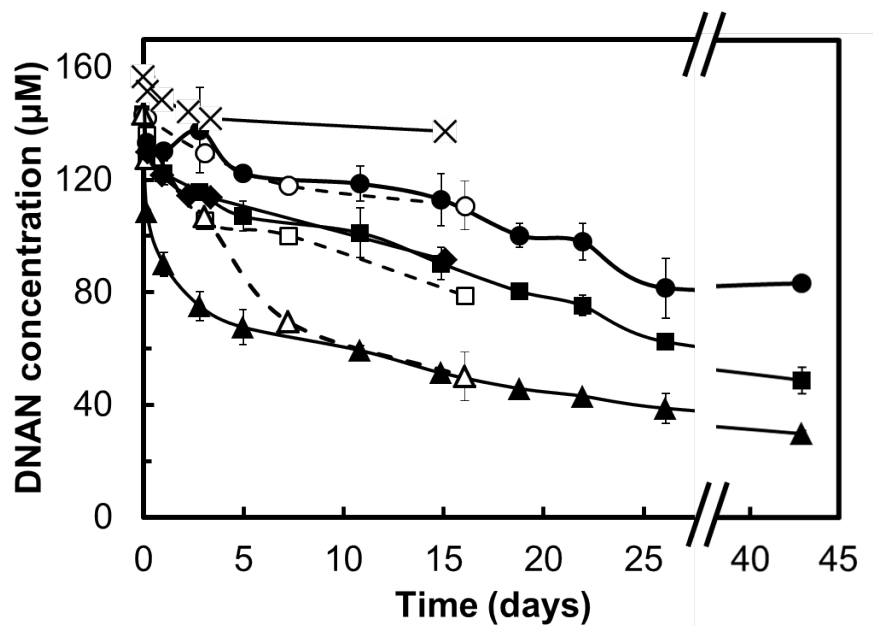


Figure 4.6-1. Aerobic removal of DNAN in soils (50 g wet wt L⁻¹) in mineral medium. Live treatments (continuous line): Camp Butner (■), Camp Ripley (●), Catlin (▲), Camp Navajo (◆), Florence (X). Heat-killed treatments (dashed line): Camp Butner (□), Camp Ripley (○), and Catlin (Δ). No heat-killed treatment available for Florence and Camp Navajo. Averages with error bars are reported

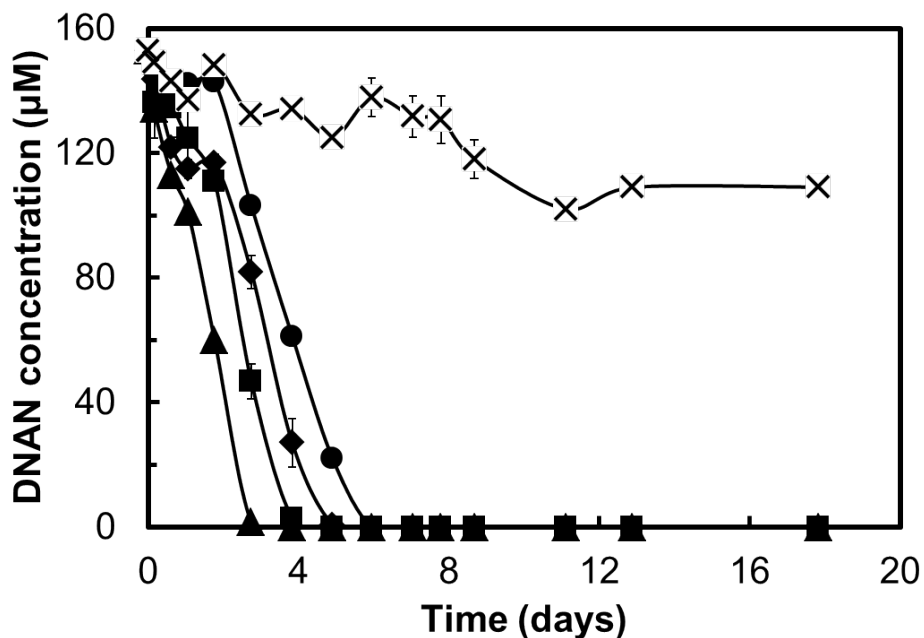


Figure 4.6-2. Anaerobic transformation of DNAN in soils (50 wet g L⁻¹) in mineral medium and amended with H₂: Camp Butner (■), Camp Ripley (●), Catlin (▲), Camp Navajo (◆), and Florence (X). Averages with error bars are reported.

Table 4.6-1. Rates of anaerobic biotransformation of DNAN with H₂ for the seven soils surveyed.

Soil	Lag phase (d)	Conversion rate DNAN [†]		Max. yield products [*]	
		($\mu\text{M d}^{-1}$)	($\mu\text{mol g}^{-1}$ dwt soil d ⁻¹)	(μM)	(%) [‡]
Roger Rd.	7.8	11.6	0.24	10	6.67
Maricopa	3.8	4.51	0.09	28	18.7
Catlin	0.2	69.3	1.43	69	46.1
Camp Ripley	1.1	38.9	0.78	107	71.3
Camp Butner	1.5	68.7	1.66	101	67.7
Camp Navajo	2.6	73.1	1.60	116	77.0
Florence	4.9	9.5	0.20	29	19.3

[†] conversion rate after lag phase.

^{*} MENA + DAAN (resolved with HPLC-DAD)

[‡] $100 \times (\text{MENA} + \text{DAAN}) / \text{DNAN}_{\text{added}} (150 \mu\text{M})$

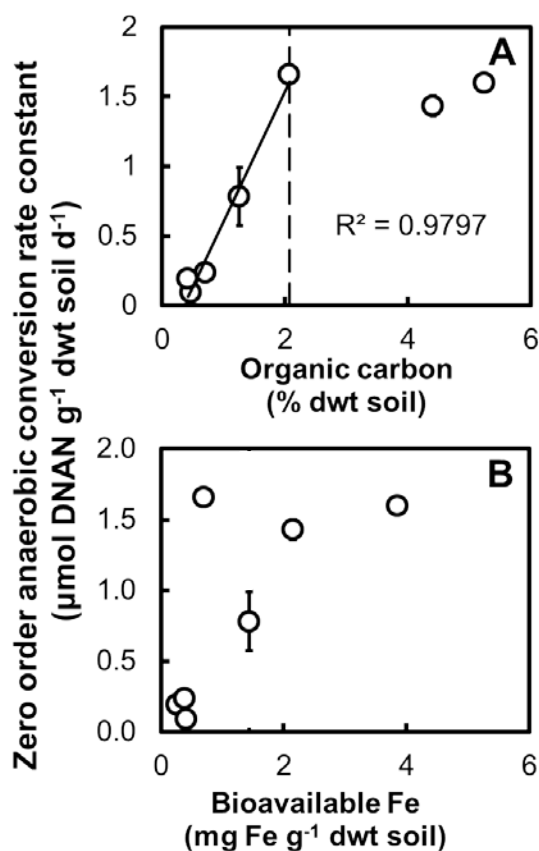


Figure 4.6-3. Correlations of zero-order rate constant with soil organic carbon (OC) content (Panel A) and soil bioavailable Fe (Panel B) during DNAN anaerobic soil biotransformation assays. Rate was calculated from the end of the lag phase (Table 4.6-1) until DNAN was no longer detected. The vertical dashed line indicates threshold of linear correlation of rate constant with OC. Linear regression for OC in Panel A valid for 0-2.07% OC. Two-sided t-test, $n = 5$, $p \leq 0.005$.

Anaerobic DNAN (bio)transformation occurred faster and to a greater extent than in aerobic conditions. In the fast degrading soils, 50% of DNAN was removed within 2-4 d under anaerobic conditions (compared to ≥ 15 days for aerobic conditions). For fast (bio)transforming soils, all DNAN was removed within 6 d, whereas in aerobic conditions, there was residual DNAN after 43 d for the same soils.

Soil parameters (OC content, bioavailable Fe, and soil texture) were tested for correlations with DNAN conversion rate. Fast DNAN-(bio)transforming soils had OC contents above 2% (Figure 4.6-3), while slow soils had a low OC content ($<1\%$). There was a strong relationship between transformation rate and OC ($R^2 = 0.9797$, $n=5$, two-sided t-test $p = 0.001$). Each percent OC means an increment of $0.593 \mu\text{mol DNAN g}^{-1}$ dry weight (dwt) soil d⁻¹ up to 2.07% OC (Figure 4.6-3). Above this value the rate did not increase. While bioavailable Fe did not show significant linear correlation at the 95% confidence level, one-way ANOVA showed that there was significant difference in the degradation rates based on its concentration (F test = 93.8, $p = 6.87 \times 10^{-5}$). Furthermore, one-way ANOVA also showed significant differences in soil texture (F test = 102, $p = 1.53 \times 10^{-5}$). Based on these observations, 2.07% OC was a threshold range that distinguished fast from slow DNAN-converting soils.

Three of the fast (bio)transforming soils were selected for further study by comparing full live treatment (containing H₂) with endogenous (no H₂ added) and heat-killed controls. DNAN conversion occurred in all cases (Figure 4.6-4). The H₂ amendment enhanced DNAN conversion by 2 to 6 fold compared to endogenous treatments. Heat-killed and endogenous treatments had similar rates, 17.9 to 44.3 and 11.1 to 47.3 $\mu\text{M d}^{-1}$, respectively, which suggest that without an electron donor amendment, abiotic transformation was dominant.

The highest yields of UHPLC-DAD detectable monomer products (MENA, DAAN) for these three fast biotransforming soils generally occurred in the H₂ amended (46.0 to 77.0% of DNAN) and the endogenous (56.8 to 68.2%) treatments. The lowest yields generally occurred in heat-killed controls (46.6 to 58.9%). In the H₂ treatments DNAN was completely eliminated and MENA and DAAN were no longer detected. This indicated the formation of transformation products that were either not amenable to UHPLC-DAD detection or the daughter products became bound to the soil.

4.6.4. Results: Products identified in UHPLC and infusion Q-ToF-MS

Ten chemical structures were detected in liquid samples using QToF-MS techniques. Table 4.6-2 shows the compounds, retention times, mass to charge ratios (m/z values as $[\text{M}+\text{H}]^+$), as well as fragments detected where available. 2,4'-dimethoxy-4-nitro-3'-nitroso-azobenzene was detected by infusion Q-ToF-MS and the rest of the compounds were detected using UHPLC-Q-ToF-MS. The high-resolution masses measured for all compounds detected were within 0.7 ppm of predicted monoisotopic masses. Mass spectral details and fragmentation patterns are provided in supplementary data of the associated publication¹²⁶. MENA and DAAN were confirmed in the samples analyzed, with $[\text{M}+\text{H}]^+$ m/z values detected 0.7 and 0.1 ppm away from the calculated ones, respectively. An isomer of MENA, 4-methoxy-5-nitroaniline (iMENA) (**J**; Figure 4.6-6) was detected and exhibited a shorter retention time (2.2 min) than MENA (5.3 min), indicative of greater hydrophilicity. The assignment is further supported due by the stronger dipole moment and lower log Kow (0.80 versus 1.47) of iMENA compared to MENA⁴⁷. In addition, the fragmentation pattern was also different between the isomers (Table 4.6-2). Since iMENA was only detected by UHPLC-Q-ToF-MS, it could be inferred that it was produced at considerably smaller amounts than MENA. To date, iMENA has only been reported in abiotic reduction of DNAN with zero-

valent iron ¹⁸³ compared to the regioselective formation of MENA in biological systems ⁴⁷. Therefore, its presence might indicate that abiotic processes contributed to in part to nitroreduction.

Besides monomeric products, a total of seven dimers were identified. Three of them have been reported during DNAN incubations with anaerobic sludge: 3,3'-diamino-4,4'-dimethoxy-azobenzene (**E**), 3,3'-diamino-4-hydroxy-4'-methoxy-azobenzene (**F**), and 4,4'-dimethoxy-3-methylamino-3'-methyleamino-azobenzene (**G**) (Table 4.6-2, Figure 4.6-6) ¹⁶⁶. The other four were new dimers identified in this study. They included: 2,4'-dimethoxy-4-nitro-3'-nitroso-azobenzene (**C**), 2,2'-dimethoxy-5-hydroxylamino-azobenzene (**D**), 4'-methoxy-3-methylamino-3'-methyleamino-azobenzene (**H**), and 3-amino-3'-nitro-4,4'-dimethoxy-azobenzene (**I**) (See Table 4.6-2 and Figure 4.6-6).

4.6.5. Discussion: Aerobic transformation

Complete DNAN (bio)conversion was restricted to anaerobic conditions. Aerobically, initial partial adsorption and subsequent slow transformation was observed in live and heat-killed soils. Rapid conversion occurred in anaerobic conditions, at a rate that was highly correlated to soil OC content up 2.07%, after which the rates were apparently saturated. An important component of the transformation was due to chemical reactivity of the soil as evidenced by transformation in heat-killed soil. However, rates in live soil were accelerated with the addition of H₂.

Aerobically, DNAN was removed initially due to putative sorption onto the soil. Hawari, et al. ⁴⁷ calculated soil OC to water partitioning coefficients for DNAN ($K_{oc} = 215\text{-}364 \text{ L kg}^{-1}$) in two soils containing 2.5-34% total OC, indicative of the strong affinity of the compound to organic matter. The adsorption of nitroaromatics, such as 2,4-dinitrotoluene, is known to be correlated with soil organic matter (SOM) ¹⁸⁴

Besides adsorption, a small fraction of DNAN underwent reduction to MENA under aerobic conditions but no further reduction to DAAN was detected. These results indicate that DNAN was also partially reduced under aerobic condition. Aerobic oxidation is problematic for compounds with electron withdrawing moieties, such as multiple nitro groups ^{30,185}. Each additional nitro group shifts the electrons away from the carbon skeleton ¹⁸⁶, making the oxidation of the carbon skeleton more difficult and the reduction to amines more likely ¹⁸⁷. While a recent study has reported aerobic DNAN mineralization by a bacterium isolated from a munitions wastewater treatment plant ⁵⁰, our findings do not show similar reactions in unacclimated soils, even after extended incubations (43 d). Therefore, reduction is the most likely pathway for DNAN biotransformation in soils, and this was clearly a much slower process in aerobic conditions.

4.6.6. Discussion: Anaerobic transformation

Under anaerobic conditions, DNAN was rapidly transformed to aromatic amines, MENA and DAAN. This is consistent with reports on anaerobic conversion of nitroaromatics with multiple nitro groups ^{42,188,189}. Previous research has also demonstrated biological anaerobic conversion of DNAN to MENA and DAAN under anaerobic conditions ^{46,47,166}.

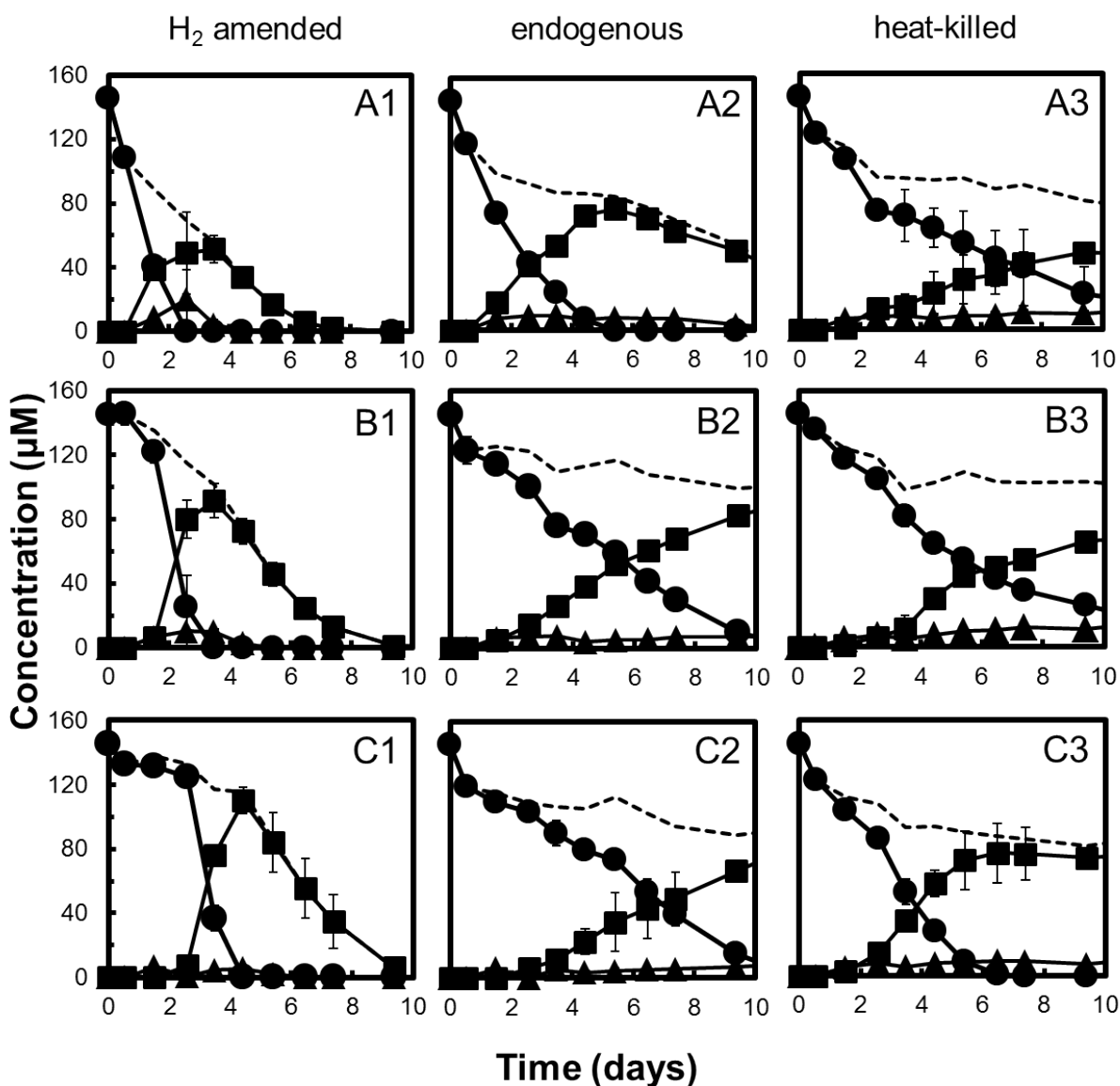


Figure 4.6-4. Concentrations of DNAN (●), MENA (■), and DAAN (▲) and their sum (---) during the anaerobic (bio)transformation of DNAN with 50 wet g L⁻¹ soil for Catlin (A), Camp Butner (B), and Camp Navajo (C) soils. H₂ added as electron donor (1), live soil (endogenous) (2), and heat-killed soil (3). Averages with error bars are reported

Table 4.6-2. Molecular Formulae, Retention Times, Calculated and Measured m/z Values, and Spectral Data Determined by UHPLC and Infusion Q-ToF-MS for the Identified Transformation Products. Retention time (RT)

Compound/ structure in Figure 4.6-6 (bold)	Molecular formula [M]	RT (min)	Calculated [M+H] ⁺	Measured [M+H] ⁺	Spectral data (*Int.)
2,4-diaminoanisole (DAAN) (B)	C ₇ H ₁₀ N ₂ O	1.9	139.0866	139.0865	139.0865 (31), 124.0635 (100), 108.0687 (28), 95.0604 (25), 80.0504 (19)
2-methoxy-5-nitroaniline (MENA) (A)	C ₇ H ₈ N ₂ O ₃	5.3	169.0608	169.0615	169.0615 (52), 154.0377 (25), 123.0683 (100), 108.0447 (49), 96.0449 (7), 80.0505 (37)
4-methoxy-5-nitroaniline (iMENA) (J)	C ₇ H ₈ N ₂ O ₃	2.2	169.0608	169.0602	169.0602 (72), 154.0366 (29), 123.0676 (16), 122.0597 (100), 108.0444 (21), 94.0649 (23), 77.0395 (18)
3,3'-diamino-4-hydroxy-4'-methoxy-azobenzene (F)	C ₁₃ H ₁₄ N ₄ O ₂	2.6	259.1190	259.1191	259.1191 (87), 242.0919 (27), 228.1005 (34), 227.0923 (100), 199.0977 (70)
4'-methoxy-3-methylamino-3'-methyleamino-azobenzene (H)	C ₁₅ H ₁₆ N ₄ O	2.3	269.1397	269.1398	269.1398 (100), 254.1167 (38), 237.1132 (57)
3,3'-diamino-4,4'-dimethoxy-azobenzene (E)	C ₁₄ H ₁₆ N ₄ O ₂	1.6	273.1346	273.1351	273.1351 (54), 256.1079 (35), 242.1161 (60), 227.0924 (100), 199.0978 (11), 151.0860 (14)
2,2'-dimethoxy-5-hydroxylamino-azobenene (D)	C ₁₄ H ₁₅ N ₃ O ₃	4.9	274.1186	274.1180	274.1180 (24), 243.1010 (100), 228.0764 (69), 200.0806 (34), 172.0863 (10), 143.0591 (10)
4,4'-dimethoxy-3-methylamino-3'-methyleamino-azobenzene (G)	C ₁₆ H ₁₈ N ₄ O ₂	3.0	299.1503	299.1509	299.1509 (100), 284.1277 (29), 267.1241 (14)
3-amino-3'-nitro-4,4'-dimethoxy-azobenzene (I)	C ₁₄ H ₁₄ N ₄ O ₄	3.4	303.1088	303.1088	303.1088 (100), 271.0810 (19), 257.0651 (19), 225.0888 (6), 227.1042 (16), 151.0856 (24)
2,4'-dimethoxy-4-nitro-3'-nitroso-azobenzene (C)	C ₁₄ H ₁₂ N ₄ O ₅	N/A [*]	317.0880	317.0879	N/A ^{**}

*Int. = % intensity normalized to highest m/z for each compound

** Compound detected in infusion-Q-ToF-MS. Fragmentation not available.

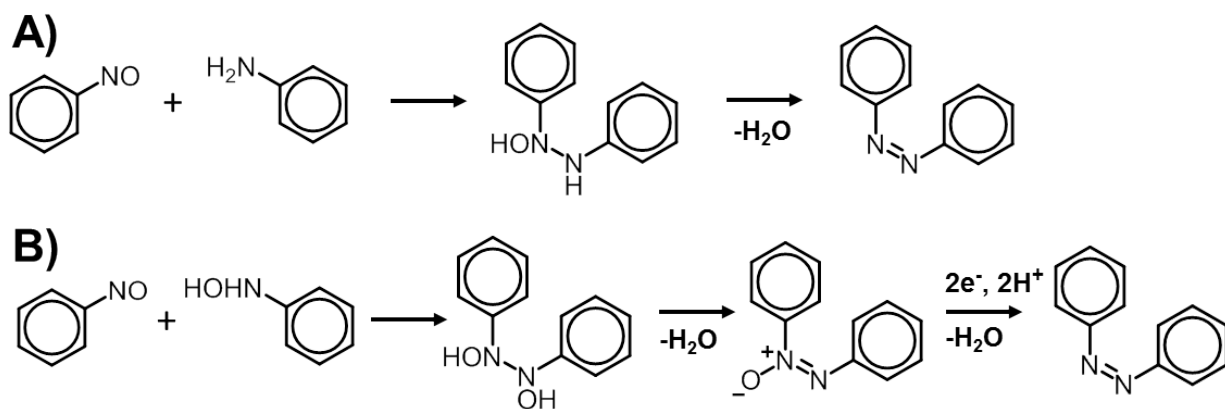


Figure 4.6-5. Possible mechanisms for coupling between reduced intermediates of nitroaromatic compounds: **A)** coupling of nitrosobenzenes with aromatic amines ^{170,171}; **B)** coupling of nitrosobenzenes with phenylhydroxylamines ¹⁷²..

In our soil assays, the transformation rates were well correlated with soil OC content. Firstly, natural decay of assimilable fractions of SOM can supply electron equivalents for reduction of nitro groups. Assimilable carbon in SOM has been demonstrated for soils ¹⁹⁰, waters ¹⁹¹, as well as anaerobic sediments ¹⁹². The decomposition of the assimilable carbon could potentially contribute to electron donating equivalents needed for nitro-group reduction. Secondly, humic material can act as electron shuttles as has been demonstrated by quinones representing redox active moieties in natural SOM that stimulate the reduction of nitroaromatics by ferrous iron and sulfide ^{40,193}. Lastly, high SOM also correlates with high bacterial counts ¹⁹⁴, which may play a role in the catalysis of nitro-group reduction.

Reduction of DNAN also occurred in heat-killed soils, particularly in Camp Navajo soil (which has the highest OC and bioavailable Fe). DNAN abiotic reduction has been reported to result from reaction with Fe(II) and with ferrous-ligand complexes ^{40,195}. Fe(II)-sorbed to Fe containing minerals are very effective in reducing nitroaromatic compounds ^{36,37}. In anaerobic sediments, SOM decomposition is known to be a major source of electron-donating substrate for Fe(III) reduction ¹⁹⁶, providing for a pool of Fe(II). Furthermore, autoclaving soils has been reported to increase 6-fold Fe(II) content due to Fe(III) reduction during heating ¹⁹⁷. Therefore, autoclaving could have reduced Fe(III) to Fe(II) coupled to SOM oxidation, which in turn could promote abiotic reduction of DNAN afterwards.

4.6.7. Discussion: Products of anaerobic conversion and biotransformation pathway

The initial reduction of DNAN occurred primarily in the ortho position, as reported previously ⁴⁶⁻⁴⁸, yielding MENA. In the endogenous and heat-killed treatments there was no further transformation (up to 9 d), except for Catlin soil. However, in the H₂ treatments, the MENA formed was readily consumed and did not result in any accumulation of DAAN. The higher reducing conditions, due to the addition of an electron donor (H₂), favored the conversion of MENA. DAAN was not detected, possibly due to binding with humic substances or coupling reactions with nitroso derivatives to form dimers, and, therefore, accounting for the lack any DAAN accumulation.

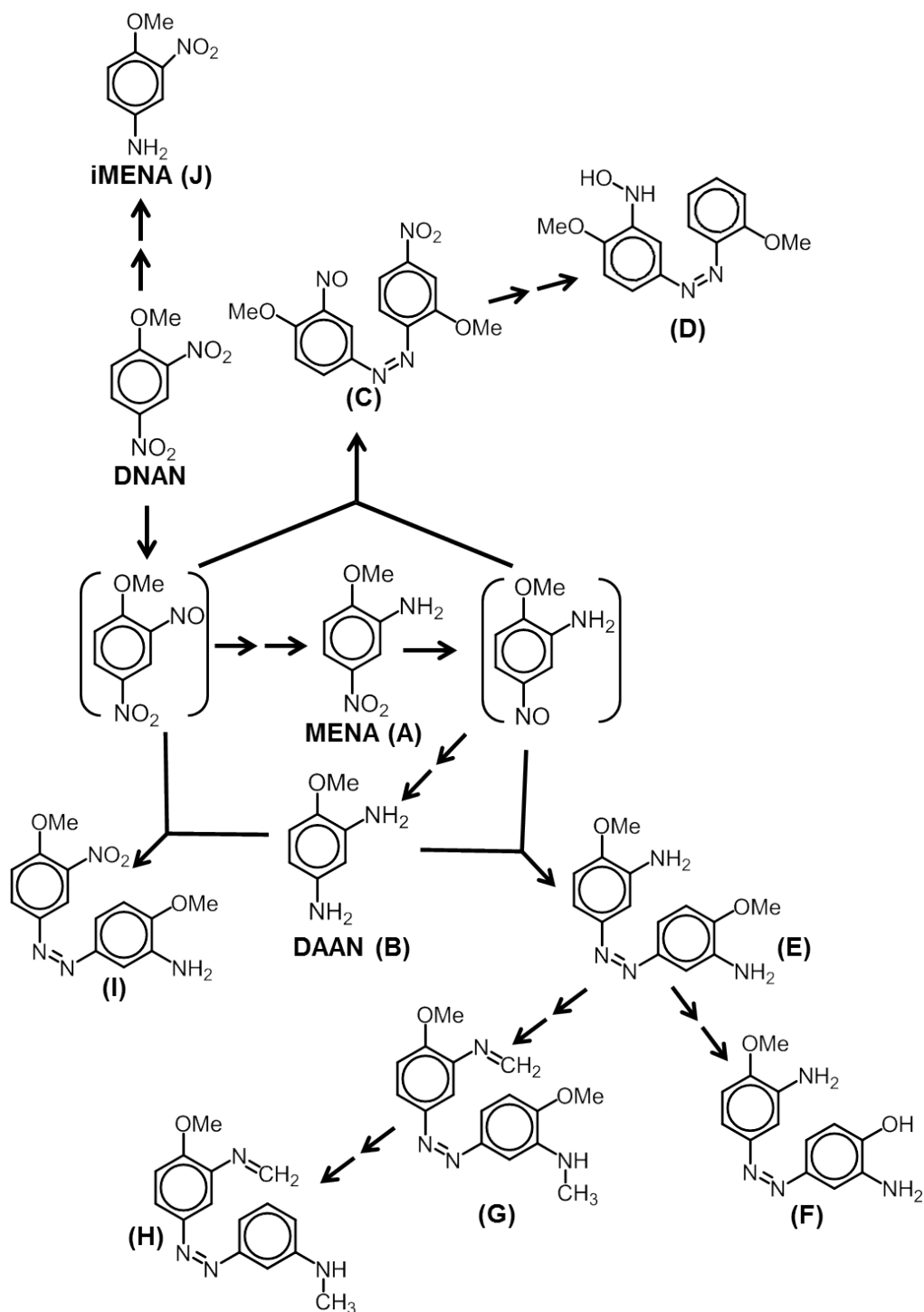


Figure 4.6-6. Metabolites detected with infusion and UHPLC Q-ToF-MS experiments and transformation pathway proposed. Compounds in parentheses were not detected in this work but are known intermediates in the literature. Double arrows indicate that reactions require multiple steps.

Q-ToF-MS indicated azo dimer formation. While these products have been regarded as artifacts formed during sample processing ⁴⁷, strict anaerobic conditions were maintained in the incubations and ascorbic acid was used as antioxidant to prevent formation of artifacts. Azo dimers were also detected previously during incubations of DNAN with anaerobic sludge ^{46,166}, as well as in similar treatments with TNT ¹⁹⁸. Furthermore, there is a body of literature that uses reductive techniques to synthesize azo dyes from nitroaromatics ^{170,171,173,199}. Therefore, we propose that azo dimers are formed as a product of (bio)transformation of nitroaromatics under anaerobic conditions. Two plausible mechanisms for azo product formation are shown in Figure 4.6-5. The most likely explanation for dimer formation under strict anaerobic conditions is a condensation reaction between a nitroso intermediate and an amino-containing compound since aromatic amines were demonstrated to accumulate. This mechanism has been proposed for azo dye synthesis by reduction of nitroaromatics with nano-iron ¹⁷⁰ and also by a one-step reaction of aromatic amines with nitroaromatics under basic conditions and high temperature (10 mM, 105 °C). ¹⁷¹. This proposed reaction would form structures **C**, **E**, and **I** in Figure 4.6-6 due to the condensation between a nitroso-bearing compound and an amino group in MENA or DAAN. 2,4'-Dimethoxy-4-nitro-3'-nitroso-azobenzene (**C**, Figure 4.6-6), provides evidence of nitroso-bearing transformation products. Alternatively, azo dimers can be formed via the reaction of nitroso-intermediates with hydroxylamine intermediates to azoxybenzenes, that can potentially be reduced to azo compounds ^{172,200}. We detected a tentative azo compound bearing a hydroxylamino group, 2,2'-dimethoxy-5-hydroxylamino-azobenzene (**D**, Figure 4.6-6). Although we did not detect any hydroxylamino-bearing monomers, Perreault, et al. ⁴⁸ detected 2-hydroxylamino-4-nitroanisole, during the reduction of DNAN in aerobic conditions. DNAN hydroxylamino intermediates might not accumulate in soil, as hydroxylamino products from TNT reduction have been reported to bind to soil irreversibly ²⁰¹.

The azo dimers can be subject to further metabolism. An additional plausible reaction is the reduction of the azo dimers to form aromatic amines again. This is a well-known reaction causing cleavage of azo dyes under reducing conditions ^{177,178,202}.

Besides the formation of dimers, other reactions are proposed based on metabolites observed with Q-ToF-MS, such as O-demethylation, two-step demethoxylation, and N-substitution. O-demethylation of the methoxy group yields a hydroxyl group in the transformation of 3,3'-diamino-4,4'-dimethoxy-azobenzene (**E**, Figure 4.6-6) to 3,3'-diamino-4-hydroxy-4'-methoxy-azobenzene (**F**, Figure 4.6-6). This reaction has been reported during anaerobic incubations of DNAN and 4-nitroanisole ^{48,166,181}. After O-demethylation, dehydroxylation could follow, together comprising a two-step demethoxylation. This series of reactions is suggested between 4,4'-dimethoxy-3-methylamino-3'-methylenamino-azobenzene (**G**, Figure 4.6-6) and 4'-methoxy-3-methylamino-3'-methylenamino-azobenzene (**H**, Figure 4.6-6). Two-step demethoxylation has been reported previously for the biotransformation of DNAN in anaerobic sludge ¹⁶⁶. Another reaction proposed is N-substitution with alkyl groups, leading to observed N-methyl and N-methylene containing dimers (**G**, **H**; Figure 4.6-6), which has also been reported previously in anaerobic sludge biotransformation ¹⁶⁶. It is possible that partially degraded labile components could be a source of alkylating amines. Finally, another compound was detected and tentatively assigned the structure 2,2'-dimethoxy-5-hydroxylamino-azobenzene (**D**, Figure 4.6-6). This dimer suggests nitrogen removal from the structure (azo dimers from DNAN have four N-bearing groups while structure **D** in Figure 4.6-6 has only three). Nitro group removal from an aromatic ring in reductive conditions can occur during nitroreduction to hydroxylamino followed by N removal as NH₄⁺ yielding a diol ¹⁸⁶. However, the diol product of this reaction scheme was not detected in

2,2'-dimethoxy-5-hydroxylamino-azobenzene (**D**). Overall, these reactions indicate that azo dimers formed from reduced products of DNAN bioconversion continue to undergo transformations in anaerobic soil environments.

4.6.8. Conclusions: (Bio)Transformation of DNAN in soils

DNAN underwent (bio)transformation in soils, particularly in anaerobic conditions, due to biotic and abiotic processes. The major reaction pathway involved nitro-group reduction to MENA, and to a minor extent, DAAN. The rate of DNAN reduction in anaerobic conditions is related to the OC content of a given soil, with higher rates occurring at high OC. Products from DNAN reduction coupled to form azo dimers that continued to be (bio)transformed with O-demethylation and N-substitution reactions. Aromatic amines such as DAAN also reacts and becomes incorporated into soil organic matter. Taken together, our results indicate that DNAN is readily reductively (bio)transformed in natural soils, and a full suite of transformation products are formed such as aromatic amines and azo dimers, which can impact the fate of DNAN in the environment.

4.7. Environmental Fate of ^{14}C -2,4-DNAN in Soil Microcosms

4.7.1 Objectives: Fate ^{14}C -DNAN in soil microcosms

Under anaerobic conditions, the nitro groups of DNAN are progressively reduced in soils forming the aromatic amines 2-methoxy-5-nitroaniline (MENA) and 2,4-diaminoanisole (DAAN)¹²⁶. The formation of aromatic amines can be attributed biological and abiotic factors. In support of the biological reduction mechanisms, the same pattern of DNAN reduction to MENA and DAAN was also observed when utilizing to pure strains of pure bacterial cultures (*Shewanella oneidensis* and *Pseudomonas fluorescens*) incubated under anaerobic conditions⁴⁷. However abiotic mechanisms may also play a role in forming these aromatic amines, since both MENA and DAAN were formed in heat sterilized soil samples albeit at slower rates compared to biologically active samples¹²⁶. This is consistent with nitro groups of nitroaromatic compounds being susceptible to abiotic reduction by Fe^{2+} adsorbed onto iron oxide minerals^{36,37} or via redox mediators, transferring electrons from hydrogen sulfide (H_2S)⁴⁰.

Aromatic amines are reactive compounds. During the anaerobic reduction of DNAN to MENA and DAAN in soil, these aromatic amines occur as fleeting intermediates that are subsequently rapidly attenuated¹²⁶. Likewise when MENA and DAAN are spiked into sterile aerobic soil microcosms, they disappear rapidly. The disappearance is partly due to sorption but mostly due to irreversible covalent binding to soil natural organic matter (NOM)⁴⁷.

There is also evidence of bound residue being formed between radiolabeled or isotope labeled TNT and soil humus during the anaerobic phase of soil bioremediation of conventional explosives. Under strictly anaerobic conditions, large percentages of ^{14}C -trinitrotoluene (^{14}C -TNT) are converted to non-extractable substances in humus (humin). After periods ranging from 35 to 51 d of anaerobic incubation, anywhere from 47 to 65% of the radiolabelled TNT was associated with the insoluble humus fraction, humin^{55,203}. ^{15}N -NMR spectra of soil incubated anaerobically with ^{15}N -TNT reveals the presence of ^{15}N in condensed moieties in the soil reminiscent of substructures expected for humus^{54,57,203}.

The objective of the present study was to provide a quantitative characterization of the fate of DNAN and its (bio)transformation products in soil utilizing radiolabeled studies with uniformly ring labelled ^{14}C -DNAN. One specific goal was to evaluate the distribution of ^{14}C in the soil, liquid, and gas phases during biotransformation. A second goal was to evaluate different strategies (aerobic/anaerobic redox conditions and additions of electron donor, soil NOM, or horseradish peroxidase) on the fate of ^{14}C , with a special focus on its irreversible covalent bonding with soil humus.

4.7.2. Results and discussion: DNAN reductive biotransformation.

The fate of DNAN was studied in Camp Navajo (CN) and Camp Butner (CB) soils. DNAN biotransformation assays inoculated with 10 g L^{-1} of soil lead to complete biotransformation of DNAN (Figure 4.7-1). However, complete conversion rate of DNAN in CN soil ($56.7\text{ }\mu\text{mol DNAN d}^{-1}\text{ dwt g}^{-1}\text{ soil}$) was four-fold higher than the rate in CB soil ($14.3\text{ }\mu\text{mol DNAN d}^{-1}\text{ dwt g}^{-1}\text{ soil}$). CN has a higher organic carbon content ($52.4\text{ mg g}^{-1}\text{ soil}$) than CB ($20.7\text{ mg g}^{-1}\text{ soil}$)¹²⁶. The higher organic carbon content may be related to improved electron donor supply as NOM is degraded and the soils with higher organic content are typically associated with higher microorganism abundance, thus providing a higher number of microorganisms capable of driving the nitroreduction with non-specific flavin containing nitroreductases³⁵. The HPLC-resolvable products expected from primary biotransformation, MENA and DAAN, only were detected

sporadically in the supernatant with the highest concentrations detected ranging from 80-135 μM , but by 50 d none of these simple aromatic amines could be detected anymore in the HPLC. Based on mass spectrometry analyses conducted in similar experiments with these soils, the secondary resolvable products found in the liquid phase are comprised by azo-dimers as assessed by the relative abundance of the ionizable products in mass spectrometry¹²⁶. Aromatic amines can also react with humic substances becoming irreversibly bound, either through substitution reactions^{61,62} or oxidative radical reactions²⁵. Thus a quantitative assessment can only be provided by analyses utilizing radiolabeled parent munitions compounds.

4.7.3. Results and discussion: ^{14}C label distribution during DNAN biotransformation

The ^{14}C distribution was monitored in aqueous, organic solvent and 0.5 M NaOH extractable and humin-bound fractions during anaerobic incubations in aqueous suspension with two soils (CN and CB) and an anaerobic sludge supplied at 10 g L⁻¹. During the time course of the incubation, the ^{14}C label was predominantly associated with the aqueous phase of the assays. This fraction accounted for 65 to 84 % of the total final label for the various soil and sludge microcosms on day 50 (Figure 4.7-1). A likely explanation is that the dominant products that remain soluble consist of azo-dimers based on our previous work characterizing the long-term species in DNAN biotransformation assays¹²⁶. Or the aromatic amines become substituted in water soluble humic materials such as the fulvic acids⁶¹. On the other hand, the methanol extracts ranged from 3 to 6% of the ^{14}C label for in the soil and sludge microcosms. The more hydrophobic ^{14}C label in the ethyl acetate remained below 1% in all microcosms.

The humus-bound ^{14}C associated with the insoluble humus (humin) of the soil and sludge significantly increased during the incubations. This is the non-extractable fraction which is combusted by the Harvey oxidizer. On d 50 this fraction accounts for 16 to 25% of the ^{14}C label in the soil and sludge microcosms. The values were highest in the anaerobic sludge microcosm where ^{14}C incorporation occurred rapidly at the start of the experiment in parallel with a rapid decrease in DNAN. To a minor extent there was also an increase in the 0.5 M NaOH extractable fraction associated with humic acid, accounting for 2 - 3% of the recovered label. The increase in ^{14}C label in the humin fraction coincided with the decrease in DNAN. Once the DNAN was depleted the ^{14}C in the humin fraction remained relatively constant, suggesting that once the supply of aromatic amines was depleted, the incorporation of ^{14}C ceased. Based on these observations, most of the ^{14}C associated with DNAN remained associated with the aqueous phase and remained soluble. Nonetheless a sizeable fraction became irreversibly incorporated into as non-soluble bound residue in the soil humin. This coincides with similar findings in experiments with TNT in soil²⁰⁴, where the humin fraction was associated with up to 52.4% of the total label.

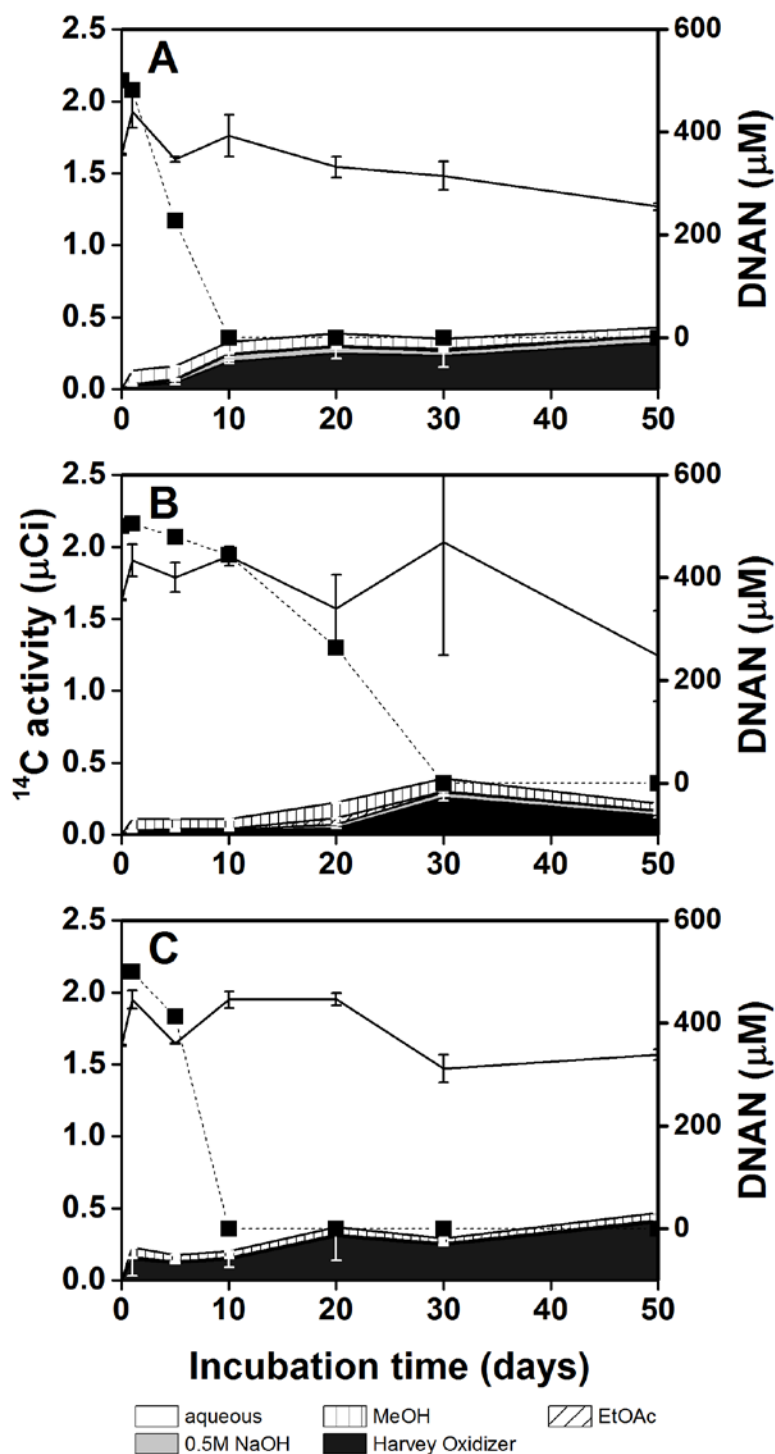


Figure 4.7-1. Incorporation of ^{14}C into soil components during DNAN (■) anaerobic (bio)transformation in soils and sludge amended with 10 mM pyruvate. Panel A: CN soil (10 g L^{-1}). Panel B: CB soil (10 g L^{-1}). Panel C: anaerobic sludge. No detectable ^{14}C label was obtained in the gas phase (volatile organic compounds (VOCs) and CO_2). In this experiment, the aqueous samples were not corrected for scintillation quenching due to coloration. The upper line is the sum of all labeled fractions.

No radiolabel above background levels was recovered in the gas phase (i.e. ^{14}C -VOCs or ^{14}C - CO_2), suggesting that ring-cleavage of DNAN is very unlikely to have occurred in CN and CB soils, as well as in anaerobic sludge. This is consistent with findings on radiolabeled ^{14}C with the chemical analog, TNT, in soils²⁰⁴ and activated sludge²⁰⁵. However, since the radiolabel only included the aromatic ring, it is possible that unlabeled CO_2 might be released from O-demethylation of the methoxy group in DNAN or its reduced products and therefore was not detected in the LSC. O-demethoxylation of DNAN bioconversion products has been detected in soils^{48,126}.

Overall, the recovery of the ^{14}C label was in general >95 % of the radiolabel added. However, at longer incubation times the recovery decreased, resulting in 76-78 % of recovered label in both soils. The aqueous phase had a stronger brown coloration at longer incubation times (>30 d), potentially attributed to fulvic and humic acids released from the soils and sludge. Coloration in LSC decreased the counting efficiency, quenching the scintillation signal. A similar phenomenon had also been observed in TNT soil radiolabeled studies²⁰⁴. To address this issue, quenching correction was performed in subsequent experiments as described in the Methods section.

4.7.4. Results and discussion: Aerobic vs. aerobic conditions

The effect of anaerobic versus aerobic soil incubations conditions on the incorporation of ^{14}C into humin from ^{14}C labeled DNAN was evaluated with 25 g L^{-1} of CN soil. Incubations under anaerobic conditions resulted in the highest incorporation of DNAN biotransformation products into the soil humus (Figure 4.7-2A). All treatments had remarkably higher incorporation of ^{14}C compared to the first experiment with just 10 g L^{-1} soil. With 10 g L^{-1} , ^{14}C incorporation was only 23%; whereas under the same pyruvate amended conditions, the same soil enables more than twice that level of incorporation when supplied at 25 g L^{-1} soil. These results clearly indicate that the quantity of soil (and perhaps its associated organic carbon) in relation to the quantity of DNAN has an important role on ^{14}C incorporation.

When comparing treatments at 25 g L^{-1} soil. The pyruvate amended anaerobic treatment had the highest incorporation of ^{14}C to humin (53.4%) after 40 d of incubation, followed by the endogenous (without pyruvate) anaerobic treatment (41.2%); whereas the aerobic treatment (25.7%) resulted in less than half of the label incorporated compared to the anaerobic pyruvate amended treatment. Moreover, the rate of incorporation was also highest for the pyruvate amended treatment (0.16 nCi mg^{-1} OC d^{-1}) (Figure 4.7-2B), which was 1.2 times the rate for the endogenous anaerobic treatment, and twice the rate compared to the aerobic treatment. In addition, incorporation into the 0.5 M NaOH extraction, operationally defined as humic acid associated fraction, ranged from 9.5-11.8% of the ^{14}C label for the three treatments. However, in the methanol extractions of the aerobic treatment there was about 2.5 times more ^{14}C - associated label than for the endogenous and pyruvate amended anaerobic treatments. No radiolabel associated with captured gas species were detected above background counts for any of the treatments. These results suggest as a whole that addition of an electron donor, such as pyruvate, could help increase the extent and rate of DNAN product-incorporation into the humin fraction in soils during biotransformation. Moreover, under aerobic conditions incorporation occurred, albeit at slower rates and lower extent.

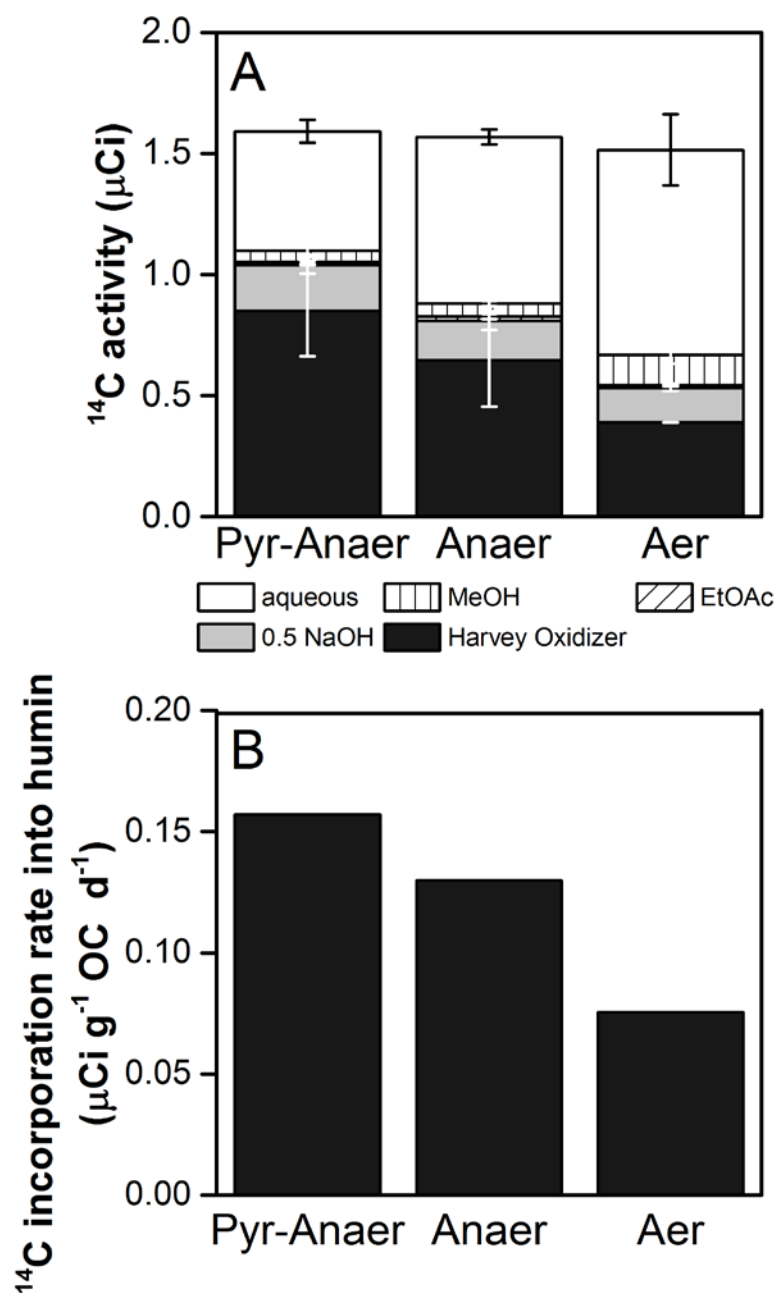


Figure 4.7-2. Impact of redox conditions on extent and rate of ^{14}C -ring DNAN labeled carbon incorporation into different extractable liquid and residual solid fractions during (bio)transformation in CN soil (25 g L^{-1}). Treatments included 10 mM pyruvate amended anaerobic (Pyr-Anaer), endogenous anaerobic without pyruvate added (Anaer) and endogenous aerobic without pyruvate added (Aer) conditions. Panel A: ^{14}C label distribution at 40 days of incubation. Panel B: ^{14}C -incorporation rate (0-40d, period of maximum slope) into the humin. Humin was measured with $^{14}\text{CO}_2$ from the combustion of the residual soil in a Harvey Oxidizer after all the extractions.

4.7.5. Anaerobic-aerobic sequential experiments.

A sequential combination of anaerobic-aerobic conditions was evaluated as strategy to increase the amount of ^{14}C incorporation into the soil humin utilizing CB soil at a concentration of 25 g L^{-1} (Figure 4.7-3). Like in the previous experiments, the majority of the label incorporated occurred in the humin phase, and pyruvate amendment increased the initial rate and extent of the ^{14}C incorporation. Upon switching to aerobic conditions, the treatment that was initially amended with pyruvate (panel B) remained relatively stable until the end of the experiment (104d), with no permanent large increase in the fraction of radioactivity incorporated into humin. On the other hand, the endogenous treatment, continued to have ^{14}C become incorporated into the humin fraction during the aerobic phase, albeit at a rate that was three-times slower than during the anaerobic portion of the experiment. By 104 d, both of these treatments had a comparable fraction of the ^{14}C label incorporated into soil humus, ranging between 63-65% of the total label.

Sequential anaerobic-aerobic treatment has been proposed for nitroaromatic compounds either for mineralization or for composting in soils, the latter being a strategy used for TNT²⁰⁶. However, in the findings here for DNAN, most of the incorporation occurred during the anaerobic phase. Although, there was continued incorporation during the aerobic regime, the rate of incorporation did not seem to be improved by switching from anaerobic to aerobic conditions. On the other hand, during the aerobic phase, addition of HRP with H_2O_2 , resulted in increasing the incorporation to the humin fraction almost instantaneously from 40 to 49.5% (Figure 4.7-3C). While the HRP was added as a single dose, humin incorporation continued to increase with time, reaching 58.8% by day 104. HRP has been used as catalyst of condensation reactions with aromatic amines^{207,208} and has been shown to catalyze incorporation reactions into soil with TNT metabolites^{209,210}.

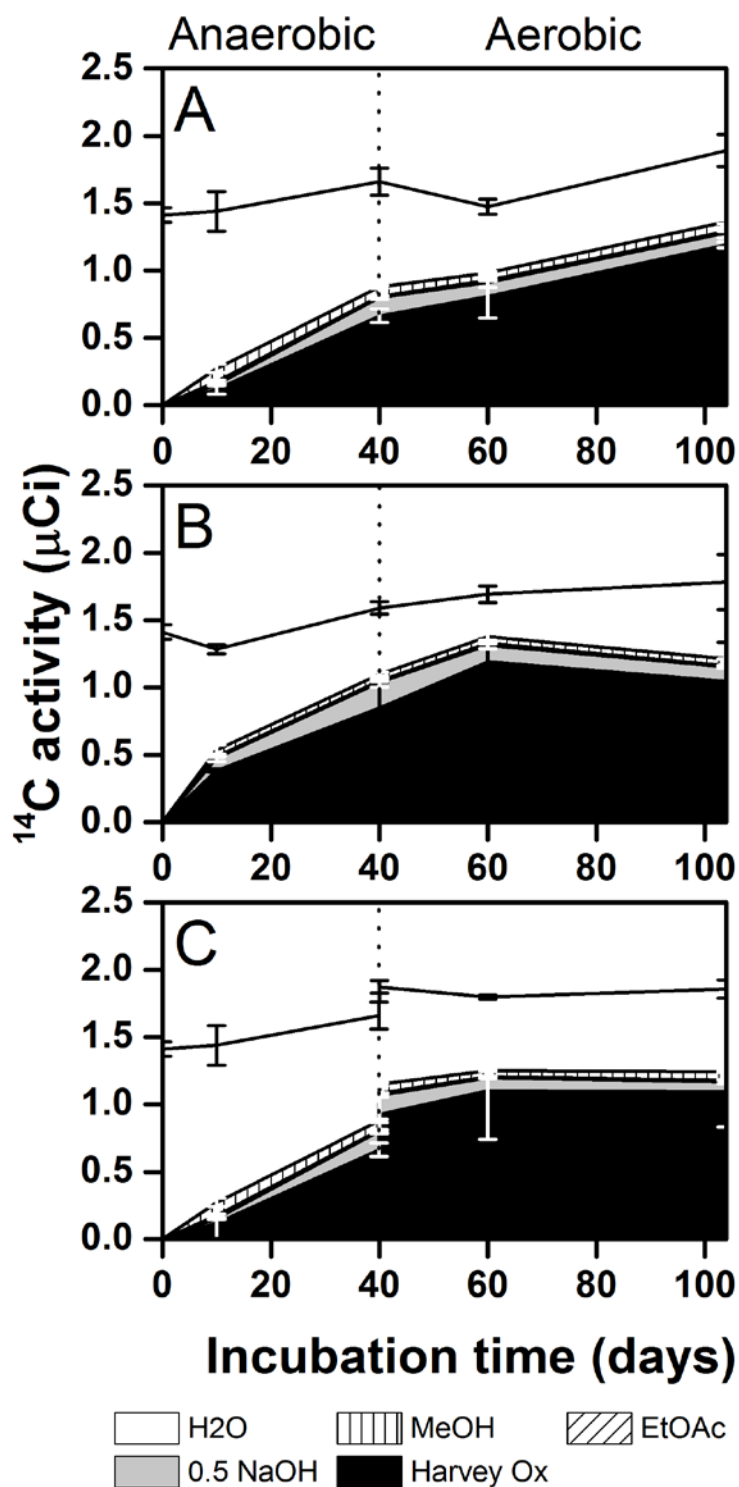


Figure 4.7-3. Effect of pyruvate and horseradish peroxidase addition on radiolabelled carbon soil incorporation during sequential anaerobic(0-40d)-aerobic(40-104d) biotransformation of ^{14}C -ring DNAN in CN soil (25 g L⁻¹). Panel A: endogenous. Panel B: amended with 10 mM pyruvate at day 0. Panel C: endogenous with horseradish peroxidase (HRP) and H₂O₂ added at day 40.

4.7.6. Humin and organic carbon addition for higher incorporation

Throughout all the biotransformation assays, performed in the present work under different redox conditions and amendments, the incorporation of ^{14}C occurred to a great extent into the humin fraction of the soil humus in CN and CB soils. Therefore, in order to analyze the role of the amount of humin available on ^{14}C incorporation, a range of soil quantities were used and in another experiment, a purified humin was artificially added to a soil and incubated until ^{14}C incorporation ceased (Figure 4.7-4). Increasing the amount of soil used in the biotransformation assays influenced greatly the amount of radiolabeled incorporated in the humin phase as determined by combustion in Harvey Oxidizer. The highest amount of label incorporated to the humin fraction (78.6%) was achieved with 50 g L^{-1} of CN as inoculant, which was $3.7\times$ higher than the treatment with the lowest amount of CN soil, 5 g L^{-1} . Similarly, addition of purified humin to CB soil, resulted in a higher incorporation of ^{14}C label (Figure 4.7-4B). Adding 20 mg of purified humin resulted in incorporation of 66.8% of the label, while using the unamended soil resulted in only 26.4 % ^{14}C incorporation.

Based on these observations, addition of soil OC (via soil or purified humin) increased the amount of irreversible binding of DNAN products into the soil. All the treatments in the present work and preliminary experiments with similar redox conditions and incubation time (anaerobic, 40 d) were compiled in Figure 4.7-5. As seen, there is a strong positive linear correlation ($R^2=0.93$) between the mass of OC to initial DNAN mass and the percentage of the ^{14}C radiolabel incorporated into the humin fraction (as operationally defined by label recovery from Harvey Oxidizer combustion of exhaustively extracted samples). That relationship holds very well up to $0.8\text{ mg OC} / \text{mg DNAN}$, thereafter there is no longer any improvement in the incorporation of ^{14}C at higher levels of OC per unit mass of DNAN. The saturation point may represent the saturation of the reaction of the two available aromatic amine groups expected to be formed from DNAN reduction to DAAN. A model in which these two groups are substituted into humic quinone moieties represented by 2-methoxy-1,4-hydroquinone is provided in Figure 4.7-6). Globally, these findings strongly suggest that organic carbon is a strong predictor of the level of incorporation of DNAN biotransformation products into the insoluble fraction of humus (humin). The OC of soil could potentially be used to estimate a maximum DNAN load a given soil can irreversibly attenuate. If the intrinsic OC levels are too low, the irreversible attenuation capacity can be improved by adding even more OC in the form of compost or peat to the soil.

Aromatic amine metabolites of TNT are known to react and become covalently bound with soil humus even under anaerobic conditions. For example, the addition of 2,4,6-triaminotoluene (TAT) to anaerobic soil cultures spiked with humus have resulted in rapid irreversible binding of TAT to the humus²⁰¹. When ^{14}C -TNT is incubated in soil anaerobically under conditions similar to our study (with addition of readily biodegradable electron donating substrates), a large fraction of the ^{14}C -label is subsequently found associated with the humin fraction^{55,203,204}. The incorporation of reduced TNT metabolites into the humus has further been confirmed by ^{15}N -NMR spectrometry^{54,57,203}.

The most likely explanation for the anaerobic irreversible binding of aromatic amines into soil humus is nucleophilic substitution of the amino group onto carbonyl structures or the double bonds of quinone subunits of humus ^{61,62}. The evidence for nucleophilic substitution reactions of quinone structures with a broad variety of aromatic amines is well documented. While there has never been a direct pairing experiment between DAAN and a quinone, we can predict the reaction shown in Figure 4.7-7. The predicted reaction shows that after the amine group substitutes into the double bond of the quinone structure, the quinone converts to a hydroquinone. In order to propagate an additional N-substitution, an additional quinone, which can be formed by the oxidation of hydroquinones. Under aerobic conditions, phenol oxidizing enzymes such as laccase are able to oxidize the hydroquinones to quinones ^{62,64}. However under anaerobic conditions, alternative mechanisms of hydroquinone oxidation are required. Fe(III) containing mineral oxides can oxidize hydroquinones to quinones ^{211,212}. The reduction of nitroaromatic compounds by reduced iron in anaerobic environments results in the formation of the Fe(III) mineral oxides ³⁷, which later can oxidize hydroquinones to quinones. Thus the nitroaromatic reduction process supplies Fe(III) for hydroquinone oxidation to quinones. These quinones can subsequently become covalently linked via nucleophilic substitution reactions with the aromatic amines that are also generated from nitroaromatic compound reduction Figure 4.7-8. If present, Mn(IV) mineral oxides also known to oxidize hydroquinones to quinones ²¹³.

A second possible explanation of the covalent bonding of aromatic amines into the soil humus under anaerobic conditions is via radical reactions initiated by a one-electron oxidation caused by Mn(IV) oxide minerals, forming a cationic amine radical ^{25,68}. These radicals can couple with each other or react with aromatic structures in the soil humus matrix. Figure 14C-9 provides a general scheme of these type of reaction based on literature data with several types of aromatic amines.

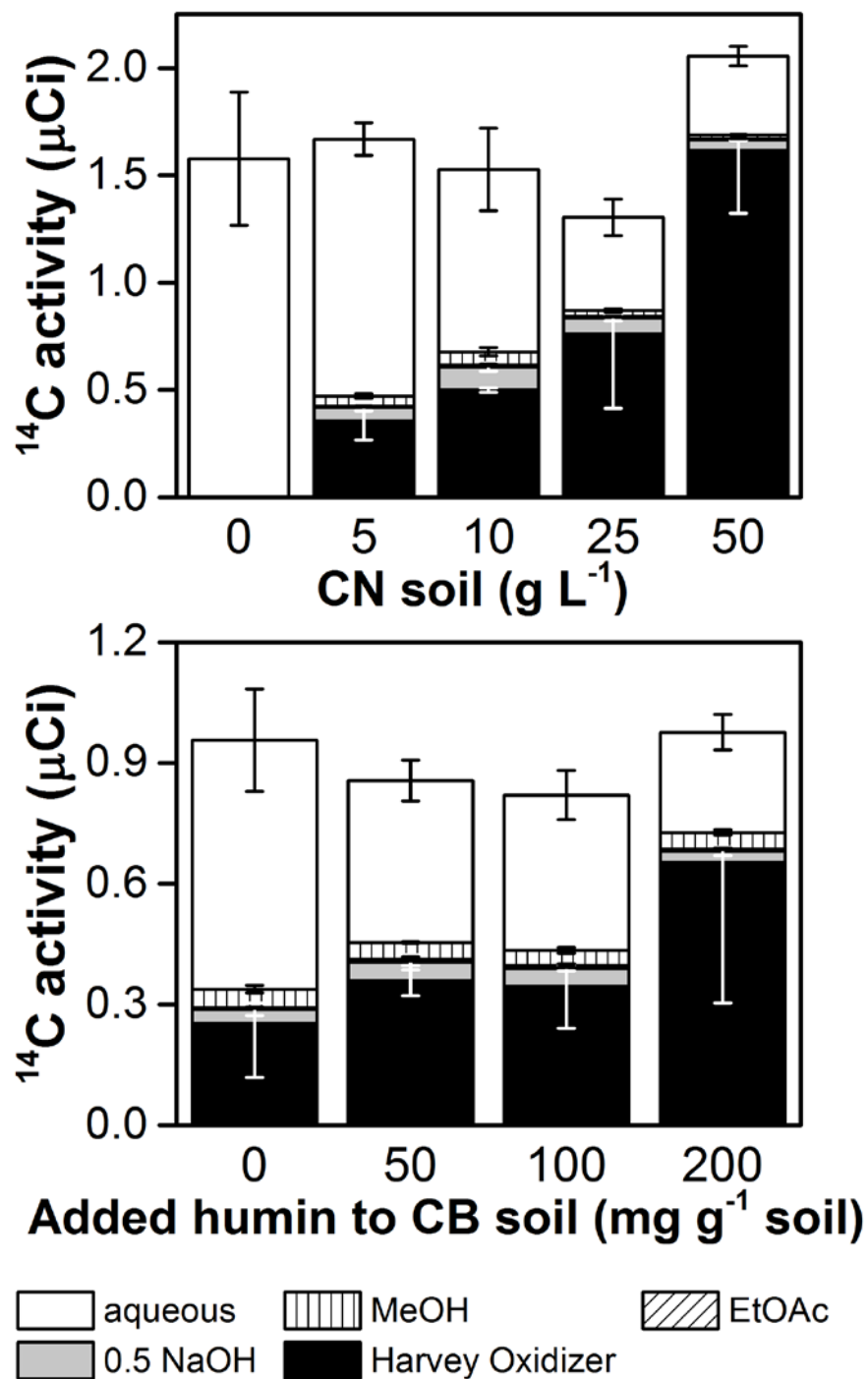


Figure 4.7-4. Increased incorporation of ^{14}C into soil humus with increased organic carbon added as natural soil or by spiking soil with humin during the course of DNAN biotransformation amended with 10 mM pyruvate in anaerobic conditions. Panel A: Incubations with different CN amounts of soil extracted at day 40. Panel B: Incubations with CB soil (25 g L^{-1}) and different amounts of purified humin added.

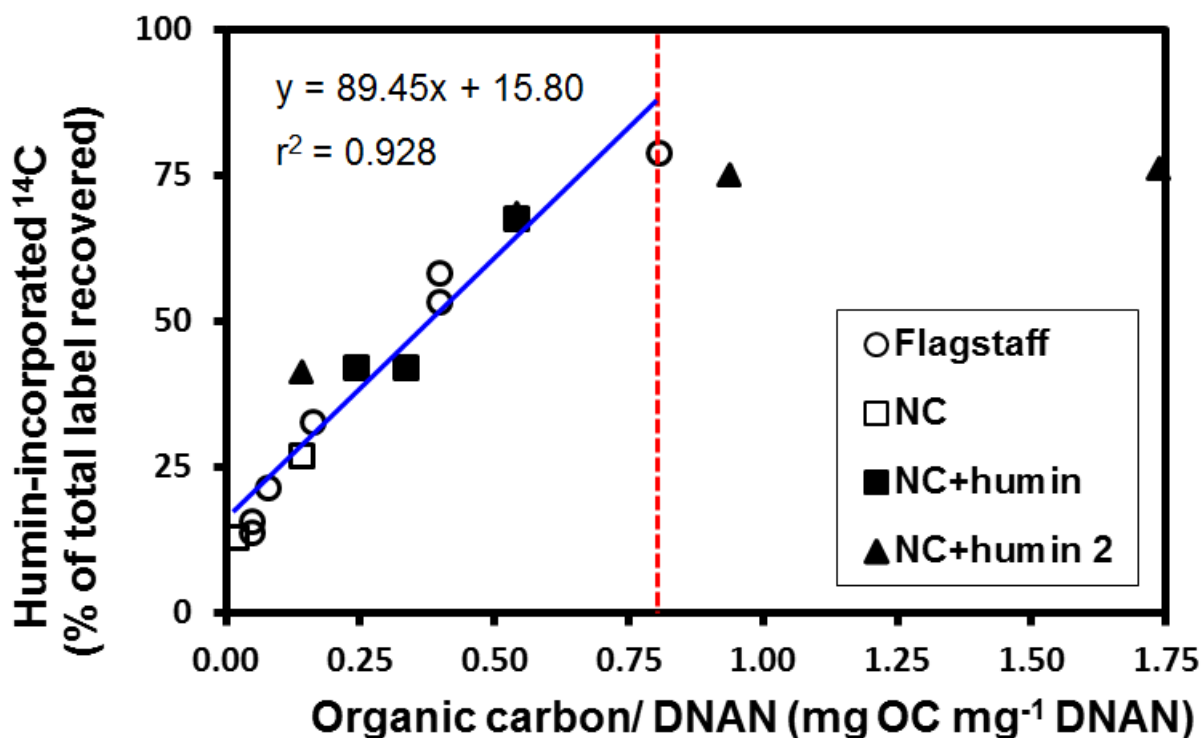


Figure 4.7-5. Correlation of organic carbon to DNAN ratio with ¹⁴C-ring labeled DNAN incorporation into humin extracted at 30-50d of anaerobic incubation amended with 10 mM pyruvate. CN soil (○), CB soil (□), CB soil amended with humin: experiment 1 (■) and experiment 2 (▲) incubations.

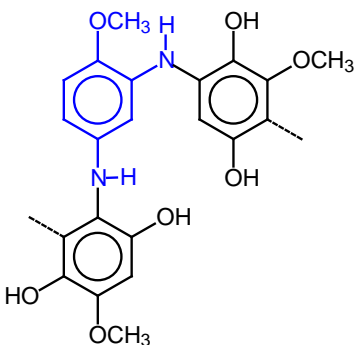


Figure 4.7-6. A suggested conceptual structure of DAAN covalently bound to two quinone moieties in humus, using 2-methoxy-1,4-hydroquinone as a model of the OC in humus. This conceptual structure would correspond to OC:DNAN (mg:mg⁻¹) ratio of 0.85.

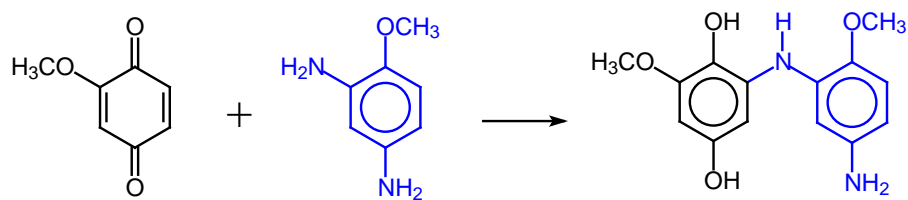


Figure 4.7-7. Predicted reaction between DAAN and 2-methoxy-1,4-benzoquinone.

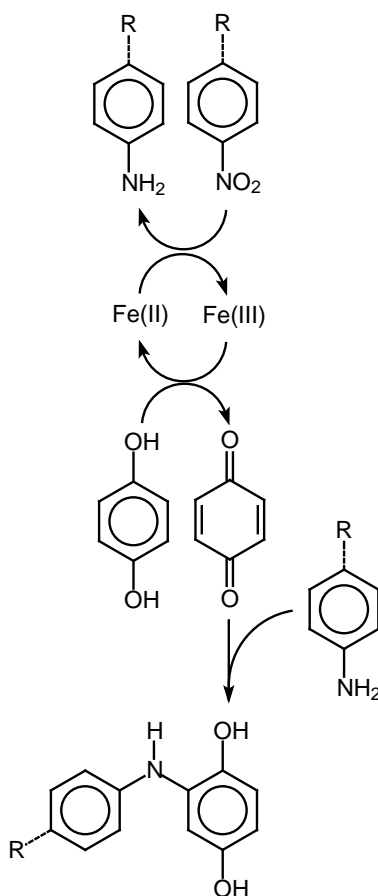


Figure 4.7-8. Hypothesized formation of Fe(III) oxide minerals during Fe^{2+} mediated reduction of nitroaromatic compounds to aromatic amines that enables the oxidation of hydroquinones to quinones which in turn can form irreversible covalent bonds with aromatic amines via nucleophilic substitution reactions. A total of 6 mol Fe(III) can be formed by reduction of each nitro group which is sufficient to oxidize 3 hydroquinones to quinone and only one quinone is required to form a covalent bond.

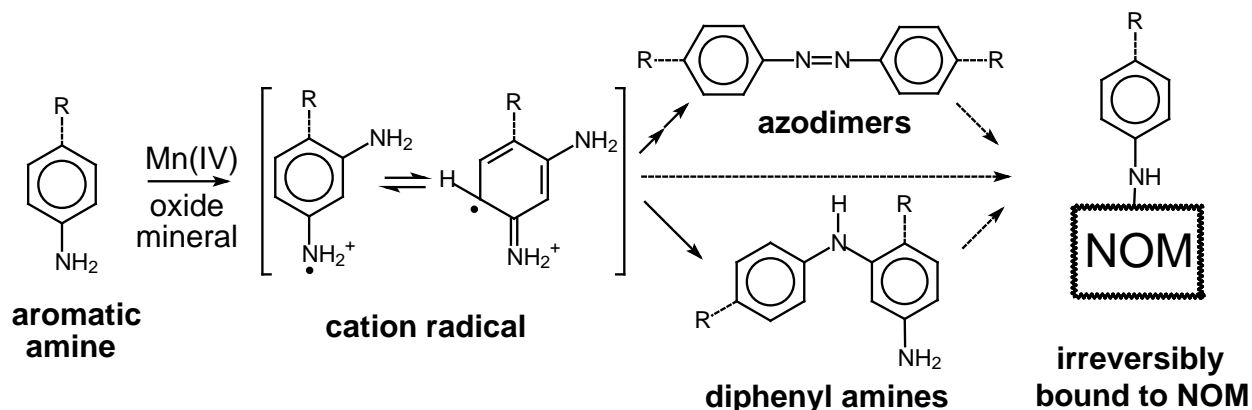


Figure 4.7-9. Reaction of aromatic amines with MnO₂ involving a cation radical mechanism, formation of dimeric intermediates and the ultimate irreversible covalent bonding of the aromatic amines and dimers with the soil humus (natural organic matter, NOM). R = rest of molecule.

4.7.7. Conclusions: Fate ¹⁴C-DNAN in soil

During incubations of ring labeled ¹⁴C-DNAN, a large fraction of water soluble radiolabel decreases and most of that decrease in radiolabel becomes incorporated into a fraction of the soil that is not extractable and is assumed to be part of the insoluble soil humus fraction known as humin. Only negligible to small recoveries of ¹⁴C label are found in the volatiles, organic extractable fractions; whereas only very modest recoveries of label are found in the NaOH extractable fraction (considered to be humic acid).

The first and foremost conclusion of the study is that OC quantity as a ratio of the initial DNAN quantity is the single most important factor dictating what fraction of the ¹⁴C-DNAN becomes incorporated into the insoluble humin fraction. The mg:mg ratio of OC: DNAN_{initial} provides a very strong prediction of the ultimate incorporation of DNAN molecules into humin. This correlation with the OC:DNAN_{initial} ratio is strong irregardless of the source of the OC (either from one of two soil types or added humin). That correlation is valid up to a ratio of 0.8 mg OC mg⁻¹ DNAN, which coincides with the two N groups in DNAN being substituted into quinone moieties of humus after DNAN is fully reduced to DAAN. Further increments in the OC:DNAN_{initial} ratio do not increase incorporation of ¹⁴C into humin because the reactive amine groups are saturated.

At a given OC:DNAN ratio, this study also evaluated the effect of different treatments on the incorporation of ¹⁴C-DNAN into humin. Globally, speaking the treatment effects were relatively small compared to the impact of the OC:DNAN ratio. Nonetheless, the more anaerobic the conditions, a greater rate and extent of ¹⁴C incorporation is observed compared to aerobic conditions. The findings are in stark contrast with the established paradigm in an important review of TNT bioremediation by Esteve-Nunez, et al.²¹⁴. The paradigm considered anaerobic conditions are solely involved in the formation of aromatic amines; whereas aerobic conditions are required to (co)polymerize and covalently link the aromatic amines into humus. The reason this paradigm can now be rejected is the compilation of evidence to the contrary showing that significant strong

sorption ²⁰¹ and covalent incorporation ^{55,203,204} of reduced TNT intermediates into humin occurs under anaerobic conditions. The results of the current study demonstrate that the same is also true for reduced DNAN intermediates because large fractions of ¹⁴C-DNAN becoming irreversibly bound in humin under highly reducing conditions.

4.8. Biotransformation and Degradation of NTO by Soil Bacterial Communities

Although there is initial evidence of NTO biotransformation and biodegradation, studies are needed to evaluate the biodegradability of NTO in soils where residues of unexploded ordnance may end up as contamination in military firing ranges. We report the biodegradation of NTO and its main metabolite ATO by microbial communities in diverse soils under aerobic and anaerobic conditions. Several different electron donors (e-donors) and the presence and absence of a nutritional amount of yeast extract (YE) were also tested. This constitutes the first study to determine if soil microbial communities can mineralize NTO nitrogen (N).

4.8.1. Results: Anaerobic reduction of NTO to ATO

In this study, microbial communities from a wide range of soils were tested in microcosms for their ability to degrade NTO. The seven soils used included five unique textural classes and covered a broad range of characteristics Table 4.8-1 (and additional supplementary data in Krzmarzick, et al. ¹⁰⁰). In anaerobic microcosms with H₂ added as an e-donor, NTO was fully biotransformed (Figure 4.8-1). No biotransformation was observed in killed- or non-inoculated controls. Endogenous controls (no external e-donor) displayed NTO bioconversions rates of 0.03 mM d⁻¹ and 0.006 mM d⁻¹ in Camp Navajo soil and in Florence soil microcosms, respectively. Amendments with H₂ as e-donor increased biotransformation rates, ranging from 0.23 (Roger Road) to 1.25 mM d⁻¹ (Camp Navajo). No clear connection between biotransformation rates and TOC or total soil N was observed. There was a negative correlation with soils with alkaline pH that corresponded to slower biotransformation rates (Spearman's $\rho = -0.85$, $P = 0.016$).

ATO was the dominant product from NTO biotransformation under anaerobic conditions. ATO formation was concomitant to the removal of NTO, and the yield of ATO production as a fraction of NTO removed was stoichiometric. Conversion NTO to ATO was very low in endogenous microcosms indicating that NTO conversion was dependent on the presence of an external e-donor. The ability of Camp Butner soil microbial communities to use various e-donors to degrade NTO was tested, both with and without a nutritional amount of yeast extract (YE) (Figure 4.8-2). In most cases, the e-donors stimulated biotransformation of NTO compared to endogenous controls and decreased the lag phase for NTO reduction.

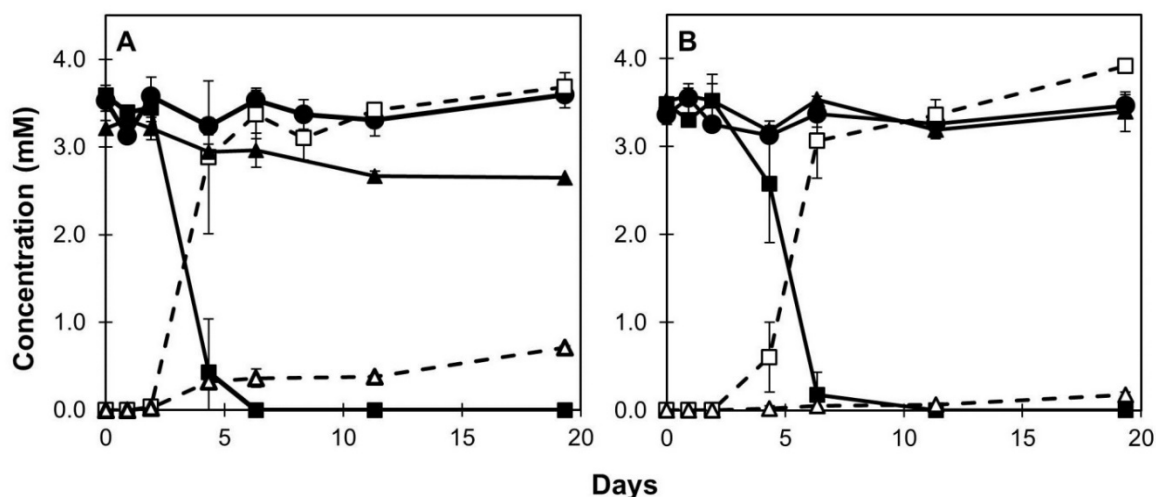


Figure 4.8.1. The anaerobic degradation of NTO to ATO in microcosms inoculated with (A) Camp Navajo (AZ) soil, and (B) Florence (AZ) soil in H₂ amended microcosms (squares) endogenous controls (triangles), and killed controls (circles). NTO concentrations are shown with solid symbols and solid lines and ATO concentrations are shown with open symbols, dotted lines). Error bars indicate standard deviation of duplicate microcosms.

YE did not improve the rates of biotransformation if the e-donor could readily serve as carbon source, such as the cases with the citrate or pyruvate amended microcosms (Figure 4.8-2. and additional supplementary data published elsewhere¹⁰⁰). Conversely, YE was responsible for a major improvement in the rate for the e-donors that did not include carbon such as with the H₂-amended microcosms Figure 4.8-2, or with the microcosms with e-donors that readily yield H₂ upon anaerobic fermentation (e.g. lactate).

With many of the electron donors, minor amounts of the intermediate HTO were observed (Figure 4.8-2). HTO did not accumulate, probably because it was quickly reduced to ATO.

4.8.1. Results: Lack of aerobic degradation of NTO

NTO was not degraded under fully aerobic conditions with any of the soils. In these microcosms, pH was maintained at 7.2 for at least 62 d (and up to 112 d). Two soils, Camp Butner and Camp Navajo, were also tested for their ability to aerobically degrade NTO with glucose addition, increased pH, and under N-limiting conditions (no exogenous N source). With these treatments, NTO was not degraded with either soil.

4.8.2. Results: Degradation of ATO

The degradation of ATO was tested under various conditions with Camp Butner and Camp Navajo soils under aerobic or anaerobic conditions, with and without glucose addition, and at pH 7.2 and 8.5 (Figure 4.8-3). ATO did not degrade under any anaerobic condition with either soil. Under aerobic conditions, ATO degraded relatively slowly with both soils as evidenced by loss of parent compound and detection of inorganic N species. With Camp Butner soil, ATO was degraded in all aerobic microcosms and the fastest degradation occurred at pH 7.2 without glucose addition. With the Camp Navajo soil, the fastest degradation occurred at pH 8.5 without glucose addition. At pH 7.2 and with glucose addition, the duplicate microcosms were dissimilar, with only one replicate degrading the ATO. Generally, nitrite was found to initially rise, followed by a permanent rise of

nitrate, far above the background amount of inorganic N (0.5 mM). In controls without ATO amendment and with killed controls and non-inoculated media-only controls, inorganic N species remained very low and did not increase.

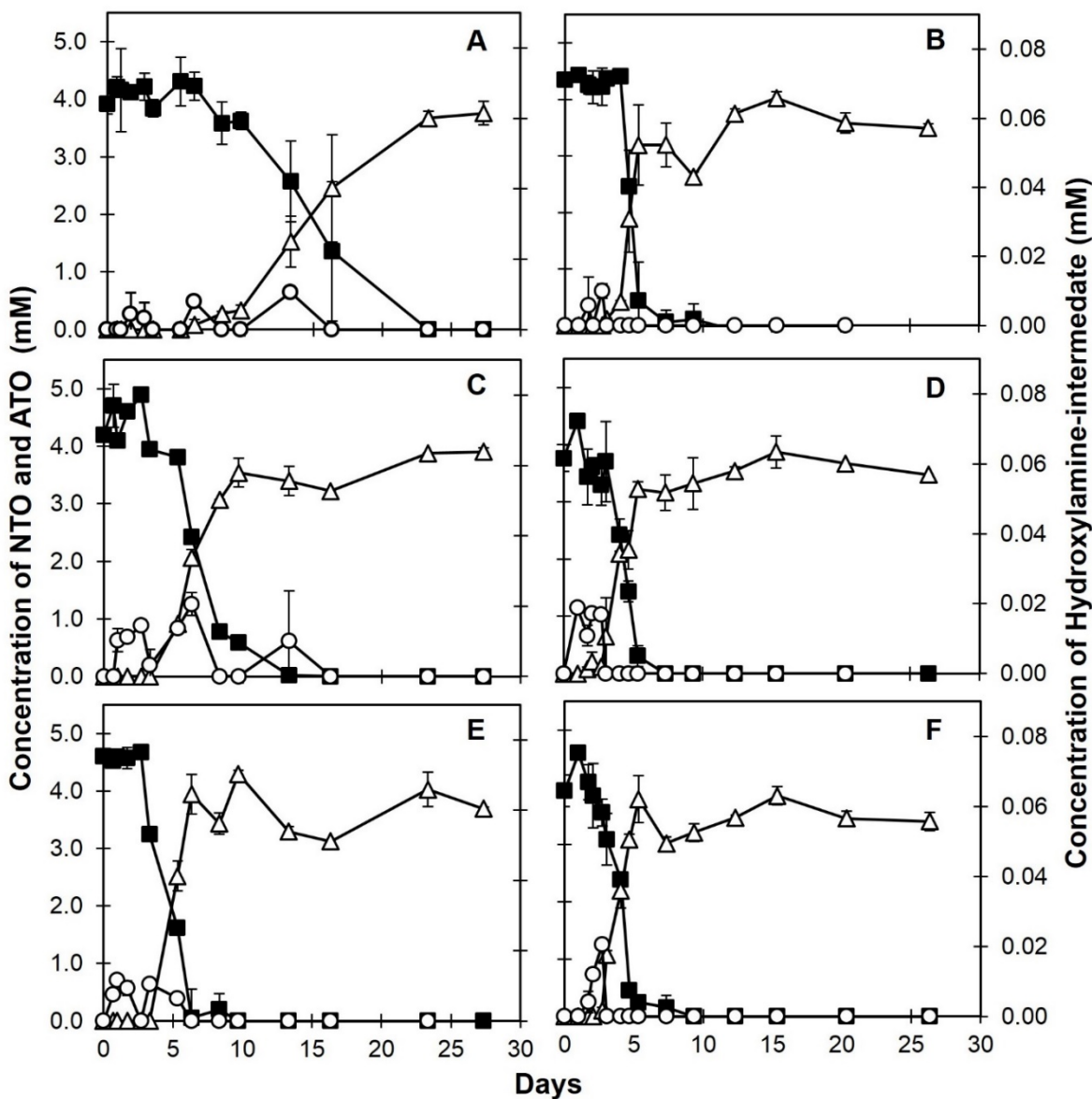


Figure 4.8-2. Degradation of NTO to ATO in microcosms with H_2 as an electron donor without YE (A) and with 10 mg L^{-1} YE (B), or with 20 mM of citrate without YE (C) and with 10 mg L^{-1} YE (D), or with 20 mM pyruvate without YE (E) and with 10 mg L^{-1} YE (F). The concentration of NTO (black squares) and ATO (triangles) are shown on the primary axis; the concentration of the hydroxyl-amino intermediate (circles) is shown on the secondary axis. Error bars indicate standard deviations of duplicate microcosms.

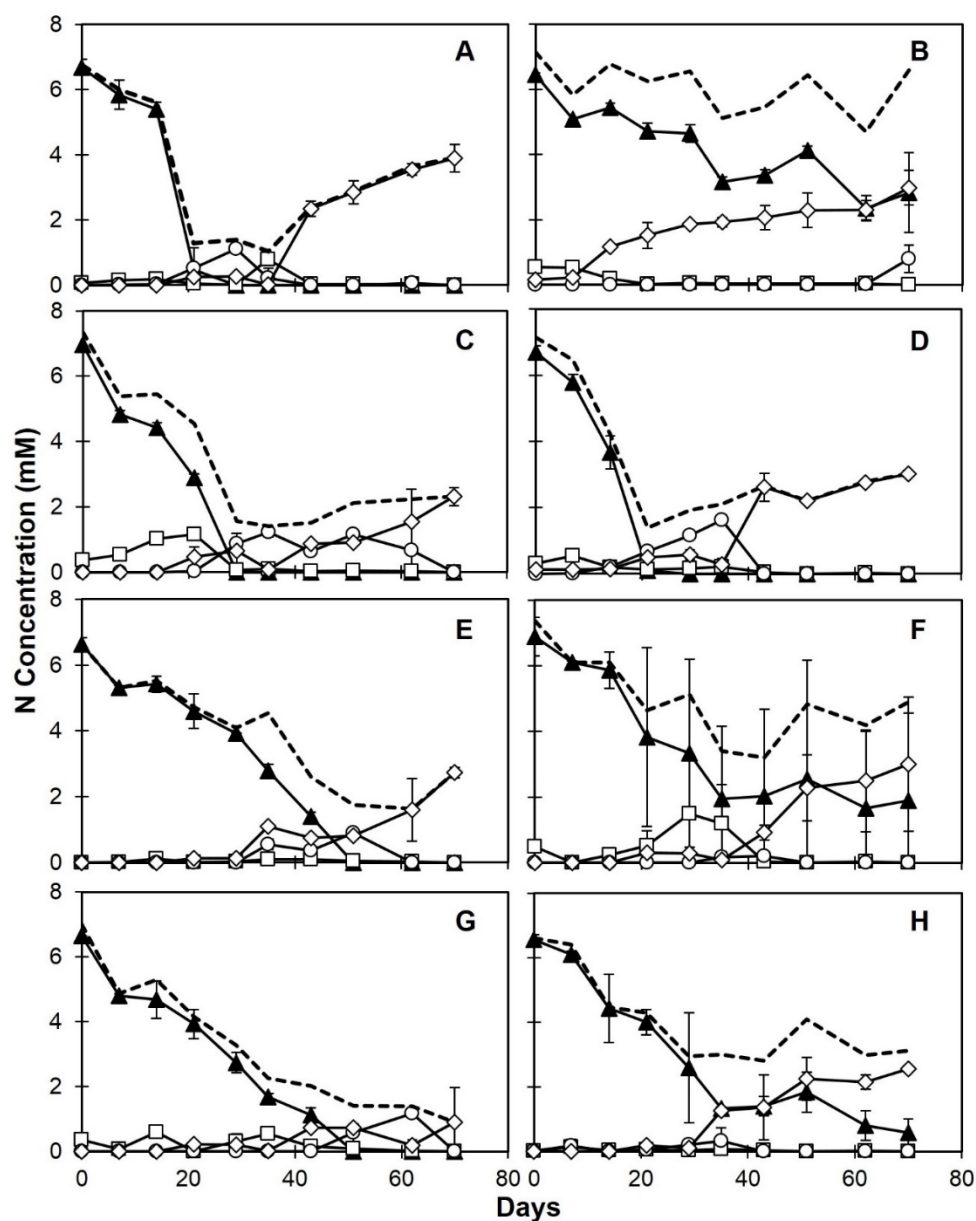


Figure 4.8.3. Degradation of ATO under aerobic conditions and release of N species: **(A)** Camp Butner soil, pH 7.2; **(B)** Camp Navajo soil, pH 7.2; **(C)** Camp Butner soil, pH 8.5; **(D)** Camp Navajo soil, pH 8.5; **(E)** Camp Butner soil, pH 7.2, with glucose; **(F)** Camp Navajo soil, pH 7.2, with glucose; **(G)** Camp Butner soil, pH 8.5, with glucose; **(H)** Camp Navajo soil, pH 8.5, with glucose. Solid triangles show ATO concentrations (as per mol of N), squares correspond to ammonia, circles to nitrite, diamonds to nitrate, and dashed line represents the sum of N species concentrations (both inorganic and ATO). Mineral medium used initially contained 0.5 mM of inorganic N (as ammonia). Results for autoclaved controls and non-inoculated controls are published elsewhere ¹.

Thus, this increase in inorganic N observed in live-soil inoculated treatments after the decrease in ATO concentration is indicative of the mineralization of the ATO in these microcosms.

Intermediate(s) between ATO and inorganic N species must exist as is seen from a lack of a molar balance between the amount of degraded ATO and the production of inorganic N products. Samples from these microcosms were analyzed with QToF-MS but no organic intermediates were detected.

4.8.3. Discussion: Lack of NTO biodegradation under aerobic conditions

Nitro groups are electron withdrawing making direct oxidation of the molecule difficult. However, nitroaromatics (NACs) with two or less nitro-groups have been degraded by several oxidative pathways²¹⁵. In other cases, aerobic bacteria will reduce NACs to aromatics with hydroxylamino groups^{215,216} or to amino- groups^{217,218}, which are then further metabolized. Less is known concerning the aerobic biodegradation of nitro-heterocyclic compounds that may also require a reduction of the nitro group, but may involve different mechanisms. The reduction of NTO to ATO in this study was only achieved under anaerobic conditions, suggesting the need of an anaerobic step for bioremediation. On the other hand, Le Campion et al.²¹⁹ and Richard and Weidhaas²²⁰ observed reduction of NTO in the presence of O₂ using high amounts of cells and rich organic broths as medium (e.g. glucose). High levels of organic substrates in those experiments may have unknowingly produced O₂-deficient conditions as the organic substrates were consumed.

Nitro-group containing organic compounds are likely difficult to biodegrade aerobically in soils. Similar to our findings, the degradation of the heterocyclic compound RDX was not degraded by soil microbial communities under aerobic conditions²²¹. TNT is also not readily degraded aerobically except when co-amended with other substrates which cause nitro group reduction to occur²²². In our study, however, the addition of glucose did not aid in the biodegradation of NTO under aerobic conditions.

4.8.4. Discussion: Anaerobic biotransformation

The anaerobic reduction of NTO to ATO occurred in all seven soils tested, indicating that this pathway (Figure 4.8-4) should be ubiquitous in soil environments if subjected to anaerobic conditions. The facile anaerobic reduction of nitro groups is common^{188,223,224}. The complete reduction of the nitro- to the amino group in NTO occurred readily with nearly stoichiometric amounts of ATO produced in nearly all cases. Stoichiometric reduction of NTO to ATO was observed in previous literature with *Bacillus licheniformis* and mammalian liver microsomes²²⁵ and has been observed in soils for RDX²²¹. The results here indicate this reduction process is very ubiquitous.

4.8.5. Discussion: Nitroreductases

Specific nitroreductase enzymes have been implicated in some aerobic NAC-degrading bacteria^{215,223}. Less specific oxygen-insensitive nitroreductases of enteric bacteria can reduce TNT and RDX^{223,226,227}. Hydrogenases and carbon monoxide dehydrogenase pyruvate:ferredoxin oxidoreductase of *Clostridia* have been shown to reduce TNT^{223,224}. Bulk reducing agents generated in anaerobic environments such as sulfide together with redox mediating NOM and Fe(II) adsorbed to iron oxide minerals are also known to reduce nitro groups abiotically^{169,228}.

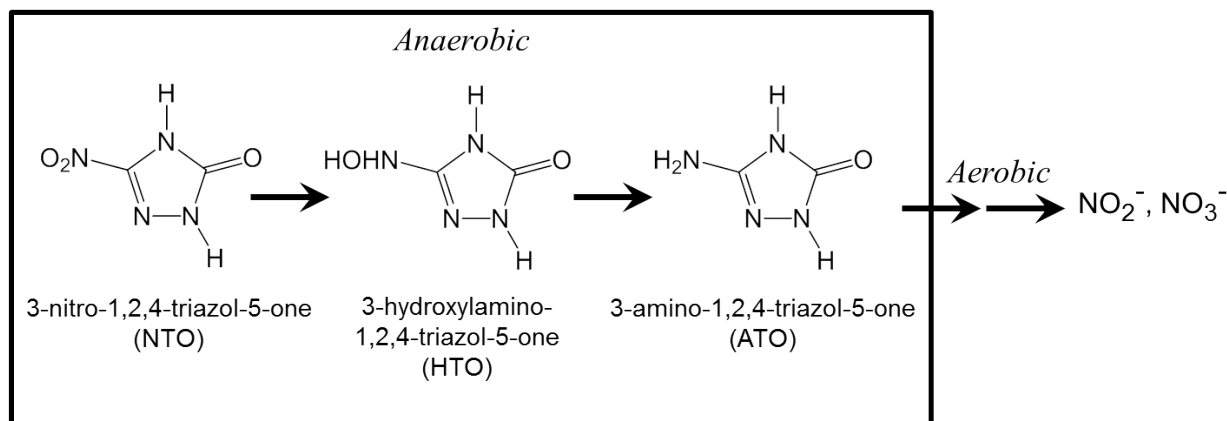


Figure 4.8-4. The biotransformation and degradation pathway of NTO found in this study.

Though such a mechanism is theoretically possible in our experiments, the relatively low concentrations of sulfate (0.4 mM) amended in the mineral medium would need to be cycled many fold in order to provide the reducing electrons needed to transform the amount of NTO added (3.8 mM). The IM compound, DNAN was transiently converted to both nitroso- and hydroxylamine intermediates as it was being reduced to 2-amino-4-nitroanisole by an aerobic soil bacteria, *Bacillus* sp. 13G²²⁹.

4.8.6. Discussion Physiology

An external e-donor was required for rapid and complete biotransformation. In previous studies, the reduction of nitrated explosives also needed e-donors, and similar to this study, diverse sources of e-donors were found suitable^{168,224,230,231}. H₂ or substrates that generate H₂ during their conversion were the best e-donors in agreement with our findings. YE provided a critical nutritional requirement to the soil microflora that enabled them to reduce NTO with a decreased lag phase with nearly every e-donor tested and an increased degradation rate with many of the e-donors. YE also increased reduction of the nitro groups in TNT by a *Pseudomonas* strain²³².

4.8.7. Discussion: Degradation products

The reduction of nitro groups occurs via three steps of two electron reductions of nitro- to nitroso-, nitroso- to hydroxylamino-, and hydroxylamino- to amino groups²²³. In this study, NTO was reduced to ATO with small amounts of the hydroxylamino intermediate (HTO) being observed temporally in some assays. The HTO as an intermediate of NTO biotransformation has not been reported previously. TNT is often observed to degrade to mixed amounts of hydroxylamino- and amino derivatives by bacteria²³³⁻²³⁵ and RDX is most commonly associated with a reduction to nitroso intermediates^{229,236,237}. Hydroxylamino intermediates are known to be reactive^{238,239}. In studies with DNAN, the mixture of hydroxylamino- and nitroso intermediates may lead to dimerization products when degraded by bacteria^{85,229}. A similar high level of reactivity was not observed in this study, since there was not a major loss in the stoichiometric yield of ATO in biodegradation tests even under conditions with the highest HTO intermediate concentration or conditions with the most prolonged exposure to HTO. Additionally, coupling products were sought using MS-QToF yet these products were not found.

ATO was never degraded in any of the anaerobic experiments in this study but degradation was observed under aerobic conditions. The N balance was incomplete after the degradation of ATO and prior to the production of inorganic N products indicating that intermediates not measured nor detected in this study were produced. Heterocyclic explosives such as RDX and HMX become unstable after initial reduction of the nitro groups due to the weak energy of C–N bond leading to abiotic hydrolysis²⁴⁰⁻²⁴². In contrast, ATO was stable in anaerobic conditions and degradation in aerobic conditions occurred slowly. Previous research shows that ATO can be ring cleaved at mildly alkaline pH²¹⁹. A higher pH did accompany a faster degradation rate in the Camp Navajo soil without glucose addition, but otherwise an increase in pH was not accompanied with significantly better degradation of ATO. Le Campion et al.^{219,225} found ring cleavage products such as CO₂ and urea. Likewise they putatively identified hydroxyurea. Urea and hydroxyurea could potentially represent N-compounds that were missing in the N-balance of this study. Additionally, denitrification may have occurred if there were anaerobic niches in the aerobic assays, causing N to be released as N₂ gas.

A recent study²²⁰ reported aerobic conversion of NTO using an enrichment culture exposed to the munitions formula IMX-101 as a N source and organic co-substrates. They indicated an NTO degradation product lacking the nitro group; however, the LC-MS evidence provided did not support the proposed structure.

4.8.7. Conclusions:

In soils, the degradation of NTO may be stimulated by promoting an initial anaerobic phase to form ATO followed by an aerobic phase for ATO biodegradation. In aerobic conditions, our research suggests that NTO will be non-biodegradable in soils. In anaerobic environments, it will most likely be readily converted to ATO, but ATO will then persist in anaerobic conditions. In aerobic conditions, ATO may be susceptible to mineralization depending on the soil microbial community and pH conditions. The addition of cosubstrates (e.g. glucose) was not observed in our study to necessarily enhance ATO degradation.

Table 4.8-1. Selected properties of the soils used in this study.

Soils	pH	BET SA [†]	TN [§]	TC [¶]	TOC [‡]	Soil Texture			
						Sand	Silt	Clay	Textural Class
		m ² g ⁻¹	-----g kg ⁻¹ -----			-----%			
Camp Ripley (MN)	6.0±0.1	1.7±0.03	1.27±0.20	12.55 ± 1.50	12.5 ± 1.50	78.2	14.0	7.8	Loamy Sand
Camp Butner (NC)	6.4±0.0	4.9±0.07	1.33 ± 0.05	20.69±1.20	20.69 ± 1.20	68.7	19.8	11.5	Sandy Loam
Florence (AZ)	7.0±0.1	32.5±1.7	0.81± 0.02	4.16±0.20	4.16 ± 0.20	44.2	28.5	27.3	Clay Loam
Camp Navajo (AZ)	6.3± 0.0	21.5±0.6	3.65 ± 0.21	52.36±3.70	52.36 ± 3.70	21.5	38.1	40.4	Clay
Maricopa (AZ)	7.8± 0.1	34.6±1.7	0.80 ± 0.05	7.07 ± 0.40	4.65 ± 0.40	37.5	22.0	40.6	Clay
Roger Road (AZ)	7.8± 0.0	27.7± 0.8	1.54 ± 0.03	18.25 ± 0.10	7.07 ± 0.40	23.3	35.1	41.6	Clay
Catlin Soil (IL)	6.4 ± 0.1	5.1± 0.4	2.81 ± 0.18	45.44 ± 1.10	44.08 ± 1.10	13.5	55.0	31.5	Silty Clay Loam

[†]Brunauer, Emmett and Teller (BET) Surface area; [§] TN = Total nitrogen; [¶] TC = Total Carbon

[‡] TOC = Total Organic Carbon.

4.9. Sequential Anaerobic-Aerobic Biodegradation of NTO

The objective of this study is to evaluate the microbial degradation of both 3-nitro-1,2,4-triazol-5-one (NTO) and its reductive daughter product, 3-amino-1,2,4-triazol-5-one (ATO), in a sequential anaerobic-aerobic batch reactor and in a continuous-flow reactor using soil microorganisms as inoculum.

4.9.1. Results: Batch bioassays

NTO biodegradation was tested under different redox regimens. Full removal of NTO was only observed in the sequenced anaerobic-aerobic treatment (Figure 4.9.1B). Under anaerobic conditions, NTO was completely transformed to ATO within 14 d, and after switching from anaerobic to aerobic conditions, ATO was fully eliminated after a lag phase of ca. 10 d. Complete NTO removal was achieved in 37 d. In the completely anaerobic regimen, all NTO was stoichiometrically converted to ATO. However, ATO was not further metabolized (Figure 4.9-1B). Under aerobic conditions, the NTO concentration was stable during the entire incubation period (Figure 4.9-1C). Anaerobic controls without addition of e-donor and yeast extract displayed a slower NTO transformation rate ($0.58 \text{ mM g}^{-1} \text{ SOC (soil organic C) d}^{-1}$). After 37 days, 44% of NTO was biotransformed. NTO transformation was also observed in the anaerobic heat-killed control, but at a constant and slower rate ($0.54 \text{ mM g}^{-1} \text{ SOC d}^{-1}$) when compared to the live culture ($1.54 \text{ mM g}^{-1} \text{ SOC d}^{-1}$). However, no transformation was observed in the anaerobic control sterilized with formaldehyde. In the media only control, NTO transformation was not observed in any of the redox regimens.

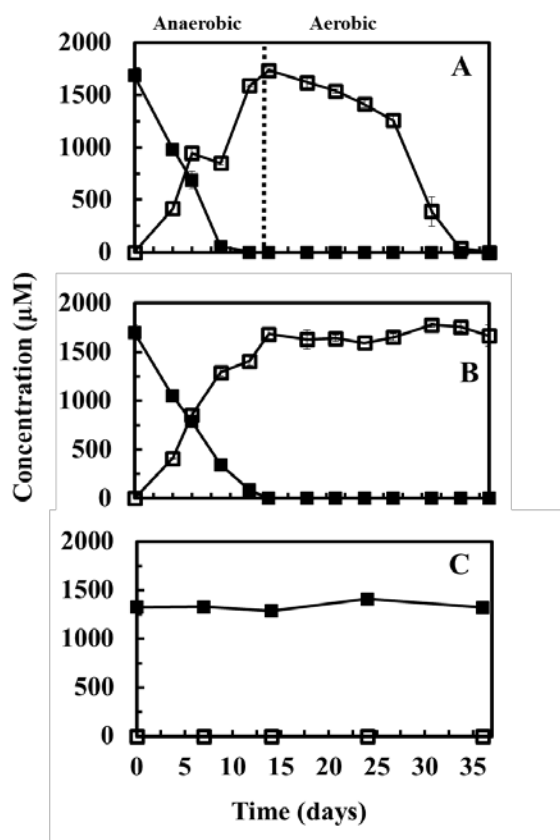


Figure 4.9-1. NTO bioconversion under various redox regimens in a soil suspension (Gortner soil 10 g L^{-1}) with pyruvate (2.7 mM). The aerobic incubation did not contain pyruvate and yeast extract. (A): Sequenced anaerobic-aerobic incubation. (B): Anaerobic incubation. (C): Aerobic incubation. Legend: NTO live culture (■), ATO live culture (□).

4.9.2. Results: Continuous flow reactor experiments

Reactor operation with ATO.

From day 0 to day 12, the reactor was operated with basal medium. During period IIa, the reactor was fed with 0.6 mM ATO as the only source of carbon and N. The analysis of the effluent indicates that all the ATO was removed during this period, since the compound was not detected in the effluent (Figure 4.9-2). During period IIb, the concentration of ATO in the influent was increased to 1.0 mM. During this period, ATO was also completely removed from the medium.

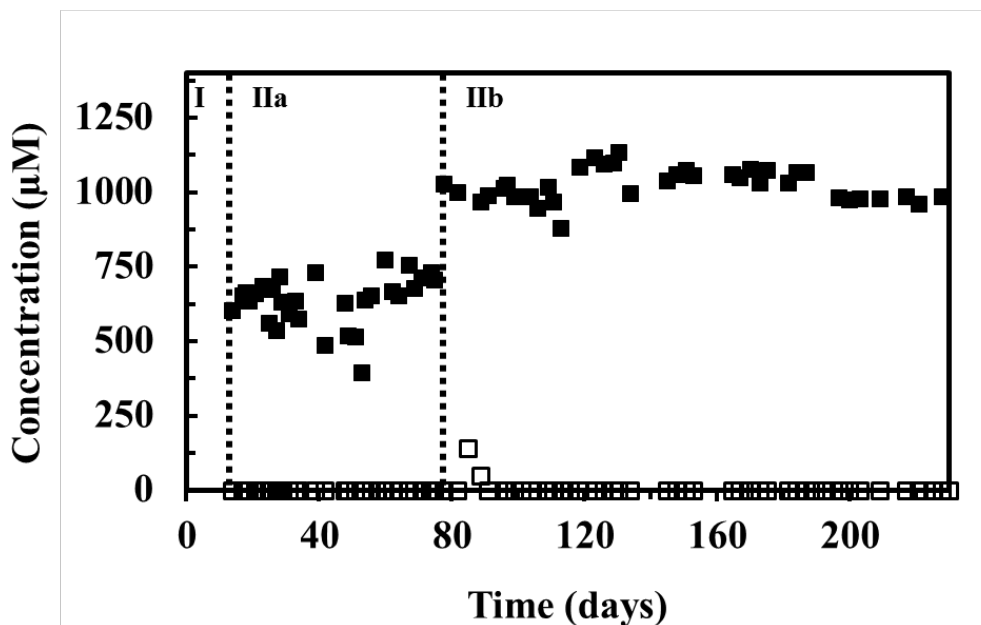


Figure. 4.9-2. Disappearance of ATO in aerated continuous flow reactor during periods I (no ATO addition, average flow rate = 154 mL day⁻¹), IIa (600 μM ATO, average flow rate = 146 mL day⁻¹), and IIb (1000 μM ATO, average flow rate = 213 mL day⁻¹). Legend: ATO concentration measured in the influent (■), ATO concentration measured in the effluent (□).

The concentration of inorganic N in the influent and in the effluent was also monitored (Figure 4.9-4A). Previously to ATO addition in the medium (Period I), very low levels of inorganic N were measured in the effluent (below 0.125 mM). During period IIa, a progressive increase in the concentration of inorganic N was observed, reaching values usually above 1000 μM, indicating that N was being released during ATO metabolism. For period IIb, the average concentration of inorganic N was about 1.50 mM. However, these values are below the expected concentration considering the complete mineralization of ATO, which would release approximately 4 mM inorganic-N. The average percent mineralization of N was 36.1% and 37.8% for periods IIa and IIb, respectively (Table 4.9.1).

Reactor operation with NTO.

In period III, the reactor was operated with 1.0 mM NTO and 1.8 mM sodium pyruvate. The concentration of NTO in the influent was relatively lower for certain samples. This variability can be explained by the partial reduction of NTO in the influent container due to the high concentration of pyruvate present in the medium, causing O₂ depletion.

Table 4.9-1. Operational conditions and performance of a laboratory-scale continuous flow reactor treating water containing ATO or NTO during different periods.

Period	Compound Added	Days	Flow rate [mL/d]	ATO influent [μM]	NTO influent [μM]	ATO removal efficiency [%]	NTO removal efficiency [%]	Nitrogen mineralization [%]
I	-	13	154 \pm 172	0 \pm 0	0 \pm 0	-	-	-
IIa	ATO	63	146 \pm 12	649 \pm 107	0 \pm 0	100 \pm 0	-	36 \pm 22
IIb	ATO	152	213 \pm 48	1024 \pm 55	0 \pm 0	100 \pm 1	-	38 \pm 5
III ^a	NTO	79	204 \pm 19	48 \pm 91	931 \pm 101	-	94 \pm 6 ^b	42 \pm 5

^a Addition of 1.8 mM sodium pyruvate as electron donor.

^b Removal efficiency after the reactor reached steady state (day 298 to 310).

in the bottom of the container. The addition of pyruvate promoted the growth of heterotrophic bacteria, leading to the consumption of oxygen and, as a consequence, creating anaerobic zones in the reactor, while at the same time providing electron donor to drive the reductive transformation of NTO to ATO. The transformation of NTO was not very significant during the first days of period III (Figure 4.9-3). However, the NTO removal efficiency gradually increased with time, and it was close to 94% after 50 days of operation. ATO was not detected in the effluent at significant concentrations during the entire period. The lack of ATO in the effluent suggests that ATO yielded from reductive NTO transformation was immediately metabolized (as witnessed in

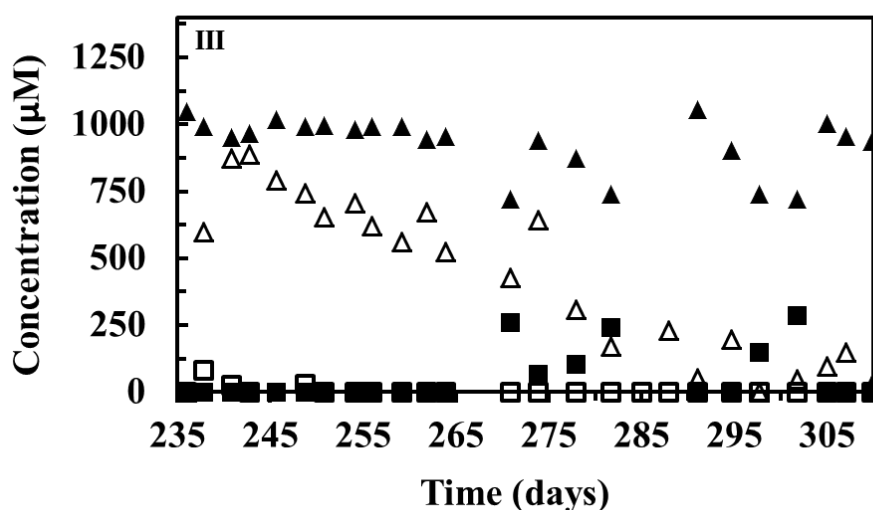


Figure 4.9-3. Disappearance of NTO and ATO in an aerated continuous-flow reactor during period III (average flow rate = 204 mL day⁻¹). NTO was added as the target substrate (1000 μM) and sodium pyruvate was added as a cosubstrate (1800 μM). Legend: NTO (\blacktriangle) and ATO (\blacksquare) concentration measured in the influent, NTO (\triangle) and ATO (\square) concentration measured in the effluent.

periods IIa and IIb) without any accumulation, which can be viewed as further evidence of ATO metabolism.

The N mineralization during period III increased with time (Figure 4.9-4A). When the reactor reached steady state (days 291-310), the average N mineralization was 41.5%, similarly to the results obtained for the periods in which the reactor was operated with ATO as the sole substrate.

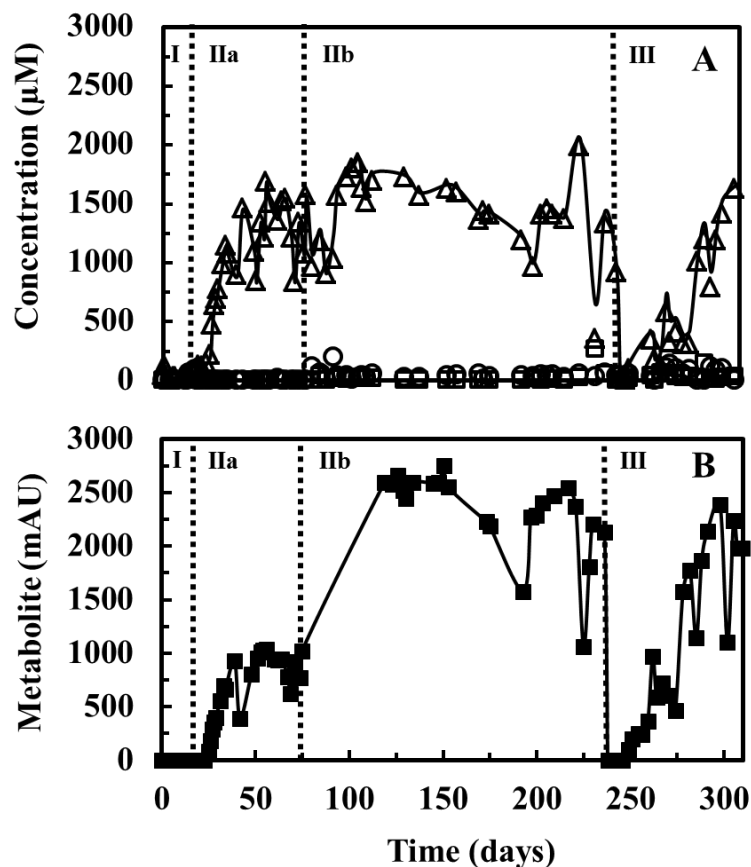


Figure 4.9-4. Mineralization of N and formation of a metabolite through ATO degradation in an aerated continuous flow reactor. (A): Concentration of inorganic N ions in the effluent. (B): Metabolite peak area measured in the effluent. Legend: Ammonium (○), nitrite (□), and nitrate (Δ) concentration, total N ions (—) concentration, and metabolite peak area (■) in the effluent.

Unidentified metabolite.

As previously stated, only around 40% of the N was recovered in the effluent, suggesting that while ATO was being removed, an N-containing-metabolite was being formed. HPLC analysis of the effluent showed the presence of a peak at a retention time of 2.9 to 3.5 min, which was analyzed at the wavelength of 216.5 nm. The metabolite was detected in the effluent consistently during the periods IIa, IIb and III, after NTO started to be metabolized (Figure 4.9-4B). During the first few weeks after initial ATO addition, ATO disappearance was complete, but N-mineralization was progressively increasing, and this was paralleled with increase in metabolite peak area. In the analysis of samples containing the metabolite in LC-MS/ToF, one compound was identified that

correlated with the peak seen in the UV-VIS from the HPLC. The unknown metabolite had a charged mass of 107.968 m/z , which was corresponded to the molecular formulas HN_3S_2 or $\text{C}_2\text{H}_2\text{NSCl}$.

A batch experiment using ^{15}N labeled nitrate was performed to evaluate the occurrence of denitrification in basal medium containing Gortner Garden soil and pyruvate. A detailed description of the experiment can be found elsewhere Madeira, et al. ¹⁰¹. The results indicate that denitrification under anaerobic conditions is very significant when compared to the control, especially when pyruvate is present as electron donor.

4.9.3. Discussion: NTO reduction

NTO was anaerobically biotransformed to ATO. However, NTO resisted transformation under aerobic conditions. These results suggest that in order to reach full removal, a combination of anaerobic and aerobic conditions must be achieved. This combination can occur as a temporal sequence of anaerobic-aerobic conditions, represented by the batch experiment (Liu et al., 2007; Franca et al., 2015), or simultaneously in a bioreactor which contains an anaerobic microbial population in a bulk aerobic environment ²⁴³⁻²⁴⁶.

In this study, NTO biotransformation in soil occurred readily under anaerobic conditions. Nonetheless, no biotransformation occurred under aerobic conditions. Similar results were also observed by Krzmarzick et al. (2015) ¹. The NTO reduction pathway is driven mainly by biological reactions. As evidence, it was observed in this study that the transformation of NTO did not occur under anaerobic conditions in a control containing soil sterilized with formaldehyde. However, heat killed controls were able to reduce NTO. The autoclaved soil is not necessarily completely comparable to the live soil, since heat treatment could cause changes in the redox active species in the soil (such as conversion Fe^{III} to Fe^{II}). According to Tratnyek and Wolfe (1993) ²⁴⁷, autoclaving the soil may have practical significance in the interpretation of environmental reduction reactions due to changes in soil properties. These changes were found to have an important effect in the reduction rate of NAC pesticides ²⁴⁸. However, NTO reduction was greatly stimulated by the addition of microbial substrate, suggesting a predominantly biological reaction during the reduction of NTO. In batch experiments conducted by Mark et al. (2016) ²⁴⁹, the contribution of biological transformation to the total attenuation of NTO in soils was assessed by comparing autoclaved to untreated soils. A significantly higher NTO mass loss was observed for the untreated soil, indicating that biodegradation plays an important role in NTO attenuation.

4.9.4. Discussion: ATO degradation

In this study, ATO was formed stoichiometrically as the main product from NTO reduction. The ATO formed, however, was not further metabolized under anaerobic conditions. ATO elimination under strict anaerobic conditions was not witnessed by Krzmarzick et al. (2015) ¹ in incubations lasting 62 days. Nevertheless, evidence of ATO metabolism under aerobic conditions was observed in two soils, which is consistent with the results of the present study.

In the bioreactor study, we demonstrated that N in ATO was converted to inorganic N species (ammonium, nitrate and nitrite), indicating the biodegradation of the compound. The incomplete conversion of ATO-nitrogen to inorganic N ions indicates that a metabolite may have accumulated. Indeed, an unknown peak with a UV spectrum similar to ATO was detected, and its area followed the concentration of N mineralized. Le Campion, et al. ²¹⁹ detected urea as an ATO degradation product by *B. licheniformis*, which was further degraded to ammonia and carbon dioxide. We did not succeed in detecting urea in our experiments using both biochemical kits and LC-MS, so the

possibility of having urea as the unknown metabolite was discarded. However, two chemical structures were found through mass spectrometry as the possible metabolite: HN_3S_2 and $\text{C}_2\text{H}_2\text{NSCl}$.

Part of the shortfall in the N mass balance can be attributed to the accumulation of biomass. In order to reduce NTO to ATO, 72 mg L^{-1} of the chemical oxygen demand (COD) of pyruvate was consumed (based on a requirement of $6 e^-$ equivalents per mole NTO). The remaining COD of pyruvate (144 mg L^{-1}) could be consumed in the aerobic phase, however, assuming a high cell yield of 50% ($\text{COD}_{\text{cells}}/\text{COD}_{\text{pyruvate}}$), the generic formula of a bacterial cell as $\text{C}_5\text{H}_7\text{O}_2\text{N}$, and the ash content of the biomass as 5%, the N uptake by the cells would account for approximately 8% and 12% of all the N in batch experiments and in the bioreactor, respectively. The occurrence of denitrification in Gortner Garden soil amended with pyruvate under anaerobic conditions indicates that a fraction of the N from ATO mineralization could form N_2 gas, since anaerobic zones are present in the reactor media.

4.9.5. Discussion: Sequential anaerobic-aerobic approach

The oxygen atoms of nitro groups are more electronegative than the nitrogen, leading the N atom to carry a partial positive charge, therefore serving as an electrophile^{215,250}. Due to this characteristic, compounds containing nitro groups are difficult to oxidize, being more prone to reduction in biological systems. In practice, NACs and other explosives persist for decades in aerobic subsurface environments^{32,251}. As evidenced by this study, NTO persisted in the soil under aerobic conditions for up to 37 days. Upon reduction of the nitro groups of explosive compounds to their amines, the molecules become more susceptible to oxidation. E-donating functional groups (e.g. amino group) facilitate the electrophilic attack by pushing electrons into the molecule skeleton, making the atoms in the ring less prone to biotransformation by reduction¹⁸⁵. Simple aromatic amines, such as aniline, are very recalcitrant under anaerobic conditions. On the other hand, aniline is readily degraded in the presence of oxygen. Wang, et al.²⁵² observed that the highest degradation levels of aniline by a *Pseudomonas* strain were detected for the highest aeration level tested (6 mg L^{-1} of dissolved oxygen).

The anaerobic step is intended to biotransform the molecule to a compound that is readily oxidizable, and the subsequent oxidation step is expected to allow for extensive biodegradation of the compound. This approach has been demonstrated for a large variety of environmental contaminants with electron withdrawing functional groups. Several N-containing aromatic compounds, such as nitrobenzene, 4-nitrophenol, aniline and 2,4-dinitrophenol, are removed simultaneously due to oxic/anoxic cycles in a sequencing batch reactor²⁵³. A sequencing anaerobic-aerobic batch reactor was also successful in the treatment of synthetic textile wastewater containing the azo dye Acid Red 14²⁵⁴. Under anaerobic conditions, the azo bond was reduced, forming two aromatic amines, which were further degraded under aerobic conditions.

4.9.6. Discussion: Concurrent aerobic and anaerobic reactions

The simultaneous presence of anaerobic and aerobic zones is possible in a biofilm. The local O_2 concentration in the biofilm matrix is determined by the balance between consumption and diffusion of dissolved O_2 ²⁵⁵. With increasing depth, the O_2 concentration decreases until it is completely depleted. Hooijmans²⁵⁶ observed that the depth of O_2 penetration in a highly active biofilm may be restricted to only 100 to 200 μm . This oxygen gradient allows for the presence of a diverse microbial community with distinct metabolisms. This is best illustrated by the degradation of ethanol by anaerobic microorganisms immobilized in anaerobic granular sludge

placed in an aerobic bulk environment ²⁴⁵. Both oxygen uptake and methanogenesis were reported to occur in parallel in the same biofilm. Furthermore, the presence of facultative substrates, such as ethanol and acetate, was found to enhance the oxygen tolerance. Beunink and Rehm ²⁴³ also observed the coupled reductive and oxidative degradation of 4-chloro-2-nitrophenol (CNP) in an aerobic bioreactor containing an immobilized mixed culture. The culture was able to reduce the nitro group of CNP in the interior of the biofilm and synchronously oxidize the intermediate, 4-chloro-2-aminophenol (CAP), in the aerobic bulk environment. A very diverse bacterial community was found in a sponge-based trickling filter ²⁴⁶. Anoxic niches within the sponge were found to provide environmental conditions which supported the growth of denitrifying bacteria, while heterotrophic bacteria with high chemical oxygen demand were more abundant at the outer part of the sponge blocks. The likely explanation for NTO degradation in the bioreactor is similar. Pyruvate added in the medium not only serves as an electron donor, but its degradation led to the depletion of oxygen in the biofilm matrix, forming anaerobic micro zones in the sponge blocks, therefore enabling NTO reduction to ATO, which subsequently was degraded in the aerobic bulk environment of the bioreactor.

4.9.7. Conclusions: Sequential biodegradation of NTO

This study demonstrates that sequencing anaerobic-aerobic biodegradation can efficiently remove NTO from the aqueous phase. NTO was not biodegradable under anaerobic conditions and ATO was not degraded under aerobic conditions. The reduction of NTO in an aerobic trickle filter bioreactor was plausible due to the presence of hypothesized anaerobic micro-zones, which were formed by addition of cosubstrate (consuming O₂ inside biofilms). The lack of NTO transformation in a sterilized control indicates that the process is driven mainly by biological reactions. The presence of inorganic N ions in the reactor effluent suggests partial NTO mineralization. However, the recovery of N as inorganic aqueous species was only ca. 40%. Denitrification, accumulation of an N-containing-metabolite formed from ATO degradation, and accumulation of N in the biomass could account for some of the missing N.

4.10. Aerobic ATO-Biodegrading Enrichment Culture Study

4.10.1. Objectives: ATO enrichment culture study

The objective of this study was to develop an aerobic enrichment culture (EC) for the biodegradation of ATO, which is the main biotransformation product of NTO^{16,90,100}. An enrichment culture was developed initially from a 10 g L⁻¹ suspension of Gortner Garden Soil, which is an organic rich soil collected from a garden on the campus of the University Minnesota. Bacterial inoculum in this sample was observed to support ATO biodegradation. The texture of the mineral matter of Gortner Garden soil was 9.8% clay, 38.9% silt and 51.3% sand the pH of the soil was 6.92, and the water content was 6.2%. The soil total organic carbon (SOC) was 24.1%⁹⁰.

The strategy of the EC is shown in Figure 4.10-2. Initially ATO was allowed to be degraded by the aqueous suspension of Gortner Garden Soil (10 g soil L⁻¹ medium). Once ATO was degraded 10% vol/vol of the culture was transferred to new medium. The EC was developed in serum flasks with 100 mL of headspace containing 20:80% O₂:N₂ (vol:vol) and 54 mL of basal mineral medium containing 1 mM ATO as the sole C and nutrient N source except for yeast extract (YE) at a concentration of 1 mg L⁻¹ (series A). After 12 transfers, a second EC was started without any YE (series B). After each transfer, the EC were incubated from 1 to 2 weeks until ATO was degraded (as determined by HPLC measurements) and subsequently 6 mL of the culture fluid was transferred to a new bottle with fresh medium (bringing the liquid volume to 60 mL) for the degradation of ATO in the subsequent EC step. In the studies reported here, the inoculum was taken after 27 to 37 transfers of the EC.

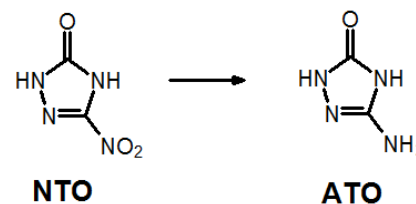


Figure 4.10-1. ATO as main daughter product of NTO.

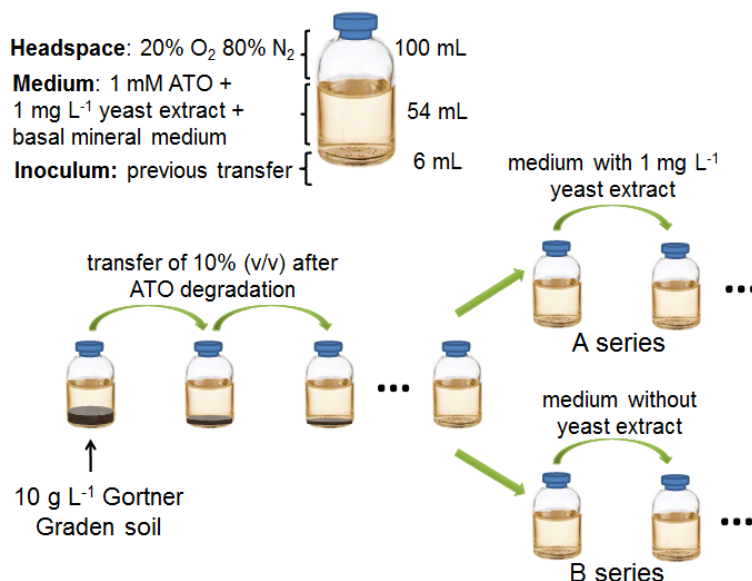


Figure 4.10-2. Schematic of the aerobic ATO enrichment culture (EC) strategy.

4.10.2. Results and discussion: ATO-carbon-mineralization

The ability of the EC to mineralize ATO to mineral forms of C and N were evaluated. First the mineralization of carbon was evaluated with 1.5 mM ATO in the medium. Using Henry's law, ideal gas law and acid-base dissociation, the expected CO₂ percentage in the headspace was calculated assuming the culture pH of and temperature of 6.8 and 30°C; respectively. ATO (1.5 mmol L⁻¹_{liq}) was expected to yield a total of 3 mmol of CO₂ L⁻¹_{liq} if the ATO carbon would be fully mineralized. The calculations indicated under the conditions of the experiment, a volumetric headspace CO₂ gas composition of 1.367% would be expected if all ATO-C was mineralized to CO₂. In the experiments, the measured CO₂ content of the headspace was normalized to this theoretical CO₂ concentration to provide % conversion of ATO-C to CO₂-C. These data were plotted along-side the percent removal of ATO to determine if the ATO disappearance was occurring concomitantly with the formation of CO₂. The results of the experiments using the series A (1 mg L⁻¹ YE) and series B (without YE) EC as inoculum are shown in Figures 4.10-3 and 4.10-4, respectively.

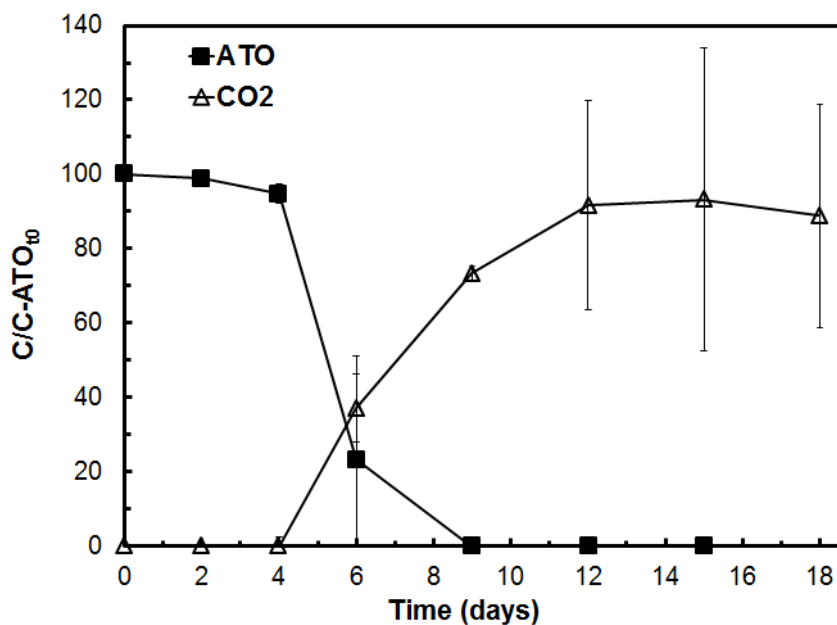


Figure 4.10-3. ATO concentration decrease in comparison with CO₂ formation by the series A enrichment culture from the 27th transfer in basal medium containing 1 mg L⁻¹ YE. The data are normalized to the C concentration of ATO at time zero. ATO was supplied at 1.5 mM.

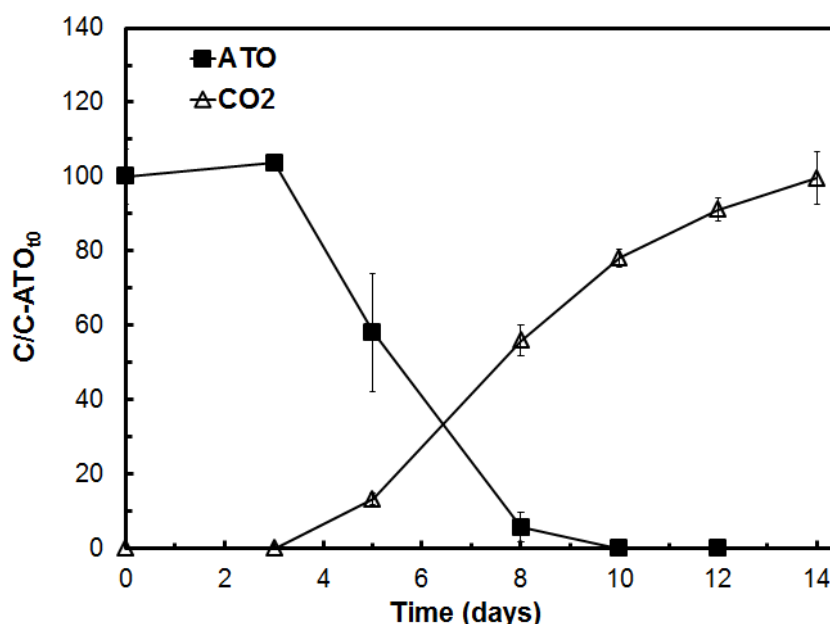


Figure 4.10-4. ATO concentration decrease in comparison with CO₂ formation by the series B enrichment culture from the 28th transfer in basal medium without YE. The data are normalized to the C concentration of ATO at time zero. ATO was supplied at 1.5 mM.

The results of the ATO-C mineralization experiments clearly indicate an extensive mineralization of organic C in ATO. The timing of the formation of CO₂ coincides well with the disappearance of ATO. In both ECs, the ATO disappearance started on day 3 or 4 which coincided with the start of the CO₂ production. In both ECs the ATO completely disappeared on day 9 or 10, which coincided with approximately 80% of the ultimate production of CO₂ and the moment in the CO₂ production when the rates began to taper off. This pattern suggests that a small pool of accumulated intermediates were still being converted to CO₂ after ATO itself was completely consumed. Lastly the ultimate production of CO₂ was consistent with the expected CO₂ production. In the the series A EC (with YE), 89.0% of the CO₂ expected was recovered, albeit the standard deviation was high. The series B EC (without YE) had a high recovery of 99.6 % of the theoretical CO₂ production expected from a fully mineralized ATO and the standard deviation was low. The CO₂ production in live control cultures lacking ATO or uninoculated cultures in medium and ATO was negligible. Collectively the data indicate that microorganisms in the ECs were fully mineralizing ATO-C. There are three lines of compelling evidence. Firstly, the CO₂ production coincided with the disappearance of ATO. Secondly, the extent of the maximum CO₂ production was consistent with the theoretically expected CO₂ from ATO biodegradation. And thirdly, controls lacking ATO or inoculum did not significantly produce CO₂.

4.10.3. Results and discussion: ATO-N mineralization

Similar to ATO-C mineralization studies, several attempts were made to study the mineralization of ATO-N to inorganic forms of nitrogen. Firstly, only the ionic N species (NH₄⁺, NO₂⁻ and NO₃⁻) that could be measured in in the ion chromatograph were monitored. In those experiments, the

sum of the ionic species only resulted in an approximate 50% recovery of the N of the ATO-N supplied initially. In the early stages of the EC, the ionic species were initially predominantly NH_4^+ but later NH_4^+ was converted to NO_2^- and afterwards to NO_3^- by nitrifying bacteria. However after many transfers (> 20), the predominant species of inorganic ionic N ions was NH_4^+ . In order to determine what N-species was responsible for the 50% gap in the N-balance, the set up and analytical methods were changed in order to enable measurement of N_2 gas which was suspected of being responsible for the gap in the N-balance. Thus the headspace gas during culturing was changed from 20:80 % vol/vol $\text{O}_2:\text{N}_2$ to 20:80 % vol/vol $\text{O}_2:\text{He}$ to avoid interference from background N_2 . Also the gas chromatograph column used was changed to a molecular sieve column in order to enable separation of N_2 and O_2 gases.

In the new N-balance experiments, N_2 mass of the headspace was measured and normalized to the initial mass of N supplied with ATO and expressed as % conversion of ATO-N to N_2 -N. In the same experiments the ionic species of N (NH_4^+ , NO_2^- and NO_3^-) were measured as described above and expressed as % conversion of ATO-N to ionic N species. The conversion of ATO-N to N_2 -N and ionic N species were summed to provide the total conversion of N to inorganic N products. These data were plotted along-side the percent removal of ATO to determine if the ATO disappearance was occurring concomitantly with the formation of inorganic N products. The results of the experiments using the series A (1 mg L^{-1} YE) and series B (without YE) EC as inoculum are shown in Figures 4.10-5 and 4.10-6, respectively.

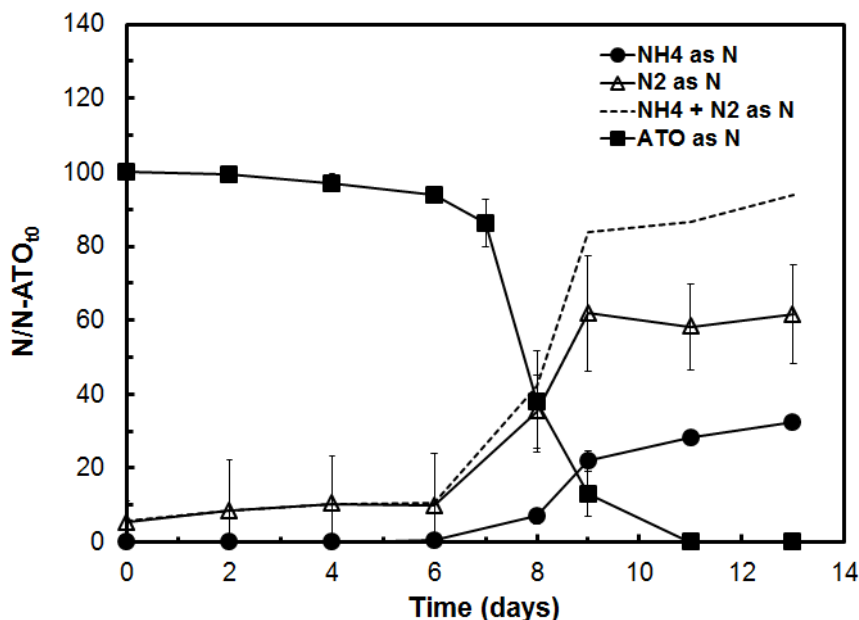


Figure 4.10-5. ATO concentration decrease in comparison with the formation of inorganic N species by the series A enrichment culture from the 37th transfer in basal medium containing 1 mg L^{-1} YE. The data are normalized to the N mass of ATO at time zero. ATO was supplied at 3.9 mM . The ionic species were composed almost exclusively of NH_4^+

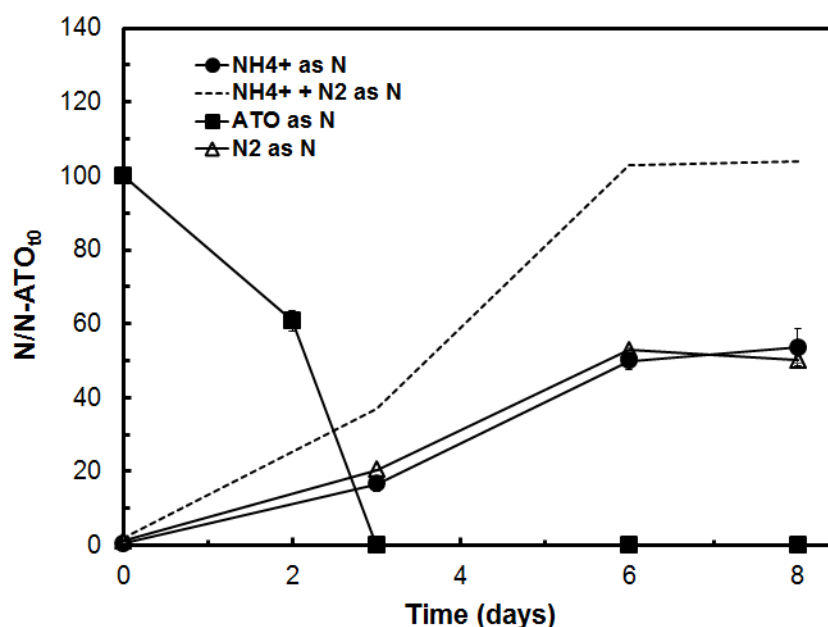


Figure 4.10-6. ATO concentration decrease in comparison with the formation of inorganic N species by the series B enrichment culture from the 35th transfer in basal medium without YE. The data are normalized to the N mass of ATO at time zero. ATO was supplied at 3.5 mM. The ionic species were composed almost exclusively of NH_4^+

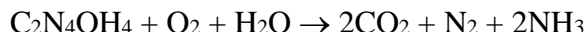
The results of the N-mineralization experiments clearly indicate an extensive mineralization of the organic N in ATO. The formation of NH_4^+ and N_2 occurred during and after the disappearance of ATO. In the A series EC (Figure 4.10-5), the start of ATO consumption coincided with the formation of inorganic N species after a lag phase of 6 days. Also the formation of inorganic stopped approximately at the same time as the ATO became completely consumed. In the B series EC (Figure 4.10-6), there was no lag phase and the inorganic N species were already forming on day 3 when ATO was completely consumed. However, the inorganic N species continued to increase up to day 6 after ATO was already eliminated, suggesting that transient intermediates were still degrading to the inorganic N species between days 3 and 6. The inorganic N species recovery (at the end of each incubation) was similar to the N in the ATO that was consumed. The recovery of ATO-N as the sum of N_2 -N and NH_4^+ -N was 94 and 104% in the A and B series, respectively. The results taken as a whole indicate that the organic N in ATO was completely mineralized.

4.10.3. Results and discussion: Stoichiometry

The results from the N mineralization experiments indicate that NH_4^+ -N and N_2 -N are produced in equal molar amounts. This is most evident in the B series EC shown in Figure 4.10-6. Thus two of the ATO-N atoms are converted to N_2 ; whereas the other two ATO N atoms are released as NH_4^+ . As was indicated previously in the ATO-C mineralization experiments, the two C atoms in ATO are released as CO_2 . The enrichment culture was tested on whether ATO could be degraded

anaerobically and the test revealed that no degradation of ATO occurred in the absence of O₂. During aerobic ATO degradation 30% of the O₂ supplied is consumed. Low levels of cell yield are observed as ATO is becoming mineralized, as evidenced by a net protein production of 3.3 mg L⁻¹. Assuming a 1:2 ratio of protein to dry biomass, only 6.6 mg dwt cells are produced compared to approximately 390 mg L⁻¹ ATO supplied corresponding to a dwt cell yield of 1.7%.

The combined information indicates an approximate molar stoichiometry as follows:



The stoichiometry indicates each mol of ATO only donates 4 electron equivalents (eeq) as it is becoming oxidized. The low eeq value is due to the release of reduced N species as products of the reaction. The stoichiometry presented does not consider the cell yield. Although the cell yield is very low on a dwt basis, the cell yield on an eeq basis (assuming 1.4 g COD/g dwt cells) is much higher, corresponding to 7.4%.

4.10.4. Results and discussion: ATO EC clone libraries

Two types of clone libraries were performed, the first was a conventional clone library using host cells and dideoxy sequencing method which used a primer set for 1495 bp length of the 16S rRNA gene. This method yielded 25-26 clones of high information content sequences. The second method utilized a second generation sequencing method utilizing an Ion Torrent Personal Genome Machine and was conducted by a service laboratory, MR DNA (Shallowater, TX), using their propriety analysis pipeline. The primer set for the high throughput method yielded much shorter sequences of 301 bp. However, the method generated high volume of sequences (from 127,239 to 152,762, depending on sample).

The results of the ATO-EC without YE and with YE are shown in Table 4.10-1 and Table 4.10-2, respectively. In those clone libraries the dominant clone produced (25% of all clones) is closely related to *Hydrogenophaga* sp. PBC which is known for its ability to aerobically biodegrade 4-amino-benzenesulfonate either in coculture with *Ralstonia* or in pure culture if supplemented with vitamins, p-aminobenzoic acid and biotin^{257,258}. *Ralstonia* was present in the EC without YE but absent in the EC with YE which may be due to vitamins supplied by YE. However, a word of caution is mentioned here because in the MR DNA method, *Ralstonia* was an important clone in background controls (accounting for 6 to 18% of the clones in those controls), thus the veracity of the presence of *Ralstonia* in the sample is suspect).

Eight percent of the clones were found with sequences very closely related to *Nitrospira* sp. which makes sense since in the early stages of the EC, nitrification of ammonia was observed, thus accounting for the presence of a nitrite oxidizing bacterium. Aside from *Hydrogenophaga* sp. PBC and *Nitrospira*, the only other clone detected worthy of mentioning is *Mesorhizobium* sp. which was 97% related to a clone from a clone library of an endocrine disrupting compounds degrading enrichment culture²⁵⁹.

In the ATO EC with YE, *Hydrogenophaga* sp. PBC was also shown to be predominant clone (27% of all clones). Two other clones were closely related to bacteria known to be involved in the degradation of pesticides with substructures related in structure to ATO. The first of these was *Pseudomonas* sp. R-41382 (7.7% of clones) implicated in the chloropropham degradation that has a side chain, R-N(H)-C(=O)-O-C(CH₃)₂, with structural similarities to ATO²⁶⁰. The second of these, *Hyphomicrobium sulfonivorans* WDL6 (7.7% of clones), is responsible for the degradation

of N,O-dimethyl-hydroxylamine ($\text{H}_3\text{C-N-OCH}_3$)²⁶¹, which is, which is an intermediate during the degradation of the pesticide, linuron. Other clones of interest were *Rhizobium* sp. R-24658 (7.7% of the clones) which is a denitrifying bacterium, and *Sphingopyxis macrogoltabida* sp EY-1 (3.8% of the clones) implicated in polyethylene glycol and glycol degradation²⁶².

The results of the high throughput MR DNA clone library are presented in Table 4.10-3. The results clearly indicate that the PCR biases are extremely different for two approaches to the clone library. In the classic method, *Hydrogenophaga* accounted for 24-27% of the clones while in the MR DNA method, *Hydrogenophaga* only accounted for 0.01 to 0.04% of the clones. On the other hand in MR DNA method *Hyphomicrobium* accounted for approximately 72% of the clones yet. However in the classic cloning approach, the genus *Hyphomicrobium* was responsible for only 3.8% of the clones and that only in the ATC EC with YE.

The high fraction of *Hyphomicrobium* clones in MR DNA and its detection by two independent methods does justify the question, why *Hyphomicrobium*? The genus *Hyphomicrobium* is well known for C1 metabolism, and members of this genus are known for metabolizing methylamines^{263,264}, or small molecules containing methylated amines²⁶¹. The structure of ATO is such that the two carbon molecules are not linked with each other, thus during degradation, one would expect the formation of C1 metabolites. The importance of C1 metabolism in the ATO EC is further manifested by the fact that the second most abundant clone in the MR DNA method is from the genus *Alkalilimnicola* known for its ability to degrade carbon monoxide²⁶⁵.

Both methods identified *Sphingopyxis* as being members of the ATO EC. In MR DNA the percentage of *Sphingopyxis* clones ranged from 1 to 1.9%; whereas, in the conventional cloning *Sphingopyxis* accounted for 3.8% of the clones in the YE containing EC. *Sphingopyxis macrogoltabida* sp EY-1, identified with the conventional cloning, is known for metabolizing glycol and polyethylene glycol²⁶². Additionally, both methods identified *Mesorhizobium* as part of the ATO ECs. *Mesorhizobium* is responsible for the biodegradation of a variety of pollutants and the clone with the highest match in the ATO EC without YE was closely related to a clone found in an endocrine disrupting compound degrading enrichment culture²⁶² as well as another bacterium responsible for N-methyl-2-pyrrolidone degradation²⁶⁶. N-methyl-2-pyrrolidone shares some structural features with ATO.

Table 4.10-1. Conventional clone library of ATO EC without YE after 17 transfer with primer set 27F and 1522R of the 16SrRNA gene. Shown are selected clones with $\geq 97\%$ sequence similarity.

Match of clone	Match	clones	clones	Functions inferred from literature
	(%)	#	(%)	
<i>Hydrogenophaga</i> sp. PBC	99	6	24.0	In co-culture degrading 4-amino-benzenesulfonate with <i>Ralstonia</i> (or as pure culture with the addition of <i>p</i> -aminobenzoate and biotin to the media)
<i>Polaromonas aquatica</i>	97	4	16.0	Isolated from tap water
<i>Ralstonia</i> sp. KN1	99	4	16.0	Phenol hydroxylase gene cometabolic TCE degradation
<i>Nitrospira</i> sp.	99	2	8.00	Nitrite oxidizer
<i>Sphingomonadaceae</i> bacterium SAP53	97	1	4.00	Bacterium associated with potato rhizosphere
<i>Pseudomonas</i> sp. DSM 29140	99	1	4.00	Bacterium isolated from milk
<i>Mesorhizobium</i> sp. clone DHy91	97	1	4.00	In clone library of an endocrine disrupting compounds degrading enrichment culture.

References: *Hydrogenophaga*^{257,258}; *Ralstonia* in coculture²⁵⁷; *Ralstonia* phenol hydroxylase²⁵⁹ and *Mesorhizobium* degradation endocrine disrupting compounds²⁶⁷ or degradation N-methyl-2-pyrrolidone²⁶⁶

Table 4.10-2. Conventional clone library of ATO EC with YE (1 mg L⁻¹) after 17 transfers with primer set 27F and 1522R of the 16SrRNA gene. Shown are selected clones with ≥97% sequence similarity.

Match of clone	Match	clones	clones	Functions inferred from literature
	(%)	#	(%)	
<i>Hydrogenophaga</i> sp. PBC	99	7	27.0	In co-culture degrading 4-amino-benzenesulfonate with <i>Ralstonia</i> (or as pure culture with the addition of <i>p</i> -aminobenzoate and biotin to the media)
<i>Brevundimonas bullata</i> IAM 13153	99	5	19.2	Associated with rhizomes and fixes N ₂
<i>Thiorhodospira</i> sp. clone 2ABC-17	99	2	7.7	Detected in soil in Korea
<i>Rhizobium</i> sp. R-24658	98	2	7.7	A denitrifying bacterium
<i>Pseudomonas</i> sp. R-41382	98	2	7.7	Present in a chloroprotham degrading enrichment culture
<i>Hyphomicrobium sulfonivorans</i> WDL6	98	1	3.8	degrades N,O-dimethyl-hydroxylamine in a linuron enrichment culture
<i>Sphingopyxis macrogoltabida</i> sp EY-1	99	1	3.8	Glycol and polyethylene glycol degrading bacterium

References: *Hydrogenophaga* ^{257,258}; *Pseudomonas* R-41382 chloroprotham ²⁶⁰; *Sphingopyxis macrogoltabida* PEG degradation ²⁶²; *Hyphomicrobium sulfonivorans* WDL6 linuron degradation ²⁶¹.

Table 4.10-3. Clones with $\geq 97\%$ sequence homology in the MR DNA clone library of ATO EC without and with YE (1 mg L^{-1}) after 34 transfers with primer set 515F and 806F for the 16SrRNA gene. Dominant clones and clones related to conventional clone library. The number of recovered sequences are 127,239 for ATO EC without YE and 152,762 for ATO SC with YE.

Match of clone	% clones		Functions inferred from literature
	EC no YE	EC YE	
<i>Hyphomicrobium</i> sp.	71.7	71.4	C1 metabolism (methylamines) and N,O-dimethylhydroxylamine degradation
<i>Alkalilimnicola</i> spp.	6.97	3.49	halophilic CO metabolism
<i>Leadbetterella</i> sp.	4.55	3.00	isolated from cotton waste compost
<i>Pseudomonas</i> spp.	3.90	5.08	degradation of a variety of pollutants
<i>Sphingopyxis</i> sp.	1.85	0.95	PEG and glycol degradation
<i>Xanthobacter flavus</i>	1.51	0.02	1,4-dioxane degradation
<i>Mesorhizobium</i> spp.	1.35	0.70	degradation of a variety of pollutants
<i>Mycobacterium</i> spp.	1.17	0.54	degradation of a variety of pollutants
<i>Agromyces mediolanus</i>	0.34	0.04	contains epoxide hydrolase
<i>Pseudoxanthomonas mexicana</i>	0.30	1.34	isolated from aerobic granular sludge
<i>Sphingomonas</i> sp.	0.28	0.50	degradation of a variety of pollutants
<i>Sphingopyxis</i> sp.	0.06	0.01	PEG and glycol degradation
<i>Hydrogenophaga</i> sp.	0.01	0.04	In co-culture degrading 4-amino-benzenesulfonate with <i>Ralstonia</i> (or as pure culture with the addition of <i>p</i> -aminobenzoate and biotin to the media)
<i>Hyphomicrobium nitrativorans</i>	0.01	0.01	Methanol denitrification

References: *Hyphomicrobium* trimethylamine metabolism ^{263,264}; *Alkalilimnicola* CO metabolism ²⁶⁵; *Mesorhizobium* degradation endocrine disrupting compounds ²⁶⁷ or degradation N-methyl-2-pyrrolidone ²⁶⁶; *Xanthobacter flavus* 1,4-dioxane degradation ²⁶⁸; *Agromyces mediolanus* epoxide hydrolase ²⁶⁹; *Ralstonia* in coculture ²⁵⁷; *Ralstonia* phenol hydroxylase ²⁵⁹; *Hyphomicrobium nitrativorans* methanol denitrification ²⁷⁰

4.10.4. Conclusions: ATO Enrichment culture

The results demonstrate that a sustainable EC can degrade ATO as the sole C and N source. The culture has been sustained for over 37 transfers of 10% v/v. We have demonstrated that the C in ATO is highly mineralized to CO₂ and that the N is mineralized for approximately 50% to NH₃ and 50% to N₂. The EC requires O₂, indicating at least one O₂- dependent step in the biodegradation pathway. Previously the mineralization of ATO to CO₂ was demonstrated during cometabolism with other substrates with the bacterium *Bacillus licheniformis* in which urea was identified as an intermediate ¹⁶. The results here extend these findings to demonstrate that an EC can grow on ATO as the sole C and N source, and the growth is sustainable with demonstrable formation of bacterial biomass as evidenced by protein production. We also demonstrate for the first time the nitrogen products of the reaction are NH₃ and N₂.

Low amounts of YE (supplied at 1 mg L⁻¹) were found not to be essential for the EC, thus the culture has the capacity to produce all the essential vitamins and cofactors from the basal inorganic nutrients in the medium, YE did however modify to a small extent the microbial composition of the community.

The results from two approaches to developing a clone library, conventional and MR DNA, indicate several members that may be playing a role in the ATO biodegradation. These include clones from the genus *Hydrogenophaga* previously implicated in oxidative 4-aminobenzenesulfonate degradation ^{257,258}. Clones from the genus *Hyphomicrobium* indicate a role of C1 metabolism in ATO biodegradation possibly including the metabolism of methylamines ^{263,264}. The importance of C1 metabolism was also strengthened by the presence of clones from *Alkalilimnicola* known for CO metabolism ²⁶⁵. The presence of *Sphingopyxis* and *Mezorhizobium* indicated other potential biodegradative mechanisms related to glycol metabolism ²⁶² and degradation of N-methyl-2-pyrrolidone ²⁶⁶.

In conclusion, ATO the major reductive biotransformation product of NTO was shown to be highly and reliably mineralized to CO₂, NH₃ and N₂ by a highly enriched culture developed from garden soil.

4.11. Microbial toxicity of DNAN and Aromatic Amine Daughter Products

4.11.1. Objectives

The objective of this study was to evaluate the inhibitory effect of DNAN and its reduced intermediates MENA and DAAN to microorganisms commonly found in the environment under different redox conditions, namely anaerobic methanogens, aerobic heterotrophs and nitrifying bacteria. The inhibitory impact of these compounds was also evaluated using the Microtox assay, a method that relies on bioluminescence measurements in cultures of the bioluminescent marine bacterium *Aliivibrio fischeri*. The results obtained will contribute to a better understanding of the environmental impact of DNAN and will facilitate the development and optimization of efficient bioremediation technologies for the removal of this nitroaromatic compound (NAC).

4.11.2. Results: Methanogenic Inhibition

Figure 4.11-1A illustrates the time course of CH₄ production in methanogenic activity assays amended with DNAN. The normalized methanogenic activity as a function of the initial DNAN concentration is shown in Figure 4.11-1A. The IC₅₀ values determined are summarized on Table 4.11-1.

The rate of methane production in all the assays spiked with DNAN was lower relative to the control indicating methanogenic inhibition. In the treatments with the highest DNAN concentrations, no CH₄ was initially produced. The onset of methane production coincided with the complete removal of DNAN due to the its reductive transformation to MENA (Figure 4.11-1B).

Figure 4.11-2A shows the normalized methanogenic activity results determined in assays with DNAN, MENA and DAAN. DNAN was found to be more toxic than MENA and DAAN. The IC₅₀ values determined for DNAN, MENA and DAAN were 41, 175, and 176 μ M, respectively (Table 4.11.1).

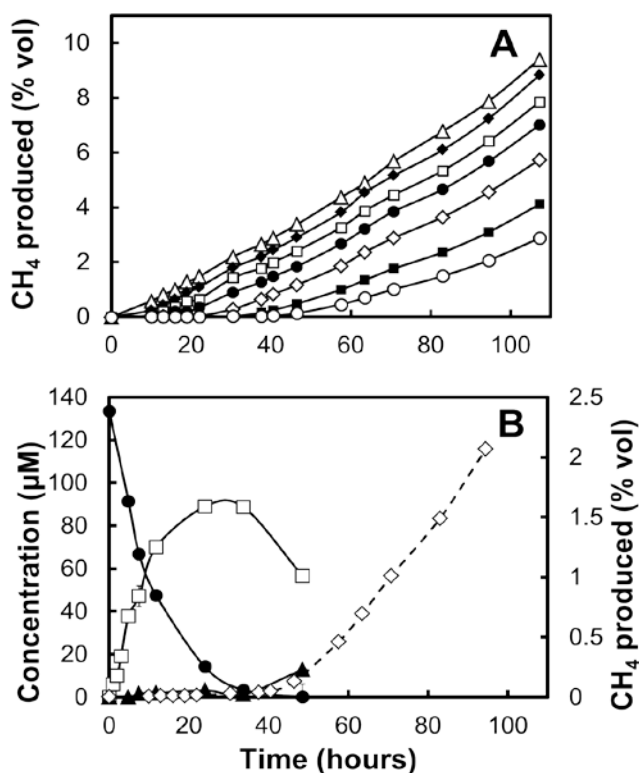


Figure 4.11-1. (A) CH₄ production by anaerobic sludge amended with acetate (26 mM) and DNAN (in μ M): 0 (Δ), 13 (\blacklozenge), 26 (\square), 52 (\bullet), 78 (\diamond), 104 (\blacksquare), and 130 (\circ). (B) DNAN bio-transformation, and formation of DNAN metabolites, and CH₄ production by anaerobic sludge amended with acetate (26 mM) and DNAN (133 μ M). Legends: DNAN (\bullet), and MENA (\square), DAAN (\blacktriangle), and methane (\diamond).

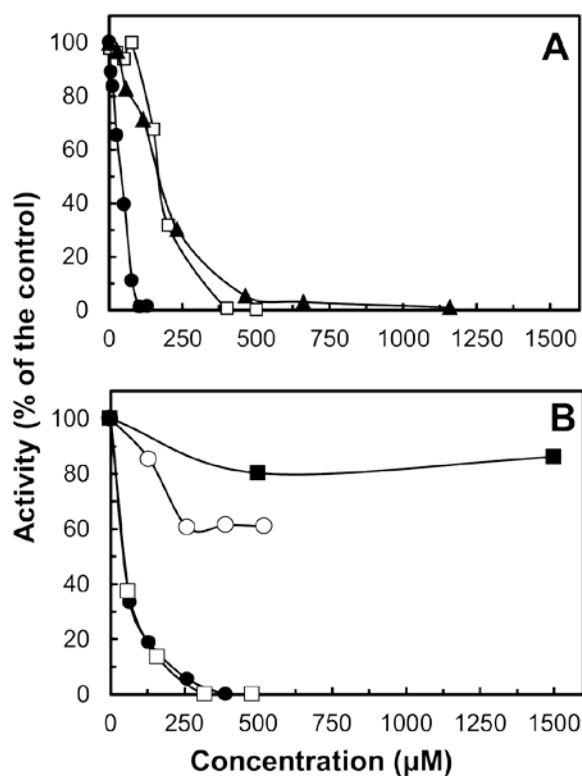


Figure 4.11-2. DNAN, MENA and DAAN inhibition (expressed as percentage of the control activity) towards methanogenic (A), and aerobic microorganisms (B). Panel A- Methanogenic assays: DNAN (●), MENA (□), DAAN (▲). Panel B- Aerobic heterotrophic assays: DNAN (○), MENA (■); Nitrification assays: DNAN (●), MENA (□).

4.11.3. Results: Inhibition of aerobic heterotrophic bacteria

The inhibitory effect of DNAN on O₂ consumption by heterotrophic bacteria in activated sludge is illustrated in Figure 4.11-3A. Figure 4.11.2B compares the normalized activity determined in these bioassays as a function of the DNAN and MENA concentration. Exposure to DNAN (390 µM) for 10 h resulted in moderate inhibition of the O₂ consumption rate by the aerobic microorganisms (39% inhibition), whereas MENA was only slightly inhibitory (14% inhibition) at concentrations as high as 1,500 µM. DAAN could not be evaluated in assays utilizing O₂ as electron acceptor, *i.e.*, aerobic heterotrophic and nitrifying bioassays, as the compound is unstable under the oxic conditions inherent of these tests.

4.11.4. Results: Inhibition of nitrification

The time course of ammonium consumption by nitrifying bacteria exposed to DNAN is shown in Figure 4.11-3B. Nitrification was completely inhibited at DNAN concentrations exceeding 260 µM. At lower concentrations, nitrifying bacteria appeared to become acclimated to the presence of DNAN with time. For example, assays exposed to DNAN concentrations ranging from 65-130 µM were completely inhibited during the first 60 h but their activity increased sharply thereafter, reaching levels close to those observed in the control without DNAN. The observed recovery may be due to transformation of DNAN to less toxic products. In this respect it is interesting to note

that chromatographic analysis of the culture samples obtained at the end of the experiment (145 h) indicated considerable removal of DNAN, ranging from 53 to 81% of the initial concentration depending on the assay. Only a small fraction of the DNAN removed was recovered as MENA and DAAN, suggesting the formation of other unidentified biodegradation products. DNAN and MENA exhibited comparable inhibition towards the nitrifying bacteria as indicated by their similar IC_{50} values (48-49 μM) (Table 4.11-1).

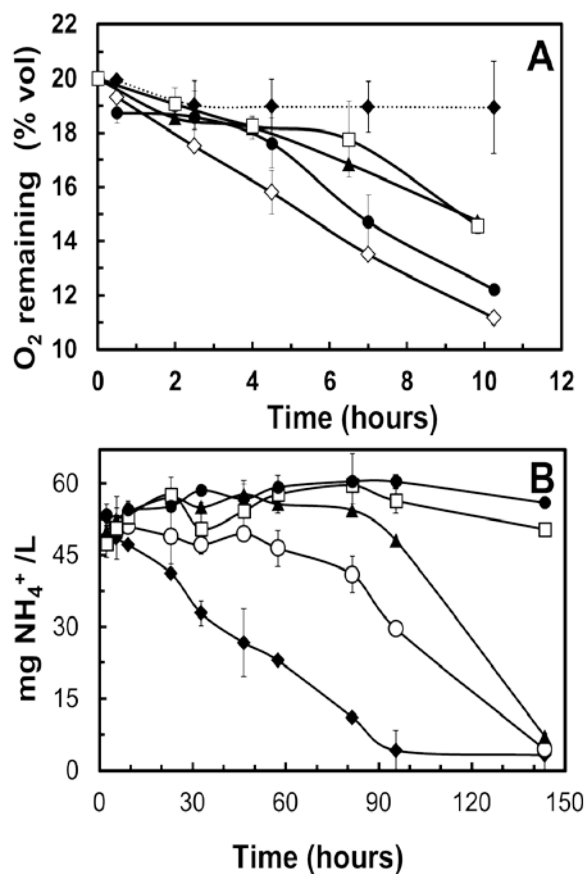


Figure 4.11-3. (A) Time course of O₂ consumption by aerobic activated sludge amended with acetate (28 mM) when exposed to DNAN (in μM): 0 (\diamond), 130 (\bullet), 260 (\blacktriangle), and 390 (\square). Endogenous control lacking acetate and DNAN (\blacklozenge). (B) Time course of NH₄⁺ consumption by nitrifiers in activated sludge in the presence of DNAN (in μM): 0 (\blacklozenge), 65 (\circ), 130 (\blacktriangle), 260 (\square), 520 (\bullet).

Table 4.11-1. Summary of inhibitory concentrations determined for DNAN and its metabolites MENA and DAAN in various microbial toxicity bioassays.

Compound	Methanogens	Aerobic heterotrophs	Nitrifiers	Microtox
	IC ₅₀	IC ₅₀	IC ₅₀	IC ₅₀
DNAN (μM)	41	NT ^{*,a}	49	57
MENA (μM)	175	NT ^b	48	48
DAAN (μM)	176	NA ^c	NA ^c	155

* NT= Not toxic at the highest concentration tested.

^a Inhibition at the highest DNAN concentration tested (390 μM) was 39%.

^b Inhibition at the highest MENA concentration tested (1,500 μM) was 13%.

^c N.A. = Not available. DAAN was not tested because the compound is very unstable (towards autoxidation) in the presence of O₂.

4.11.5. Results: Inhibition towards *Aliivibrio fischeri*

Figure 4.11-4 illustrates the impact of exposure to varying concentrations of DNAN, MENA, and DAAN on the bioluminescence activity of *A. fischeri* ²⁷¹. DAAN was the least toxic of the compounds tested and its IC₅₀ value (155 μ M) was approximately 3-fold higher compared to those of the other NACs. DNAN and MENA showed very similar inhibitory potential as indicated by their close IC₅₀ values, 57 and 48 μ M, respectively.

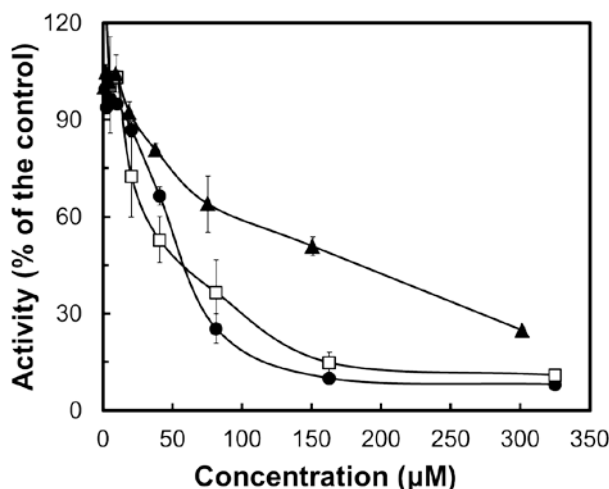


Figure 4.11-4. Toxicity of DNAN (●), MENA (□), and DAAN (▲) to *A. fischeri* after 30 min of exposure. Toxicity is expressed as percentage of toxicant-free activity.

4.11.6. Discussion: Microbial toxicity of DNAN

This study was undertaken to examine the microbial toxicity of DNAN and several of its reduction metabolites to ecologically relevant microbial activity. Only one previous study has attempted to characterize the toxicological profile of DNAN ²⁷² and information on the microbial toxicity of DNAN is largely lacking. We are only aware of a previous study where DNAN was identified as an inhibitor of perchlorate-reducing bacteria ¹⁸³. Complete inhibition of the perchlorate-reducing activity of activated sludge was observed in batch assays spiked with 126 μ M DNAN.

The results obtained demonstrated that the inhibitory impact of DNAN varied widely depending on the target microbial population. While respiration activity by aerobic heterotrophs was only partly impacted at the highest concentration tested (39% inhibition at 390 μ M DNAN), all other microbial targets were severely inhibited at relatively low concentrations (Table 4.11-1). Previous studies have also demonstrated that NACs are highly toxic to methanogens ²⁷³⁻²⁷⁶ and *A. fischeri* ²⁷⁷⁻²⁷⁹. On the other hand, the sensitivity of aerobic heterotrophs to these pollutants appears to differ widely. Gram-negative organisms have been found to be more tolerant to NACs than Gram-positive bacteria ^{280,281}. Fuller and Manning ²⁸⁰ observed that the growth of pure cultures of aerobic Gram-positive bacteria was severely inhibited by concentrations of TNT as low as 44 μ M, whereas most Gram-negative organisms were unaffected by concentrations approaching the water solubility of TNT (440 μ M). Similarly, growth of the Gram-negative bacterium, *Pseudomonas putida*, was not inhibited by TNT and 11 other NACs, including several TNT metabolites ²⁷⁷. DNAN might be somewhat less toxic to microorganisms. Most notably, the 30-min IC₅₀ value (57 μ M) determined for DNAN in luminescence assays with *A. fischeri* is several times higher compared to those previously reported for TNT (2-16 μ M) ²⁷⁷⁻²⁷⁹.

The mechanisms responsible for the inhibitory effects of DNAN have not been investigated to date, but they are likely to overlap to some degree with those of other NACs. Many nitrophenols are potent uncouplers of oxidative phosphorylation²⁸². DNAN was also reported recently to be a mitochondrial uncoupler²⁸³. The inhibitory effect of NACs has also been related to their hydrophobic character. We have previously demonstrated that the methanogenic toxicity exerted by N-substituted phenols (aminophenols and nitrophenols) was closely correlated with compound apolarity ($R^2 = 0.95$)²⁷³, suggesting that partitioning of NACs into the lipophilic microbial membranes may have a role in the toxicity.

4.11.7. Discussion: Microbial toxicity of DNAN metabolites

Results obtained for several DNAN metabolites and related N-substituted compounds indicate that the reduction of nitro to amino groups on the aromatic ring was generally associated with a decreased toxicity. The inhibitory impact of DNAN and MENA towards nitrifying bacteria and *A. fischeri* was very similar indicating that reduction of a single nitro group was not sufficient to alleviate the inhibitory effect of the parent compound (Table 4.11-1). In contrast, MENA was significantly less inhibitory towards methanogens than DNAN. Microbial reduction of the two nitro groups with formation of DAAN led to significant detoxification in bioassays with methanogens and *A. fischeri*. In agreement with these findings, aromatic amines have been reported to be generally less toxic than their corresponding NAC analogs in studies with several microorganisms, including methanogenic archaea^{168,273}, *A. fischeri*^{277,284-286}, and in studies with other aquatic (algae, fish) and terrestrial targets, including mammalian cells^{277,284,286,287}.

Although the primary metabolites of DNAN reduction, particularly the diamino compound DAAN, were found to be generally less toxic than the parent compound, it is unclear whether microbial reduction of DNAN would lead ultimately to detoxification of the NAC. Anaerobic biotransformation of MENA and DAAN has been reported to result in an array of secondary metabolites including azo and hydrazine dimer derivatives^{85,103}. Azoxy- and azo-dimers have also been detected during aerobic biotransformation of DNAN²²⁹. In soil environments, these reduction products are likely to bind to humic compounds, forming humus-bound residue, as reported for TNT and other NACs²⁸⁸⁻²⁹⁰. The inhibitory impact of polymeric DNAN derivatives and soil conjugates is yet to be characterized. Previous studies comparing the toxicity of TNT and two of its dimeric azoxy metabolites (4,4',6,6'-tetrinitro-2,2'-azoxytoluene and 2,2',6,6'-tetrinitro-4,4'-azoxytoluene) have shown that the three compounds were equally cytotoxic²⁸⁶. However, dimeric metabolites detected in microbial transformation studies with DNAN lacked nitro groups. Based on the lower toxicity generally observed when nitro groups are reduced to amine moieties, DNAN dimers are likely to be less toxic than the nitrated TNT dimers.

4.11.8. Conclusions: Microbial toxicity of DNAN and its daughter products

Taken as a whole these results indicate that DNAN causes strong acute cytotoxicity in methanogenic and nitrification microbial populations. Preliminary results suggest that microbial reductive transformation may reduce the inhibitory impact of DNAN but does not completely remove toxicity. Additional toxicity studies with secondary dimeric metabolites of DNAN and their soil conjugates are needed to better characterize the hazard associated with metabolites of this emerging energetic compound. In addition to cytotoxicity, there is a need to understand the mutagenicity of aromatic amines formed during DNAN metabolism.

4.12. Microbial Toxicity of DNAN (Bio)Transformation Products and Mixtures characterized by LC-QTOF-MS

4.12.1. Objectives: Microbial toxicity of DNAN biotransformation products/mixtures

The objectives of this work were to assay microbial toxicity of individual transformation products and/or best available surrogate compounds to acetoclastic methanogens and the marine bacterium *Allivibrio fischeri*; and determine biotransformation product profiles for DNAN incubated anaerobically in soils and in sludge and link the profile mixture composition to toxicity changes during transformation using acetoclastic methanogens and *A. fischeri*, as microbial toxicity models.

4.12.2. Results and Discussion: Toxicity of model compounds and surrogates.

The chemical structure of the commercial transformation products and/or best available surrogate compounds tested for inhibition towards acetoclastic methanogens and the marine bacterium *A. fischeri* are shown on Figure 4.12-1.

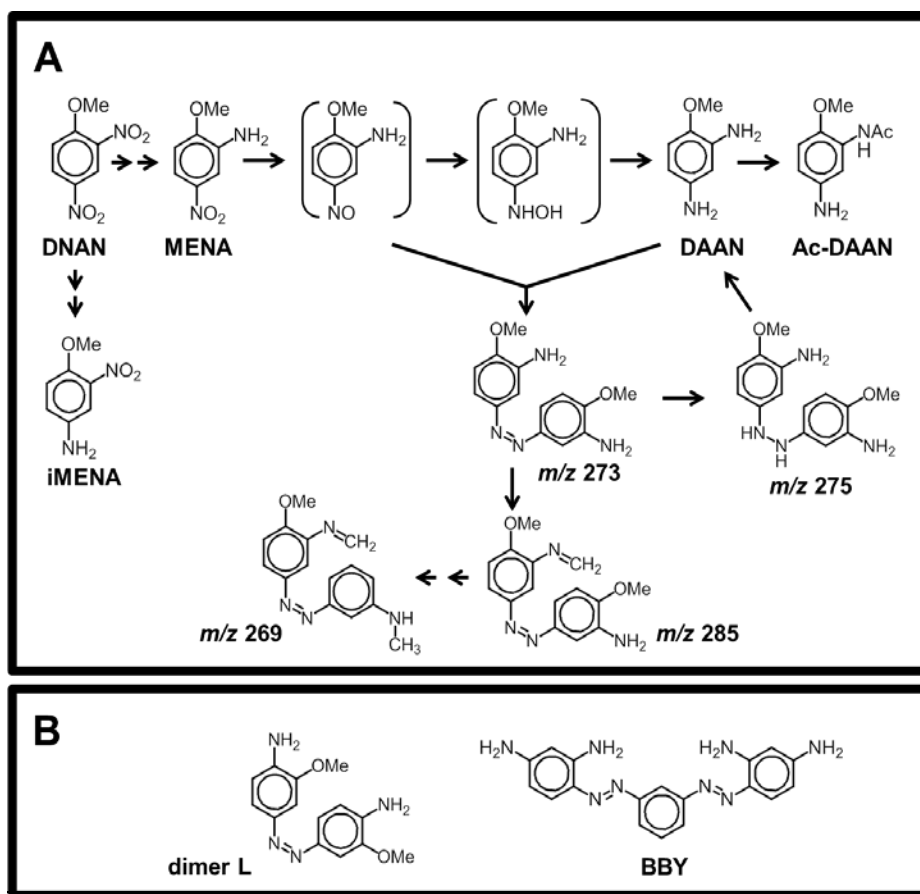


Figure 4.12-1. Panel A: (Bio)transformation pathways of DNAN in anaerobic incubations of soils and sludge. Microbial toxicity was evaluated for shown monomer compounds. Panel B: Azo-oligomer surrogate compounds used for microbial toxicity. Notation: OMe = methoxy; Ac = acetyl.

Monomeric biotransformation products as pure compounds

Most monomeric metabolites from DNAN reduction had partially decreased microbial toxicity with the exception of the MENA isomers (Table 4.12-1, Figure 4.12-3). DAAN and especially Ac-DAAN were many fold less toxic than DNAN, whereas one of the isomers, iMENA and MENA, was more toxic than DNAN in the case of methanogens and Microtox, respectively. Nitroaniline isomers from nitro reduction of 2,4-dinitrotoluene have been shown to be more toxic than the parent compound in *A. fischeri* ²⁹¹. In addition, nitroanilines were also the most toxic compounds in an extensive evaluation of the methanogenic toxicity of 24 different amino- and nitro-substituted benzenes ²⁷³. During the course of (bio)transformation, regio-specificity in DNAN (bio)conversion could impact the overall toxicity. For instance, nitro reduction of DNAN has predominantly been reported in the *ortho* nitro group in biological systems ^{47,85,229}, whereas evidence of *para*-NO₂ reduction has been found primarily in abiotic systems ²⁴¹, with one account of biological production ²⁹². Dominance of nitro reduction in the *ortho* group has been attributed to overall molecular stability due to H-bonding with the neighboring methoxy group ⁴⁷. Given these considerations, the toxicity of the nitroaniline isomers formed from DNAN nitro reduction is expected to be driven by MENA.

Table 4.12-1. Summary of inhibitory concentrations for DNAN, (bio)transformation products and best available surrogates to acetoclastic methanogens and *A. fischeri* (Microtox).

Compound	Methanogens	Microtox		Source
	IC ₅₀	IC ₅₀	0	
	-----μM-----			
DNAN	41	57		²⁹³
MENA	175	48		²⁹³
DAAN	176	155		²⁹³
iMENA	25	219		This study
Ac-DAAN	>8000 ^c	911		This study
Dimer L	65	29.8		This study
BBY	0.71	0.7		This study

^a302 μM DAAN caused 75% inhibition to *A. fischeri*.

^b446 μM iMENA caused 62% inhibition to *A. fischeri*.

^c8000 μm Ac-DAAN caused 2% inhibition to acetoclastic methanogens.

On the other hand, there are other reactions during (bio)transformation that could yield to less toxic products. Complete nitro reduction to aromatic amines has been considered as a detoxification mechanism ²²⁴, and aromatic amines were generally less cytotoxic than NACs to methanogens ^{273,294} and *A. fischeri* ^{277,294}. In a previous study we reported DAAN as less toxic than DNAN or MENA in both microbial assays ²⁹⁴. In addition, other transformation pathways could further decrease the inhibition potential of aromatic amines. For instance, DAAN N-acetylation resulted in a considerable decrease in toxicity (Figure 4.12-2A1, 4.12-2B1 and Figure 4.12-3). Ac-DAAN was the least toxic of all monomers, and did not cause inhibition up to 8 mM to acetoclastic

methanogens and had a 50% inhibition concentration (IC₅₀) of 911 μ M in Microtox. N-acetylation has been reported as a detoxification mechanism for amine moieties in aromatic compounds^{288,295}.

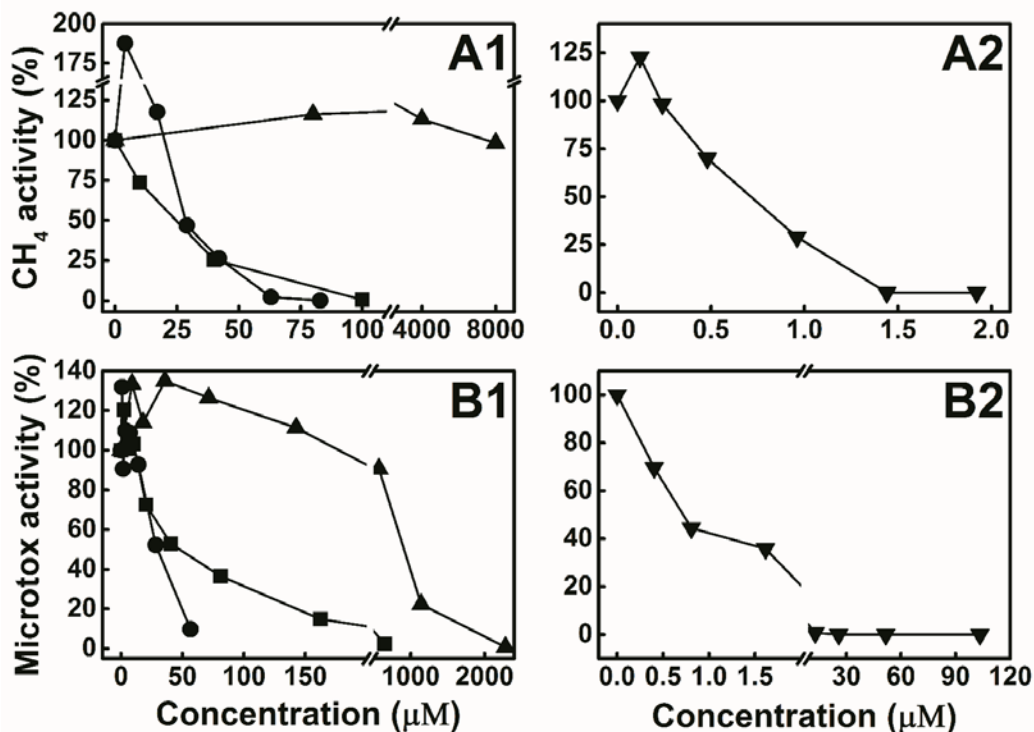


Figure 5.12-2. Methanogenic inhibition (A1, A2) and *A. fischeri* bioluminescence (B1, B2) based on toxicant concentration. Column 1: iMENA (■), Ac-DAAN (▲), dimer L (●). Column 2: BBY (▼).

Surrogates of dimers and trimers

The azo-oligomers tested, dimer L and BBY, were among the compounds causing the strongest toxicity. Dimer L was a potent toxicant to *A. fischeri* (IC₅₀ = 30 μ M) and methanogens (IC₅₀ = 65 μ M). While there is limited information on toxicity of oligomers formed during the biotransformation of explosives, a study on the cytotoxicity of TNT and its degradation products to H4IIE cells and Chinese hamster ovary-K1 (CHO) cells found that the azoxy-dimers were as toxic as the parent compound²⁸⁶. BBY was the most toxic of all compounds tested with an IC₅₀ in each of the microbial systems of 0.7 μ M. Even though both systems had the same IC₅₀, *A. fischeri* were more sensitive than methanogens, since complete inhibition occurred at 1.4 μ M (Figure 4.12-2A2).

Despite the severe inhibition posed by the oligomers, at very low concentrations, dimer L stimulated the methanogenic activity rate. Up to 188% of the test compound-free control activity at 4 μ M of the dimer (Figure 4.12-2A1). A similar phenomenon was detected for BBY but at a lower concentration range (125% stimulation at 1.23 μ M of trimer). Azo-oligomers are highly conjugated molecules that are reminiscent of phenazines, which are electron transport molecules in the respiratory chain of methanogens^{296,297}. Recently, the application of a phenazine, Neutral Red, was claimed in a patent application to increase the rate of methanogenesis²⁹⁸.

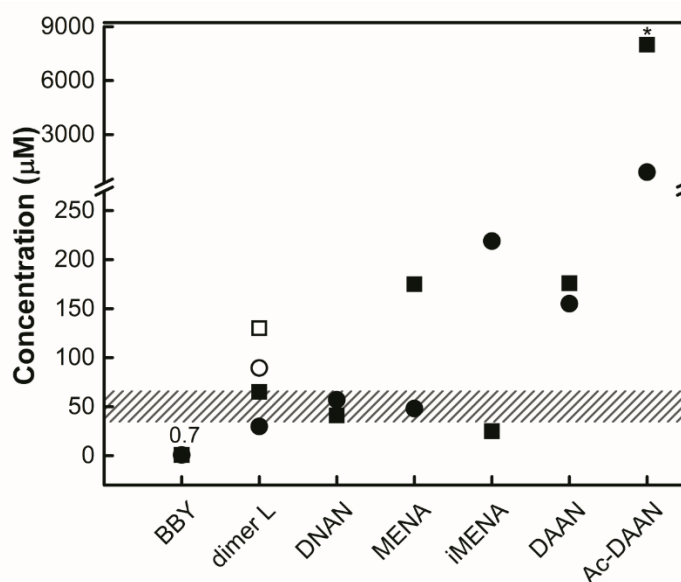


Figure 4.12-3. Fifty-percent inhibition concentrations (IC₅₀) for acetoclastic methanogens (■) and *A. fischeri* (●) for DNAN and its (bio)transformation products and azo-oligomer surrogates. Shaded area indicates DNAN IC₅₀ range. Open symbols in dimer L show adjusted concentrations to monomer equivalents. Ac-DAAN did not cause inhibition to methanogens and the highest concentration tested (8000 μM) is shown instead with an asterisk above the symbol. The BBY IC₅₀ for both models was 0.7 μM.

4.12.3. Results and Discussion: Exposures to DNAN (bio)transformation mixtures *Biotransformation product profiles.*

DNAN was incubated anaerobically in soil or sludge microcosms to obtain mixtures of products formed at different stages of (bio)transformation (See Materials and methods for details). Tubes were incubated at different times so that when liquid samples were collected at the same day, the overall (bio)transformation time elapsed would be 0, 1, 5, 10, 20, 30, 40, 50 days of anaerobic incubation. A diagram depicting the staggered (bio)transformation assays and overall workflow is shown in Figure 4.12-4.

MENA, DAAN and oligomer transformation products present in the liquid phase were semi-quantitated by LC-QToF-MS. Table 4.12-2 provides a list of selected parent/daughter ions used for semi-quantitative LC-MS determination of soluble products formed during anaerobic MENA soil (bio)transformation. The individual profile of (bio)transformation product mixtures formed at different stages of DNAN (bio)transformation for the two soils, Camp Butner (Figure 4.12-5) and Camp Navajo (Figure 4.12-6A), as well as for the anaerobic sludge (Figure 4.12-7A), were determined using LC-QToF-MS to detect products that were below detection in HPLC-DAD. Overall, the rate of DNAN conversion affected the rate of production of monomer and oligomer products. MENA and DAAN were detected primarily between 10-30 d of incubation in Camp Navajo soil, but were detected only sporadically in the Camp Butner soil. Unlike the soils, in the anaerobic sludge a consistent amount of DAAN was detected throughout 0-50 d of incubation, accounting for slightly less than a third of the total product peak area (3×10^7 area units for DAAN). A higher amount of DAAN in the system might require more reducing conditions. For instance, 2,4,6-triaminotoluene from TNT reduction has only been reported below -200 mV²⁹⁹. In the

systems studied in this work, hydrazo compounds had a higher occurrence in the sludge (m/z 275 in Figures 4.12-1 and 4.12-7), and as an intermediate formed during the reductive cleavage of azo-dimers, its presence points to a source of DAAN.

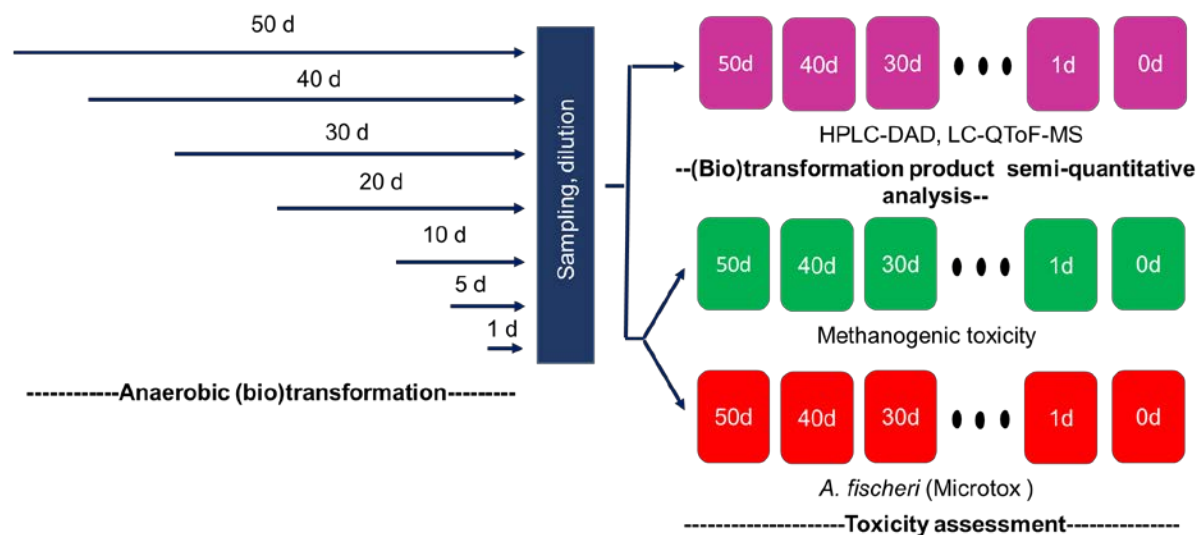


Figure 4.12-4. Workflow pictogram for DNAN staggered (bio)transformation assay, followed by product mixture semi-quantitative analysis and microbial toxicity assessment. Anaerobic incubations were set starting at different days so that when all the samples were taken the (bio)transformation product mixture would be a representative mixture for different stages of DNAN (bio)transformation (0, 1, 5, 10, 20, 30, 40, and 50 days of incubation). Samples were collected for (semi)-quantitation of the products formed, and subjected to methanogen and Microtox toxicity assays in order to reconstruct the changes in toxicity of the aqueous phase during the course of DNAN (bio)transformation.

Other monomer products, such as iMENA and Ac-DAAN were detected in smaller quantities than MENA or DAAN. For iMENA, the highest amount detected was 2×10^6 area units in Camp Butner soil at 20 d of (bio)transformation, but overall MENA was at least twice as much more abundant than its isomer. For Ac-DAAN, the largest amount detected was in sludge (8×10^5 area units), but its signal was on average two orders of magnitude smaller than DAAN. Azo-dimer products were detected concomitantly with the formation of QToF-MS detectable MENA, iMENA, DAAN, and Ac-DAAN in all three systems studied, suggesting that dimerization occurs very rapidly during the period nitro groups are being reduced. However, at longer incubation times (9-30 days), the major abundant species were comprised of products with ion m/z > 200 , attributed to azo-dimers. Based on common dominant (bio)transformation products detected across all systems, dimers underwent other reactions, such as N-substitution and O-demethoxylation.

Besides common dominant products, the relative abundance of each product varied depending on the system. For example, in Camp Butner soil incubations, the most abundant ions included m/z 269 and 285, 4'-methoxy-3-methylamino-3'-methylethylamino-azobenzene and 4,4'-dimethoxy-3-methylamino-3'-methylethylamino-azobenzene. In Camp Navajo, the primary products were m/z 247 and 274 (putatively with molecular formulas $C_7H_9N_3O_7^-$ and $C_9H_{11}N_3O_7^-$,

respectively), followed by m/z 269 and 285, like in Camp Butner. The ions m/z 247 and 274 have not been characterized, but could be a product formed during incorporation of DNAN reduced (bio)transformation products with humic substances. Covalent binding between quinone-like and reduced TNT products, a chemical analog to DNAN, have been found in ^{15}N studies with soil humic substances in aerobic conditions ²⁹⁰. Moreover, sediment-aromatic amine reactions have been detected and kinetically studied ³⁰⁰. In the anaerobic sludge, the primary dimers detected included m/z 285 and 269, with significant contributions of m/z 273 and 275, 4,4'-dimethoxy-3,3'-diamino-azobenzene and 4,4'-dimethoxy-3,3'-diamino-hydrazobenzene, respectively.

The largest cumulative amount of products in the aqueous phase, as quantified by peak area, occurred in Camp Butner soil and in the anaerobic sludge (1.2×10^6 area units). On the other hand, Camp Navajo soil, had two orders of magnitude less products at longer incubation times (40-50 d). A higher abundance in Camp Navajo was also observed with compounds with the highest molecular weight in the list, such as m/z 325 and 327, which were detected in all systems more often after DNAN was depleted ⁸⁷. Their concentration was in the range of $\sim 10^5$ area units for Camp Butner and sludge, but $\sim 10^4$ for Camp Navajo. The metabolite m/z 431, a potential trimer based on the molecular mass, was detected only in Camp Navajo soil at a 2.5-fold higher amount than m/z 325 and 327 ⁸⁷. Camp Navajo has more organic carbon than Camp Butner (5.24 versus 2.07 % dwt soil) ¹, and the difference in amount of products recovered may be due to irreversible adsorption and covalent incorporation into soil humus. In studies with ^{14}C radiolabeled TNT incubated with soil, more than half of the label was incorporated into different soil humic fractions ⁹⁸.

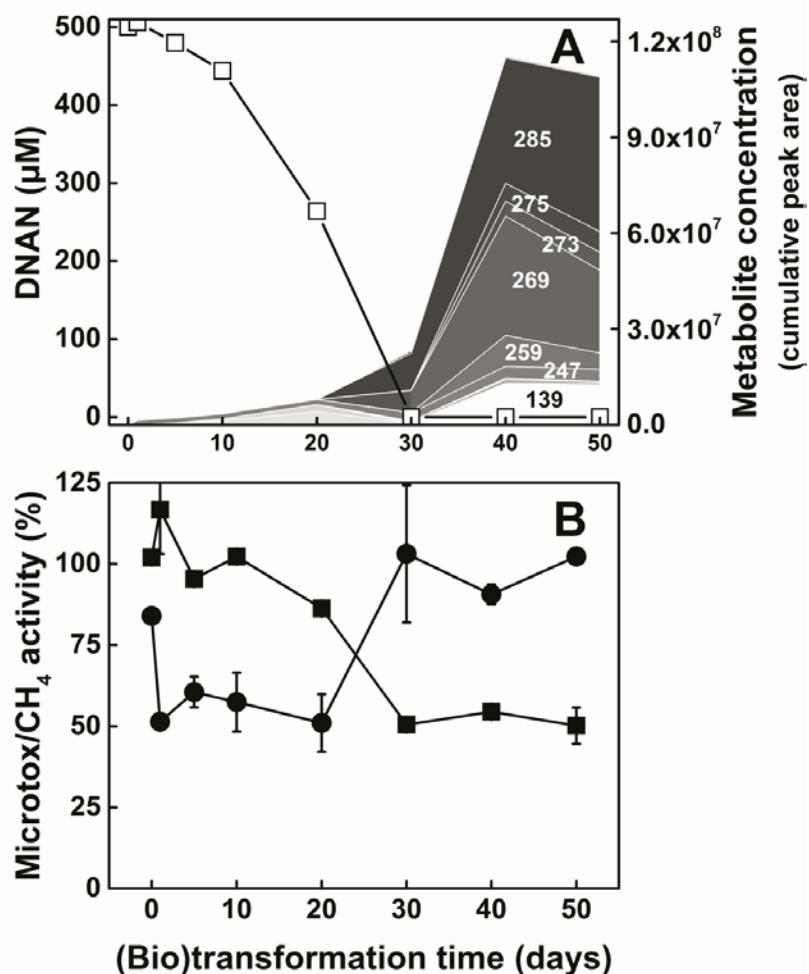


Figure 4.12-5. DNAN anaerobic (bio)transformation in Camp Butner soil and their collective toxicity impact. Panel A: DNAN (□) formed transformation products (stacked area, from light to dark in ascending molecular mass): 139.0866, 165.0659, 169.0608, 181.0972, 185.0652, 193.0607, 228.0768, 243.0877, 243.1241, 245.1300, 247.0425, 259.1190, 267.0975, 269.1397, 273.1347, 274.0715, 275.1503, 285.1347, 299.1179, 301.1289, 313.1289, 325.1659, 327.1452, 431.1569. Predominant $[M+H]^+$ values are shown. Panel B: Impact of mixtures of transformation products formed during (bio)transformation on *A. fischeri* bioluminescence (■) and acetoclastic methanogens (●).

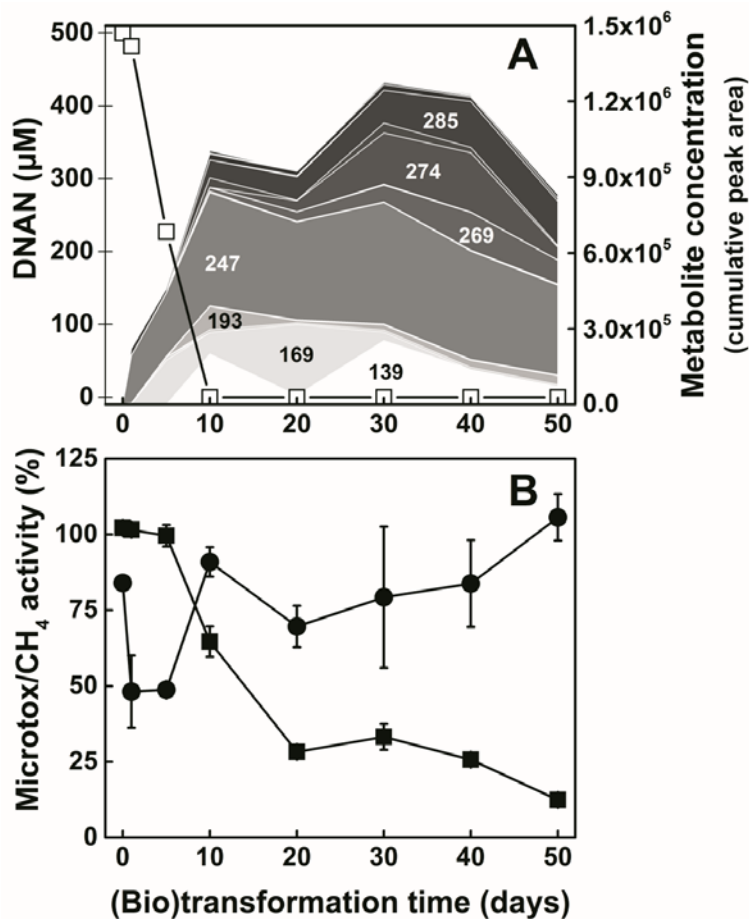


Figure 4.12-6. DNAN anaerobic (bio)transformation in Camp Navajo soil and their collective toxicity impact. Panel A: DNAN (□) formed transformation products (stacked area, from light to dark in ascending molecular mass): 139.0866, 165.0659, 169.0608, 181.0972, 185.0652, 193.0607, 228.0768, 243.0877, 243.1241, 245.1300, 247.0425, 259.1190, 267.0975, 269.1397, 273.1347, 274.0715, 275.1503, 285.1347, 299.1179, 301.1289, 313.1289, 325.1659, 327.1452, 431.1569. Predominant $[M+H]^+$ values are shown. Panel B: Impact of mixtures of transformation products formed during (bio)transformation on *A. fischeri* bioluminescence (■) and acetoclastic methanogens (●).

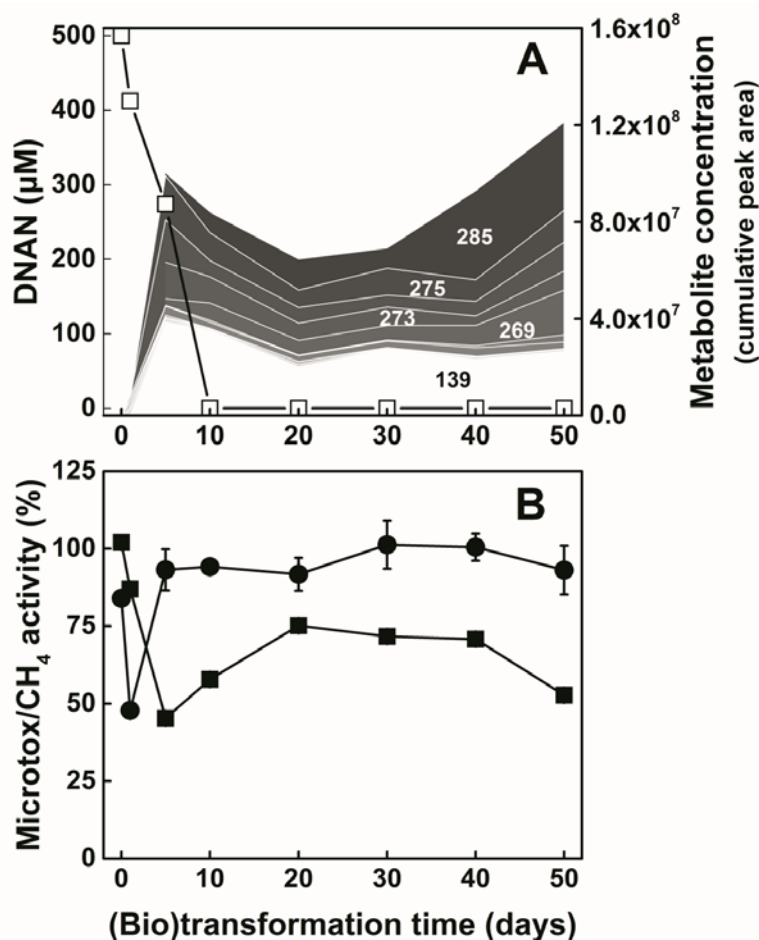


Figure 4.12-7. DNAN anaerobic (bio)transformation in anaerobic sludge and their collective toxicity impact. Panel A: DNAN (□) formed transformation products (stacked area, from light to dark in ascending molecular mass): 139.0866, 165.0659, 169.0608, 181.0972, 185.0652, 193.0607, 228.0768, 243.0877, 243.1241, 245.1300, 247.0425, 259.1190, 267.0975, 269.1397, 273.1347, 274.0715, 275.1503, 285.1347, 299.1179, 301.1289, 313.1289, 325.1659, 327.1452, 431.1569. Predominant $[M+H]^+$ values are shown. Panel B: Impact of mixtures of transformation products formed during (bio)transformation on *A. fischeri* bioluminescence (■) and acetoclastic methanogens (●).

Table 4.12-2. Selected parent/daughter ion list for semi-quantitative LC-MS determination of soluble products formed during anaerobic MENA soil (bio)transformation. Daughter ions shown indicate they were used to determine the abundance of the products. A total tolerance of 10 ppm for the mass bias was allowed for peak integration of the measured $[M+H]^+$ ions.

Chemical compound (identifier); Molecular formula;	CAS #	Measured $[M+H]^+$	Retention time (min)
2,4-diaminoanisole (DAAN); $C_7H_{10}N_2O$	615-05-4	139.0866	2.51
2-methoxy-5-nitroaniline (MENA); $C_7H_8N_2O_3$	99-59-2	169.0608	6.23
3-nitro-4-methoxyaniline (iMENA); $C_7H_8N_2O_3$	577-72-0	169.0608	2.99
N-(5-amino-2-methoxyphenyl) acetamide (Ac-DAAN); $C_9H_{12}N_2O_2$	64353-88-4	181.0972	2.14
3-amino-3'-nitro-azobenzene (m/z 243); $C_{12}H_{10}N_4O_2$	61390-99-6	243.0877	1.87
4'-methoxy-3-methylamino-3'-methylethylamino-azobenzene (m/z 269); $C_{15}H_{16}N_4O$	N/A	269.1397	5.09
3,3'-diamino-4,4'-dimethoxy-azobenzene (m/z 273); $C_{14}H_{16}N_4O_2$	N/A	273.1347	13.75
3,3'-Diamino-4,4'-dimethoxy-hydrazobenzene (m/z 275); $C_{14}H_{18}N_4O_2$	N/A	275.1503	3.48
5-((3-Amino-4-methoxyphenyl)diazonyl)-2-methoxy-N-methylethylamine (m/z 285); $C_{15}H_{16}N_4O_2$	N/A	285.1347	10.61

Toxicity profile during (bio)transformation.

Acetoclastic methanogenic and *A. fischeri* bioluminescent inhibition assays were used to assess the overall toxicity of the aqueous extracts of DNAN (bio)transformation product mixtures sampled from the biotransformation assays at different times of anaerobic incubation. Both microbial toxicity models were very susceptible to toxicity of the mixture of (bio)transformation. The samples mixtures had to be diluted significantly (1:54 for methanogens and 1:36 for *A. fischeri*) before exposure, since at lower dilutions, there was complete inhibition in both assays which did not allow to observe differences in inhibition potential across the (bio)transformation timeline.

At early stages of DNAN (bio)conversion, methanogenic activity dropped sharply as the parent compound disappeared, across all systems assayed (Figures 4.12.5B through 4.12-7B). This period of increased inhibition lasted as long as DNAN was detectable in aqueous solutions. This period of enhanced toxicity was directly dependent on the rate of DNAN (bio)transformation. The dip in activity was the shortest in anaerobic sludge (1 d) (Figure 4.12-7B), while for Camp Butner (with the slowest rate of DNAN (bio)conversion), lasted for 30 days (Figure 4.12-5B).

The increase in methanogenic inhibition could be attributed to putative reactive intermediates formed during nitro reduction of DNAN, such as nitroso- and hydroxylamino-derivatives. Nitroso and hydroxylamino products have been identified as potentially responsible for methanogen cell lysis (and methanogenic inhibition) during nitro reduction²²⁴. Cytotoxicity studies on TNT and its reduced (bio)transformation products, showed that 4-hydroxylamino,2,6-dinitrotoluene could be as toxic or more toxic than TNT²⁸⁶. DNAN nitroso-derivatives have been found in abiotic⁴⁷ and biotic¹⁰², as well as for other nitroaromatic compounds such as 2,4-dinitrotoluene³⁰¹. Hydroxylamino products have also been reported in DNAN^{102,229} and TNT³⁰² reductive (bio)transformation studies. Furthermore, azo-dimers detected in this work could be indirect evidence of the occurrence of these intermediates since classic azo formation involves coupling of nitroso-bearing products with either hydroxylamino¹⁷² or amino derivatives^{303,304}.

At longer incubation times (30-50 d), the diluted mixtures of metabolites present at this stage of (bio)transformation caused very low inhibition to methanogens. Compared to earlier incubation times, when the toxicity was maximum, there was clearly a decrease in toxicity associated with the formation of azo-dimers. This recovery of activity might be attributed to the disappearance of a steady supply of reactive intermediates from nitroreduction once DNAN is depleted from the system. An additional factor could be the stimulation of methanogenic activity by azo-dimers, such as the effect observed with dimer L exposure up to 17 μM to methanogens in this work. Since the mixtures were diluted 54-fold, this would imply a maximum azo-dimer concentration of 4.6 μM (or 9.2 μM monomer equivalents). The theoretical maximum azo-dimer concentration would be in the stimulatory region. In all cases, after the initial inhibition, there was a consistent recovery and detoxification compared to the initial portion of (bio)transformation, eventually achieving restoration 100% activity compared to the test-compound free controls.

For *A. fischeri*, there was little inhibition during initial conversion DNAN in all systems, but inhibition started to increase when more than half of the DNAN had been converted (Figures 4.12-5B through 4.12-7B). Unlike methanogens, *A. fischeri* might not be affected by the reactive nitroso and hydroxylamino intermediates if coping mechanisms against radicals and N-reactive species are present. Recently, flamohaemoglobin Hmp in *A. fischeri* has been attributed to protect against NO and reactive oxygen produced by the host squid as an antimicrobial agent during colonization in *A. fischeri*-squid symbiosis³⁰⁵. However, at the latter part of DNAN reduction and after DNAN was completely (bio)transformed, there was increased inhibition of bioluminescence. During these stages of (bio)transformation, there were

also significant detection of dimer products ($m/z > 200$), which could be directly responsible for affecting bioluminescence. In Camp Navajo, the highest inhibition (88%) occurred at 50 days. However, in Camp Butner soil and in the anaerobic sludge, the maximum inhibition was 50%. In the anaerobic sludge there was a temporary decrease in inhibition from 20-40 d which occurred at the same time as the amount of detected dimers decreased, and by 50 d the inhibition increased again concomitantly with the dimers products. Based on the 1:36 dilution used in Microtox, the maximum theoretical concentration of azo-dimers would be 6.9 μM (or 13.8 μM monomer equivalents), which would be in the inhibitory range based on surrogate L dimer toxicity test.

4.12.3. Implications of microbial toxicity and (bio)transformation product profiles

A workflow integrating transformation product semi-quantitation with microbial toxicity provided information about scenarios expected in soils and wastewater sludge systems polluted with DNAN. Two key events during (bio)transformation were identified as potential toxicity drivers. Methanogenic increased inhibition during nitro reduction of DNAN was attributed to reactive hydroxylamino and nitroso intermediates, while azo-dimers rich mixtures were severely toxic to *A. fischeri*. On the other hand, N-acetylation greatly reduced toxicity of DNAN. N-acetylation and azo-dimerization of amines are transformation pathways that have been reported to be in direct competition with each other²⁹⁵. Both of these processes have been identified in microbial systems in presence of DNAN^{85,229}, although azo-dimerization seems to be the dominant route based on semi-quantitative analysis of this work. However, devising strategies to increase N-acetylation reactions could be exploited in bioremediation efforts to yield non-toxicant products in systems polluted with DNAN.

4.13. Zebrafish Embryo Toxicity of DNAN Anaerobic Biotransformation Products .

4.13.1. Objectives: Zebrafish embryo toxicity

The objective of this work was to evaluate developmental effects of DNAN (bio)transformation products (or best commercially-available surrogates) using zebrafish (*Danio rerio*) as a toxicology model. We also tested mixtures of the products formed at different stages of (bio)transformation during anaerobic incubations of soils using as a starting point the primary DNAN transformation product, MENA. Toxicological testing was supported by detailed mass spectrometry studies (using ultra-high performance liquid chromatography coupled to quadrupole time-of-flight mass spectrometry, UHPLC-Q-ToF-MS) to characterize transformation product mixture profiles.

In the ecotoxicology field, zebrafish embryos have become widely used to monitor water quality and to aid in environmentally safe product development^{306,307}. The embryonic zebrafish model is amenable for high-throughput studies and allows evaluation of developmental and behavioral endpoints in addition to acute toxicity³⁰⁸. Early development is very similar to higher order vertebrates and its transparency allows for non-invasive and specific developmental assessment endpoints³⁰⁹. Moreover, a vast amount of transcriptomic information along an expanding library of toxicants tested can provide mechanistic insights of the toxicity effects in zebrafish^{105,307,310,311}.

4.13.2. Results and Discussion: Toxicity of model biotransformation products

The library of compounds tested included DNAN monomer (bio)transformation products^{85,103,229} and best available surrogates for azo dimers and trimers, since no dimer metabolites were commercially available (Table 4.13-1 and Figure 4.12-1). DNAN was not tested in this work due to the commercialization, transportation, and export control restrictions established by the International Traffic in Arms Regulations (ITAR) of the US Department of State³¹². Instead MENA was used as the reference parent compound.

Mortality.

No statistically significant mortality at 24 and 120 hpf was detected for any of the pure compounds tested (0-640 μ M for MENA and DAAN; 0-64 μ M for iMENA, Ac-DAAN, dimer A, dimer L, and BBY). Mortality charts for each compound tested can be found elsewhere⁹⁴. In this study, which used zebrafish embryos with intact chorions, no adverse lethal effect were detected for MENA concentrations up to 640 μ M. However, in a previous study with dechorionated zebrafish embryos on compounds from the U.S. EPA ToxCast phase 1 and 2 lists, which included MENA, the 120-hpf mortality lowest observable effect level (LOEL) was reported at 64 μ M¹⁰⁵. Since the chorion is the primary exposure route before hatching³⁰⁸, this discrepancy suggests that the presence of the chorion could be limiting the diffusion of aromatic amines like MENA.

Similar to the monomeric compounds tested in this work, the azo-dimers and trimer (BBY) evaluated did not result in zebrafish mortality at concentrations up to 64 μ M. Azo dye dimers and trimers have been tested in aquatic ecotoxicity models, including an extensive dye survey on fathead minnows (*P. promelas*)³¹³, and more recently on guppy fish (*Poecilia reticulata*)³¹⁴, and the Western clawed frog (*Silurana tropicalis*)³¹⁵. In contrast with the lack of lethal effects detected in our study, the 96-h LC₅₀ value reported in guppy fish for Methyl Red (CAS# 493-52-7), an azo-dimer with N-methyl, amino, and carboxylic acid substituents, was 89 μ M³¹⁴, and for Basic Brown 4 (CAS# 5421-66-9), an azo trimer with amino and methyl substituents, in fathead minnows it was 12.1 μ M.

Overall, the low mortality counts obtained with the pure compounds tested suggest that the individual transformation products/surrogates evaluated in this study pose little acute

toxicity risk ($\leq 64 \mu\text{M}$). This argument is strengthened by the observed decrease in toxicity of TNT on fathead minnows, as TNT was reduced to dinitroaniline products ³¹⁶.

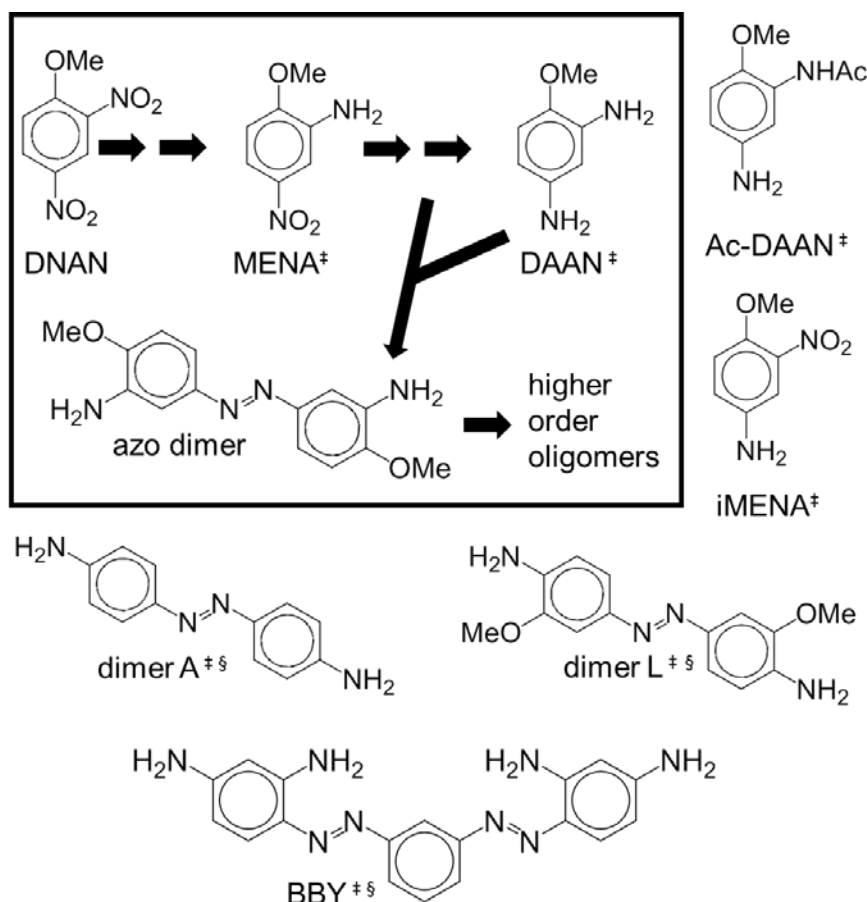


Figure 4.13-1. Main anaerobic DNAN (bio)transformation pathway (structures inside box): DNAN undergoes nitro reduction to MENA and DAAN ⁸⁵. Reactive intermediates formed during nitro-group reduction enable coupling reactions that form dimers and other oligomers by reacting with aromatic amines ^{303,304}. Chemical structures of individual compounds tested based on previously identified DNAN (bio)transformation products ([‡]) or best available surrogates ([§]).

Developmental toxicity

Detailed developmental endpoint scoring for all the chemicals tested in this work is provided elsewhere ⁹⁴. While most of the compounds tested did not cause developmental abnormalities, dimer L and iMENA caused significant malformations in zebrafish embryos (Table 4.13-1). iMENA had a developmental LOEL of $6.4 \mu\text{M}$ based on yolk sac edema formation, but no other abnormalities were detected. The rest of monomer compounds did not show developmental activity. Developmental toxicity studies with the monomeric compounds tested here have not been previously reported. However, some aromatic amines, such as aniline have been shown to cause developmental toxicity in African clawed frog (*Xenopus laevis*) embryos, albeit at much higher concentrations, 3.9 mM ³¹⁷. Of the dimers and trimer tested, only dimer L caused significant developmental abnormalities in the embryos ⁹⁴. Dimer L caused a significant occurrence of yolk sac and pericardial edemas (LOEL = $6.4 \mu\text{M}$), and several malformations in six other endpoints at $64 \mu\text{M}$ (Figure 4.13-2). A photograph illustrating some of these abnormalities is shown in Figure 4.13-3. While BBY and dimer A did not show any developmental toxicity in the tested range, BBY has been reported to cause malformations in

Western clawed frogs at 2.4 mM³¹⁵.

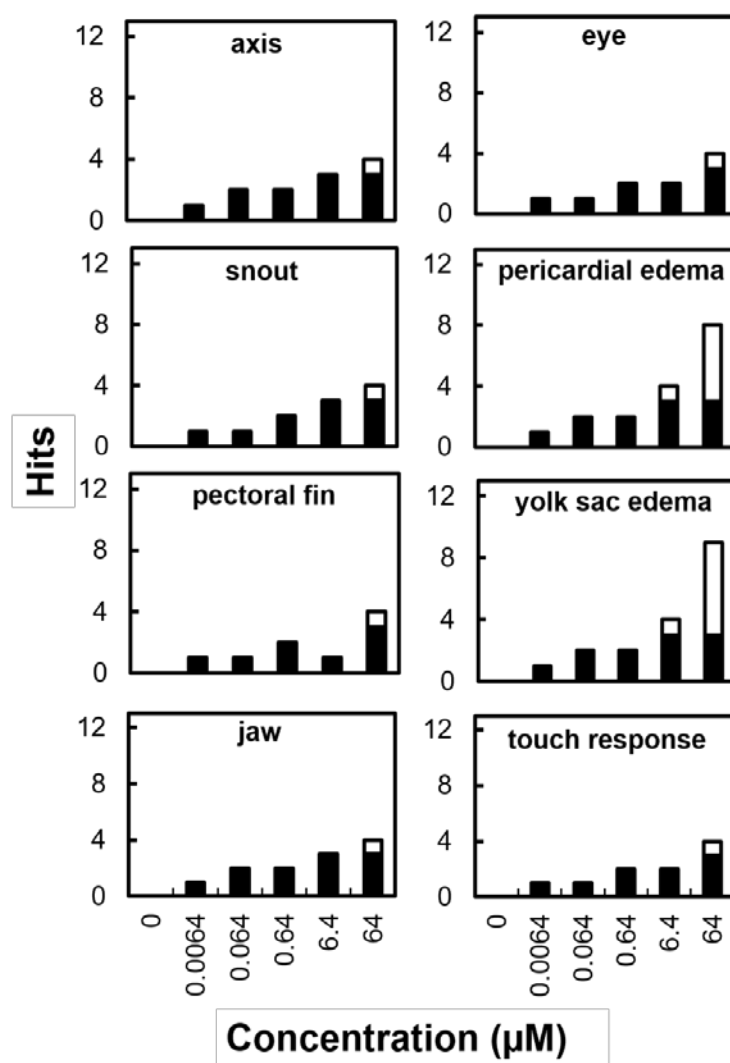


Figure 4.13-2. Developmental endpoints that caused significant malformations in the zebrafish embryo assay for dimer L. White bars indicate hits above the statistically significant threshold ($p \leq 0.05$). The rest of the endpoints did not show significant activity.

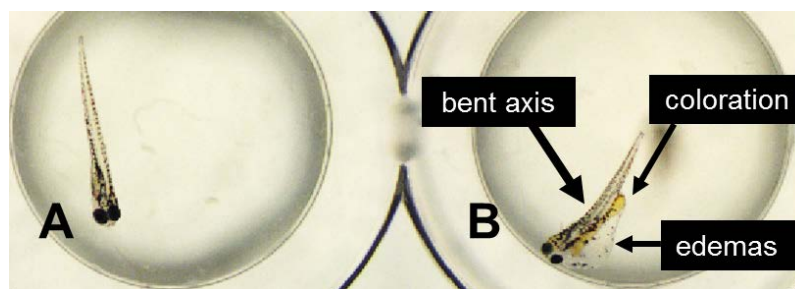


Figure 4.13-3. Representative visual comparison between 120 hpf zebrafish embryos: Control (A), 64 μ M dimer L (B). The embryo exposed to dimer L showed developmental abnormalities and visible dimer L uptake (coloration).

Locomotor behavior assay

The impact of the various model compounds on zebrafish swimming locomotor behavior was also tested at 120 hpf. Zebrafish are more static in presence of light compared to dark periods, and comparing the difference in light/dark cycles can indicate changes in behavior due to exposure to toxicants¹⁰⁶. In this study, long distance swimming motion ranged from 18 to 30 mm in the dark, while it was below 5 mm in light (Figure 4.13-4). There were no detectable effects in locomotion for any of the chemicals tested, except for DAAN. While there were some minor variations in the distance swum in the dark periods when considering most compounds, the average movement in zebrafish that had been exposed to 640 μ M DAAN (4 mm), was eight-fold less than the toxicant-free control (32 mm). Since there were no developmental active endpoints for DAAN⁹⁴, the lack of response to light/dark periods is not associated with swimming impairment due to malformations. Therefore, this suggests that exposure to 640 μ M DAAN could have neurotoxicity effects. To the best of our knowledge, this is the first work to study potential locomotor effects caused by a NAC, an aromatic amine, and an azo-dimer exposure in zebrafish during the developmental stage.

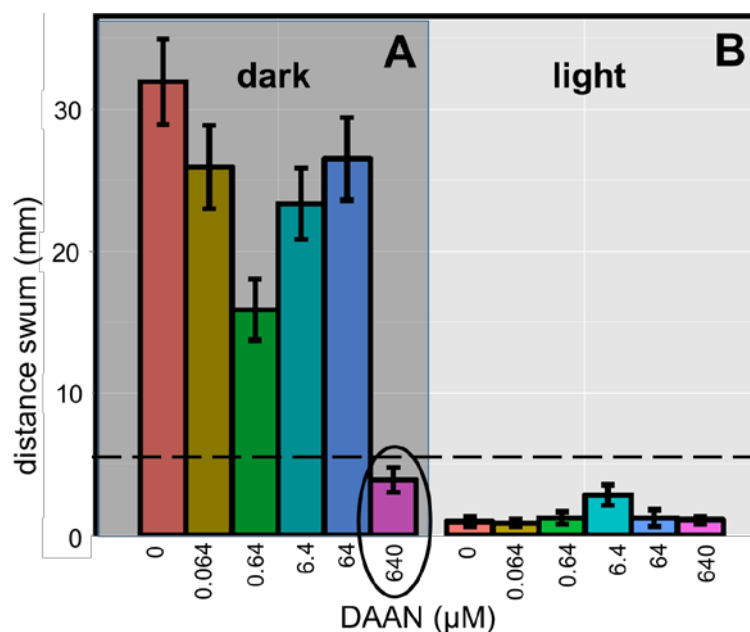


Figure 4.13-4. Average long distance swum recorded in locomotor response Viewpoint assay for 120 hpf zebrafish larvae exposed to DAAN (0-640 μ M) in dark (A) and light (B) stages.

4.13.3. Results and Discussion: Toxicity of MENA (bio)transformation products in anaerobic soil microcosms

Product characterization and semi-quantitation

Based on UHPLC-Q-ToF-MS analyses, six parent ions were selected for semi-quantitation according to their chromatogram peak area abundance (> 1000) (Table 4.13-2). From these compounds, three had been reported previously as monomer products formed during DNAN (bio)transformation in anaerobic conditions: DAAN and Ac-DAAN⁸⁵. In this work, we report a new transformation product, 3-amino-3'-nitro-azobenzene (m/z 243, as well as two parent ions that have not been assigned chemical structures $[M+H]^+$ m/z 313.1343 (putative molecular formula $C_{16}H_{16}N_4O_3$) and 393.0836 (putative molecular formula $C_{19}H_{12}N_4O_6$). Based on these formulae, these ions could represent a dimer and a trimer, respectively. Transformation products were quantified using parent ions (m/z $[M+H]^+$), or daughter ion (m/z $[M+H-R]^+$) transitions when the daughter yielded a stronger ionization signal than the precursor (Table 4.13-2). While standards were available for DAAN and Ac-DAAN, the rest of the analytes were not commercially available, difficult to synthesize, and potentially not stable in air. For consistency, all analytes are reported in peak area units based on UHPLC-Q-ToF-MS, which cannot be unequivocally translated to concentration because of potential variation in ionization efficiencies (Figure 4.13-5A). MENA was not added to the selected ion list since it ionized several orders of magnitude more strongly than the rest of the analytes. Therefore, its concentration during the (bio)transformation is reported in μ M as quantified using UHPLC-DAD (Figure 4.13-5B).

From initial time to 6 days of (bio)transformation, trace amounts of all of the analytes were detected, but 23% of MENA had already been removed, indicating possible formation of transformation products not shown in Table 4.13-2. From day 6 to 9 the formation of oligomers (mainly m/z 243, 313, 393) was visible, followed by accumulation of DAAN and Ac-DAAN

after day 10. The concentration of all of the analytes increased until day 30, with exception of DAAN, which decreased by 40% from days 20-30.

In order to consider transformation products that might be difficult to separate chromatographically or ionize in the Q-ToF-MS, UV-VIS spectra were also recorded along the course of the (bio)transformation of MENA. Since oligomers were detected in Q-ToF-MS, the spectral data are summarized as an oligomer index, based on the ratio of absorbance at 400 to 254 nm (Figure 4.13-5B), the former wavelength being chosen to quantify polymers⁹⁵ that have visible absorbance (e.g. azo dyes), and the latter a common wavelength for aromaticity. The 400/254 nm ratio increased from days 1-6, reached a maximum at 9 days of incubation, and then decreased until day 30. The initial increase might be due to the onset of oligomer formation as evidenced by Q-ToF-MS data, whereas the subsequent decrease following day 9 indicates precipitation of larger insoluble oligomers out of solution, even if soluble dimers such as m/z 243 continue being formed.

Zebrafish mortality and absence of developmental abnormalities.

Mortality assessed at 120 hpf was statistically significant only for the sample taken at 9 days of (bio)transformation (Figure 4.13-5A), coinciding with the maxima recorded for the 400/254 nm absorbance oligomer index (Figure 4.13-5B) and slightly after the onset of oligomer formation. This suggests that the early formation of azo dimers is responsible for an increase in zebrafish embryo mortality. Oligomerization occurs when reactive nitroso-intermediates react with amines to cause coupling reactions^{303,304}. Thus, mortality is potentially associated with the reactive intermediates.

Table 4.13-1. Developmental Lowest Observable Effect Levels (LOELs) and endpoints with significant morbidity.

Chemical compound (identifier)	Surrogate for	Developmental LOEL (μM)	Active Endpoints (μM)
2-methoxy-5-nitroaniline (MENA)	N/A	>640	N.D.
3-nitro-4methoxyaniline (iMENA)	N/A	6.4	yolk sac edema (6.4)
2,4-diaminoanisole (DAAN)	N/A	>640	N.D.
N-(5-amino-2-methoxyphenyl) acetamide (Ac-DAAN)	N/A	>64	N.D.
4,4'-azodianiline (dimer A)	azo dimer	>64	N.D.
2,2'-dimethoxy-4,4'-azodianiline (dimer L)	azo dimer	6.4	yolk sac and pericardial edemas (6.4); axis, eye, snout, jaw, pectoral fin, touch response (64)
Bismarck Brown Y (BBY)	azo trimer	>64	N.D.

N/A = Not applicable; N.D. = None detected

Table 4.13-2. Selected parent/daughter ion list for semi-quantitative LC-MS determination of soluble products formed during anaerobic MENA soil (bio)transformation. Daughter ions shown indicate they were used to determine the abundance of the products.

Chemical compound or identifier; Molecular formula	CAS #	Calculated	Measured		Retention time (min)
		Parent [M+H] ⁺	Parent [M+H] ⁺	Daughter [M+H-R] ⁺	
2,4-diaminoanisole (DAAN); C ₇ H ₁₀ N ₂ O	615-05-4	139.0866	139.0866	N/A	2.86
N-(5-amino-2-methoxyphenyl) acetamide (Ac-DAAN); C ₉ H ₁₂ N ₂ O ₂	64353-88-4	181.0972	181.0972	N/A	2.36
3-amino-3'-nitro-azobenzene (<i>m/z</i> 243) [§] ; C ₁₂ H ₁₀ N ₄ O ₂	61390-99-6	243.0877	243.0870	N/A	2.3
(<i>m/z</i> 313) ^{*§} ; C ₁₆ H ₁₆ N ₄ O ₃	N/A	313.1295	313.1312	250.8794	1.60
(<i>m/z</i> 393) ^{*§} ; C ₁₉ H ₁₂ N ₄ O ₆	N/A	393.0830	393.0836	276.0833	1.59

N/A = Not applicable.

* These ions detected have not been assigned a chemical structure.

§ These compounds are reported for the first time as (bio)transformation products.

There were no active developmental endpoints in any of the samples collected during MENA biotransformation. The absence of developmental abnormalities in the assay could be due to several factors, which may contribute synergistically. Firstly, the compound mixtures were produced at very low concentrations and below any LOEL. Secondly, fewer oligomers may be bioavailable to the embryos if extensive polymerization occurs that result in oligomers precipitating from solution or oligomer incorporation into the soil humus⁹⁸. These mechanisms are supported by the overall decrease of aromaticity of the aqueous phase as evidenced by the decline in 254 nm absorbance during the course of the (bio)transformation⁹⁴. Aromatic amines and azo polymers from similar NACs, such as DNAN and TNT, bind irreversibly to soil humic substances^{47,98}.

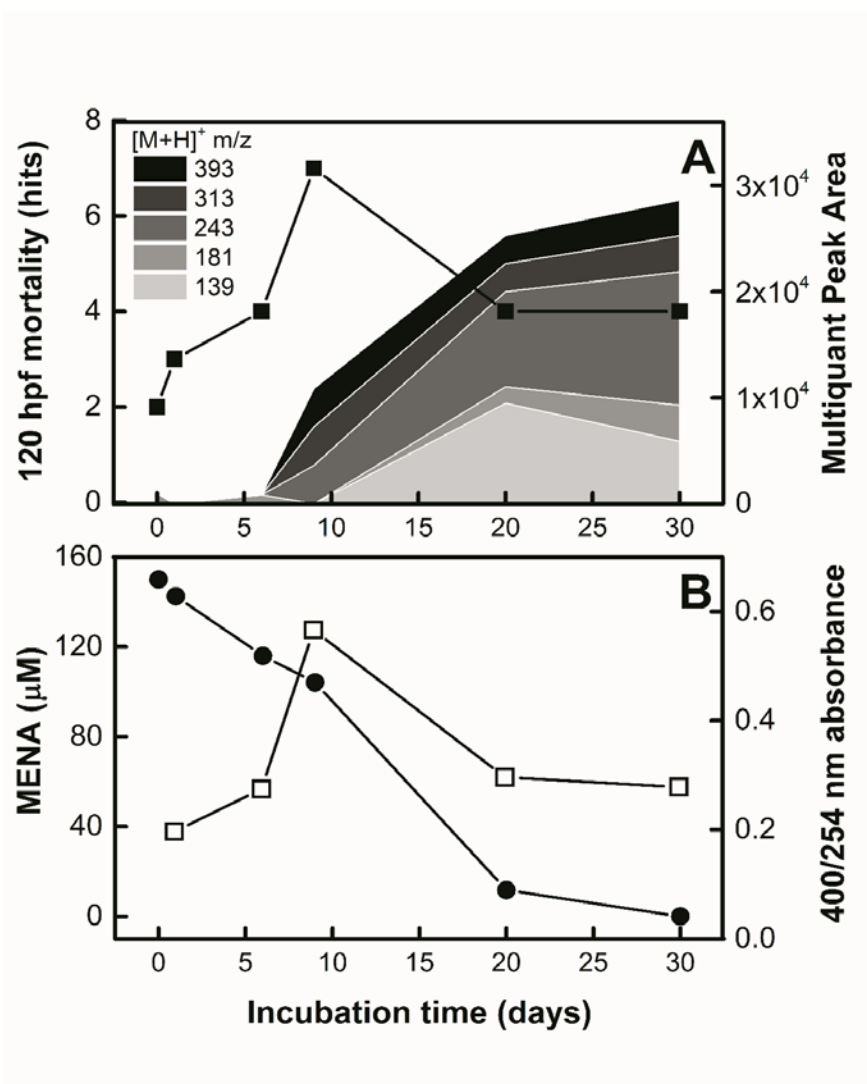


Figure 4.13-5. Characterization of products formed during MENA (bio)transformation coupled to zebrafish toxicity. Panel A: Temporal semi-quantitation of transformation products ($[M+H]^+$ m/z = 139, 181, 243, 313, 393) shown with stacked areas and increasing m/z shown with darker shades and zebrafish mortality assessed at 120 hpf (■). Mortality statistical significance ($p < 0.05$) is above 4 hits ($n = 32$). Panel B: MENA concentration (●) and 400 nm/ 254 nm absorbance index (□) during MENA (bio)transformation.

4.13.4. Toxicity implications of DNAN biotransformation

The results of this study demonstrate that intermediates of DNAN biotransformation can cause detectable developmental and behavioral toxicity endpoints in zebrafish embryos. Most concerning was the high level of developmental toxicity caused by a surrogate azo-dimer intermediate (dimer L) and iMENA (both at 6.4 μM) as well as evidence of locomotor toxicity caused by DAAN at higher concentrations. Our work approach coupled transformation product identification with toxicological testing to determine the environmental impact of organic pollutants as they undergo transformation in natural systems. These findings will help to advance understanding of the potential adverse impacts of DNAN biotransformation products in natural systems to aquatic species and vertebrates in general.

5. CONCLUSIONS

5.1. Reactivity of IMCs and IMC Daughter Products with Soil Minerals

5.1.1. Adsorption

The adsorption and reactivity of IMCs with clay mineral and Fe and Mn oxide mineral constituents was determined as a means to better assess contaminant mobility and bioavailability in soils and sediments. Adsorption of IMCs at mineral surfaces is governed not only by functional group composition and charge of the IMCs themselves, but also by the surface functional group chemistry and exchangeable cation (in the case of montmorillonite) composition of the mineral adsorbents. None of the minerals served as a high affinity adsorbent for all of the IMCs and daughter compounds tested. However, each of the compounds did exhibit a high adsorption affinity for at least one of the adsorbent types examined. This suggests that each of the compounds would be subjected to adsorptive retardation during subsurface transport, but likely as a result of accumulation at distinct mineral surfaces. NACs (DNAN and MENA) exhibited significant affinity for layer silicate clays; whereas, the nitroheterocyclic compounds (NHCs), NTO and ATO, showed greater affinity for the Fe(III) and Mn(IV) metal oxide minerals (goethite and birnessite, respectively).

NAC adsorption to layer silicate clays was apparently favored by inner-sphere complexation between nitro functional groups and exchangeable cations. The strength of this adsorption can be greatly increased with K^+ exchangeable cations versus other cations (e.g. Na^+) due to the lower hydration of K^+ enhancing the innersphere complexes. On the other hand, NHC adsorption was insignificant on the silicate clays because of charge repulsion. Conversely, NTO exhibited strong affinity for adsorption to both goethite and birnessite mineral surfaces. The reduction of DNAN and NTO is expected to occur in sub-oxic soil pore waters and our results indicate that such bio-reduction to MENA and ATO, respectively, can alter subsequent contaminant reactivity with mineral surfaces (more mobile). Specifically, reduction of nitro substituents to amine functionality diminishes NAC affinity for layer silicate surfaces, due to a decrease in nitro-groups available for ternary complexes with adsorbed metal cations as well as weakening of electron-donor-acceptor complexes of NAC π system with the clay's siloxane oxygen. Nitro group reduction also decreases NHC sorptive affinity for goethite.

5.1.2. Transformation

DNAN Transformation by minerals

The results of this study suggest that the progressive replacement of electron withdrawing nitro groups by amino groups, that occurs during reductive biotransformation of DNAN, increases the susceptibility of IMC molecules to oxidation by naturally occurring metal oxides in soil. The parent compound, DNAN, was completely resistant to oxidation by both birnessite (MnO_2) and ferrihydrite. In contrast, the first daughter product DNAN reduction, MENA in which one of the nitro groups is replaced with an amine group, was reactive with birnessite but not with ferrihydrite. The second daughter product DAAN in which the two of the nitro groups of DNAN are replaced with an amine groups, was reactive with both with birnessite and ferrihydrite, but birnessite was 6-fold more reactive. Likewise DAAN was 5-fold more reactive compared to MENA, highlighting the large increases in reactivity afforded by the progressive conversion of nitro groups to amines.

These results indicate that metal oxides in soil play a very important role in remediation of reduced IMC daughter products in the natural environment.

NTO transformation by minerals

The study of parent compound NTO and daughter product ATO reactivity with birnessite and ferrihydrite improves the understanding of the fate of these compounds on mineral surfaces. NTO was resistant to oxidation by both the birnessite and ferrihydrite at the tested concentrations. However, NTO was strongly adsorbed to the ferrihydrite surface, indicating an important potential mechanism for its attenuation in soils. Given the overwhelming consensus view that NTO does not adsorb to soils, an update on the view needs to include the possibility that NTO is effectively adsorbed by iron oxides. ATO was also found to be adsorbed to the ferrihydrite surface but more weakly than NTO. However, ATO, which is readily formed from NTO nitro-group biotransformation to an amine group in suboxic soil microniches, was found to be highly reactive with birnessite. By comparison, the parent compound was completely nonreactive with birnessite indicating the importance of converting the electron-withdrawing nitro-group to an amine to make the molecule highly susceptible to an oxidation reaction with the minerals. The reaction of ATO with birnessite resulted in its transformation to urea, N₂ and CO₂, indicating complete breakdown to safe end products. The results

Reduction of DNAN and NTO by green rust

Green rust in aqueous suspension (1% w/w) is capable of reductive transformation of IMCs (0.5 mM) to their respective amines concomitantly as green rust is oxidized in the process to lepidocrocite. The reductive transformation of DNAN and NTO resulted in the formation of reduced, aminated daughter products. DNAN transformation displayed a highly unique staggered regioselectivity. First it was converted in by reduction of *para* nitro-group but after 10 minutes the regioselectivity rapidly changed to reducing the *ortho* nitro-group, and thereafter DAAN was gradually formed in the time-scale of a few days. On the other hand the conversion of NTO to ATO was almost complete converted in 10 minutes, indicating an extraordinary reactivity of green rust with NTO. The findings provide important clues on the fate and reactivity IMCs on green rust mineral surfaces highlighting the importance for the geochemical transformation of these compounds in soil. This study also adds insight into the mechanism of contaminant transformation by reaction with zero valent iron (ZVI) since green rust is a major intermediate during ZVI corrosion. The results taken as a whole indicate that green rust, either directly or indirectly as a product of ZVI, could be a useful approach for abiotic transformation of munitions compounds.

5.2. Bioconversion DNAN

5.2.1. DNAN transformation in anaerobic sludge

DNAN was reduced by sludge to two MENA and DAAN as the main metabolites, under all of the different conditions tested. The highest DNAN biotransformation rate was observed in anaerobic conditions enhanced by the addition of H₂, as an electron-donating cosubstrate. The nitro group in the *ortho* position was first reduced to an amine to yield MENA, then the *para* nitro group was reduced to an amine to produce DAAN. During the reductive biotransformation, covalent coupling of DNAN intermediates occurred, yielding azo-linked dimers. These products were further reduced to hydrazine dimers. In addition, a diversity of products was created by parallel pathways of N-methylation, and N-acetylation of primary amines, as well as O-demethylation and

subsequent dehydroxylation of methoxy groups. The results provide insights on the fate and biotransformation of DNAN which will help in understanding environmental health risks from DNAN and provide clues for the bioremediation of DNAN contamination.

5.2.2. DNAN transformation in soil

DNAN underwent (bio)transformation in soils, particularly in anaerobic conditions. The reactions were catalyzed by both biotic and abiotic processes. The major reaction pathway involved nitro-group reduction to MENA, and to a lesser extent, DAAN. The rate of DNAN biotransformation was highly correlated with soil organic carbon content up to 2% OC. Products from DNAN reduction coupled to form azo dimers that continued to be (bio)transformed with O-demethylation and N-substitution reactions. Aromatic amines such as DAAN also reacted and became incorporated into soil organic matter. Taken together, our results indicate that DNAN is readily reductively (bio)transformed in natural soils, and a full suite of transformation products such as aromatic amines and azo dimers that are further subjected to secondary metabolism which collectively impact the fate of DNAN in the environment.

5.2.3. ^{14}C -DNAN study

During incubations of ring labeled ^{14}C -DNAN, a large fraction of water soluble radiolabel becomes incorporated into a non-extractable fraction of the soil and assumed to be part of the insoluble soil humus fraction known as humin. Only negligible to small recoveries of ^{14}C label are found in the volatiles, organic extractable fractions; and only a modest recovery of label is found in the NaOH extractable fraction (considered to be humic acid). The most important conclusion of the study is that OC quantity as a ratio of the initial DNAN quantity is an important factor dictating what fraction of the ^{14}C -DNAN becomes incorporated into the insoluble humin fraction. The mg:mg ratio of OC: DNAN_{initial} provides a very strong prediction of the ultimate incorporation of DNAN product molecules into humin. This correlation is strong regardless of the source of the OC (either from one of two soil types or added purified humin). The correlation is valid up to a ratio of 0.8 mg OC mg⁻¹ DNAN_{initial}, which coincides with the two N groups in of fully reduced DNAN products being substituted into quinone moieties of humus. Beyond 0.8 mg OC mg⁻¹ DNAN_{initial} the reactive amine groups are saturated and there is no longer any increased incorporation of ^{14}C into the humin fraction. The effect of different treatments on the incorporation of ^{14}C -DNAN into humin were evaluated. Globally, speaking the treatment effects were relatively small compared to the impact of the OC:DNAN mass ratio. Nonetheless, the more anaerobic the conditions, a greater rate and extent of ^{14}C incorporation was observed compared to aerobic conditions. The findings are in stark contrast with the established paradigm. The paradigm considers anaerobic conditions are solely involved in the formation of aromatic amines; whereas aerobic conditions are required to (co)polymerize and covalently link the aromatic amines into humus. The reason this paradigm can now be rejected is the compilation of evidence to the contrary, showing that significant strong sorption and covalent incorporation of reduced TNT intermediates into humin occurs under anaerobic conditions. The results of the current study demonstrate that the same is also true for reduced DNAN intermediates.

5.3. Bioconversion NTO

5.3.1. Biotransformation of NTO in soil

Reductive biotransformation of NTO can be stimulated by promoting an initial anaerobic phase by supplying electron donating substrates to form ATO. In aerobic conditions, our research suggests that NTO will persist in soils. In anaerobic environments, NTO was readily converted to ATO. However ATO was found to persist in anaerobic conditions. In aerobic conditions, ATO was susceptible to mineralization depending on the soil microbial community and pH conditions. The addition of cosubstrates (e.g. glucose) was not observed to enhance aerobic ATO degradation.

5.3.2. Sequential anaerobic-aerobic biodegradation of NTO

The sequencing of anaerobic-aerobic condition promotes the full biodegradation NTO. NTO reduction to ATO occurs under reducing conditions. ATO in turn is removed when conditions are switched to aerobic conditions. There is no biotransformation of NTO under aerobic conditions; likewise only the conversion of NTO to ATO without any removal of ATO occurs when conditions are only anaerobic. ATO and NTO degradation were observed in a continuously fed aerobic biotrickle reactor. The reduction of NTO in an aerobic bulk environment of the reactor was plausible due to the presence of hypothesized anaerobic micro-zones in biofilms, which were formed by addition of cosubstrate (pyruvate). The lack of NTO transformation in a sterilized control indicates that the process is driven mainly by biological reactions. The presence of inorganic N ions in the reactor effluent suggested that at least partial mineralization NTO was occurring.

5.3.3. ATO-degrading enrichment culture

ATO can be degraded as the sole C and N source by a sustainable enrichment culture (EC). The C in ATO is highly mineralized to CO₂ and the N in ATO is mineralized for approximately 50% to NH₃ and 50% to N₂. The EC requires O₂, indicating at least one O₂- dependent step in the biodegradation pathway. Low amounts of yeast extract (YE) (1 mg L⁻¹) were found not to be essential for the EC, thus the culture has the capacity to produce all the essential vitamins and cofactors from the basal inorganic nutrients in the medium. Two approaches to were used to obtain a clone library, one was a conventional approach, the other utilized MR DNA (based on ion torrent sequencing technology). These two approaches indicated that several members of the clone library may be playing a role in the ATO biodegradation. These include clones from the genus *Hydrogenophaga* previously implicated in oxidative 4-aminobenzenesulfonate degradation. Clones from the genus *Hyphomicrobium* indicate a role of C1 metabolism in ATO biodegradation possibly including the metabolism of methylamines. The importance of C1 metabolism was also strengthened by the presence of clones from *Alkalilimnicola* known for CO metabolism. The presence of *Sphingopyxis* and *Mezorhizobium* indicated other potential biodegradative mechanisms related to glycol metabolism and degradation of N-methyl-2-pyrrolidone, respectively. In conclusion, ATO the major reductive biotransformation product of NTO was shown to be highly reliably mineralized to CO₂, NH₃ and N₂ by a highly enriched culture developed from soil. The EC can potentially be utilize to bioaugment NTO contaminated soil lacking ATO-degrading capacity to accelerate complete bioremediation of reductively biotransformed NTO

5.4. Toxicity

5.4.1. Microbial toxicity of DNAN

Taken as a whole microbial toxicity results indicate that DNAN causes strong acute cytotoxicity to methanogenic and nitrifying microbial populations as well as the marine bioluminescent bacterium, *Aliivibrio fischeri*, used in the Microtox test. The 50% inhibitory concentration for these impacted microorganisms ranges from 41 to 57 μM . Preliminary results suggest that microbial reductive transformation of DNAN to aromatic amines may reduce the inhibitory impact of DNAN to these microbial groups. Aerobic heterotroph bacterial activity was not impacted by the presence of DNAN. Additional toxicity studies with secondary dimeric metabolites of DNAN and their soil con

5.4.2. Microbial Toxicity of DNAN (bio)transformation products and product mixtures

The goal of this work was to assess microbial toxicity of individual transformation products and/or best available surrogate compounds to acetoclastic methanogens and the marine bacterium *Allivibrio fischeri*; while in parallel determine biotransformation product profiles for DNAN incubated anaerobically in soils and anaerobic sludge and link the profile mixture composition to toxicity changes during transformation as measured by UHPLC-QToF-MS. The latter was performed with a staggered toxicity test in which toxicity of a given initial concentration of DNAN was evaluated as a function of biotransformation time in soil or sludge. The staggered toxicity test demonstrated two key events during (bio)transformation as potential toxicity drivers. The inhibition of methanogens increased during nitro reduction of DNAN and this behavior was attributed to reactive hydroxylamino and nitroso intermediates. As soon as nitro-reduction ceased, the inhibition decreased again. In contrast, the inhibition to *A. fischeri* steadily increased as azo-dimers rich mixtures were progressively being formed. In the experiments with individual compounds, The heightened toxicity of azo dimers was also confirmed in inhibition tests with azo-dimer and trimer surrogates. Additionally, an N-acetylated metabolite of DAAN was shown to have greatly reduced toxicity compared to DNAN and its primary daughter products. This indicates that N-acetylation reactions could be exploited in bioremediation efforts to yield non-toxicant products in systems polluted with DNAN and prevent dimerization.

5.4.3. Zebrafish Embryo Toxicity of Anaerobic DNAN Biotransformation Products

The goal of zebrafish (*Danio rerio*) embryo study was to evaluate developmental effects of DNAN (bio)transformation products. Individual biotransformation products/surrogates or mixtures of the products formed at different stages of DNAN (bio)transformation in soil the starting point the primary DNAN transformation product, MENA. The toxicological testing was supported by detailed mass spectrometry studies (UHPLC QToF-MS) to characterize transformation product mixture profiles. The results of the study demonstrated that intermediates of DNAN biotransformation can cause detectable developmental and behavioral toxicity endpoints in zebrafish embryos. Most concerning was the high level of developmental toxicity caused by a surrogate azo-dimer intermediate (dimer L) and 4-methoxy-5nitroaniline (iMENA) (both at 6.4 μM) as well as evidence of locomotor toxicity caused by DAAN at higher concentrations. The linking of biotransformation product identification with toxicological testing indicated the there was a significant increase in acute cytotoxicity to zebrafish embryo during the stage of biotransformation when azo-dimers start to form. The study demonstrates a methodology to study the ecotoxicity of organic pollutants as they undergo transformation in natural systems. These

findings will help to advance understanding of the potential adverse impacts of DNAN biotransformation products in natural systems to aquatic species and vertebrates in general.

5.5. Overview and Benefits.

The most important benefit of the project is the recognition that IMCs can be converted by a sequence of reduction and oxidation (or substitution) reactions to environmentally safe end points. DNAN and NTO have shared and divergent pathways as shown in Figure 5.5-1.

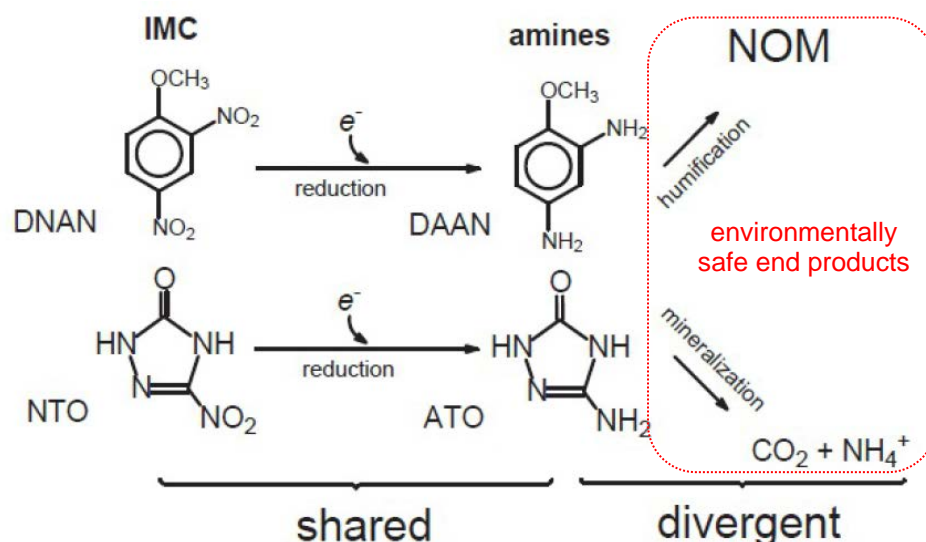


Figure 5.5-1. Shared and divergent pathways of IMC biotransformation to environmentally safe end products (NOM refers to natural organic matter or humus).

The nitro-groups of DNAN and NTO are readily reduced to yield amine intermediates. However the pathways diverge afterwards. The aromatic amines daughter products of DNAN become irreversibly covalently incorporated into the insoluble fraction of humus, known as humin. The proposed pathway involves either a nucleophilic substitution reaction in which aromatic amines react with quinone moieties of humus or an oxidation reaction of the aromatic amines by MnO_2 or iron oxides to produce cation amine radicals that couple covalently with humus. The heterocyclic amine, ATO, which is the reduced product of NTO, is oxidatively mineralized by aerobic soil bacteria or extensively oxidized by reaction with MnO_2 producing benign end-products: CO_2 , NH_3 , N_2 and/or urea. The complete sequence of events is required since our study shows that primary daughter products are still quite toxic. The implication is that just removing IMCs by primary transformation does not necessarily remove toxicity. The sequence is also required because the reductive step converts IMC molecules to amines that are significantly more prone to oxidation or substitution reactions. The latter reactions are necessary to achieve environmentally safe end

points. The project demonstrates the importance of both soil minerals and microbial activity in the transformation of IMCs.

Other benefits of this project include the discovery that iron oxides in soil can significantly adsorb NTO dispelling a popular belief there is no sorption of NTO by soils. Adsorption of DNAN in clay soils can be significantly increased by an order of magnitude with the addition K^+ to soil. This project has identified a parameter that can predict the extent of this incorporation based on the mass ratio of OC to DNAN. The addition of humic materials was shown to greatly enhance the irreversible covalent incorporation of DNAN metabolites into humus and such additions could potentially enhance the remediation of DNAN. And lastly, an enrichment culture was developed that reliably mineralizes ATO as sole C and N-source to simple non-toxic products: CO_2 , NH_3 and N_2 . Several species identified in the clone libraries provided clues on possible degradation mechanisms and how to monitor for responsible bacteria. The enrichment culture could potentially be utilized through a bioaugmentation strategy to enhance the complete biodegradation of NTO in soils or subsurface sites lacking a natural population of ATO-degraders,

6. LITERATURE CITED

- 1 Krzmarzick, M. J. *et al.* Biotransformation and degradation of the insensitive munitions compound, 3-nitro-1,2,4-triazol-5-one, by soil bacterial communities. *Environ. Sci. Technol.* **49**, 5681-5688 (2015).
- 2 Davies, P. J. & Provatas, A. Characterisation of 2,4-dinitroanisole an ingredient for use in low sensitivity melt cast formulations. Weapons Systems Division, Defence Science and Technology Organisation (DSTO), Edinburgh, South Australia. . (2006).
- 3 Spear, R. J. & Davis, L. M. An Australian Insensitive Munitions Policy: A working paper prepared for the Australian Ordnance Council. (General Document MRL-GD-0020) Materials Research Laboratory, Defence Science and Technology Organisation (DTSO), Department of Defence, Melbourne, Victoria (1989).
- 4 Zeman, S. & Jungová, M. Sensitivity and Performance of Energetic Materials. *Propellants, Explosives, Pyrotechnics* **41**, 426-451, doi:10.1002/prop.201500351 (2016).
- 5 Powell, I. J. Insensitive Munitions - Design Principles and Technology Developments. *Propellants Explosives Pyrotechnics* **41**, 409-413, doi:10.1002/prop.201500341 (2016).
- 6 Pagoria, P. A Comparison of the Structure, Synthesis, and Properties of Insensitive Energetic Compounds. *Propellants, Explosives, Pyrotechnics* **41**, 452-469, doi:10.1002/prop.201600032 (2016).
- 7 Smith, M. W. & Cliff, M. D. NTO-based explosive formulations: A technology review (DSTO-TR-0796). Weapons Systems Division, Aeronautical and Maritime Research Laboratory. Defence Science and Technology, Australian Department of Defence, Salisbury, South Australia., (1999).
- 8 Boddu, V. M., Abburi, K., Maloney, S. W. & Damavarapu, R. Thermophysical Properties of an Insensitive Munitions Compound, 2,4-Dinitroanisole. *Journal of Chemical & Engineering Data* **53**, 1120-1125, doi:10.1021/je7006764 (2008).
- 9 Lee, K.-Y., Chapman, L. B. & Cobura, M. D. 3-Nitro-1,2,4-triazol-5-one, a less sensitive explosive. *Journal of Energetic Materials* **5**, 27-33, doi:10.1080/07370658708012347 (1987).
- 10 Bhatnagar, N., Kamath, G. & Potoff, J. J. Prediction of 1-octanol-water and air-water partition coefficients for nitro-aromatic compounds from molecular dynamics simulations. *Physical Chemistry Chemical Physics* **15**, 6467-6474, doi:10.1039/c3cp44284e (2013).
- 11 Brannon, J. M. & Pennington, J. C. Environmental Fate and Transport Process Descriptors for Explosives (ERDC/EL TR-02-10). US Army Corps of Engineers, Engineer research and Development Center. Environmental laboratory. Vicksburg, MS. (2002).
- 12 Liang, Y. Z., Kuo, D. T. F., Allen, H. E. & Di Toro, D. M. Experimental determination of solvent-water partition coefficients and Abraham parameters for munition constituents. *Chemosphere* **161**, 429-437, doi:10.1016/j.chemosphere.2016.07.028 (2016).
- 13 Boddu, V. M., Abburi, K., Maloney, S. W. & Damavarapu, R. Thermophysical properties of an insensitive munitions compound, 2,4-dinitroanisole. *J Chem Eng Data* **53**, 1120-1125, doi:Doi 10.1021/Je7006764 (2008).
- 14 Smith, M. & Cliff, M. NTO-based explosives: A technology review Report No. Report nr AR-010-873, (Melbourne: DTSO Aeronautical Maritime Research Laboratory 1999).

- 15 Olivares, C., Liang, J. D., Abrell, L., Sierra-Alvarez, R. & Field, J. A. Pathways of reductive 2,4-dinitroanisole (DNAN) biotransformation in sludge. *Biotechnol Bioeng* **110**, 1595-1604, doi:Doi 10.1002/Bit.24820 (2013).
- 16 Le Campion, L., Vandais, A. & Ouazzani, J. Microbial remediation of NTO in aqueous industrial wastes. *Fems Microbiology Letters* **176**, 197-203, doi:10.1111/j.1574-6968.1999.tb13662.x (1999).
- 17 Boyd, S. A., Sheng, G. Y., Teppen, B. J. & Johnston, C. J. Mechanisms for the adsorption of substituted nitrobenzenes by smectite clays. *Environ Sci Technol* **35**, 4227-4234, doi:Doi 10.1021/Es010663w (2001).
- 18 Haderlein, S. B., Weissmahr, K. W. & Schwarzenbach, R. P. Specific adsorption of nitroaromatic: Explosives and pesticides to clay minerals. *Environ Sci Technol* **30**, 612-622, doi:Doi 10.1021/Es9503701 (1996).
- 19 Johnston, C. T., Khan, B., Barth, E. F., Chattopadhyay, S. & Boyd, S. A. Nature of the Interlayer Environment in an Organoclay Optimized for the Sequestration of Dibenzo-p-dioxin. *Environ Sci Technol* **46**, 9584-9591, doi:Doi 10.1021/Es300699y (2012).
- 20 Weissmahr, K. W., Haderlein, S. B., Schwarzenbach, R. P., Hany, R. & Nuesch, R. In situ spectroscopic investigations of adsorption mechanisms of nitroaromatic compounds at clay minerals. *Environ Sci Technol* **31**, 240-247, doi:Doi 10.1021/Es960381+ (1997).
- 21 Chattopadhyay, S. & Traina, S. J. Spectroscopic study of sorption of nitrogen heterocyclic compounds on phyllosilicates. *Langmuir* **15**, 1634-1639, doi:Doi 10.1021/La980607h (1999).
- 22 Chorover, J., Amistadi, M. K., Burgos, W. D. & Hatcher, P. G. Quinoline sorption on kaolinite-humic acid complexes. *Soil Sci Soc Am J* **63**, 850-857 (1999).
- 23 Hanna, K. Sorption of two aromatic acids onto iron oxides: Experimental study and modeling. *J Colloid Interf Sci* **309**, 419-428, doi:DOI 10.1016/j.jcis.2007.01.004 (2007).
- 24 Nilsson, N., Persson, P., Lovgren, L. & Sjoberg, S. Competitive surface complexation of o-phthalate and phosphate on goethite (alpha-FeOOH) particles. *Geochim Cosmochim Acta* **60**, 4385-4395, doi:Doi 10.1016/S0016-7037(96)00258-X (1996).
- 25 Laha, S. & Luthy, R. G. Oxidation of aniline and other primary aromatic-amines by manganese-dioxide. *Environmental Science & Technology* **24**, 363-373, doi:10.1021/es00073a012 (1990).
- 26 Li, H., Lee, L. S., Schulze, D. G. & Guest, C. A. Role of soil manganese in the oxidation of aromatic amines. *Environmental Science & Technology* **37**, 2686-2693, doi:10.1021/es0209518 (2003).
- 27 Majcher, E. H., Chorover, J., Bollag, J. M. & Huang, P. M. Evolution of CO₂ during birnessite-induced oxidation of C-14-labeled catechol. *Soil Sci Soc Am J* **64**, 157-163 (2000).
- 28 Sposito, G. *The Surface Chemistry of Natural Particles*. (Oxford University Press, 2004).
- 29 Lenke, H., Achtnich, C. & Knackmuss, H.-J. in *Biodegradation of nitroaromatic compounds and explosives* (eds J. C. Spain, J. B. Hughes, & H.-J. Knackmuss) 91-126 (Lewis Publishers, 2000).
- 30 Knackmuss, H.-J. Basic knowledge and perspectives of bioelimination of xenobiotic compounds. *Journal of Biotechnology* **51**, 287-295, doi:[http://dx.doi.org/10.1016/S0168-1656\(96\)01608-2](http://dx.doi.org/10.1016/S0168-1656(96)01608-2) (1996).

- 31 Amaral, H. I. F., Fernandes, J., Berg, M., Schwarzenbach, R. P. & Kipfer, R. Assessing TNT and DNT groundwater contamination by compound-specific isotope analysis and H-3-He-3 groundwater dating: A case study in Portugal. *Chemosphere* **77**, 805-812, doi:10.1016/j.chemosphere.2009.08.011 (2009).
- 32 Bradley, P. M., Chapelle, F. H., Landmeyer, J. E. & Schumacher, J. G. Microbial transformation of nitroaromatics in surface soils and aquifer materials. *Applied and Environmental Microbiology* **60**, 2170-2175 (1994).
- 33 Ju, K.-S. & Parales, R. E. Nitroaromatic compounds, from synthesis to biodegradation. *Microbiol Mol Biol Rev* **74**, 250-272, doi:10.1128/mmbr.00006-10 (2010).
- 34 Ahmad, F. & Hughes, J. B. in *Biodegradation of nitroaromatic compounds and explosives* (eds J. C. Spain, J. B. Hughes, & H-J. Knackmuss) 185-212 (Lewis Publishers, 2000).
- 35 Roldan, M., Perez-Reinado, E., Castillo, F. & Moreno-Vivian, C. Reduction of polynitroaromatic compounds: the bacterial nitroreductases. *Fems Microbiology Reviews* **32**, 474-500, doi:10.1111/j.1574-6976.2008.00107.x (2008).
- 36 Elsner, M., Schwarzenbach, R. P. & Haderlein, S. B. Reactivity of Fe(II)-bearing minerals toward reductive transformation of organic contaminants. *Environmental Science & Technology* **38**, 799-807, doi:10.1021/es0345569 (2004).
- 37 Hofstetter, T. B., Heijman, C. G., Haderlein, S. B., Holliger, C. & Schwarzenbach, R. P. Complete reduction of TNT and other (poly)nitroaromatic compounds under iron reducing subsurface conditions. *Environmental Science & Technology* **33**, 1479-1487, doi:10.1021/es9809760 (1999).
- 38 Wang, S. & Arnold, W. A. Abiotic reduction of dinitroaniline herbicides. *Water Research* **37**, 4191-4201, doi:[http://dx.doi.org/10.1016/S0043-1354\(03\)00340-3](http://dx.doi.org/10.1016/S0043-1354(03)00340-3) (2003).
- 39 Borch, T., Inskeep, W. P., Harwood, J. A. & Gerlach, R. Impact of ferrihydrite and anthraquinone-2,6-disulfonate on the reductive transformation of 2,4,6-trinitrotoluene by a gram-positive fermenting bacterium. *Environmental Science & Technology* **39**, 7126-7133, doi:10.1021/es0504441 (2005).
- 40 Schwarzenbach, R. P., Stierli, R., Lanz, K. & Zeyer, J. Quinone and iron porphyrin mediated reduction of nitroaromatic compounds in homogeneous aqueous-solution. *Environmental Science & Technology* **24**, 1566-1574, doi:10.1021/es00080a017 (1990).
- 41 Bae, S., Lee, Y., Kwon, M. J. & Lee, W. Riboflavin-mediated RDX transformation in the presence of *Shewanella putrefaciens* CN32 and lepidocrocite. *Journal of Hazardous Materials* **274**, 24-31, doi:10.1016/j.jhazmat.2014.04.002 (2014).
- 42 Boopathy, R., Kulpa, C. F. & Manning, J. Anaerobic biodegradation of explosives and related compounds by sulfate-reducing and methanogenic bacteria: A review. *Bioresource Technology* **63**, 81-89, doi:10.1016/s0960-8524(97)00083-7 (1998).
- 43 Gorontzy, T., Kuver, J. & Blotvogel, K. H. Microbial transformation of nitroaromatic compounds under anaerobic conditions. *Journal of General Microbiology* **139**, 1331-1336 (1993).
- 44 Rafii, F., Franklin, W., Heflich, R. H. & Cerniglia, C. E. Reduction of nitroaromatic compounds by anaerobic-bacteria isolated from the human gastrointestinal-tract. *Applied and Environmental Microbiology* **57**, 962-968 (1991).
- 45 Watrous, M. M. *et al.* 2,4,6-trinitrotoluene reduction by an Fe-only hydrogenase in *Clostridium acetobutylicum*. *Applied and Environmental Microbiology* **69**, 1542-1547, doi:10.1128/aem.69.3.1542-1547.2003 (2003).

- 46 Platten, W. E., Bailey, D., Suidan, M. T. & Maloney, S. W. Treatment of Energetic Wastewater Containing 2,4-Dinitroanisole and N-Methyl Paranitro Aniline. *Journal of Environmental Engineering-Asce* **139**, 104-109, doi:10.1061/(asce)ee.1943-7870.0000592 (2013).
- 47 Hawari, J. *et al.* Environmental fate of 2,4-dinitroanisole (DNAN) and its reduced products. *Chemosphere* **119**, 16-23 (2015).
- 48 Perreault, N. N. *et al.* Aerobic biotransformation of 2,4-dinitroanisole in soil and soil *Bacillus* sp. *Biodegradation* **23**, 287-295, doi:10.1007/s10532-011-9508-7 (2012).
- 49 Karthikeyan, S. & Spain, J. C. Biodegradation of 2,4-dinitroanisole (DNAN) by *Nocardioide* sp JS1661 in water, soil and bioreactors. *Journal of Hazardous Materials* **312**, 37-44, doi:10.1016/j.jhazmat.2016.03.029 (2016).
- 50 Fida, T. T., Palamuru, S., Pandey, G. & Spain, J. C. Aerobic Biodegradation of 2,4-Dinitroanisole by *Nocardioide* sp Strain JS1661. *Applied and Environmental Microbiology* **80**, 7725-7731, doi:10.1128/aem.02752-14 (2014).
- 51 Le Campion, L., Delaforge, M., Noel, J. P. & Ouazzani, J. Metabolism of C-14-labelled 5-nitro-1,2,4-triazol-3-one by rat liver microsomes - Evidence for the participation of cytochrome P-450. *European Journal of Biochemistry* **248**, 401-406 (1997).
- 52 Mark, N., Arthur, J., Dontsova, K., Brusseau, M. & Taylor, S. Adsorption and attenuation behavior of 3-nitro-1,2,4-triazol-5-one (NTO) in eleven soils. *Chemosphere* **144**, 1249-1255, doi:10.1016/j.chemosphere.2015.09.101 (2016).
- 53 Richard, T. & Weidhaas, J. Biodegradation of IMX-101 explosive formulation constituents: 2,4-Dinitroanisole (DNAN), 3-nitro-1,2,4-triazol-5-one (NTO), and nitroguanidine. *Journal of Hazardous Materials* **280**, 372-379, doi:10.1016/j.jhazmat.2014.08.019 (2014).
- 54 Bruns-Nagel, D. *et al.* Characterization of (15)N-TNT residues after an anaerobic/aerobic treatment of soil/molasses mixtures by solid state (15)N NMR spectroscopy. 2. Systematic investigation of whole soil and different humic fractions. *Environmental Science & Technology* **34**, 1549-1556, doi:10.1021/es990757u (2000).
- 55 Drzyzga, O. *et al.* Incorporation of (14)C-labeled 2,4,6-trinitrotoluene metabolites into different soil fractions after anaerobic and anaerobic-aerobic treatment of soil/molasses mixtures. *Environmental Science & Technology* **32**, 3529-3535, doi:10.1021/es980090w (1998).
- 56 Pennington, J. C. *et al.* Fate of 2,4,6-trinitrotoluene in a simulated compost system. *Chemosphere* **30**, 429-438, doi:10.1016/0045-6535(94)00422-q (1995).
- 57 Knicker, H., Achtnich, C. & Lenke, H. Solid-state nitrogen-15 nuclear magnetic resonance analysis of biologically reduced 2,4,6-trinitrotoluene in a soil slurry remediation. *Journal of Environmental Quality* **30**, 403-410 (2001).
- 58 Lenke, H. *et al.* Biological treatment of TNT contaminated soil. 2. Biologically induced immobilization of the contaminants and full-scale application. *Environmental Science & Technology* **32**, 1964-1971, doi:10.1021/es970950t (1998).
- 59 Bruns-Nagel, D., Steinbach, K., Gemsa, D. & von Low, E. in *Biodegradation of Nitroarmatic Compounds and Explosives* (eds J. C. Spain, J. B. Hughes, & H-J. Knackmuss) Ch. 13, 357-394 (Lewis Publishers, 2000).
- 60 Elovitz, M. S. & Weber, E. J. Sediment mediated reduction of 2,4,6-trinitrotoluene and fate of the resulting aromatic (poly)amines. *Environmental Science & Technology* **33**, 2617-2625, doi:10.1021/es980980b (1999).

- 61 Thorn, K. A., Pettigrew, P. J. & Goldenberg, W. S. Covalent binding of aniline to humic substances .2. N-15 NMR studies of nucleophilic addition reactions. *Environmental Science & Technology* **30**, 2764-2775, doi:10.1021/es9509339 (1996).
- 62 Gulkowska, A., Sander, M., Hollender, J. & Krauss, M. Covalent Binding of Sulfamethazine to Natural and Synthetic Humic Acids: Assessing Laccase Catalysis and Covalent Bond Stability. *Environmental Science & Technology* **47**, 6916-6924, doi:10.1021/es3044592 (2013).
- 63 Gulkowska, A., Thalmann, B., Hollender, J. & Krauss, M. Nonextractable residue formation of sulfonamide antimicrobials: New insights from soil incubation experiments. *Chemosphere* **107**, 366-372, doi:10.1016/j.chemosphere.2013.12.093 (2014).
- 64 Dawel, G. *et al.* Structure of a laccase-mediated product of coupling of 2,4-diamino-6-nitrotoluene to guaiacol, a model for coupling of 2,4,6-trinitrotoluene metabolites to a humic organic soil matrix. *Applied and Environmental Microbiology* **63**, 2560-2565 (1997).
- 65 Ichinohe, D., Muranaka, T., Sasaki, T., Kobayashi, M. & Kise, H. Oxidative polymerization of phenylenediamines catalyzed by horseradish peroxidase. *Journal of Polymer Science Part a-Polymer Chemistry* **36**, 2593-2600, doi:10.1002/(sici)1099-0518(199810)36:14<2593::aid-pola19>3.0.co;2-d (1998).
- 66 Karamyshev, A. V., Shleev, S. V., Koroleva, O. V., Yaropolov, A. I. & Sakharov, I. Y. Laccase-catalyzed synthesis of conducting polyaniline. *Enzyme and Microbial Technology* **33**, 556-564, doi:10.1016/s0141-0229(03)00163-7 (2003).
- 67 Kim, S.-C. *et al.* Synthesis of polyaniline derivatives via biocatalysis. *Green Chemistry* **9**, 44-48, doi:10.1039/b606839a (2007).
- 68 Klausen, J., Haderlein, S. B. & Schwarzenbach, R. P. Oxidation of substituted anilines by aqueous MnO₂: Effect of co-solutes on initial and quasi-steady-state kinetics. *Environmental Science & Technology* **31**, 2642-2649, doi:10.1021/es970053p (1997).
- 69 Dodard, S. G. *et al.* Ecotoxicological assessment of a high energetic and insensitive munitions compound: 2,4-dinitroanisole (DNAN). *J. Hazard. Mater.* **262**, 143-150 (2013).
- 70 Kennedy, A. J. *et al.* Inter- and intraspecies chemical sensitivity: A case study using 2,4-dinitroanisole. *Environ. Toxicol. Chem.* **34**, 402-411 (2015).
- 71 Prasath, A., Panneerselvan, L., Provatas, A., Naidu, R. & Megharaj, M. Genotoxicity assessment of acute exposure of 2, 4-dinitroanisole, its metabolites and 2, 4, 6-trinitrotoluene to *Daphnia carinata*. *Ecotoxicology (London, England)*, doi:10.1007/s10646-016-1709-8 (2016).
- 72 Stanley, J. K., Lotufo, G. R., Biedenbach, J. M., Chappell, P. & Gust, K. A. Toxicity of the conventional energetics TNT and RDX relative to new insensitive munitions constituents DNAN and NTO in *Rana pipiens* tadpoles. *Environ. Toxicol. Chem.* **34**, 873-879, doi:10.1002/etc.2890 (2015).
- 73 Ou, C. *et al.* Removal of multi-substituted nitroaromatic pollutants by zero valent iron: a comparison of performance, kinetics, toxicity and mechanisms. *Phys. Chem.* **17**, 22072-22078, doi:10.1039/c5cp02518d (2015).
- 74 Kennedy, A. J., Poda, A. R., Melby, N. & Gust, K. A. in *SETAC North America 36th Annual Meeting. Platform 383* (Salt Lake City, UT, 2015).

- 75 Tan, E. L., Ho, C. H., Griest, W. H. & Tyndall, R. L. Mutagenicity of trinitrotoluene and its metabolites formed during composting. *J. Toxicol. Environ. Health* **36**, 165-175 (1992).
- 76 Padda, R. S., Wang, C., Hughes, J. B., Kutty, R. & Bennett, G. N. Mutagenicity of nitroaromatic degradation compounds. *Environ. Toxicol. Chem.* **22**, 2293-2297 (2003).
- 77 Purohit, V. & Basu, A. K. Mutagenicity of nitroaromatic compounds. *Chem. Res. Toxicol.* **13**, 673-692 (2000).
- 78 Pearson, J. G., Glennon, J. P., Barkley, J. J. & Highfill, J. W. in *Aquat. Toxicol. ASTM STP 667*. 284 (ASTM International).
- 79 Taylor, S., Dontsova, K., Walsh, M. E. & Walsh, M. R. Outdoor dissolution of detonation residues of three insensitive munitions (IM) formulations. *Chemosphere* **134**, 250-256 (2015).
- 80 Haley, M. V., Kuperman, R. G. & Checkai, R. T. Aquatic Toxicity of 3-Nitro-1,2,4-Triazol-5-One. (Edgewood Chemical Biological Center, U.S. Army Research, Development and Engineering Command, Aberdeen Proving Ground, Ft. Belvoir, 2009).
- 81 Reddy, G. *et al.* Genotoxicity assessment of an energetic propellant compound, 3-nitro-1,2,4-triazol-5-one (NTO). *Mutat. Res.* **719**, 35-40 (2011).
- 82 Krzmarzick, M. J. *et al.* Biotransformation and degradation of the insensitive munitions compound, 3-nitro-1,2,4-triazol-5-one, by soil bacterial communities. *Environmental Science & Technology* **49**, 5681-5688, doi:10.1021/acs.est.5b00511 (2015).
- 83 Linker, B. R. *et al.* Adsorption of novel insensitive munitions compounds at clay mineral and metal oxide surfaces. *Environmental Chemistry* **12**, 74-84, doi:<http://dx.doi.org/10.1071/EN14065> (2015).
- 84 Le Campion, L. & Ouazzani, J. Synthesis of 5-amino-1,2,4-triazole-3-one through the nitroreduction of 5-nitro-1,2,4-triazole-3-one. Comparison between chemical and microbiological catalysis. *Biocatal. Biotransfor.* **17**, 37-44 (1999).
- 85 Olivares, C., Liang, J., Abrell, L., Sierra-Alvarez, R. & Field, J. A. Pathways of reductive 2,4-dinitroanisole (DNAN) biotransformation in sludge. *Biotechnol. Bioeng.* **110**, 1595–1604 (2013).
- 86 Liang, J., Olivares, C., Field, J. A. & Sierra-Alvarez, R. Microbial toxicity of the insensitive munitions compound, 2,4-dinitroanisole (DNAN), and its aromatic amine metabolites. *Journal of Hazardous Materials* **262**, 281-287, doi:<http://dx.doi.org/10.1016/j.jhazmat.2013.08.046> (2013).
- 87 Olivares, C. I. *et al.* Microbial toxicity and characterization of DNAN (bio)transformation product mixtures. *Chemosphere* **154**, 499-506, doi:<http://dx.doi.org/10.1016/j.chemosphere.2016.04.007> (2016).
- 88 Olivares, C. I. *et al.* Continuous treatment of the insensitive munitions compound N-methyl-p-nitro aniline (MNA) in an upflow anaerobic sludge blanket (UASB) bioreactor. *Chemosphere* **144**, 1116-1122, doi:<http://dx.doi.org/10.1016/j.chemosphere.2015.09.092> (2016).
- 89 Dontsova, K. M., Hayes, C., Pennington, J. C. & Porter, B. Sorption of high explosives to water-dispersible clay: influence of organic carbon, aluminosilicate clay, and extractable iron. *J. Environ. Qual.* **38**, 1458-1465 (2009).
- 90 Madeira, C. L. *et al.* Sequential anaerobic-aerobic biodegradation of emerging insensitive munitions compound 3-nitro-1,2,4-triazol-5-one (NTO). *Chemosphere* **167**, 478-484 (2017).

- 91 Chiou, C. T., Kile, D. E., Rutherford, D. W., Sheng, G. & Boyd, S. A. Sorption of selected organic compounds from water to a peat soil and its humic-acid and humin fractions: potential sources of the sorption nonlinearity. *Environ. Sci. Technol.* **34**, 1254-1258, doi:10.1021/es990261c (2000).
- 92 Le Campion, L., Adeline, M. T. & Ouazzani, J. Separation of NTO related 1,2,4-triazole-3-one derivatives by a high performance liquid chromatography and capillary electrophoresis. *Propell. Explos. Pyrot.* **22**, 233-237 (1997).
- 93 Ochoa-Herrera, V. *et al.* Toxicity of fluoride to microorganisms in biological wastewater treatment systems. *Water Research* **43**, 3177-3186, doi:<http://dx.doi.org/10.1016/j.watres.2009.04.032> (2009).
- 94 Olivares, C. I. *et al.* Zebrafish embryo toxicity of anaerobic biotransformation products from the insensitive munitions compound 2,4-dinitroanisole (DNAN). *Environ. Toxicol. Chem.*, doi:10.1002/etc.3446 (2016).
- 95 Koch, M., Yediler, A., Lienert, D., Insel, G. & Kettrup, A. Ozonation of hydrolyzed azo dye reactive yellow 84 (CI). *Chemosphere* **46**, 109-113, doi:10.1016/s0045-6535(01)00102-3 (2002).
- 96 Storer, D. A. A simple high sample volume ashing procedure for determination of soil organic matter. *Communications in Soil Science and Plant Analysis* **15**, 759-772, doi:10.1080/00103628409367515 (1984).
- 97 Perdrial, N., Rivera, N., Thompson, A., O'Day, P. A. & Chorover, J. Trace contaminant concentration affects mineral transformation and pollutant fate in hydroxide-weathered Hanford sediments. *Journal of Hazardous Materials* **197**, 119-127, doi:<http://dx.doi.org/10.1016/j.jhazmat.2011.09.063> (2011).
- 98 Drzyzga, O., Bruns-Nagel, D., Gorontzy, T., Blotvogel, K. H. & von Low, E. Anaerobic incorporation of the radiolabeled explosive TNT and metabolites into the organic soil matrix of contaminated soil after different treatment procedures. *Chemosphere* **38**, 2081-2095, doi:10.1016/s0045-6535(98)00426-3 (1999).
- 99 Pell, M., Stenström, J. & Granhall, U. in *Microbiological methods for assessing soil quality* (eds Jaap Bloem, David W Hopkins, & Anna Benedetti) 117-126 (CABI, 2005).
- 100 Krzmarzick, M. *et al.* Biotransformation and Degradation of the Insensitive Munitions Compound, 3-nitro-1,2,4-triazol-5-one (NTO), by Soil Bacterial Communities. *Environmental Science & Technology* **49**, 5681-5688 (2015).
- 101 Madeira, C. L. *et al.* Sequential anaerobic-aerobic biodegradation of emerging insensitive munitions compound 3-nitro-1,2,4-triazol-5-one (NTO). *Chemosphere (In press)* (2016).
- 102 Olivares, C. I. *et al.* (Bio)transformation of 2,4-dinitroanisole (DNAN) in soils. *J. Hazard. Mater.* **304**, 214-221, doi:<http://dx.doi.org/10.1016/j.jhazmat.2015.10.059> (2016).
- 103 Platten, W. E., Bailey, D., Suidan, M. T. & Maloney, S. W. Biological transformation pathways of 2,4-dinitroanisole and N-methylparanitroaniline in anaerobic fluidized-bed bioreactors. *Chemosphere* **81**, 1131-1136 (2010).
- 104 Bulich, A. A. & Isenberg, D. L. Use of the luminescent bacterial system for the rapid assessment of aquatic toxicity. *ISA T.* **20**, 29-33 (1981).
- 105 Truong, L. *et al.* Multidimensional in vivo hazard assessment using zebrafish. *Toxicol. Sci.* **137**, 212-233 (2014).
- 106 Truong, L., Saili, K. S., Miller, J. M., Hutchison, J. E. & Tanguay, R. L. Persistent adult zebrafish behavioral deficits results from acute embryonic exposure to gold

- nanoparticles. *Comp. Biochem. Phys. C* **155**, 269-274, doi:10.1016/j.cbpc.2011.09.006 (2012).
- 107 Atkinson, R. J., Posner, A. M. & Quirk, J. P. Adsorption of potential-determining ions at the ferric oxide-aqueous electrolyte interface. *The Journal of Physical Chemistry* **71**, 550-558, doi:10.1021/j100862a014 (1967).
- 108 McKenzie, R. M. The synthesis of birnessite, cryptomelane, and some other oxides and hydroxides of manganese. *Mineralogical Magazine* **38**, 493-502, doi:citeulike-article-id:9697695
doi: 10.1180/minmag.1971.038.296.12 (1971).
- 109 Chorover, J. & Amistadi, M. K. Reaction of forest floor organic matter at goethite, birnessite and smectite surfaces. *Geochimica et Cosmochimica Acta* **65**, 95-109, doi:[http://dx.doi.org/10.1016/S0016-7037\(00\)00511-1](http://dx.doi.org/10.1016/S0016-7037(00)00511-1) (2001).
- 110 Schwertmann, U. & Cornell, R. M. *Iron oxides in the laboratory preparation and characterization*. 143-145 (1991).
- 111 Caporaso, J. G. *et al.* Global patterns of 16S rRNA diversity at a depth of millions of sequences per sample. *Proceedings of the National Academy of Sciences of the United States of America* **108**, 4516-45122 (2011).
- 112 Giovannoni, S., p. . , . in *Nucleic Acid Techniques in Bacterial Systematics* (eds E. Stackebrandt & M. Goodfellow) 175-201 (John Wiley & Sons, 1991).
- 113 Tamura, K., Stecher, G., Peterson, D., Filipski, A. & Kumar, S. MEGA6: Molecular Evolutionary Genetics Analysis version 6.0. . *Molecular Biology and Evolution* **30** 2725-2729 (2013).
- 114 Area diffraction machine software (2007-2010).
- 115 Tournassat, C. & Appelo, C. A. J. Modelling approaches for anion-exclusion in compacted Na-bentonite. *Geochim Cosmochim Ac* **75**, 3698-3710 (2011).
- 116 Gimsing, A. L., Sorensen, J. C., Strobel, B. W. & Hansen, H. C. B. Adsorption of glucosinolates to metal oxides, clay minerals and humic acid. *Appl Clay Sci* **35**, 212-217 (2007).
- 117 Zhang, L. C., Luo, L. & Zhang, S. Z. Adsorption of phenanthrene and 1,3-dinitrobenzene on cation-modified clay minerals. *Colloid Surface A* **377**, 278-283, doi:DOI 10.1016/j.colsurfa.2011.01.017 (2011).
- 118 Polubesova, T. & Borisover, M. Two components of chloride anion exclusion volume in montmorillonitic soils. *Colloid Surface A* **347**, 175-179, doi:DOI 10.1016/j.colsurfa.2009.04.002 (2009).
- 119 Chorover, J. in *Encyclopedia of soils in the environment* (ed D. Hillel and D.L. Sparks) (Elsevier Ltd, 2005).
- 120 Chorover, J. & Brusseau, M. L. in *Kinetics of Water-Rock Interaction* (eds Susan L. Brantley, James D. Kubicki, & Art F. White) Ch. 4, 109-149 (Springer New York, 2008).
- 121 Tebo, B. M. *et al.* Biogenic manganese oxides: Properties and mechanisms of formation. *Annu Rev Earth Pl Sc* **32**, 287-328, doi:DOI 10.1146/annurev.earth.32.101802.120213 (2004).
- 122 He, Y. *et al.* Oxidative transformation of carbamazepine by manganese oxides. *Environ Sci Pollut R* **19**, 4206-4213, doi:DOI 10.1007/s11356-012-0949-2 (2012).
- 123 Cerrato, J. M., Hochella, M. F., Jr., Knocke, W. R., Dietrich, A. M. & Cromer, T. F. Use of XPS to identify the oxidation state of Mn in solid surfaces of filtration media oxide

- samples from drinking water treatment plants. *Environmental Science & Technology* **44**, 5881-5886, doi:10.1021/es100547q (2010).
- 124 Ju, K.-S. & Parales, R. E. Nitroaromatic compounds, from synthesis to biodegradation. *Microbiology and Molecular Biology Reviews* **74**, 250-+, doi:10.1128/mmbr.00006-10 (2010).
- 125 Niedzwiecka, J. B. & Finneran, K. T. Combined biological and abiotic reactions with iron and Fe(III)-reducing microorganisms for remediation of explosives and insensitive munitions (IM). *Environmental Science-Water Research & Technology* **1**, 34-39, doi:10.1039/c4ew00062e (2015).
- 126 Olivares, C. I. *et al.* (Bio)transformation of 2,4-dinitroanisole (DNAN) in soils. *Journal of Hazardous Materials* **304**, 214-221, doi:10.1016/j.jhazmat.2015.10.059 (2016).
- 127 Olivares, C., Liang, J., Abrell, L., Sierra-Alvarez, R. & Field, J. A. Pathways of reductive 2,4-dinitroanisole (DNAN) biotransformation in sludge. *Biotechnology and Bioengineering* **110**, 1595-1604, doi:10.1002/bit.24820 (2013).
- 128 Colon, D., Weber, E. J. & Baughman, G. L. Sediment-associated reactions of aromatic amines. 2. QSAR development. *Environmental Science & Technology* **36**, 2443-2450, doi:10.1021/es0113551 (2002).
- 129 Pizzigallo, M. D. R., Ruggiero, P., Crecchio, C. & Mascolo, G. Oxidation of chloroanilines at metal oxide surfaces. *Journal of Agricultural and Food Chemistry* **46**, 2049-2054, doi:10.1021/jf9707905 (1998).
- 130 Anschutz, A. J. & Penn, R. L. Reduction of crystalline iron(III) oxyhydroxides using hydroquinone: Influence of phase and particle size. *Geochemical Transactions* **6**, 60-66, doi:10.1063/1.2037887 (2005).
- 131 Essington, M. E. *Soil and water chemistry: An integrative approach*. 2nd ed. edn, (CRC Press, 2015).
- 132 Salter-Blanc, A. J., Bylaska, E. J., Lyon, M. A., Ness, S. C. & Tratnyek, P. G. Structure-Activity Relationships for Rates of Aromatic Amine Oxidation by Manganese Dioxide. *Environmental Science & Technology* **50**, 5094-5102, doi:10.1021/acs.est.6b00924 (2016).
- 133 Laha, S. & Luthy, R. G. Oxidation of aniline and other primary aromatic-amines by manganese-dioxide. *Environmental Science & Technology* **24**, 363-373, doi:10.1021/es00073a012 (1990).
- 134 Kersten, P. J., Kalyanaraman, B., Hammel, K. E., Reinhammar, B. & Kirk, T. K. Comparison of lignin peroxidase, horseradish-peroxidase and laccase in the oxidation of methoxybenzenes. *Biochemical Journal* **268**, 475-480 (1990).
- 135 Li, C., Zhang, B., Ertunc, T., Schaeffer, A. & Ji, R. Birnessite-induced binding of phenolic monomers to soil humic substances and nature of the bound residues. *Environmental Science & Technology* **46**, 8843-8850, doi:10.1021/es3018732 (2012).
- 136 Kang, K. H., Lim, D. M. & Shin, H. Oxidative-coupling reaction of TNT reduction products by manganese oxide. *Water Research* **40**, 903-910, doi:10.1016/j.watres.2005.12.036 (2006).
- 137 Kang, K.-H., Lim, D.-M. & Shin, H.-S. A novel solution for hydroxylated PAHs removal by oxidative coupling reaction using Mn oxide. *Water Science and Technology* **58**, 171-178, doi:10.2166/wst.2008.637 (2008).

- 138 Nyanhongo, G. S., Couto, S. R. & Guebitz, G. M. Coupling of 2,4,6-trinitrotoluene (TNT) metabolites onto humic monomers by a new laccase from *Trametes modesta*. *Chemosphere* **64**, 359-370, doi:10.1016/j.chemosphere.2005.12.034 (2006).
- 139 Zhao, H. *et al.* Formation of todorokite from "c-disordered" H⁺-birnessites: the roles of average manganese oxidation state and interlayer cations. *Geochemical Transactions* **16**, doi:10.1186/s12932-015-0023-3 (2015).
- 140 Bargar, J. R. *et al.* Biotic and abiotic products of Mn(II) oxidation by spores of the marine *Bacillus* sp. strain SG-1. *American Mineralogist* **90**, 143-154, doi:10.2138/am.2005.1557 (2005).
- 141 Zhu, M., Ginder-Vogel, M., Parikh, S. J., Feng, X.-H. & Sparks, D. L. Cation effects on the layer structure of biogenic Mn-oxides. *Environmental Science & Technology* **44**, 4465-4471, doi:10.1021/es1009955 (2010).
- 142 Grangeon, S., Lanson, B. & Lanson, M. Solid-state transformation of nanocrystalline phyllosulfate into tectosulfate: influence of initial layer and interlayer structure. *Acta Crystallographica Section B-Structural Science Crystal Engineering and Materials* **70**, 828-838, doi:10.1107/s2052520614013687 (2014).
- 143 Zhao, H. *et al.* Redox reactions between Mn(II) and hexagonal birnessite change its layer symmetry. *Environmental Science & Technology* **50**, 1750-1758 (2016).
- 144 Field, J. A., Stams, A. J. M., Kato, M. & Schraa, G. Enhanced biodegradation of aromatic pollutants in cocultures of anaerobic and aerobic bacterial consortia. *Antonie Van Leeuwenhoek International Journal of General and Molecular Microbiology* **67**, 47-77, doi:10.1007/bf00872195 (1995).
- 145 Field, J. A., Stams, A. J. M., Kato, M. & Schraa, G. Enhanced biodegradation of aromatic pollutants in cocultures of anaerobic and aerobic bacterial consortia. *Antonie Van Leeuwenhoek International Journal of General and Molecular Microbiology* **67**, 47-77, doi:10.1007/bf00872195 (1995).
- 146 Essington, M. E. & Vergeer, K. A. Adsorption of antimonate, phosphate, and sulfate by manganese dioxide: Competitive effects and surface complexation modeling. *Soil Science Society of America Journal* **79**, 803-814, doi:10.2136/sssaj2014.12.0482 (2015).
- 147 Patterson, A. L. The Scherrer formula for x-ray particle size determination. *Physical Review* **56**, 978-982, doi:10.1103/PhysRev.56.978 (1939).
- 148 Chorover, J. Zero-charge points. *Encyclopedia of Soils in the Environment* (Elsevier: Oxford, UK), 367-373 (2005).
- 149 Smith, M. W. & Cliff, M. D. NTO-based explosive formulations: A technology review. (1999).
- 150 Koutsospyros, A. *et al.* Degradation of high energetic and insensitive munitions compounds by Fe/Cu bimetal reduction. *Journal of Hazardous Materials* **219**, 75-81, doi:10.1016/j.jhazmat.2012.03.048 (2012).
- 151 Platten, W. E., III, Bailey, D., Suidan, M. T. & Maloney, S. W. Biological transformation pathways of 2,4-dinitro anisole and N-methyl paranitro aniline in anaerobic fluidized-bed bioreactors. *Chemosphere* **81**, 1131-1136, doi:10.1016/j.chemosphere.2010.08.044 (2010).
- 152 Ou, C. *et al.* Enhanced reductive transformation of 2,4-dinitroanisole in an anaerobic system: the key role of zero valent iron. *Rsc Advances* **5**, 75195-75203, doi:10.1039/c5ra11197h (2015).

- 153 Ou, C. *et al.* Removal of multi-substituted nitroaromatic pollutants by zero valent iron: a comparison of performance, kinetics, toxicity and mechanisms. *Physical Chemistry Chemical Physics* **17**, 22072-22078, doi:10.1039/c5cp02518d (2015).
- 154 Ahn, S. C., Cha, D. K., Kim, B. J. & Oh, S.-Y. Detoxification of PAX-21 ammunitions wastewater by zero-valent iron for microbial reduction of perchlorate. *Journal of Hazardous Materials* **192**, 909-914, doi:10.1016/j.jhazmat.2011.05.104 (2011).
- 155 Gorontzy, T., Kuver, J. & Blotevogel, K. H. Microbial transformation of nitroaromatic compounds under anaerobic conditions. *Journal of General Microbiology* **139**, 1331-1336 (1993).
- 156 Yang, H., Halasz, A., Zhao, T. S., Monteil-Rivera, F. & Hawari, J. Experimental evidence for in situ natural attenuation of 2,4-and 2,6-dinitrotoluene in marine sediment. *Chemosphere* **70**, 791-799, doi:10.1016/j.chemosphere.2007.07.014 (2008).
- 157 Hawari, J. *et al.* Characterization of metabolites in the biotransformation of 2,4,6-trinitrotoluene with anaerobic sludge: Role of triaminotoluene. *Applied and Environmental Microbiology* **64**, 2200-2206 (1998).
- 158 Liu, A., Liu, J., Pan, B. & Zhang, W.-x. Formation of lepidocrocite (γ -FeOOH) from oxidation of nanoscale zero-valent iron (nZVI) in oxygenated water. *Rsc Advances* **4**, 57377-57382, doi:10.1039/c4ra08988j (2014).
- 159 Refait, P., Gehin, A., Abdelmoula, M. & Genin, J. M. R. Coprecipitation thermodynamics of iron(II-III) hydroxysulphate green rust from Fe(II) and Fe(III) salts. *Corrosion Science* **45**, 659-676, doi:10.1016/s0010-938x(02)00138-5 (2003).
- 160 Satapanajaru, T., Shea, P. J., Comfort, S. D. & Roh, Y. Green rust and iron oxide formation influences metolachlor dechlorination during zerovalent iron treatment. *Environmental Science & Technology* **37**, 5219-5227, doi:10.1021/es0303485 (2003).
- 161 Boparai, H. K. *et al.* Abiotic transformation of high explosives by freshly precipitated iron minerals in aqueous Fe-II solutions. *Chemosphere* **79**, 865-872, doi:10.1016/j.chemosphere.2010.02.037 (2010).
- 162 Chaves, L. H. G. The role of green rust in the environment: A review. *Revista Brasileira de Engenharia Agrícola e Ambiental* **9**, 284-288, doi:10.1590/s1415-43662005000200021 (2005).
- 163 Yin, W. *et al.* Reductive transformation of pentachloronitrobenzene by zero-valent iron and mixed anaerobic culture. *Chemical Engineering Journal* **210**, 309-315, doi:10.1016/j.cej.2012.09.003 (2012).
- 164 Schwertmann, U. & Fechter, H. The formation of green rust and its transformation to lepidocrocite. *Clay Mineralogy*, 87-98 (**1994**).
- 165 Carlson, L. & Schwertmann, U. The effect of CO₂ and oxidation rate on the formation of goethite versus lepidocrocite from an Fe(II) system at pH-6 and pH-7. *Clay Minerals* **25**, 65-71, doi:10.1180/claymin.1990.025.1.07 (1990).
- 166 Olivares, C., Liang, J., Abrell, L., Sierra-Alvarez, R. & Field, J. A. Pathways of reductive 2,4-dinitroanisole (DNAN) biotransformation in sludge. *Biotechnol. Bioeng.* **110**, 1595-1604 (2013).
- 167 Bryant, C. & DeLuca, M. Purification and characterization of an oxygen-insensitive NAD(P)H nitroreductase from *Enterobacter cloacae*. *J. Biol. Chem.* **266**, 4119-4125 (1991).

- 168 Donlon, B. A., Razo-Flores, E., Lettinga, G. & Field, J. A. Continuous detoxification, transformation, and degradation of nitrophenols in upflow anaerobic sludge blanket (UASB) reactors. *Biotechnol. Bioeng.* **51**, 439-449 (1996).
- 169 Dunnivant, F. M., Schwarzenbach, R. P. & Macalady, D. L. Reduction of substituted nitrobenzenes in aqueous solutions containing natural organic matter. *Environ. Sci. Technol.* **26**, 2133-2141, doi:10.1021/es00035a010 (1992).
- 170 Moglie, Y., Vitale, C. & Radivoy, G. Synthesis of azo compounds by nanosized iron-promoted reductive coupling of aromatic nitro compounds. *Tetrahedron Letters* **49**, 1828-1831, doi:10.1016/j.tetlet.2008.01.053 (2008).
- 171 Zhao, R. *et al.* One step synthesis of azo compounds from nitroaromatics and anilines. *Tetrahedron Letters* **52**, 3805-3809, doi:10.1016/j.tetlet.2011.05.054 (2011).
- 172 Smith, M. B. & March, J. in *March's Advanced Organic Chemistry* 752-852 (John Wiley & Sons, Inc., 2006).
- 173 Wang, J. Q. *et al.* Catalysis by Pd nanoclusters generated in situ of high-efficiency synthesis of aromatic azo compounds from nitroaromatics under H₂ atmosphere. *Rsc Advances* **3**, 4899-4902, doi:10.1039/c3ra23004j (2013).
- 174 Bin, Y. *et al.* Expression and characteristics of the gene encoding azoreductase from *Rhodobacter sphaeroides* AS1.1737. *FEMS Microbiol. Lett.* **236**, 129-136 (2004).
- 175 Nakanishi, M., Yatome, C., Ishida, N. & Kitade, Y. Putative ACP phosphodiesterase gene (*acpD*) encodes an azoreductase. *Journal of Biological Chemistry* **276**, 46394-46399, doi:10.1074/jbc.M104483200 (2001).
- 176 Hu, T. L. Decolourisation of reactive azo dyes by transformation with *Pseudomonas luteola*. *Bioresource Technology* **49**, 47-51, doi:10.1016/0960-8524(94)90172-4 (1994).
- 177 van der Zee, F. P., Lettinga, G. & Field, J. A. Azo dye decolourisation by anaerobic granular sludge. *Chemosphere* **44**, 1169-1176 (2001).
- 178 Stolz, A. Basic and applied aspects in the microbial degradation of azo dyes. *Appl. Microbiol. Biot.* **56**, 69-80 (2001).
- 179 Gilcrease, P. C. & Murphy, V. G. Bioconversion of 2,4-diamino-6-nitrotoluene to a novel metabolite under anoxic and aerobic conditions. *Appl Environ Microb* **61**, 4209-4214 (1995).
- 180 Sim, E., Walters, K. & Boukouvala, S. Arylamine N-acetyltransferases: from structure to function. *Drug metabolism reviews* **40**, 479-510 (2008).
- 181 Schäfer, A., Harms, H. & Zehnder, A. J. Biodegradation of 4-nitroanisole by two *Rhodococcus* spp. *Biodegradation* **7**, 249-255 (1996).
- 182 Boll, M. & Fuchs, G. Unusual reactions involved in anaerobic metabolism of phenolic compounds. *Biological Chemistry* **386**, 989-997 (2005).
- 183 Ahn, S. C., Cha, D. K., Kim, B. J. & Oh, S.-Y. Detoxification of PAX-21 ammunitions wastewater by zero-valent iron for microbial reduction of perchlorate. *J. Hazard. Mater.* **192**, 909-914, doi:10.1016/j.jhazmat.2011.05.104 (2011).
- 184 Zhang, D., Zhu, D. & Chen, W. Sorption of nitroaromatics to soils: Comparison of the importance of soil organic matter versus clay. *Environmental Toxicology and Chemistry* **28**, 1447-1454, doi:10.1897/08-406.1 (2009).
- 185 Field, J. A., Stams, A. J., Kato, M. & Schraa, G. Enhanced biodegradation of aromatic pollutants in cocultures of anaerobic and aerobic bacterial consortia. *Antonie van Leeuwenhoek* **67**, 47-77 (1995).

- 186 Stenuit, B., Eyers, L., Fantroussi, S. & Agathos, S. Promising strategies for the mineralisation of 2,4,6-trinitrotoluene. *Rev. Environ. Sci. Biotechnol.* **4**, 1-2 (2005).
- 187 Rieger, P. G. & Knackmuss, H. J. in *Biodegradation of nitroaromatic compounds* (ed Jim C. Spain) Ch. 1, 1-18 (Plenum Press, 1995).
- 188 Razo-Flores, E., Lettinga, G. & Field, J. A. Biotransformation and biodegradation of selected nitroaromatics under anaerobic conditions. *Biotechnol. Progr.* **15**, 358-365, doi:10.1021/bp9900413 (1999).
- 189 Kwon, S. H. & Yen, T. F. Metabolism of 2, 4, 6 -trinitrotoluene by n populations in digested sewage sludge under strict anaerobic conditions. *J. Environ. Sci. Heal. A* **32**, 2669-2682 (1997).
- 190 Grigatti, M., Perez, M. D., Blok, W. J., Ciavatta, C. & Veeken, A. A standardized method for the determination of the intrinsic carbon and nitrogen mineralization capacity of natural organic matter sources. *Soil Biol. Biochem.* **39**, 1493-1503 (2007).
- 191 Hem, L. Assimilable organic carbon in molecular weight fractions of natural organic matter. *Water Res.* **35**, 1106-1110 (2001).
- 192 Lee, C. Controls on organic carbon preservation: The use of stratified water bodies to compare intrinsic rates of decomposition in oxic and anoxic systems. *Geochim. Cosmochim. Ac.* **56**, 3323-3335 (1992).
- 193 Glaus, M., Heijman, C., Schwarzenbach, R. & Zeyer, J. Reduction of nitroaromatic compounds mediated by *Streptomyces* sp. exudates. *Appl. Environ. Microbiol.* **58**, 1945-1951 (1992).
- 194 Anderson, T.-H. & Domsch, K. H. Ratios of microbial biomass carbon to total organic carbon in arable soils. *Soil Biol. Biochem.* **21**, 471-479 (1989).
- 195 Niedwiecka, J. B. & Finneran, K. T. Combined biological and abiotic reactions with iron and Fe(III)-reducing microorganisms for remediation of explosives and insensitive munitions (IM). *Environ. Sci. Water Res. Technol.* **1**, 34-39, doi:10.1039/c4ew00062e (2015).
- 196 Lovley, D. R. & Phillips, E. J. Organic matter mineralization with reduction of ferric iron in anaerobic sediments. *Appl. Environ. Microbiol.* **51**, 683-689 (1986).
- 197 Weiss, J. V., Emerson, D. & Megonigal, J. P. Geochemical control of microbial Fe(III) reduction potential in wetlands: comparison of the rhizosphere to non-rhizosphere soil. *FEMS Microbiol. Ecol.* **48**, 89-100 (2004).
- 198 Hawari, J. *et al.* Characterization of metabolites in the biotransformation of 2,4,6-trinitrotoluene with anaerobic sludge: role of triaminotoluene. *Appl Environ Microb* **64**, 2200-2206 (1998).
- 199 Hu, L. *et al.* A Highly Active Nano-Palladium Catalyst for the Preparation of Aromatic Azos under Mild Conditions. *Organic Letters* **13**, 5640-5643, doi:10.1021/ol202362f (2011).
- 200 Pizzolatti, M. G. & Yunes, R. A. Azoxybenzene formation from nitrosobenzene and phenylhydroxylamine. A unified view of the catalysis and mechanisms of the reactions. *J. Chem. Soc. Perkin Trans. 2*, 759-764 (1990).
- 201 Daun, G., Lenke, H., Reuss, M. & Knackmuss, H.-J. Biological treatment of TNT-contaminated soil. 1. Anaerobic cometabolic reduction and interaction of TNT and metabolites with soil components. *Environ. Sci. Technol.* **32**, 1956-1963 (1998).

- 202 Burger, S. & Stolz, A. Characterisation of the flavin-free oxygen-tolerant azoreductase
from *Xenophilus azovorans* KF46F in comparison to flavin-containing azoreductases.
Appl. Microbiol. Biot. **87**, 2067-2076 (2010).
- 203 Achtnich, C., Fernandes, E., Bollag, J. M., Knackmuss, H. J. & Lenke, H. Covalent
binding of reduced metabolites of N-15(3) TNT to soil organic matter during a
bioremediation process analyzed by N-15 NMR spectroscopy. *Environmental Science &
Technology* **33**, 4448-4456, doi:10.1021/es990427+ (1999).
- 204 Drzyzga, O., Bruns-Nagel, D., Gorontzy, T., Blotevogel, K.-H. & von Löw, E. Anaerobic
incorporation of the radiolabeled explosive TNT and metabolites into the organic soil
matrix of contaminated soil after different treatment procedures. *Chemosphere* **38**, 2081-
2095, doi:[http://dx.doi.org/10.1016/S0045-6535\(98\)00426-3](http://dx.doi.org/10.1016/S0045-6535(98)00426-3) (1999).
- 205 Carpenter, D. F., McCormick, N. G., Cornell, J. H. & Kaplan, A. M. Microbial
transformation of ¹⁴C-labeled 2,4,6-trinitrotoluene in an activated-sludge system.
Applied and Environmental Microbiology **35**, 949-954 (1978).
- 206 Nishino, S. F., Spain, J. C. & He, Z., . In Biodegradation of nitroaromatic compounds and
explosives,, Eds. CRC Press: . (eds J. C. Spain, J. B. Hughes, & H. J. Knackmuss) 7-61
(CRC Press, 2000).
- 207 Giurg, M. *et al.* Catalytic Oxidative Cyclocondensation of o -Aminophenols to 2-
Amino -β-Henoxazin- 3- ones. *Synthetic Communications* **37**, 1779-1789,
doi:10.1080/00397910701316136 (2007).
- 208 Van der Zee, J., Duling, D. R., Mason, R. P. & Eling, T. E. The oxidation of N-
substituted aromatic amines by horseradish peroxidase. *Journal of Biological Chemistry*
264, 19828-19836 (1989).
- 209 Thorn, K. A. & Kennedy, K. R. ¹⁵N NMR Investigation of the Covalent Binding of
Reduced TNT Amines to Soil Humic Acid, Model Compounds, and Lignocellulose.
Environmental Science & Technology **36**, 3787-3796, doi:10.1021/es011383j (2002).
- 210 Achtnich, C., Sieglén, U., Knackmuss, H.-J. & Lenke, H. Irreversible binding of
biologically reduced 2,4,6-trinitrotoluene to soil. *Environmental Toxicology and
Chemistry* **18**, 2416-2423 (1999).
- 211 Anschutz, A. J. & Penn, R. L. Reduction of crystalline iron(III) oxyhydroxides using
hydroquinone: Influence of phase and particle size. *Geochemical Transactions* **6**, 60-60,
doi:10.1186/1467-4866-6-60 (2005).
- 212 Kung, K. H. & McBride, M. B. Electron-transfer processes between hydroquinone and
iron-oxides. *Clays and Clay Minerals* **36**, 303-309, doi:10.1346/ccmn.1988.0360403
(1988).
- 213 Liu, M. M. *et al.* Structural controls on the catalytic polymerization of hydroquinone by
birnessites. *Clays and Clay Minerals* **59**, 525-537, doi:10.1346/ccmn.2011.0590510
(2011).
- 214 Esteve-Nunez, A., Caballero, A. & Ramos, J. L. Biological degradation of 2,4,6-
trinitrotoluene. *Microbiology and Molecular Biology Reviews* **65**, 335-352,
doi:10.1128/mmbr.65.3.335-352.2001 (2001).
- 215 Ju, K. S. & Parales, R. E. Nitroaromatic Compounds, from Synthesis to Biodegradation.
Microbiol. Mol. Biol. R. **74**, 250-272, doi:10.1128/mmbr.00006-10 (2010).
- 216 Marvin-Sikkema, F. D. & de Bont, J. A. M. Degradation of nitroaromatic compounds by
microorganisms. *Appl. Microbiol. Biot.* **42**, 499-507 (1994).

- 217 Boopathy, R. & Melancon, E. Metabolism of compounds with nitro-functions by
Klebsiella pneumoniae isolated from a regional wetland. *Int. Biodeterior. Biodegr.* **54**,
269-275 (2004).
- 218 Wang, J., Zhou, J.-T., Zhang, A.-L. & Hong, L. U. Aerobic degradation of nitrobenzene
by Pseudomonas sp. JX165 and its intact cells. *China Environ. Sci.* **21**, 144-147 (2001).
- 219 Le Campion, L., Vandais, A. & Ouazzani, J. Microbial remediation of NTO in aqueous
industrial wastes. *FEMS Microbiol. Lett.* **176**, 197-203, doi:10.1111/j.1574-
6968.1999.tb13662.x (1999).
- 220 Richard, T. & Weidhaas, J. Biodegradation of IMX-101 explosive formulation
constituents: 2,4-dinitroanisole (DNAN), 3-nitro-1,2,4-triazol-5-one (NTO), and
nitroguanidine. *J. Hazard. Mater.* **280**, 372-379, doi:10.1016/j.jhazmat.2014.08.019
(2014).
- 221 Jayamani, I., Manzella, M. P. & Cupples, A. M. RDX degradation potential in soils
previously unexposed to RDX and the identification of RDX-degrading species in one
agricultural soil using stable isotope probing. *Water Air Soil Poll.* **224**, 1-15 (2013).
- 222 Lewis, T. A., Ederer, M. M., Crawford, R. L. & Crawford, D. L. Microbial
transformation of 2,4,6-trinitrotoluene. *J. Ind. Microbiol. Biot.* **18**, 89-96,
doi:10.1038/sj.jim.2900258 (1997).
- 223 Roldan, M., Perez-Reinado, E., Castillo, F. & Moreno-Vivian, C. Reduction of
polynitroaromatic compounds: the bacterial nitroreductases. *FEMS Microbiol. Rev.* **32**,
474-500, doi:10.1111/j.1574-6976.2008.00107.x (2008).
- 224 Gorontzy, T., Küver, J. & Blotevogel, K. H. Microbial transformation of nitroaromatic
compounds under anaerobic conditions. *J. Gen. Microbiol.* **139**, 1331-1336 (1993).
- 225 Le Campion, L., Delaforge, M., Noel, J. P. & Ouazzani, J. Metabolism of ¹⁴C-labelled 5-
nitro-1,2,4-triazol-3-one (NTO): comparison between rat liver microsomes and bacterial
metabolic pathways. *J. Mol. Catal. B-Enzym.* **5**, 395-402 (1998).
- 226 Kitts, C. L., Green, C. E., Otley, R. A., Alvarez, M. A. & Unkefer, P. J. Type I
nitroreductases in soil enterobacteria reduce TNT (2,4,6-trinitrotoluene) and RDX
(hexahydro-1,3,5-trinitro-1,3,5-triazine). *Can. J. Microbiol.* **46**, 278-282 (2000).
- 227 Koder, R. L., Haynes, C. A., Rodgers, M. E., Rodgers, D. W. & Miller, A. F. Flavin
thermodynamics explain the oxygen insensitivity of enteric nitroreductases.
Biochemistry. **41**, 14197 - 14205 (2002).
- 228 Elsner, M., Schwarzenbach, R. P. & Haderlein, S. B. Reactivity of Fe(II)-bearing
minerals toward reductive transformation of organic contaminants. *Environ. Sci. Technol.*
38, 799-807, doi:10.1021/es0345569 (2004).
- 229 Perreault, N. N. *et al.* Aerobic biotransformation of 2, 4-dinitroanisole in soil and soil
Bacillus sp. *Biodegradation* **23**, 287-295 (2012).
- 230 Adrian, N. R., Arnett, C. M. & Hickey, R. F. Stimulating the anaerobic biodegradation of
explosives by the addition of hydrogen or electron donors that produce hydrogen. *Water
Res.* **37**, 3499 - 3507 (2003).
- 231 Boopathy, R., Kulpa, C. F. & Manning, J. Anaerobic biodegradation of explosives and
related compounds by sulfate-reducing and methanogenic bacteria: A review.
Bioresource Technol. **63**, 81-89, doi:10.1016/s0960-8524(97)00083-7 (1998).
- 232 Oh, B.-T., Shea, P. J., Drijber, R. A., Vasilyeva, G. K. & Sarath, G. TNT
biotransformation and detoxification by a Pseudomonas aeruginosa strain.
Biodegradation **14**, 309-319, doi:10.1023/a:1025656325834 (2003).

- 233 Fleischmann, T. J., Walker, K. C., Spain, J. C., Hughes, J. B. & Craig, A. M. Anaerobic transformation of 2,4,6-TNT by bovine ruminal microbes. *Biochem. Bioph. Res. Co.* **314**, 957-963, doi:10.1016/j.bbrc.2003.12.193 (2004).
- 234 Preuss, A., Fimpel, J. & Diekert, G. Anaerobic transformation of 2,4,6-trinitrotoluene (TNT). *Arch. Microbiol.* **159**, 345-353, doi:10.1007/bf00290917 (1993).
- 235 Yin, H., Wood, T. K. & Smets, B. F. Reductive transformation of TNT by *Escherichia coli*: pathway description. *Appl. Microbiol. Biot.* **67**, 397-404, doi:10.1007/s00253-004-1736-x (2005).
- 236 Khan, M. I., Lee, J. & Park, J. Microbial degradation and toxicity of hexahydro-1,3,5-trinitro-1,3,5-triazine. *J. Microbiol. Biotechn.* **22**, 1311-1323, doi:10.4014/jmb.1203.04002 (2012).
- 237 McCormick, N. G., Cornell, J. H. & Kaplan, A. M. Biodegradation of hexahydro-1,3,5-trinitro-1,3,5-triazine. *Appl. Environ. Microb.* **42**, 817-823 (1981).
- 238 Hughes, J. B. *et al.* Bamberger rearrangement during TNT metabolism by *Clostridium acetobutylicum*. *Environ. Sci. Technol.* **32**, 494-500 (1998).
- 239 Maeda, T., Nakamura, R., Kadokami, K. & Ogawa, H. I. Relationship between mutagenicity and reactivity or biodegradability for nitroaromatic compounds. *Environ. Toxicol. Chem.* **26**, 237-241, doi:10.1897/06-019r1.1 (2007).
- 240 Bhushan, B. *et al.* Biotransformation of hexahydro-1,3,5-trinitro-1,3,5-triazine (RDX) by a rabbit liver cytochrome P450: insight into the mechanism of RDX biodegradation by *Rhodococcus* sp. strain DN22. *Appl. Environ. Microb.* **69**, 1347-1351 (2003).
- 241 Hawari, J. in *Biodegradation of nitroaromatic compounds and explosives* (eds J. C. Spain, J. B. Hughes, & H. J. Knackmuss) 277-310 (Lewis Publishers, 2000).
- 242 Halasz, A. & Hawari, J. in *Aquatic Redox Chemistry Vol. 1071 ACS Symposium Series* (eds P. G. Tratnyek, T. J. Grundl, & S. B. Haderlein) 441-462 (2011).
- 243 Beunink, J. & Rehm, H.-J. Coupled reductive and oxidative degradation of 4-chloro-2-nitrophenol by a co-immobilized mixed culture system. *Applied Microbiology and Biotechnology* **34**, 108-115 (1990).
- 244 Chae, K.-J. *et al.* Spatial distribution and viability of nitrifying, denitrifying and ANAMMOX bacteria in biofilms of sponge media retrieved from a full-scale biological nutrient removal plant. *Bioprocess and Biosystems Engineering* **35**, 1157-1165, doi:10.1007/s00449-012-0701-9 (2012).
- 245 Kato, M. T., Field, J. A. & Lettinga, G. High tolerance of methanogens in granular sludge to oxygen. *Biotechnology and bioengineering* **42**, 1360-1366 (1993).
- 246 Mac Conell, E. F. A., Almeida, P. G. S., Martins, K. E. L., Araujo, J. C. & Chernicharo, C. A. L. Bacterial community involved in the nitrogen cycle in a down-flow sponge-based trickling filter treating UASB effluent. *Water Science and Technology* **72**, 116-122, doi:10.2166/wst.2015.154 (2015).
- 247 Tratnyek, P. G. & Wolfe, N. L. Oxidation and acidification of anaerobic sediment-water systems by autoclaving. *Journal of environmental quality* **22**, 375-378 (1993).
- 248 Tratnyek, P. G. & Macalady, D. L. Abiotic reduction of nitro aromatic pesticides in anaerobic laboratory systems. *Journal of Agricultural and Food Chemistry* **37**, 248-254 (1989).
- 249 Mark, N., Arthur, J., Dontsova, K., Brusseau, M. & Taylor, S. Adsorption and attenuation behavior of 3-nitro-1, 2, 4-triazol-5-one (NTO) in eleven soils. *Chemosphere* **144**, 1249-1255 (2016).

- 250 Spain, J. C. Biodegradation of nitroaromatic compounds. *Annu. Rev. Microbiol.* **49**, 523-555 (1995).
- 251 Amaral, H. I. F., Fernandes, J., Berg, M., Schwarzenbach, R. P. & Kipfer, R. Assessing TNT and DNT groundwater contamination by compound-specific isotope analysis and ^3H - ^3He groundwater dating: A case study in Portugal. *Chemosphere* **77**, 805-812 (2009).
- 252 Wang, L., Barrington, S. & Kim, J.-W. Biodegradation of pentyl amine and aniline from petrochemical wastewater. *Journal of environmental management* **83**, 191-197 (2007).
- 253 Liu, X.-Y. *et al.* Simultaneous biodegradation of nitrogen-containing aromatic compounds in a sequencing batch bioreactor. *Journal of Environmental Sciences* **19**, 530-535 (2007).
- 254 Franca, R. D. *et al.* Effect of an azo dye on the performance of an aerobic granular sludge sequencing batch reactor treating a simulated textile wastewater. *Water research* **85**, 327-336 (2015).
- 255 Stewart, P. S. & Franklin, M. J. Physiological heterogeneity in biofilms. *Nature Reviews Microbiology* **6**, 199-210 (2008).
- 256 Hooijmans, C. M. Diffusion coupled with bioconversion in immobilized systems: use of an oxygen microsensor. (1990).
- 257 Gan, H. M., Shahir, S., Ibrahim, Z. & Yahya, A. Biodegradation of 4-aminobenzenesulfonate by *Ralstonia* sp. PBA and *Hydrogenophaga* sp. PBC isolated from textile wastewater treatment plant. *Chemosphere* **82**, 507-513, doi:<http://dx.doi.org/10.1016/j.chemosphere.2010.10.094> (2011).
- 258 Gan, H. M., Chew, T. H., Tay, Y. L., Lye, S. F. & Yahya, A. Genome Sequence of *Hydrogenophaga* sp Strain PBC, a 4-Aminobenzenesulfonate-Degrading Bacterium. *Journal of Bacteriology* **194**, 4759-4760, doi:10.1128/jb.00990-12 (2012).
- 259 Nakamura, K., Ishida, H. & Iizumi, T. Constitutive trichloroethylene degradation led by tac promoter chromosomally integrated upstream of phenol hydroxylase genes of *Ralstonia* sp. KN1 and its nucleotide sequence analysis. *Journal of Bioscience and Bioengineering* **89**, 47-54, doi:[http://dx.doi.org/10.1016/S1389-1723\(00\)88049-4](http://dx.doi.org/10.1016/S1389-1723(00)88049-4) (2000).
- 260 Verhagen, P., De Gelder, L., Hoefman, S., De Vos, P. & Boon, N. Planktonic versus Biofilm Catabolic Communities: Importance of the Biofilm for Species Selection and Pesticide Degradation. *Applied and Environmental Microbiology* **77**, 4728-4735, doi:10.1128/aem.05188-11 (2011).
- 261 Breugelmans, P. *et al.* Architecture and spatial organization in a triple-species bacterial biofilm synergistically degrading the phenylurea herbicide linuron. *FEMS Microbiology Ecology* **64**, 271-282, doi:10.1111/j.1574-6941.2008.00470.x (2008).
- 262 Hu, X. P., Fukutani, A., Liu, X., Kimbara, K. & Kawai, F. Isolation of bacteria able to grow on both polyethylene glycol (PEG) and polypropylene glycol (PPG) and their PEG/PPG dehydrogenases. *Applied Microbiology and Biotechnology* **73**, 1407-1413, doi:10.1007/s00253-006-0616-y (2007).
- 263 Meiberg, J. B. M. & Harder, W. AEROBIC AND ANAEROBIC METABOLISM OF TRIMETHYLAMINE, DIMETHYLAMINE AND METHYLAMINE IN *HYPHOMICROBIUM*-X. *Journal of General Microbiology* **106**, 265-276 (1978).
- 264 Kim, S. G., Bae, H. S. & Lee, S. T. A novel denitrifying bacterial isolate that degrades trimethylamine both aerobically and anaerobically via two different pathways. *Archives of Microbiology* **176**, 271-277, doi:10.1007/s002030100319 (2001).

- 265 King, G. M. Carbon monoxide as a metabolic energy source for extremely halophilic microbes: Implications for microbial activity in Mars regolith. *Proceedings of the National Academy of Sciences of the United States of America* **112**, 4465-4470, doi:10.1073/pnas.1424989112 (2015).
- 266 Ruzicka, J. *et al.* Microbial degradation of N-methyl-2-pyrrolidone in surface water and bacteria responsible for the process. *Water Science and Technology* **73**, 643-647, doi:10.2166/wst.2015.540 (2016).
- 267 Villemur, R. *et al.* Biodegradation of Endocrine Disruptors in Solid-Liquid Two-Phase Partitioning Systems by Enrichment Cultures. *Applied and Environmental Microbiology* **79**, 4701-4711, doi:10.1128/aem.01239-13 (2013).
- 268 Chen, D. Z. *et al.* Intermediates and substrate interaction of 1,4-dioxane degradation by the effective metabolizer *Xanthobacter flavus* DT8. *International Biodeterioration & Biodegradation* **106**, 133-140, doi:10.1016/j.ibiod.2015.09.018 (2016).
- 269 Xue, F., Liu, Z. Q., Wan, N. W., Zhu, H. Q. & Zheng, Y. G. Engineering the epoxide hydrolase from *Agromyces mediolanus* for enhanced enantioselectivity and activity in the kinetic resolution of racemic epichlorohydrin. *Rsc Advances* **5**, 31525-31532, doi:10.1039/c5ra02492g (2015).
- 270 Martineau, C., Mauffrey, F. & Villemur, R. Comparative Analysis of Denitrifying Activities of *Hyphomicrobium nitrivorans*, *Hyphomicrobium denitrificans*, and *Hyphomicrobium zavarzinii*. *Applied and Environmental Microbiology* **81**, 5003-5014, doi:10.1128/aem.00848-15 (2015).
- 271 Urbanczyk, H., Ast, J. C., Higgins, M. J., Carson, J. & Dunlap, P. V. Reclassification of *Vibrio fischeri*, *Vibrio logei*, *Vibrio salmonicida* and *Vibrio wodanis* as *Aliivibrio fischeri* gen. nov., comb. nov., *Aliivibrio logei* comb. nov., *Aliivibrio salmonicida* comb. nov. and *Aliivibrio wodanis* comb. nov. *Int. J. Syst. Evol. Micr.* **57**, 2823-2829 (2007).
- 272 Davies, P. J. & Provatas, A. Characterisation of 2,4-dinitroanisole an ingredient for use in low sensitivity melt cast formulations. (Science Defence Technology Organization. Weapons Systems Divison., Edinburgh, Australia, 2006).
- 273 Donlon, B. A., Razo-Flores, E., Field, J. A. & Lettinga, G. Toxicity of N-substituted aromatics to acetoclastic methanogenic activity in granular sludge. *Appl. Environ. Microb.* **61**, 3889-3893 (1995).
- 274 Uberoi, V. & Bhattacharya, S. K. Toxicity and degradability of nitrophenols in anaerobic systems. *Water Environment Research* **69**, 146-156, doi:10.2175/106143097x125290 (1997).
- 275 Haghighi-Podeh, M. R. & Bhattacharya, S. K. Fate and toxic effects of nitrophenols on anaerobic treatment systems. *Water Science and Technology* **34**, 345-350, doi:10.1016/0273-1223(96)00664-6 (1996).
- 276 Boyd, S. A., Shelton, D. R., Berry, D. & Tiedje, J. M. Anaerobic biodegradation of phenolic compounds in digested sludge. *Appl. Environ. Microb.* **46**, 50-54 (1983).
- 277 Neuwoehner, J. *et al.* Toxicological characterization of 2,4,6-trinitrotoluene, its transformation products, and two nitramine explosives. *Environ. Toxicol. Chem.* **26**, 1090-1099 (2007).
- 278 Frische, T. Screening for soil toxicity and mutagenicity using luminescent bacteria- A case study of the explosive 2,4,6-Trinitrotoluene (TNT). *Ecotoxicology and Environmental Safety* **51**, 133-144 (2002).

- 279 Drzyzga, O., Gorontzy, T., Schmidt, A. & Blotevogel, K. H. Toxicity of explosives and related compounds to the luminescent bacterium *Vibrio fischeri* NRRL-B-11177. *Arch. Environ. Contam. Toxicol.* **28**, 229-235 (1995).
- 280 Fuller, M. & Manning, J. F. Aerobic gram-positive and gram-negative bacteria exhibit differential sensitivity to and transformation of 2,4,6-trinitrotoluene (TNT). *Curr. Microbiol.* **35**, 77-83 (1997).
- 281 Klausmeier, R. E., Osmon, J. L. & Walls, D. R. The effect of trinitrotoluene on microorganisms. *Dev. Ind. Microbiol.* **15**, 309-317 (1973).
- 282 Terada, H. The interaction of highly-active uncouplers with mitochondria. *Biochim. Biophys. Acta* **639**, 225-242 (1981).
- 283 Arechederra, M. N., Fischer, C. N., Wetzel, D. J. & Minteer, S. D. Evaluation of the electron transport chain inhibition and uncoupling of mitochondrial bioelectrocatalysis with antibiotics and nitro-based compounds. *Electrochimica Acta* **56**, 938-944, doi:10.1016/j.electacta.2010.09.069 (2010).
- 284 Lachance, B. *et al.* Cytotoxic and genotoxic effects of energetic compounds on bacterial and mammalian cells in vitro. *Mutat. Res-Gen. Tox. En.* **444**, 25-39 (1999).
- 285 Won, W. D., Disalvo, L. H. & Ng, J. Toxicity and mutagenicity of 2,4,6-trinitrotoluene and its microbial metabolites. *Appl. Environ. Microb.* **31**, 576-580 (1976).
- 286 Honeycutt, M. E., Jarvis, A. S. & McFarland, V. A. Cytotoxicity and mutagenicity of 2,4,6-trinitrotoluene and its metabolites. *Ecotox. Environ. Safe* **35**, 282-287 (1996).
- 287 Lachance, B., Renoux, A. Y., Sarrazin, M., Hawari, J. & Sunahara, G. I. Toxicity and bioaccumulation of reduced TNT metabolites in the earthworm *Eisenia andrei* exposed to amended forest soil. *Chemosphere* **55**, 1339-1348 (2004).
- 288 Bruns-Nagel, D. *et al.* Characterization of ¹⁵N-TNT residues after an anaerobic/aerobic treatment of soil/molasses mixtures by solid-state ¹⁵N NMR spectroscopy. 2. Systematic investigation of whole soil and different humic fractions. *Environ. Sci. Technol.* **34**, 1549-1556 (2000).
- 289 Dawel, G. *et al.* Structure of a laccase-mediated product of coupling of 2,4-diamino-6-nitrotoluene to guaiacol, a model for coupling of 2,4,6-trinitrotoluene metabolites to a humic organic soil matrix. *Appl. Environ. Microb.* **63**, 2560-2565 (1997).
- 290 Thorn, K. A. & Kennedy, K. R. N-15 NMR investigation of the covalent binding of reduced TNT amines to soil humic acid, model compounds, and lignocellulose. *Environ. Sci. Technol.* **36**, 3787-3796 (2002).
- 291 Dodard, S. G. *et al.* Ecotoxicity characterization of dinitrotoluenes and some of their reduced metabolites. *Chemosphere* **38**, 2071-2079 (1999).
- 292 Schroer, H. W., Langenfeld, K. L., Li, X., Lehmler, H.-J. & Just, C. L. Stable isotope-enabled pathway elucidation of 2,4-dinitroanisole metabolized by *Rhizobium litchii*. *Environ. Sci. Technol. Lett.* **2**, 362-366, doi:10.1021/acs.estlett.5b00278 (2015).
- 293 Liang, J. D., Olivares, C., Field, J. A. & Sierra-Alvarez, R. Microbial toxicity of the insensitive munitions compound, 2,4-dinitroanisole (DNAN), and its aromatic amine metabolites. *Journal of Hazardous Materials* **262**, 281-287, doi:10.1016/j.jhazmat.2013.08.046 (2013).
- 294 Liang, J., Olivares, C., Field, J. A. & Sierra-Alvarez, R. Microbial toxicity of the insensitive munitions compound, 2,4-dinitroanisole (DNAN), and its aromatic amine metabolites. *J. Hazard. Mater.* **262**, 281-287 (2013).

- 295 Tweedy, B. G., Loeppky, C. & Ross, J. A. Metobromuron: Acetylation of the aniline moiety as a detoxification mechanism. *Science* **168**, 482-483, doi:10.1126/science.168.3930.482 (1970).
- 296 Beifuss, U. & Tietze, M. in *Natural products synthesis II: Targets, methods, concepts Topics in current chemistry* (ed J. Mulzer) 77-113 (2005).
- 297 Murakami, E., Deppenmeier, U. & Ragsdale, S. W. Characterization of the intramolecular electron transfer pathway from 2-hydroxyphenazine to the heterodisulfide reductase from *Methanosarcina thermophila*. *J. Biol. Chem.* **276**, 2432-2439, doi:10.1074/jbc.M004809200 (2001).
- 298 Beckmann, S., Lee, M. J., Manefield, M. & Oo, Y. M. Enhances biogas production. Australia Patent Application # AU2014202663. (2014).
- 299 Esteve-Núñez, A., Caballero, A. & Ramos, J. L. Biological degradation of 2,4,6-trinitrotoluene. *Microbiol. Mol. Biol. R.* **65**, 335-352 (2001).
- 300 Colón, D., Weber, E. J. & Baughman, G. L. Sediment-associated reactions of aromatic amines. 2. QSAR development. *Environ. Sci. Technol.* **36**, 2443-2450, doi:10.1021/es0113551 (2002).
- 301 Padda, R. S., Wang, C. Y., Hughes, J. B. & Bennett, G. N. Mutagenicity of trinitrotoluene and metabolites formed during anaerobic degradation by *Clostridium acetobutylicum* ATCC 824. *Environ. Toxicol. Chem.* **19**, 2871-2875 (2000).
- 302 Knicker, H., Achtnich, C. & Lenke, H. Solid-state nitrogen-15 nuclear magnetic resonance analysis of biologically reduced 2,4,6-trinitrotoluene in a soil slurry remediation. *J. Environ. Qual.* **30**, 403-410 (2001).
- 303 Moglie, Y., Vitale, C. & Radivoy, G. Synthesis of azo compounds by nanosized iron-promoted reductive coupling of aromatic nitro compounds. *Tetrahedron Lett.* **49**, 1828-1831 (2008).
- 304 Zhao, R. *et al.* One step synthesis of azo compounds from nitroaromatics and anilines. *Tetrahedron Lett.* **52**, 3805-3809 (2011).
- 305 Wang, Y. *et al.* *Vibrio fischeri* flavohaemoglobin protects against nitric oxide during initiation of the squid-*Vibrio* symbiosis. *Mol. Microbiol.* **78**, 903-915 (2010).
- 306 Lin, H. C. & Hwang, P. P. Acute and chronic effects of gallium chloride (GaCl₃) on tilapia (*Oreochromis mossambicus*) larvae. *B. Environ. Contam. Tox.* **60**, 931-935 (1998).
- 307 Kim, K.-T. & Tanguay, R. L. Integrating zebrafish toxicology and nanoscience for safer product development. *Green Chem.* **15**, 872-880 (2013).
- 308 Scholz, S. *et al.* The zebrafish embryo model in environmental risk assessment—applications beyond acute toxicity testing. *Environ. Sci. Pollut. R.* **15**, 394-404, doi:10.1007/s11356-008-0018-z (2008).
- 309 Truong, L., Harper, S. L. & Tanguay, R. L. in *Drug Safety Evaluation* Vol. 691 *Methods in Molecular Biology* (ed Jean-Charles Gautier) Ch. 16, 271-279 (Humana Press, 2011).
- 310 Dai, Y.-J. *et al.* Zebrafish as a model system to study toxicology. *Environ. Toxicol. Chem.* **33**, 11-17 (2014).
- 311 Howe, K. *et al.* The zebrafish reference genome sequence and its relationship to the human genome. *Nature* **496**, 498-503 (2013).
- 312 Vol. 79 Fed. Reg. 34 34-47 (2014).
- 313 Little, L. W. & Lamb, J. C. I. Acute toxicity of 46 selected dyes to the fathead minnow, *Pimephales promelas*. Final Report to the American Dye Manufacturers Institute, Inc. UNC Wastewater Research Center, Department of Environmental Sciences and

- Engineering. School of Public Health. University of North Carolina, Chapel Hill, NC., (1972).
- 314 Sharma, S., Upreti, N. & Sharma, K. P. Monitoring toxicity of an azo dye methyl red and a heavy metal Cu, using plant and animal bioassays. *Toxicol. Environ. Chem.* **91**, 109-120, doi:10.1080/02772240802010987 (2009).
- 315 Soriano, J., Mathieu-Denoncourt, J., Norman, G., de Solla, S. & Langlois, V. Toxicity of the azo dyes Acid Red 97 and Bismarck Brown Y to Western clawed frog (*Silurana tropicalis*). *Environmental Science and Pollution Research* **21**, 3582-3591, doi:10.1007/s11356-013-2323-4 (2014).
- 316 Lotufo, G. R., Rosen, G., Wild, W. & Carton, G. Summary review of the aquatic toxicology of munitions constituents. (US Army Corps of Engineers. Engineer Research and Development Center, Environmental Laboratory Vicksburg, MS., 2013).
- 317 Davis, K. R., Schultz, T. W. & Dumont, J. N. Toxic and teratogenic effects of selected aromatic amines on embryos of the amphibian *Xenopus laevis*. *Arch. Environ. Contam. Toxicol.* **10**, 371-391 (1981).

APPENDIX

A. Supporting Data

All supporting data is stored with the supplementary data of the cited journals

B. Scientific Publications

Peer reviewed journal publications

1. Jagadish, B.; Field, J. A.; Chorover, J.; Sierra-Alvarez, R.; Abrell, L.; Mash, E. A., Synthesis of ¹³C and ¹⁵N labeled 2,4-dinitroanisole. *Journal of Labelled Compounds and Radiopharmaceuticals* 2014, 57, (6), 434-436.
2. Krzmarzick, M. J.; Khatiwada, R.; Olivares, C. I.; Abrell, L.; Sierra-Alvarez, R.; Chorover, J.; Field, J. A., Biotransformation and Degradation of the Insensitive Munitions Compound, 3-Nitro-1,2,4-triazol-5-one, by Soil Bacterial Communities. *Environmental Science & Technology* 2015, 49, (9), 5681-5688.
3. Liang, J.; Olivares, C.; Field, J. A.; Sierra-Alvarez, R., Microbial toxicity of the insensitive munitions compound, 2,4-dinitroanisole (DNAN), and its aromatic amine metabolites. *Journal of Hazardous Materials* 2013, 262, 281-287.
4. Linker, B. R.; Khatiwada, R.; Perdrial, N.; Abrell, L.; Sierra-Alvarez, R.; Field, J. A.; Chorover, J., Adsorption of novel insensitive munitions compounds at clay mineral and metal oxide surfaces. *Environmental Chemistry* 2015, 12, (1), 74-84.
5. Madeira, C. L.; Speet, S. A.; Nieto, C. A.; Abrell, L.; Chorover, J.; Sierra-Alvarez, R.; Field, J. A., Sequential anaerobic-aerobic biodegradation of emerging insensitive munitions compound 3-nitro-1,2,4-triazol-5-one (NTO). *Chemosphere* 2017, 167, 478-484.
6. Olivares, C.; Liang, J.; Abrell, L.; Sierra-Alvarez, R.; Field, J. A., Pathways of reductive 2,4-dinitroanisole (DNAN) biotransformation in sludge. *Biotechnol. Bioeng.* 2013, 110, (6), 1595–1604.
7. Olivares, C. I.; Abrell, L.; Khatiwada, R.; Chorover, J.; Sierra-Alvarez, R.; Field, J. A., (Bio)transformation of 2,4-dinitroanisole (DNAN) in soils. *J. Hazard. Mater.* 2016, 304, 214-221.
8. Olivares, C. I.; Sierra-Alvarez, R.; Abrell, L.; Chorover, J.; Simonich, M.; Tanguay, R. L.; Field, J. A., Zebrafish embryo toxicity of anaerobic biotransformation products from the insensitive munitions compound 2,4-dinitroanisole (DNAN). *Environ. Toxicol. Chem.* 2016.
9. Olivares, C. I.; Sierra-Alvarez, R.; Alvarez-Nieto, C.; Abrell, L.; Chorover, J.; Field, J. A., Microbial toxicity and characterization of DNAN (bio)transformation product mixtures. *Chemosphere* 2016, 154, 499-506.
10. Olivares, C. I.; Wang, J.; Silva Luna, C. D.; Field, J. A.; Abrell, L.; Sierra-Alvarez, R., Continuous treatment of the insensitive munitions compound N-methyl-p-nitro aniline (MNA) in an upflow anaerobic sludge blanket (UASB) bioreactor. *Chemosphere* 2016, 144, 1116-1122.

Conference publications

1. Field, J. A.; Sierra, R.; Olivares, C.; Cameron, S.; Krzmarzick, M.; Amezcuita Garcia, H.; Abrell, L.; Chorover, J.; Khatiwada, R.; Coffey II, J. In *Biotransformation of Insensitive Munition Components in Soil Microbial Cultures*, JANNAF Workshop Proceedings - Fate, Transport And Effects of Insentitive Munitions: Issues and Recent Data, Charleston, South Carolina, 2014; Johnson, M. S., Ed. Charleston, South Carolina, 2014; pp 67-72

Conference abstracts

1. Abrell, L.; Olivares, C. I.; Chorover, J.; Sierra-Alvarez, R.; Field, J. A., New 2,4-dinitroanisole (DNAN; munitions chemical) (bio)transformation products discovered and bioassayed using high resolution UPLC-QToFMS. In *64th ASMS Conference on Mass Spectrometry*, San Antonio, TX, USA, 2016. [ORAL]
2. Olivares, C. I.; Abrell, L.; Sierra-Alvarez, R.; Chorover, J.; Field, J. A., Characterization of products of 2,4-dinitroanisole (DNAN) microbial biotransformation and their inhibitory impact to microorganisms. In *250th American Chemical Society National Meeting*, Boston, MA., USA, 2015. [ORAL]
3. Field, J., Sierra-Alvarez, R., Krzmarzick, M., Madeira, C., Olivares, C., Chorover J., Abrell, L. Biotransformation and biodegradation of insensitive munitions compounds in soil. Environmental Chemistry Session, Microbial and Molecular Tools to Determine the Fate and Biotransformation of Emerging Contaminants at 252nd American Chemical Society National Meeting in Philadelphia, PA, August 21-25, 2016. [Keynote talk]
4. Field, J.A, Sierra-Alvarez, R., Krzmarzick, M., Madeira, C.L., Olivares, C.I., Chorover, J., Abrell, L. Biotransformation pathways dictating the fate in soil of insensitive munition compounds, 2,4-dinitroanisole (DNAN) and 3-nitro-1,2,4-triazole-5-one (NTO). 2016 Society of Industrial Microbiology and Biotechnology Annual Meeting. New Orleans, LA. July 27, 2016. [ORAL]
5. Madeira, C.L., Speet, S.A., Abrell, L., Chorover, J., Sierra-Alvarez, R., Field, J.A. 2016. Biodegradation of the Insensitive Munitions Compound 3-nitro-1,2,4-triazol-5-one (NTO). 7th SETAC World Congress/37th SETAC North America Annual Meeting, Nov. 6-10, 2016. Orlando, FL. [POSTER]
6. Olivares, C. I.; Abrell, L.; Simonich, M.; Chorover, J.; Sierra-Alvarez, R.; Tanguay, R. L.; Field, J. A., Coupling biotransformation of 2,4-dinitroanisole (DNAN) in anaerobic soil microcosms to a multidimensional toxicity assay using zebrafish embryos. In *Society of Environmental Toxicology and Chemistry North America 36th Annual Meeting*, Salt Lake City, UT., USA, 2015. [ORAL]
7. Olivares, C. I.; Madeira, C. L.; Abrell, L.; Chorover, J.; Sierra-Alvarez, R.; Field, J. A., Environmental fate of ¹⁴C-ring labeled 2,4-dinitroanisole (DNAN) in anaerobic saturated soils. In *250th American Chemical Society National Meeting*, Boston, MA., USA, 2015. [ORAL]
8. Olivares, C. I.; Sierra-Alvarez, R.; Abrell, L.; Chorover, J.; Field, J. A., Biotransformation and Microbial Toxicity of 2,4-Dinitroanisole (DNAN). In *Society*

- of Environmental Toxicology and Chemistry North America 35TH Annual Meeting*, Vancouver, B.C., Canada, 2014. [ORAL]
9. Olivares, C. I.; Sierra-Alvarez, R.; Abrell, L.; Chorover, J.; Field, J. A., Biotransformation and Microbial Toxicity of 2,4-Dinitroanisole (DNAN). In *Association of Environmental Engineering & Science Professors 2015 Conference*, Yale, CT., USA, 2015. [POSTER]
 10. Field, J. A. R. Sierra, C. Olivares, S. Cameron, M. Krzmarzick, H. Amezcuita Garcia, C. Alvarez Nieto, L. Abrell, J. Chorover, R. Khatiwada and John Coffey II. Biotransformation of Insensitive Munition Compounds in Soil Microbial Cultures. JANNAF Interagency Propulsion Committee. 61st JANNAF Propulsion Meeting (JPM), Charleston, SC, USA 19 – 22 May 2014 [ORAL].

Book chapters

1. Olivares, C. I.; Abrell, L.; Chorover, J.; Simonich, M.; Tanguay, R. L.; Sierra-Alvarez, R.; Field, J. A. Identifying toxic biotransformation products of the insensitive munitions compound, 2,4-dinitroanisole (DNAN), using liquid chromatography coupled to quadrupole time-of-flight mass spectrometry (LC-QToF-MS). In *Towards Harmonized Strategies and Workflows to Assess Transformation Products of Chemicals of Emerging Concern by Non-Target and Suspect Screening*, Drewes, J.; Letzel, T., Eds. American Chemical Society: 2016 (*in press*)

C. Other Supporting Materials

None